Alaska Department of Transportation & Public Facilities

Research & Technology Transfer

ALASKA DEPARTMENT OF TRANSPORTATION

Seismic Retrofit of CISS Pile Bent Cap Connections

Prepared by: Center for Infrastructure Engineering Studies
University of Missouri-Rolla
223 Engineering Research Lab
1870 Miner Circle
Rolla, MO 65409-0710

October 2006

Prepared for:
Alaska Department of Transportation
Statewide Research Office
3132 Channel Drive
Juneau, AK 99801-7898

FHWA-AK-RD-06-06

Notice

This document is disseminated under the sponsorship of the U.S. Department of Transportation in the interest of information exchange. The U.S. Government assumes no liability for the use of the information contained in this document.

The U.S. Government does not endorse products or manufacturers. Trademarks or manufacturers' names appear in this report only because they are considered essential to the objective of the document.

Quality Assurance Statement

The Federal Highway Administration (FHWA) provides high-quality information to serve Government, industry, and the public in a manner that promotes public understanding. Standards and policies are used to ensure and maximize the quality, objectivity, utility, and integrity of its information. FHWA periodically reviews quality issues and adjusts its programs and processes to ensure continuous quality improvement.

Author's Disclaimer

Opinions and conclusions expressed or implied in the report are those of the author. They are not necessarily those of the Alaska DOT&PF or funding agencies.

REPORT DOCUMENTATION PAGE

Form approved OMB No.

Public reporting for this collection of information is estimated to average 1 hour per response, including the time for reviewing instructions, searching existing data sources, gathering and maintaining the data needed, and completing and reviewing the collection of information. Send comments regarding this burden estimate or any other aspect of this collection of information, including suggestion for reducing this burden to Washington Headquarters Services, Directorate for Information Operations and Reports, 1215 Jefferson Davis Highway, Suite 1204, Arlington, VA 22202-4302, and to the Office of Management and Budget, Paperwork Reduction Project (0704-1833), Washington, DC 20503

1. AGENCY USE ONLY (LEAVE BLANK)	2. REPORT DATE	3. REPORT TYPE AND DATES COVERED
FHWA-AK-RD-06-06	October 2006	Final

4. TITLE AND SUBTITLE

Seismic Retrofit of CISS Pile Bent Cap Connections

5. FUNDING NUMBERS

T2-03-02
RES-02-008

6. AUTHOR(S)

Michael C. Lubiewski, Pedro F. Silva, Ph.D., P.E., Genda Chen, PhD., P.E.

7. PERFORMING ORGANIZATION NAME(S) AND ADDRESS(ES)

Center for Infrastructure Engineering Studies
University of Missouri-Rolla
223 Engineering Research Lab
1870 Miner Circle
Rolla, MO 65409-0710

8. PERFORMING ORGANIZATION REPORT NUMBER

CIES 06-64

9. SPONSORING/MONITORING AGENCY NAME(S) AND ADDRESS(ES)

State of Alaska, Alaska Dept. of Transportation and Public Facilities
Research and Technology Transfer
2301 Peger Rd
Fairbanks, AK 99709-5399

10. SPONSORING/MONITORING AGENCY REPORT NUMBER

FHWA-AK-RD-06-06

11. SUPPLENMENTARY NOTES

Performed in cooperation with the U.S. Department of Transportation, Federal Highway Administration.
Research Project Title: "Bridge Seismic Retrofit"

12a. DISTRIBUTION / AVAILABILITY STATEMENT

No restrictions.
This document is available to the public through the National Technical Information Service, Springfield, VA 22161

12b. DISTRIBUTION CODE

13. ABSTRACT (Maximum 200 words)

Three 4/5-scale units were cast, retrofitted, and tested under simulated seismic loads. These units were built to model a bridge bent consisting of a cast in place steel shell (CISS) column foundation shaft and a bent cap configured to form a tee connection. Each unit was retrofitted in the column, bent cap, and their connection according to current seismic design standards. The main objective was to ensuring ductile performance under lateral loads.

Specific seismic improvements made to the column and the bent cap system were: (1) the moment capacity of the column was reduced by cutting a portion of the column longitudinal reinforcement at the connection to the bent cap to levels that can ensure a proper ductile seismic response, (2) a section of the steel shell was cut and removed leaving a gap between the steel shell and the bent cap, and (3) the bent cap dimensions were increased to ensure proper reinforcement spacing and to install additional flexure and joint shear reinforcement.

Empirical models were developed that account for the effects of joint rotation and damage.

14. KEYWORDS : Testing, Investigation of Structures, Structural Analysis, Structural Models, Structural Design, Earthquake Resistant Design, Bridge Foundations

15. NUMBER OF PAGES
136

16. PRICE CODE
N/A

17. SECURITY CLASSIFICATION OF REPORT	18. SECURITY CLASSIFICATION OF THIS PAGE	19. SECURITY CLASSIFICATION OF ABSTRACT	20. LIMITATION OF ABSTRACT
Unclassified	Unclassified	Unclassified	N/A

SI* (MODERN METRIC) CONVERSION FACTORS

APPROXIMATE CONVERSIONS TO SI UNITS

Symbol	When You Know	Multiply By	To Find	Symbol
		LENGTH		
in	inches	25.4	millimeters	mm
ft	feet	0.305	meters	m
yd	yards	0.914	meters	m
mi	miles	1.61	kilometers	km
		AREA		
in^2	square inches	645.2	square millimeters	mm^2
ft^2	square feet	0.093	square meters	m^2
yd^2	square yard	0.836	square meters	m^2
ac	acres	0.405	hectares	ha
mi^2	square miles	2.59	square kilometers	km^2
		VOLUME		
fl oz	fluid ounces	29.57	milliliters	mL
gal	gallons	3.785	liters	L
ft^3	cubic feet	0.028	cubic meters	m^3
yd^3	cubic yards	0.765	cubic meters	m^3
	NOTE: volumes greater than 1000 L shall be shown in m^3			
		MASS		
oz	ounces	28.35	grams	g
lb	pounds	0.454	kilograms	kg
T	short tons (2000 lb)	0.907	megagrams (or "metric ton")	Mg (or "t")
		TEMPERATURE (exact degrees)		
^oF	Fahrenheit	5 (F-32)/9 or (F-32)/1.8	Celsius	^oC
		ILLUMINATION		
fc	foot-candles	10.76	lux	lx
fl	foot-Lamberts	3.426	candela/m^2	cd/m^2
		FORCE and PRESSURE or STRESS		
lbf	poundforce	4.45	newtons	N
lbf/in^2	poundforce per square inch	6.89	kilopascals	kPa

APPROXIMATE CONVERSIONS FROM SI UNITS

Symbol	When You Know	Multiply By	To Find	Symbol
		LENGTH		
mm	millimeters	0.039	inches	in
m	meters	3.28	feet	ft
m	meters	1.09	yards	yd
km	kilometers	0.621	miles	mi
		AREA		
mm^2	square millimeters	0.0016	square inches	in^2
m^2	square meters	10.764	square feet	ft^2
m^2	square meters	1.195	square yards	yd^2
ha	hectares	2.47	acres	ac
km^2	square kilometers	0.386	square miles	mi^2
		VOLUME		
mL	milliliters	0.034	fluid ounces	fl oz
L	liters	0.264	gallons	gal
m^3	cubic meters	35.314	cubic feet	ft^3
m^3	cubic meters	1.307	cubic yards	yd^3
		MASS		
g	grams	0.035	ounces	oz
kg	kilograms	2.202	pounds	lb
Mg (or "t")	megagrams (or "metric ton")	1.103	short tons (2000 lb)	T
		TEMPERATURE (exact degrees)		
^oC	Celsius	1.8C+32	Fahrenheit	^oF
		ILLUMINATION		
lx	lux	0.0929	foot-candles	fc
cd/m^2	candela/m^2	0.2919	foot-Lamberts	fl
		FORCE and PRESSURE or STRESS		
N	newtons	0.225	poundforce	lbf
kPa	kilopascals	0.145	poundforce per square inch	lbf/in^2

*SI is the symbol for the International System of Units. Appropriate rounding should be made to comply with Section 4 of ASTM E380.
(Revised March 2003)

CENTER FOR INFRASTRUCTURE ENGINEERING STUDIES

SEISMIC RETROFIT OF CISS PILE BENT CAP CONNECTIONS

by

MICHAEL LUBIEWSKI

PEDRO SILVA

GENDA CHEN

University of Missouri-Rolla

CIES 06-64

April 2006

DISCLAIMER

The contents of this report reflect the views of the authors, who are responsible for the facts and the accuracy of the information presented herein. This document is disseminated under the sponsorship of the Center for Infrastructure Engineering Studies (CIES), University of Missouri-Rolla, in the interest of information exchange. CIES assumes no liability for the contents or use thereof.

CIES MISSION

The mission of CIES is to provide leadership in research and education for solving society's problems affecting the nation's infrastructure systems. CIES is the primary conduit for communication among those on the UMR campus interested in infrastructure studies and provides coordination for collaborative efforts. CIES activities include interdisciplinary research and development with projects tailored to address needs of federal agencies, state agencies, and private industry as well as technology transfer and continuing/distance education to the engineering community and industry.

Center for Infrastructure Engineering Studies (CIES)
University of Missouri-Rolla
223 Engineering Research Lab
1870 Miner Circle
Rolla, MO 65409-0710
Tel: (573) 341-6223; fax -6215
E-mail: cies@umr.edu
Web Page: www.cies.umr.edu

ACKNOWLEDGEMENTS

The research reported in this report was funded by the Alaska Department of Transportation and the University Transportation Center located at the University of Missouri Rolla. Material donations were also made possible by the Headed Reinforcement Corporation, Ambassador Steel Corporation, and the Concrete Reinforcing Steel Institute Heart of America Chapter. All support is greatly appreciated. The views expressed in this report do not necessarily reflect the views of the sponsors. Assistance was provided by various students at the University of Missouri – Rolla and by the support staff for the laboratory, all of which is appreciated.

Seismic Retrofit of CISS Pile Bent Cap Connections

by

Michael Lubiewski
Graduate Research Assistant

Pedro Silva
Assistant Professor of Civil Engineering

Genda Chen
Associate Professor of Civil Engineering

Final Report

Report No. CIES 06-64

Department of Civil, Architectural and Environmental Engineering
Center for Infrastructure Engineering Studies
University of Missouri – Rolla

April 2006

TABLE OF CONTENTS

TABLE OF CONTENTS vi
LIST OF SYMBOLS ix
LIST OF FIGURES xi
LIST OF TABLES xvi
ABSTRACT xvii
1. INTRODUCTION 1
1.1. Overview 1
1.2. Research Significance 2
1.3. Literature Review 2
1.4. Scope of Research 4
1.5. Research Findings and General Design Recommendations 5
1.5.1. Unit 2 – Permissible Design Levels 6
1.5.2. Unit 3 – Permissible Design Levels 6
1.6. Report Layout 7
2. EXPERIMENTAL PROGRAM AND AS-BUILT SECTIONS 8
2.1. Test Matrix 8
2.2. Test Setup 8
2.3. As-Built Sections 9
2.3.1. Column Reinforcement 10
2.3.2. Bent Cap Reinforcement 11
2.4. Material Properties 11
3. RETROFIT AND UPGRADE DESIGN OF UNIT 1 13
3.1. Column Design Considerations 13
3.1.1. Moment-Curvature Analysis 14
3.2. Bent Cap Design Considerations 16
3.2.1. Moment-Curvature Analysis 17
3.2.2. Retrofitted Bent Cap Sizing 18
3.3. Joint Design Considerations 19
3.3.1. Joint Principle Stress Evaluation 19
3.3.2. Joint Shear Reinforcement 21
3.3.3. Additional Longitudinal Reinforcement 23
3.3.4. Additional Internal and External Vertical Reinforcement 24
3.3.5. Additional Horizontal Reinforcement 24
3.4. Construction of The As-built Section 27
3.5. Construction of Unit 1 Upgrade Section 28
4. RETROFIT AND UPGRADE DESIGN OF UNIT 2 31

4.1. Construction of Unit 2 Upgrade Section....32
5. RETROFIT AND UPGRADE DESIGN OF UNIT 3.... 34
5.1. Introduction....34
5.2. Moment-Curvature Analysis....35
5.3. Joint Principle Stress Determination....36
5.4. Construction of Unit 3 Upgrade Section....39
6. INSTRUMENTATION Layout.... 40
6.1. Strain Gauges....40
6.1.1. Column Section.... 40
6.1.2. Bent Cap As-Built Section.... 41
6.1.3. Bent Cap Retrofit Section.... 42
6.2. Load Cells....43
6.3. LVDT's....44
7. Predicted Load-deformation Response.... 46
7.1. One-Component Nonlinear Giberson Model....46
7.2. Force-Displacement Response not Considering Joint Degradation....47
7.3. Loading Protocol....49
8. EXPERIMENTAL RESULTS – UNIT 1.... 51
8.1. General Test Observations....51
8.1.1. Force Control Load Cycles.... 51
8.1.2. Displacement Control Load Cycles.... 52
8.2. Load Deformation Response....63
8.3. Load vs. Curvature Response....65
8.4. Column Longitudinal Reinforcement Strains....66
8.5. Joint Shear Reinforcement Strain Profiles....69
8.6. Bent Cap Longitudinal Reinforcement Strains....71
8.6.1. Strain Profiles - Bottom Reinforcement.... 71
8.6.2. Strain Profiles - Top Reinforcement.... 73
8.7. Joint Shear Analysis....74
8.8. Relevant Experimental Results used in the Design of Unit 2....77
9. EXPERIMENTAL RESULTS – UNIT 2.... 78
9.1. General Test Observations....78
9.1.1. Force Control Load Cycles.... 78
9.1.2. Displacement Control Load Cycles.... 80
9.2. Load Deformation Response....90
9.3. Load vs. Curvature Response....92
9.4. Column Longitudinal Reinforcement Strains....93

9.5. Joint Shear Reinforcement Strain Profiles 94
9.6. Bent Cap Longitudinal Reinforcement Strains 96
9.6.1. Strain Profiles - Bottom Reinforcement 96
9.7. Joint Shear Analysis 98
10. EXPERIMENTAL RESULTS – UNIT 3 101
10.1. General Test Observations 101
10.1.1. Force Control Load Cycles 101
10.1.2. Displacement Control Load Cycles 101
10.2. Load Deformation Response 111
10.3. Load vs. Curvature Response 113
10.4. Column Longitudinal Reinforcement Strains 113
10.5. Joint Shear Reinforcement Strain Profiles 116
10.6. Bent Cap Longitudinal Reinforcement Strains 117
10.7. Joint Shear Analysis 119
11. DISCUSSION OF EXPERIMENTAl RESULTS 121
11.1. General 121
11.2. Comparison of Dissipated Energy for the Three Test units 121
11.3. Strength Degradation under Reversed cyclic loading 122
11.4. Joint Performance 123
11.5. Post-Test Analysis 126
12. CONCLUSIONS 128
12.1. General Overview 128
12.2. General Conclusions 129
12.3. Seismic Design Recommendations 129
12.3.1. Column Design 130
12.3.2. Bent Cap Design 131
12.3.3. Reinforced Concrete Joint Design 131
REFERENCES 134

LIST OF SYMBOLS

A_{jh} = Area of horizontal joint shear reinforcement

A_{jv} = Area of vertical joint shear reinforcement

A_{jv}^{ext} = Area of external vertical joint shear reinforcement, outside the joint region

A_{jv}^{int} = Area of internal vertical joint shear reinforcement, within the joint region

A_{sc} = Area of the column longitudinal reinforcement

b_{je} = Width of the joint over which the shear force is applied

d_b = Bar diameter

D_c = Inside diameter of CISS steel shell

$D_c^{'}$ = Diameter of column concrete core

E_s = Modulus of elasticity of reinforcement steel

f_a = Axial stress

$f_c^{'}$ = Concrete compressive strength

f_l = Joint confining pressure

f_{sh} = Stress in the horizontal confining steel

f_y = Reinforcement yield stress

$f_{y,b}$ = Bent cap longitudinal reinforcement yield stress

$f_{y,c}$ = Column reinforcing specified yield strength

f_{yc}^{o} = Overstrength stress in the column longitudinal reinforcement, $f_{yc}^{o} = \lambda_0 f_y$

$f_{c,b}^{'}$ = Bent cap specified design compressive concrete strength

f_p = Transverse presstressing stress

H = Distance from the centerline of the retrofitted bent cap to the centerline of the applied lateral load

h_b = Height of the retrofitted bent cap

L = Distance between the end supports

l_a = Anchorage length of column longitudinal reinforcement, $l_a = 0.7h_b$

l_d = Development length

L_1 = Distance between the bridge girders

M_b^D = Bent cap centerline moment at node D

M_c^F = Column centerline moment at node F

P = Axial force in the column

p_c = Principle compressive stress

p_t = Principle tensile stress

$p_{t,m}$ = Principle tensile stress limit requiring full joint shear reinforcement

v_h = Joint shear stress

V_h = Shear force in joint due to applied moment

α = Factor to calculate moment at column face

β = Factor to calculate moment at column face

ΔA_{bb} = Additional bottom beam longitudinal reinforcement

ΔA_{tb} = Additional top beam longitudinal reinforcement

λ = Principle stress determined from Eigenvector

λ_0 = material over strength factor, equal to 1.4 for when design yield strength is used

σ_{xx} = Stress in the x-x direction

σ_{yy} = Stress in the y-y direction, $\sigma_{yy} = f_a$

σ_{zz} = Stress in the z-z direction, $\sigma_{zz} = f_p$

ρ_l = Column longitudinal reinforcement ratio

ρ_s = Column volumetric transverse reinforcement ratio

τ_{xy} = Shear stress in x-y direction, $\tau_{xy} = v_h$

τ_{zx} = Shear stress in the z-x direction

τ_{zy} = Shear stress in the z-y direction

μ = Displacement ductility level

LIST OF FIGURES

Figure 2-1. Test Setup 9
Figure 2-2. As-Built Reinforcement Layout 10
Figure 3-1. Unit 1 Retrofitted Cross-Section 13
Figure 3-2. Cut Longitudinal Reinforcement 14
Figure 3-3. Column Moment Curvature 15
Figure 3-4. Bent Cap Moment Demand Design Considerations 16
Figure 3-5. Bent Cap Moment Curvature 17
Figure 3-6. Joint Shear Forces in Bridge Tee Joints 19
Figure 3-7. Joint Principle Tensile Stresses - Retrofitted Column 21
Figure 3-8. Joint Force Transfer Model (Sritharan, 1999) 22
Figure 3-9. Joint Shear Reinforcements 23
Figure 3-10. Unit 1 Bent Cap Reinforcement Layout 26
Figure 3-11. Column Strut Forces 26
Figure 3-12. Column & Cap Reinforcing Cage 27
Figure 3-13. Bent Cap Reinforcing Cage 27
Figure 3-14. Bent Cap Inside Form Work 27
Figure 3-15. Colum Reinforcing Cage 27
Figure 3-16. Installation of Column Cage 28
Figure 3-17. Casting of the Bent Cap 28
Figure 3-18. Construction of the Load Stub 28
Figure 3-19. Completed As-Built Section 28
Figure 3-20. Cutting Steel Shell Casing 29
Figure 3-21. Installing Headed Reinforcing 29
Figure 3-22. Retrofit Section Reinforcing Cage 29
Figure 3-23. Joint Region Detail 29
Figure 3-24. Retrofit Section Reinforcing Cage 30
Figure 3-25. Forming Retrofit Section 30
Figure 3-26. Completed Unit 1 Before Testing 30
Figure 4-1. Unit 2 Retrofit Cross-Section 31
Figure 4-2. Unit 2 Retrofit Reinforcement Layout 32
Figure 4-3. Detail at Bent Cap Interface 33
Figure 4-4. Detail at Bent Cap Interface 33
Figure 4-5. Bent Cap Retrofit Section 33
Figure 4-6. Bent Cap Retrofit Section 33
Figure 5-1. Unit 3 Retrofit Cross-Section 34
Figure 5-2. Unit 3 Retrofit Reinforcement Layout 35

Figure 5-3. Unit 3 Pre-stressed Joint 35
Figure 5-4. Unit 3 Moment-Curvature 36
Figure 5-5. 3-D Stress Cube 37
Figure 5-6. Unit 3 Principle Stresses 38
Figure 5-7. Pre-Drilled Holes 39
Figure 5-8. Installed Headed Reinforcement 39
Figure 5-9. Unit Before Casting of Upgrade Section 39
Figure 5-10. Completed Test Unit 39
Figure 6-1. Column Reinforcement and Steel Shell Strain Gauges 40
Figure 6-2. As-Built Bent Cap Strain Gauges 41
Figure 6-3. As-Built Bent Cap Shear Strain Gauges 41
Figure 6-4. Retrofit Bent Cap Strain Gauges 42
Figure 6-5. Retrofit Bent Cap Shear Strain Gauges 43
Figure 6-6. Retrofit Transverse Headed Reinforcement Strain Gauges 43
Figure 6-7. Retrofit Vertical Headed Reinforcement Strain Gauges 43
Figure 6-8. Load Cells for Axial Load 43
Figure 6-9. Joint LVDT's 44
Figure 6-10. Joint Strain Calculation 45
Figure 7-1. Predicted Force-Displacement Response of Units 1, 2 and 3 48
Figure 7-2. Loading Protocol Sequence 50
Figure 8-1. Bent Cap Cracking at 1.00V_y 51
Figure 8-2. Bent Cap Cracking at 1.00 V_y 52
Figure 8-3. Joint Cracking at 1.0 μ_Δ 54
Figure 8-4. Bent Cap Cracking at 1.0 μ_Δ 54
Figure 8-5. Joint Cracking at 1.5 μ_Δ 55
Figure 8-6. Bent Cap Cracking at 1.5 μ_Δ 55
Figure 8-7. Joint Cracking at 2.0 μ_Δ 56
Figure 8-8. Bent Cap Cracking at 2.0 μ_Δ 56
Figure 8-9. Joint Cracking at 4.0 μ_Δ 57
Figure 8-10. Bent Cap Cracking at 4.0 μ_Δ 57
Figure 8-11. Joint Crack Width at 4.0 μ_Δ 58
Figure 8-12. Column Concrete Crushing at 4.0 μ_Δ 58
Figure 8-13. Joint Cracking at 6.0 μ_Δ 59
Figure 8-14. Column Concrete Crushing at 6.0 μ_Δ 59
Figure 8-15. Bent Cap Bottom Cracking at 6.0 μ_Δ 60
Figure 8-16. Column Longitudinal Bar Buckling at 6.0 μ_Δ 60

Figure 8-17. Bent Cap Cracking at 8.0 μ_Δ 61
Figure 8-18. Column Longitudinal Bar Fracture at 8.0 μ_Δ 61
Figure 8-19. Bent Cap Bottom Spalling at 8.0 μ_Δ 62
Figure 8-20. Joint Cracking at 8.0 μ_Δ 62
Figure 8-21. Bent Cap Ultimate Damage 63
Figure 8-22. Unit 1 - Load Displacement Response 64
Figure 8-23. Unit 1 – Load versus Curvature Response 66
Figure 8-24. Strain Gauge History – C4a 67
Figure 8-25. Strain Gauge History – C4b 67
Figure 8-26. Strain Gauge Profile – Side “A” 68
Figure 8-27. Strain Gauge Profile – Side “B” 68
Figure 8-28. Strain Profiles – As-Built Section 70
Figure 8-29. Strain Profiles – Retrofit Section 70
Figure 8-30. Strain Profiles – As-Built Section 72
Figure 8-31. Strain Profiles – Retrofit Section 72
Figure 8-32. Confinement of Column Anchorage Failure 73
Figure 8-33. Strain Profiles – Retrofit Section 73
Figure 8-34. Joint Shear Deformation 75
Figure 8-35. Unit 1 Principle Tensile Stress vs. Joint Shear Strain 76
Figure 8-36. Underside of Bent Cap Cracking Pattern 76
Figure 9-1. Bent Cap Cracking at $0.50V_y$ 78
Figure 9-2. Bent Cap Cracking at $0.75V_y$ 79
Figure 9-3. Bent Cap Cracking at $1.00V_y$ 79
Figure 9-4. Joint Cracking at $1.00V_y$ 80
Figure 9-5. Joint Cracking at 1.0 μ_Δ 82
Figure 9-6. Bent Cap Cracking at 1.0 μ_Δ 82
Figure 9-7. Joint Cracking at 1.5 μ_Δ 83
Figure 9-8. Bent Cap Cracking at 1.5 μ_Δ 83
Figure 9-9. Joint Cracking at 2.0 μ_Δ 84
Figure 9-10. Bent Cap Cracking at 2.0 μ_Δ 84
Figure 9-11. Joint Cracking at 4.0 μ_Δ 85
Figure 9-12. Bent Cap Cracking at 4.0 μ_Δ 85
Figure 9-13. Joint Cracking at 6.0 μ_Δ 86
Figure 9-14. Bent Cap Cracking at 6.0 μ_Δ 86
Figure 9-15. Bottom Cracking at 8.0 μ_Δ 87
Figure 9-16. Joint Cracking at 8.0 μ_Δ 87

Figure 9-17. Column Crushing at 8.0 μ_Δ 88
Figure 9-18. Final Damage 88
Figure 9-19. Hoop Buckling Side "A" 89
Figure 9-20. Hoop Buckling Side "B" 89
Figure 9-21. Unit 2 – Load Displacement Response 90
Figure 9-22. Unit 2 Joint Shear Cracks 91
Figure 9-23. Cracking on Underside of Bent Cap 92
Figure 9-24. Unit 2 – Load versus Curvature Response 92
Figure 9-25. Strain Gauge History – C4a 93
Figure 9-26. Strain Gauge History – C4b 93
Figure 9-27. Strain Gauge Profile – Side "A" 94
Figure 9-28. Strain Gauge Profile – Side "B" 94
Figure 9-29. Strain Profiles – As-Built Section 95
Figure 9-30. Strain Profiles – Retrofit Section 96
Figure 9-31. Strain Profiles – As-Built Section 97
Figure 9-32. Strain Profiles – Retrofit Section 97
Figure 9-33. Specimen #2 Joint Shear Deformation 98
Figure 9-34. Unit 2 Headed Transverse Reinforcement Strain History 99
Figure 9-35. Unit 2 Top Transverse Reinforcement Strain Profile 99
Figure 9-36. Unit 2 Principle Tensile Stress vs. Joint Shear Strain 100
Figure 10-1. Bent Cap Cracking at 1.00V_y 101
Figure 10-2. Joint Cracking at 1.0 μ_Δ 103
Figure 10-3. Bent Cap Cracking at 1.0 μ_Δ 103
Figure 10-4. Joint Cracking at 1.5 μ_Δ 104
Figure 10-5. Bent Cap Cracking at 1.5 μ_Δ 104
Figure 10-6. Joint Cracking at 2.0 μ_Δ 105
Figure 10-7. Bent Cap Cracking at 2.0 μ_Δ 105
Figure 10-8. Joint Cracking 4.0 μ_Δ 106
Figure 10-9. Bent Cap Cracking at 4.0 μ_Δ 106
Figure 10-10. Joint Cracking at 6.0 μ_Δ 107
Figure 10-11. Bent Cap Cracking at 6.0 μ_Δ 107
Figure 10-12. Joint Cracking at 8.0 μ_Δ 108
Figure 10-13. Bent Cap Cracking – Side "A" at 8.0 μ_Δ 108
Figure 10-14. Bent Cap Cracking – Side "B" at 8.0 μ_Δ 109
Figure 10-15. Bent Cap Underside Cracking at 8.0 μ_Δ 109
Figure 10-16. Bent Cap Cracking Ultimate Damage 110

Figure 10-17. Column Crushing Ultimate Damage 110
Figure 10-18. Underside of Bent Cap Ultimate Damage 111
Figure 10-19. Unit 3 - Load Displacement Response 111
Figure 10-20. Unit 3 Joint Shear Cracks 112
Figure 10-21. Unit 3 – Load versus Curvature Response 113
Figure 10-22. Strain Gauge History – C4a 114
Figure 10-23. Strain Gauge History – C4b 114
Figure 10-24. Strain Gauge Profile – Side “A” 115
Figure 10-25. Strain Gauge Profile – Side “B” 115
Figure 10-26. Strain Profiles – As-Built Section 116
Figure 10-27. Strain Profiles – Retrofit Section 117
Figure 10-28. Strain Profiles – As-Built Section 118
Figure 10-29. Strain Profiles – Retrofit Section 118
Figure 10-30. Unit 3 Joint Shear Deformation 119
Figure 10-31. Unit 3 Principle Tensile Stress vs. Joint Shear Strain 120
Figure 10-32. Unit 3 Top Transverse Reinforcement Strain Profile 120
Figure 11-1. Cumulative Dissipated Energy 122
Figure 11-2. Strength Degradation under Reversed cyclic loading 123
Figure 11-3. Normalized Principle Stresses vs. Computed Joint Rotation 125
Figure 11-4. Joint models 126
Figure 11-5. Post-Test Analysis 127

LIST OF TABLES

Table 2-1. Concrete Material Properties 12
Table 2-2. Reinforcing Steel Material Properties – As Built Section 12
Table 2-3. Reinforcing Steel Material Properties – Retrofit Section 12
Table 5-1. Bilinear Moment Curvature 36
Table 7-1. Bilinear Force Deformation 48
Table 11-1. Peak Values 121
Table 12-1. Allowable 132
Table 12-2. Modified Displacement Ductility Capacity 133

ABSTRACT

This report presents and discusses results from a research investigation of three 4/5-scale units that were cast, retrofitted, and tested under simulated seismic loads at the University of Missouri Rolla experimental facilities and sponsored under a research grant from the State of Alaska Department of Transportation and Public Facilities. These units were built to model a bridge bent consisting of a cast in place steel shell (CISS) column foundation shaft and a bent cap configured to form a tee connection. In this report these units were designated as Unit 1, 2, and 3. Each unit was retrofitted in the column, bent cap, and their connection according to current seismic design standards with the main objective of ensuring a ductile performance under lateral loads.

Specific seismic improvements made to the column and the bent cap system were: (1) the moment capacity of the column was reduced by cutting a portion of the column longitudinal reinforcement at the connection to the bent cap to levels that can ensure a proper ductile seismic response, (2) a section of the steel shell was cut and removed leaving a gap between the steel shell and the bent cap, and (3) the bent cap dimensions were increased to ensure proper reinforcement spacing and to install the additional flexure and joint shear reinforcement, which was designed according to well established joint shear force transfer mechanism models. Before testing the lateral deformation response of the test units was performed using well-established moment rotation models. Based on test results these moment-rotation models were revised and an empirical model was proposed to include the contribution of joint flexibility and damage into the lateral response of the test units. These models account for the flexibility of the retrofitted and as described in this report the post-test results matched well the experimental results. This report presents the test results, design philosophy of the upgrade method along with design recommendations, and recommendations for future research in order to improve the proposed retrofit scheme.

1. INTRODUCTION

1.1. OVERVIEW

Seismic design in the United States has improved significantly since the 1971 San Fernando Earthquake in California (Buckle, 2000; Krawinkler, 1995; 1999). During the aftermath of this earthquake a large number of bridges failed catastrophically due to insufficient confinement of plastic hinges and span seating. In response to these failures, the California Department of Transportation (Caltrans, 2001, 2004) initiated a retrofit program to retrofit all bridges against premature failure in the plastic hinge zones and unseating (DesRoches and Fenves, 2001; Priestley et al., 1995). Then, following the 1989 Loma Prieta Earthquake in California, major advances were implemented in seismic design of joints leading to the current capacity philosophy for the seismic design of bridges. According to the capacity design philosophy the main performance goal is to allow the development of plastic hinges at both ends of columns for optimum energy dissipation. This can be realized by carefully selecting and detailing the plastic hinge areas, while the remaining regions are designed to remain elastic for the design seismic event (Priestley *et al.*, 1996; Mazzoni and Moehle, 2001; ATC-32, 1996).

It is well documented in current seismic design codes that the purpose of limiting the plastic hinges at both ends of columns is because post-earthquake repair may be completed without disruption to the daily traffic flow (Caltrans, 2004). Another benefit of this practice is that post-earthquake inspection consisting of nondestructive measures can be easily undertaken. Previous research has shown that existing bridges built in the state of Alaska do not comply with current seismic design principles leaving them prone to significant damage and undesirable failure modes when subjected to seismic events. A common practice in the construction of bridge bents in Alaska and other regions that experience long winter and deicing seasons is the use of a thick steel shell to form a cast-in-drilled-hole (CIDH) foundation shaft system and to act as the external longitudinal and transverse reinforcement for the system. The shell, which improves constructability for the bent by serving as a casing for the CIDH shaft and formwork for the column, have been typically embedded into the bent cap and the connection to the bent cap consists of mild steel longitudinal reinforcement. Based on a preliminary evaluation of existing bridges built in the state of Alaska, (Silva *et al.*, 1999), some of the design deficiencies common to these as-built bridges are:

1) The CISS column foundation shafts have excessive longitudinal reinforcement ratios, which impose high demands in the joints and the bent caps.

2) The yield moment capacity of the bent cap is below the maximum feasible moment demand that develops at the column faces, which leads to the formation of plastic hinges in the bent cap.

3) The steel shells are partially embedded in the joint region, which under low levels of rotation impose extensive damage on the bent cap, and

4) The joints have inadequate amounts of joint shear reinforcement to sustain the levels of principal tensile stresses that develop within the joint region, which leads to anchorage failure of the column longitudinal reinforcement and significant strength degradation below yielding of the column longitudinal reinforcement.

Under seismic loading, these design deficiencies lead to damage of the bent cap and joint, which do not meet current capacity design standards for a proper seismic response of bent cap systems (AASHTO, 1996; Caltrans, 2001; Priestley, 1996). Because of the design deficiencies outlined above, there is a need to develop procedures for the seismic upgrade of these systems. As such, the main objective of this research program was to provide upgrade design guidelines and evaluation methodologies for bridge system consisting of CIDH foundation shafts.

1.2. RESEARCH SIGNIFICANCE

This research program investigated an upgrade method for improving the seismic performance of bridge bents built in the state of Alaska. Research results were then used to establish reliable displacement ductility levels and joint principle tensile stress limits for design of bridge bents using the proposed upgrade method. As such, a laboratory model was designed, constructed, and tested under simulated seismic loads with the main goal of investigating the feasibility for field implementation of the proposed upgrade scheme.

1.3. LITERATURE REVIEW

Most of reinforced concrete (RC) columns built prior to the 1970's were deficient in shear strength and flexural ductility (Sanders et al., 1992; Priestley *et al*., 1995). Each of these design deficiencies corresponds to a potential failure mode that is associated with insufficient amounts of transverse reinforcement and/or seismic detailing. However, the associated failure modes are mostly eliminated when using steel shells encasing reinforced or unreinforced concrete sections, because of the satisfactory seismic performance of steel casings to enhance the ductility capacity through confinement of the concrete core (Chai *et al.*, 1991; Priestley *et al.*, 1995; Silva *et al.*, 1997). With the presence of the steel shells undesirable failure modes are prevented under reversed cyclic loading and, as such, no retrofit is required in these members. However; up until recently, the steel shells in these CIDH shafts have been embedded into the bent cap. This detail has been experimentally investigated to cause extensive damage to the joint region due to the the steel shell prying action expected under reversed cyclic loading (Silva and Seible, 2001). As demonstrated by Silva *et al.* (1997), such damage can be easily prevented by terminating the

steel shells below the bent cap. This detail was also adopted in this research program and the corresponding construction/upgrade details are clearly described in Section 3.1.

Recent earthquakes worldwide have illustrated the vulnerability of existing RC beam-column joints to seismic loading (Sritharan, 1998). Poorly detailed joints have been identified as critical structural elements because of their undesirable performance when subjected to seismic loading (Mazzoni and Moehle, 2001). Strengthening of RC joints is a difficult task posing major construction challenges. A variety of techniques applicable to concrete elements have also been applied to joints with the most common ones being the construction of concrete jackets with or without the use of longitudinal or transverse prestressing (Mazzoni and Moehle, 2001; Ingham, 1995).

Longitudinal prestressing of a beam-column joint has two major advantages; namely, it reduces the tendency for joint cracking due to an increase in horizontal plane stresses, and secondly it increases the joint shear strength of the bent cap. Prestressing can also be designed to increase the bent cap shear and flexural strength sufficiently to ensure that column plastic hinges are developed for both positive and negative moments. However, prestressing the joint also increases the principal compressive stresses within the joint, and design of the prestressing force should not lead to principle compressive stresses in excess of $0.3f'_c$. In this research program post tensioning was also evaluated; but in this case, only stressing in the transverse direction of the bent cap was implemented. Unlike longitudinal prestressing, transverse prestressing only merits by increasing the strength of the joint to resist the input tensile stresses, but it does not either lead to a reduction in the principle tensile stresses nor does it increases the shear and flexural strength of the bent cap. Although not as effective as prestressing in the longitudinal direction because of these reasons, this is a detail solution that has not been previously investigated, and merits investigation for its usefulness in field applications.

Longitudinal external prestressing is likely to be the most effective retrofit technique when the principal tensile stresses within the joint can be reduced below $0.25\sqrt{f'_c}$ [MPa]. For higher levels of principal tensile stresses it may be unfeasible or even impractical to solely use prestressing. In this case, jacketing the joint by concrete, steel, or composite-materials may be also required to ensure that the performance of the joint is not likely to degrade under reversed cyclic loading (Gergely *et al.*, 2000; Chen *et al.*, 2005). Joint degradation leads to increased drift levels and subsequently anchorage failure of the column longitudinal reinforcement. Typically, the concrete jacket is dimensioned to ensure that the principle tensile stresses are properly dissipated over a wider region (Sritharan, 1998). Jacketing can also be used to increase the joint dimensions, thus reducing the principle stress levels. Extending the size of the joint into the existing column and

bent cap also increases the development length of the column longitudinal reinforcement and it creates new critical sections for moment capacity at the edge of the jacket. These details were further evaluated and implemented in this research program to enhance the seismic performance of the bent cap and joint region. Construction and design details implemented in the three test units are clearly described in Sections 3, 4, and 5.

Analytical models in the form of strut-and-tie models have been developed and successfully used to design the shear reinforcement within the joint region. For example, Priestley (1993) developed a three point stress-strain model for poorly confined joints using these limits as starting points for joint design and assessment. As such, strut-and-tie models discussed in the literature were also used in this research program (Sritharan, 1998). Test results along with recommended procedures for seismic design and implementation of the retrofit schemes are presented and discussed in detail in the body of this report.

1.4. SCOPE OF RESEARCH

A prototype unit consisting of an interior column and corresponding bent cap was designed and constructed in a T-configuration by including the deficiencies discussed in Section 1.1. After construction, the as-built portion of the test units was modified in order to investigate seismic improvements and propose procedures for field implementation. The proposed seismic upgrade procedures were experimentally investigated in this research program and are presented in this report. Briefly, the seismic improvements made to the column and the bent cap system were:

1) The moment capacity of the column was reduced by cutting a portion of the column longitudinal reinforcement at the connection to the bent cap to levels that can ensure a proper ductile seismic response. Although current seismic design practices in the State of Alaska limits the longitudinal reinforcement ratio to 3% in order to minimize strength reductions resulting from joint degradation, previous research has shown that column reinforcement ratios in the order of 4.0% can be achieved provided that joint shear stresses are limited and congestion of reinforcement is avoided within the joint region (Priestley *et. al*, 1995, Silva *et. al*, 1999). As such, this limit was also used as a benchmark for this research program for retrofit applications.

2) A section of the steel shell was cut and removed leaving a gap between the steel shell and the bent cap. As before, previous research has shown that leaving this gap avoids significant damage to the bent cap under small rotations because the prying action of the steel shell against the surrounding concrete is avoided (Silva *et. al*, 1999). In addition, the steel shell was removed to provide access to cut the column longitudinal reinforcement thereby reducing the reinforcement ratio as designated above.

3) The bent cap dimensions were increased to ensure proper reinforcement spacing and to install the additional flexure and joint shear reinforcement, which was designed according to well established joint shear force transfer mechanism models (Sritharan and Ingham, 2003). Increasing the bent cap sizes also reduced the principle tensile stresses and provides for a better transfer of stresses within the joint region. In addition, enlarging the bent cap also provides for a greater development length of the column longitudinal reinforcement, thereby increasing the anchorage capacity of this reinforcement. Lastly, the bent cap was enlarged to levels that can prevent reinforcement congestion within the joint region.

1.5. RESEARCH FINDINGS AND GENERAL DESIGN RECOMMENDATIONS

Preliminary analytical investigations on the selected prototype structure have shown that joint shear failure was expected below first-yielding of the column longitudinal reinforcement. This is a clear indication that retrofitting/upgrade of the prototype structure was indeed necessary to achieve a desirable seismic performance. To achieve this objective, seismic improvements were made to the prototype structure and construction and design implementation of these seismic upgrade details are discussed and presented in greater detail within this report.

As clearly shown in Sections 3.3, 4, 5.3, and 11.1, the retrofit scheme was slightly different for each of the three tested units and consisted primarily of variations in the: i) steel shell gap length, and ii) horizontal joint shear reinforcement. In Units 1 and 2 the steel shell gap length was 51mm (2in.), and for Unit 3 the gap length was reduced to 13mm (1/4in.). Regarding the horizontal joint shear reinforcement; in Unit 1, this reinforcement was installed in two separate pieces and was inserted from either side of the bent cap. In Unit 2 this reinforcement was installed as a single piece and was installed continuously through the joint region. Finally, Unit 3 was transversely post-tensioned through the existing bent cap section and the new section was built over it. A detailed explanation for the reasoning behind each of these variations is presented in Design Sections 4 and 5.1 and in the Experimental Results Sections 8, 9, and 10.

After retrofit, results from the cyclic testing of the upgraded units showed a ductile response up to the displacement ductility of 4 for the three units without significant decreases in the strength of the test units. Beyond this ductility level, the main failure mode of Unit 1 was attributed to joint shear failure due to excessive transverse dilations in the joint region. An improved joint detail was implemented for Unit 2, and the main failure mode was attributed to low cyclic fatigue of the column longitudinal reinforcement. Joint degradation was also recorded beyond the displacement ductility of 6, but this degradation was lower than the values registered for Unit 1. In Unit 3 the joint was post-tensioned in the transverse direction while also decreasing the gap length between the steel shell and the bent cap. Beyond ductility level 6 degradation of the lateral

load capacity of the column occurred due to joint shear failure. Although, strength degradation was higher than in Unit 2, this was attributed to the reduction of the steel shell gap and as a first recommendation it is suggested that the steel shell gap be within 38 to 51mm.
Test results also indicate that the computed principal tensile stresses, observed levels of joint damage, and energy dissipation capacity were different in each of the test units. Regarding Units 1 and 2, these units reached principle tensile stresses in the order of $0.42\sqrt{f_c^{'}}$ [MPa] before experiencing decreases in the lateral load capacity. In Unit 3, principle tensile stresses as high as $0.54\sqrt{f_c^{'}}$ [MPa] were registered before the unit reached its peak lateral load. While Unit 1 experienced higher levels of joint damage, strength degradation and losses in the energy dissipation capacity, Units 2 and 3 performed within a more acceptable capacity design approach. Detailed description for the design of these units and experimental results are discussed within this report. Based on these test results, the research team proposes the following:

1.5.1. Unit 1 – Permissible Design Levels

It is recommended that the details used in the construction of this test unit be limited to design conditions when the principle tensile stress limits do not exceed $\phi_f \times 0.42\sqrt{f_c^{'}}$ [MPa]. Furthermore, a limiting force reduction factor of 4 should be employed in retrofit conditions using the upgrade details discussed in this report for Unit 1.

1.5.2. Unit 2 – Permissible Design Levels

For this unit the research team proposes two limiting design values. One is for cases when the principle tensile stress limits do not exceed $\phi_f \times 0.42\sqrt{f_c^{'}}$ [MPa]. Under these conditions no limit should be imposed on the displacement ductility capacity beyond those currently stipulated for bent design. For other cases when the principle tensile stress limits exceed this value a limiting force reduction factor of 4 should be employed in the retrofit design. However, the principle tensile stress limits should not exceed $0.42\sqrt{f_c^{'}}$ [MPa] at ductility levels in excess of 4.

1.5.3. Unit 3 – Permissible Design Levels

For Unit 3 the research team proposes that the steel shell gap be within 38 to51mm. Under these conditions when the principle tensile stress limits do not exceed $\phi_f \times 0.55\sqrt{f_c^{'}}$ [MPa] no extra limitation should be imposed on the displacement ductility capacity currently stipulated for bent design. For other cases when the principle tensile stress limits exceed this value a limiting force reduction factor of 4 should be employed in the retrofit design. However, the principle tensile stress limits should not exceed $0.55\sqrt{f_c^{'}}$ [MPa] at ductility levels in excess of 4.

Based on this design philosophy it is expected that some level of strength degradation will be observed in the column when the limiting principle tensile stress limits are achieved, but by imposing a limiting value on the dependable displacement ductility capacity it is expected that this will not either cause significant decrease in the column axial capacity nor significant wide open cracks in the joint region. Furthermore, any cracks at this level will close under the gravity loads. In other conditions, for bent caps with lower principle tensile stress limits the full dependable moment capacity and displacement ductility of the column can be expected to develop. As such, for these columns higher displacement ductility levels may be accepted in design. These recommendations along with other test results are described in further detail in this report.

1.6. REPORT LAYOUT

Following an introduction to the seismic design of reinforced concrete bridge bents, and scope of the current study in this section, Section 2 describes the test matrix, the geometry of the test setup and loading protocol, the reinforcement layout for the test as-built section and the material properties. Following description of the as-built section in Section 2, Section 3 describes in detail the design considerations for the column, bent cap and joint region for Unit 1, along with the analytical predictions and evaluation for this test unit. Section 4 describes the design procedure for Unit 2, while Section 5 covers the design of Unit 3, and Section 6 describes the instrumentation layout for the three test units. In Section 7 the predicted response of the test units was developed using well established moment-rotation models and results from these analyses are discussed. In Sections 8, 9, and 10 experimental results are described in great detail for Units 1, 2, and 3, respectively. Following the description of the test results, a detailed discussion and development of an empirical model is presented at length in Section 11, which were then used to obtain the post-test lateral deformation response of the test units. Finally, this report concludes with specific recommendations for the seismic upgrade of reinforced concrete bridge bents with cast-in-place steel shell pile-shaft/columns, as presented in Section 12.

2. EXPERIMENTAL PROGRAM AND AS-BUILT SECTIONS

2.1. TEST MATRIX

In this research program three test units, designated as Units 1, 2, and 3, were tested under reversed seismic loads. The main objective of this research was to investigate different retrofit/upgrade schemes with the main goal of increasing the performance of bridge bents under seismic loads. In these units the retrofit scheme for the bent cap was identical, to the exception that within the column and joint region a few minor modifications were implemented as discussed in Sections 4, and 5. Design of Unit 2 was accomplished after testing of Unit 1; meanwhile, design of Unit 3 was accomplished after testing of Unit 2.

2.2. TEST SETUP

Laboratory conditions placed a limit on the size and setup for the test units. For safety precautions the test units were built and tested in an inverted position, as shown in Figure 2-1. The test units consisted of a column and respective bent cap arranged in a tee configuration. In the as-built conditions, the columns were 610 mm in diameter with a height from the bent cap interface to the height of load application of 2.87 m. The bent caps were 737 mm (wide) x 743 mm (depth) x 5.18m (length) with a clear span between supports of 4.57 mm.

After retrofitting, the bent cap size dimensions were increased to 1,054 mm (wide) x 895 mm (depth), resulting in a reduced column height of 2.72 m or an aspect ratio of 4.5. Design considerations for the retrofit and upgrade of the test units are presented in detail in Sections 3, 4, and 5 of this report.

As shown in Figure 2-1 for application of the simulated gravity and lateral loads, the top of the columns was terminated in the form of a cubic load stub. On the top surface of the load stub a hydraulic jack was used to apply the simulated gravity load. This axial load was then transferred to the bent cap through I-sections to simulate as closely as possible the position of the prototype bridge girders. These I-sections were positioned on the underside of the bent cap at a distance of 1.83 m, and the total axial load applied on the column was 710 kN, which corresponds to an estimated axial load ratio of 8%. On the side surface, a servo-controlled hydraulic actuator was connected to apply the simulated reversed cyclic lateral loads. The lateral loading protocol is described in further detail in Section 7.3.

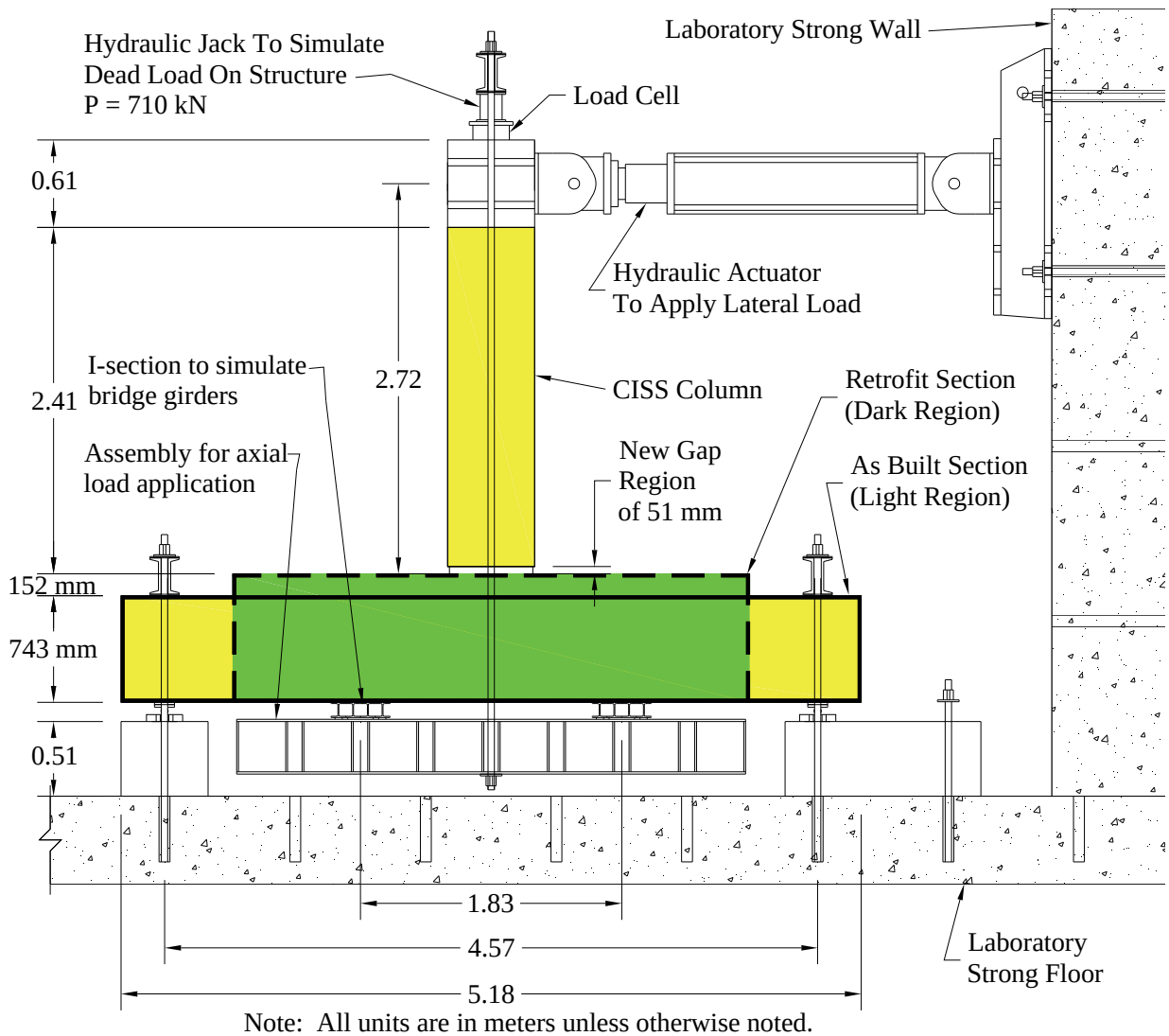

Note: All units are in meters unless otherwise noted.

Figure 2-1. Test Setup

2.3. AS-BUILT SECTIONS

The three test units were constructed in a similar manner as in field conditions. However, in order to ensure proper safety precautions during and after construction and testing, each unit was built in an inverted position. Construction of the three test units was performed in two phases. In the first phase the corresponding as-built section was built. In the second phase, the as-built segment was modified as needed, and the new retrofit section was added. The as-built section was identical in all the three test units; however, the retrofit section in all three test units was constructed with minor deviations for investigation of different retrofit details, which will be discussed in detail in Sections 3, 4, and 5. The as-built column and bent cap cross sections and reinforcement layout are shown in Figure 2-2.

As previously discussed and based on current seismic evaluation methodologies, in its as-built condition the main failure mode of these units was by flexural yielding of the bent cap longitudinal reinforcement with significant shear deformations within the joint regions. Each of these failure modes do not comply with current seismic design criteria for the response of bridge bents under seismic loads. According to these failure modes, plastic hinges form in the bent cap and joint shear failure, leading to anchorage failure of the column longitudinal reinforcement at displacement levels below yielding of the column, which are insufficient to sustain the design seismic event. In Section 3 of this report a detailed analytical investigation of the as-built system is presented in further detail along with the recommended design improvements and the proposed methodology.

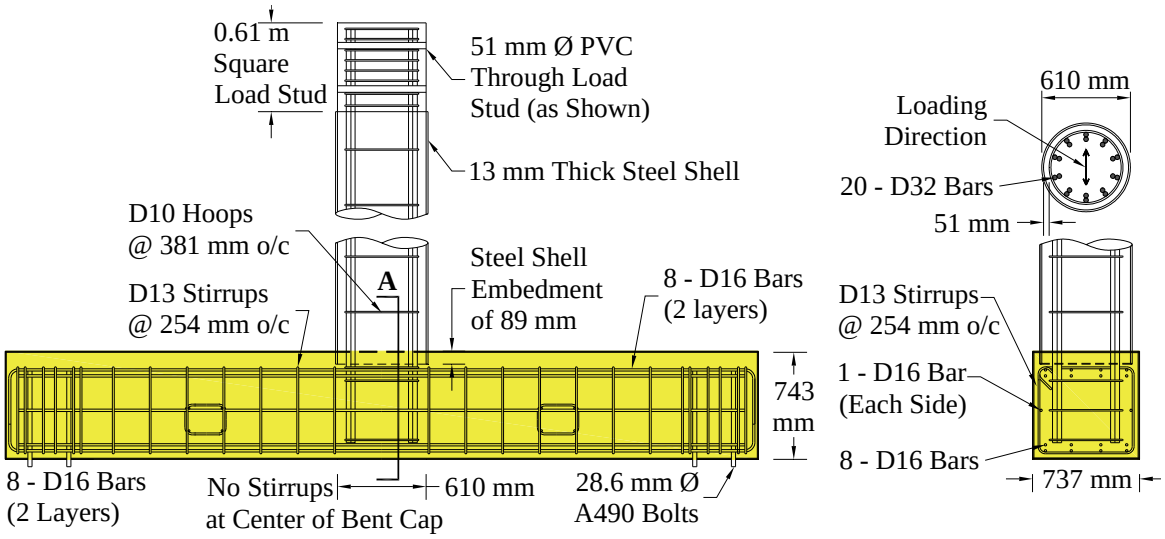

(a) Longitudinal Cross-Section **(b)** Cross-Section

Figure 2-2. As-Built Reinforcement Layout

2.3.1. Column Reinforcement

The as-built column section consisted of 20 – D32 bars for the longitudinal reinforcement that were encased in a 13 mm thick steel shell with a cover concrete of 51 mm leading to a longitudinal reinforcement ratio of 6.1%. Furthermore, the steel shell was embedded 89 mm into the bent cap and the anchorage length of the column longitudinal reinforcement was 690 mm. The transverse reinforcement in the column was only provided for construction purposes, which under typical field conditions consists of D10 hoops at 381 mm on centers. By providing this large level of column longitudinal reinforcement ratio poses severe difficulties in providing for a reliable joint shear force transfer mechanism model and subsequently design of the joint shear reinforcement.

In addition, previous research has clearly shown that by embedding the steel shell into the bent cap imposes significant damage within the seating region due to the prying action of the steel shell (Silva *et al.*, 1999). Meanwhile, one of the main advantages in using steel shells encasing reinforced concrete sections, especially in seismic regions, is the satisfactory performance of steel casings to enhance the ductility capacity of reinforced concrete sections through confinement of the concrete core.

2.3.2. Bent Cap Reinforcement

The main longitudinal reinforcement for the bent cap was the same for both the top and bottom layers and consisted of 8 – D16 bars that were placed in two layers. The clear distance between the two layers was 25.4 mm and the distance between the centroid of the top and bottom layer was nearly 198 mm, leading approximately to a reinforcement ratio of 0.40%. As discussed in Sections 3 and 5, this level of longitudinal reinforcement ratio is not appropriate to develop the yielding moment capacity necessary to ensure that the bent cap will remain essentially elastic under the input column plastic moment. Matching the as-built bent cap, no transverse reinforcement was provided within the joint region. The transverse reinforcement consisted of closed D13 stirrups spaced at 254 mm to either side of the columns (see Figure 2-2). However, it is important to emphasize that this construction detail does not comply with existing seismic design standards, and large inelastic actions are expected under reversed cyclic loading. As such, the retrofit and/or upgrade details discussed in Sections 3, 4, and 5 of this report investigate the feasibility of mediating the response of bridge bents under seismic loadings.

2.4. MATERIAL PROPERTIES

In Sections 3 and 5, analytical investigations of the as-built and new retrofit sections are presented in detail. In this section a detailed list of all the material properties used in these analyses are presented. Concrete and steel properties used in the analysis are presented in Table 2-1 through Table 2-3, respectively. Concrete cylinders (102 x 203 mm) were cast for each lift of concrete and stored next to the test unit. Rebar samples were taken from each lot of steel and tested. Reinforcing steel material properties for the as-built and retrofit sections are shown, respectively in Table 2-2 and Table 2-3. All material tests for either the concrete or reinforcing steel were done in sets of three and averaged.

Table 2-1. Concrete Material Properties

Unit No.	Test *	Column	Bent Cap	
			As-Built	Retrofit
1	28 Day (MPa)	27.1	29.0	33.8
	Day of Test (MPa)	29.3	33.8	36.9
2	28 Day (MPa)	28.0	33.5	36.6
	Day of Test (MPa)	30.8	38.3	38.9
3	28 Day (MPa)	39.3	26.2	36.6
	Day of Test (MPa)	43.7	27.1	38.8

* Specified nominal strength was 34.5 MPa

Table 2-2. Reinforcing Steel Material Properties – As Built Section

Unit No.	Bar Size	Bar Location	f_y (MPa)	f_u (MPa)	E (GPa)
1 and 2	D10	Column Hoops	310	474	215
	D13	Bent Shear	425	638	195
	D16	Bent Longitudinal	554	689	196
	D32	Column Longitudinal*	519	671	189
3	D10	Column Hoops	435	632	174
	D13	Bent Shear	503	669	192
	D16	Bent Longitudinal	476	702	195
	D32	Column Longitudinal	497	746	209

* Calculated yield strain of 2,740 $\mu\varepsilon$

Table 2-3. Reinforcing Steel Material Properties – Retrofit Section

Unit No.	Bar Size	Bar Location	f_y (MPa)	f_u (MPa)	E (GPa)
1	D13	Bent Shear	506	674	215
	D16	Bent Transverse	486	652	200
	D19	Bent Longitudinal	493	775	195
2	D13	Bent Shear	503	669	192
	D16	Bent Transverse	476	645	193
	D19	Bent Longitudinal	472	696	182
3	D13	Bent Shear	506	674	215
	D16	Bent Transverse	486	652	200
	D19	Bent Longitudinal	493	775	195
	D19*	Pre-Stress Rods	517	689	200

* Threaded Rod, Manufacturer's Specifications

3. RETROFIT AND UPGRADE DESIGN OF UNIT 1

As previously discussed, after the as-built section was constructed, modifications were implemented according to well established seismic design principles. The overall section dimensions and reinforcement layout of the modified cross section for Unit 1 are shown in Figure 3-1. In this figure the shaded region represents the as-built bent cap section. Further modifications were implemented in the design of Units 2 and 3, which are discussed in further detail in Sections 4 and 5. In this section, design of the upgrade scheme for Unit 1 is explained in further detail.

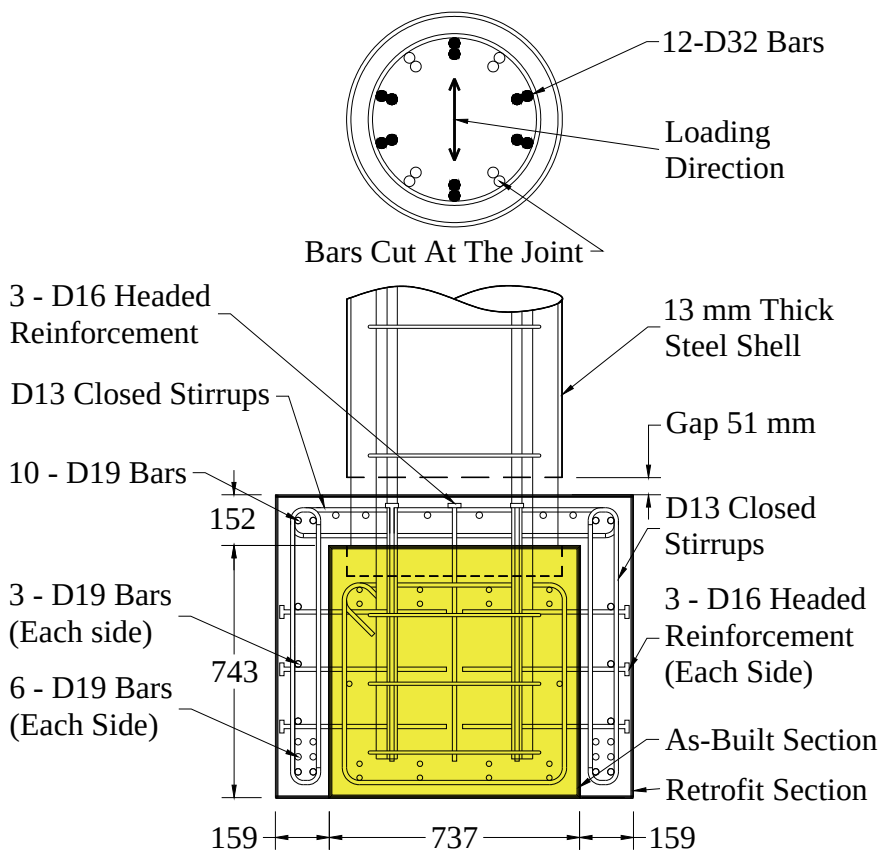

Note: All units are in mm unless otherwise noted

Figure 3-1. Unit 1 Retrofitted Cross-Section

3.1. COLUMN DESIGN CONSIDERATIONS

In the joint region the column longitudinal reinforcement was reduced to a reinforcement ratio below 4.0%, as suggested by Priestley *et al.* (1996). This reinforcement ratio has been suggested as an upper limit to avoid excessive amounts of joint shear reinforcement, which can lead to reinforcement congestion within the joint region. As such, eight of the twenty column longitudinal bars were cut, thereby reducing the reinforcement ratio from 6.1 % to 3.7%.

Current seismic design practices in the State of Alaska limits the longitudinal reinforcement ratio to 3%. As such, this design value should also be used in retrofit applications provided that by reducing the reinforcement ratio to this level does not impose significant demands on the existing columns in terms of either ductility or inelastic strength. Otherwise, it is practical to increase this limit to 4% without significant strength degradation resulting from joint damage (Priestley *et. al*, 1995, Silva *et. al*, 1999).

In order to access the column longitudinal reinforcement, the steel shell was also cut and a portion removed. After the steel shell was cut and the column reinforcement was exposed by removing the cover concrete, the designated column bars were cut immediately above the as-built bent cap section, as shown in Figure 3-2. The new column section consisted of 12 – D32 longitudinal reinforcement and a gap region of 51 mm was left between the steel shell and the new bent cap section as shown in Figure 3-1.

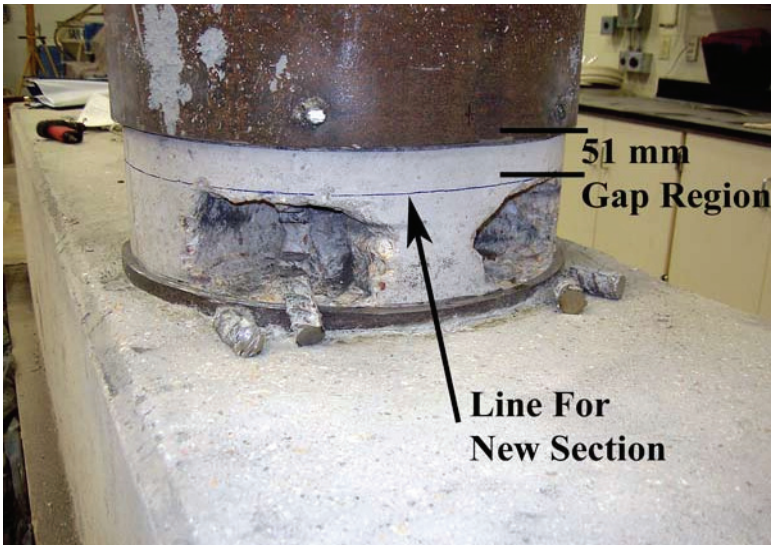

Figure 3-2. Cut Longitudinal Reinforcement

3.1.1. Moment-Curvature Analysis

A moment-curvature analysis was performed for both of these reinforcement ratios (i.e. 6.1% and 3.7%) corresponding to the as-built and the retrofitted sections. Results of this analysis are shown in Figure 3-3.

For the as-built section, the moment curvature analysis was implemented considering that in the compression block the concrete, longitudinal reinforcement and steel shell are effective in transferring forces (Silva, 1997). Meanwhile within the tension block, only the longitudinal reinforcement was considered effective in transferring forces. Furthermore, the entire concrete

compression block was assumed confined by the action provided by the steel shell based on expressions developed by Chai *et al.* (1991). Based on this analysis the ultimate moment capacity for the as-built column section was computed at 2,736 kN-m with an ultimate curvature ductility capacity of approximately 17.

For the retrofitted section and since the steel shell was cut at the bent cap interface to provide for a gap between the steel shell and the increased bent cap, the moment curvature analyses was implemented considering that in the compression block only the concrete and longitudinal reinforcement are effective in transferring forces (Silva, 1997). In this case the concrete compression block was assumed confined by an equivalent spiral confined section with a spiral size and pitch of 13x13 mm and 51 mm, respectively. These numbers correspond to the steel shell thickness and the gap at the interface with the bent cap (see Figure 3-1). Based on this analysis the ultimate moment demand for the modified column section was computed at 1,414 kN-m with an ultimate curvature ductility capacity of approximately 18.

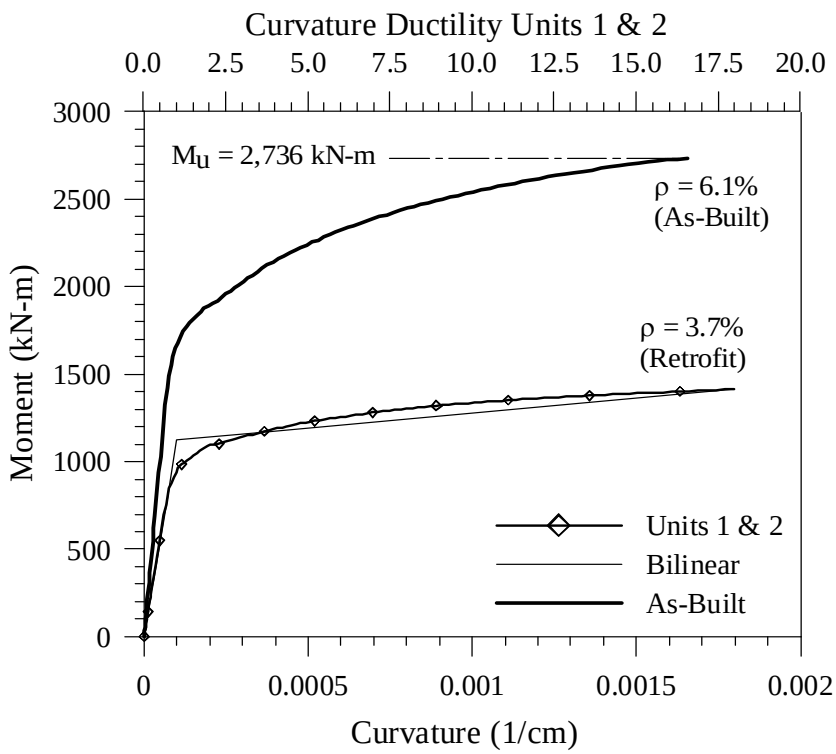

Figure 3-3. Column Moment Curvature

Referring to this figure, it is clear that the moment capacity of the retrofitted section (i.e. 3.7%) was reduced by nearly a factor of 2. Proportionally, this decrease is much less than the decrease in the reinforcement ratio or by a factor of 1.66. This can be explained because in addition to a decrease in the reinforcement ratio, the gap between the steel shell and the new bent cap section

also decreased the confinement action of the steel shell and the effects of the steel shell on the bending moment capacity of the column section. In addition, analysis for the reduced reinforcement ratio without the compression action of the steel shell shows a pronounced elasto-plastic response when compared against the original section. This is also a desirable characteristic in the seismic design of structures because it sets the limiting actions in the system at low displacement ductility levels as compared to the as-built section where the capacity of the section increases up to ultimate. This new reinforcement ratio of 3.7%, was then used as the parameter to design the additional flexural, shear, and joint shear reinforcement for the bent cap.

3.2. BENT CAP DESIGN CONSIDERATIONS

The moment demand placed on the bent cap was determined based on the ultimate moment capacity of the column, the applied axial load, and the structural layout of the test unit. Then an analysis was performed along the centerline of the bent cap at the critical locations, as shown in Figure 3-4(a). Based on the bending moment diagram depicted in Figure 3-4(b), the critical location used for design of the bent cap was established at node F.

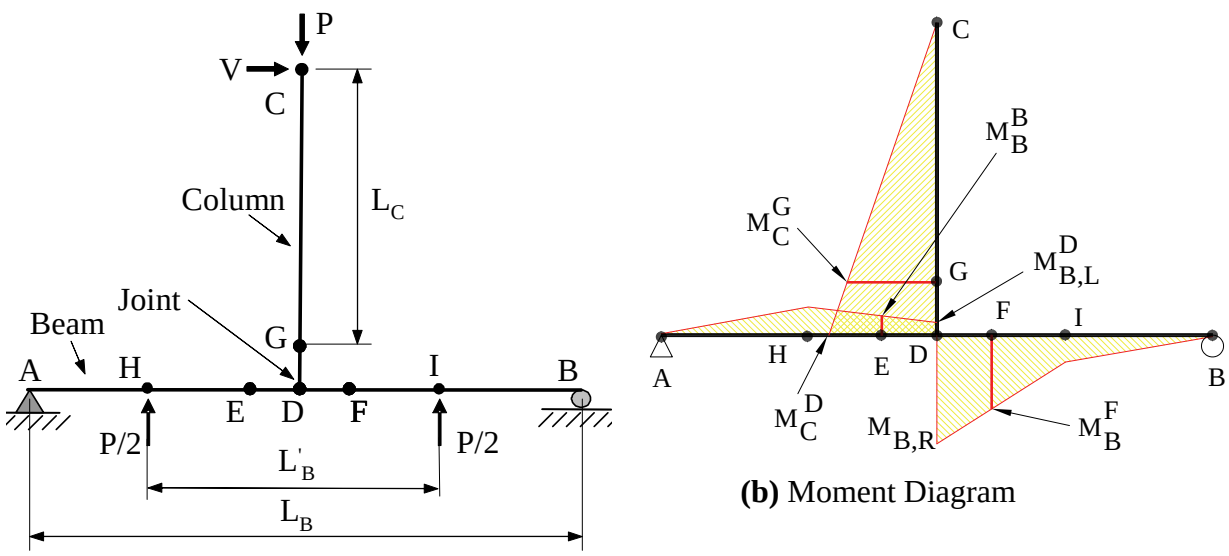

(b) Moment Diagram

(a) Model Structure

Figure 3-4. Bent Cap Moment Demand Design Considerations

The maximum moment demand placed on the bent cap was determined according to the bending moment diagram presented in Figure 3-4(b) and computed at node F based on the expression

$$M_B^F = \frac{M_C^G}{2}\left(\frac{L_C + h_b/2}{L_C}\right)\left(\frac{L_B - D_c}{L_B}\right) + P\left(\frac{L'_B - D_c}{4}\right) \qquad (3\text{-}1)$$

Referring to Figure 3-4, M_B^F is the bent cap centerline moment at the critical node F, M_C^G is the retrofitted column bending moment capacity estimated according to the moment curvature analysis presented in Figure 3-3 for the column with the reduced reinforcement ratio, ρ_l, of 3.7%, L'_B is the distance between the bridge girders, which for these test units was modeled at 1.83 m, as shown in Figure 2-1, D_c for CISS sections is the inside diameter of the steel shell or 584 mm for these test units, and P is the axial load applied to the column. Furthermore, h_b is the height of the retrofitted bent cap, L_C is the distance from the top surface of the bent cap to the centerline of the applied lateral load or the distance between nodes C and G, and L_B is the distance between the end supports or the distance between nodes A and B or 4.57 m, as shown in Figure 2-1 and Figure 3-4(a).

3.2.1. Moment-Curvature Analysis

From the moment-curvature analysis depicted in Figure 3-5, it can be shown that the as-built bent cap moment capacity was deficient compared to the moment demand obtained by using Eq. (3-1). In this analysis the column capacity was evaluated based on the section with the reduced reinforcement ratio of 3.7%. As such, additional longitudinal reinforcement was added to the bent cap to increase its yield moment capacity above the moment demand imposed on the bent cap from the column, M_c^G.

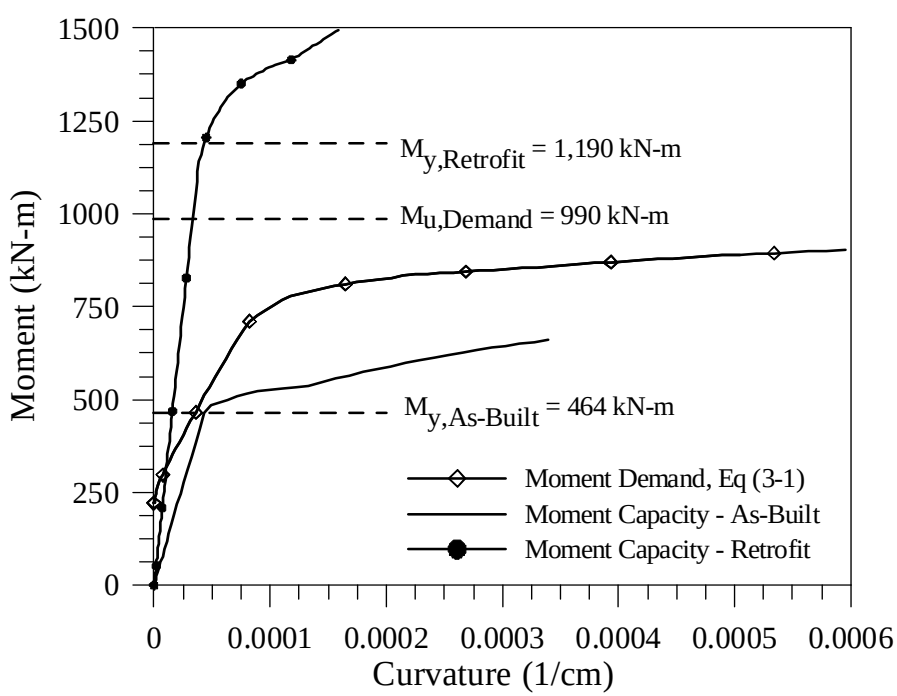

Figure 3-5. Bent Cap Moment Curvature

Referring to Figure 3-5, the maximum moment demand that can be imposed on the bent cap was nearly 990 kN-m and the computed yield moment capacity of the as-built bent cap was nearly 464 kN-m. Previous research by Silva *et al.* (1999) has suggested that the first yield moment capacity of the bent cap, $M_{y,b}$, should be at least 1,110 kN-m as given by

$$M_{y,b} = \frac{\lambda_o}{\phi_f} M_b^D = \frac{1.0}{0.9} \times 990 = 1{,}100\, kN - m \qquad (3\text{-}2)$$

Where λ_0 is the material over-strength factor equal to 1.4 when the nominal reinforcement design yield stress is used, otherwise λ_0 is 1.0, M_B^F is the bent cap centerline moment at location F given by Eq. (3-1), and ϕ_f is the flexural strength reduction factor equal to 0.9. In order to increase the yield moment capacity of the bent cap to 1,100 kN-m, additional longitudinal reinforcement in the amount of approximately 800 mm^2 top and bottom were required along with increasing the bent cap dimensions. This limit required a total of 3-D19 bars; as although, as shown in Figure 3-1, the total amount of additional reinforcement provided in the bent cap was 10-D19 on the top and 12-D19 on the bottom. These values exceed the required limit because of joint shear design considerations, which will be discussed in Section 3.3.3. However it is important to note that the moment curvature analysis presented in Figure 3-5 was evaluated for a bent cap section with the new dimensions shown in Figure 3-1 but including only these new 3-D19 bars along with the as-built reinforcement.

3.2.2. Retrofitted Bent Cap Sizing

In order to install the longitudinal reinforcement in the bent cap and to meet current seismic design standards, the minimum width of the bent cap, W_b, required was

$$W_b = 1.5 D_c = 1.5 \times 584 mm = 876\, mm \qquad (3\text{-}3)$$

However, the required width of the bent cap necessary to meet current ACI (ACI 2002) bar spacing and cover concrete specifications (see Figure 3-1) was 1,054 mm. Completing the bent cap resizing design, the height of the bent cap was determined based on limits to provide adequate anchorage length for the column longitudinal reinforcement. Using Priestley's (1996) recommendations, the development length, l_d, was computed based on the expression

$$l_d = 0.3 d_b \frac{f_{yc}}{\sqrt{f'_{cb}}} = 0.3 \times 32 mm \times \frac{414 MPa}{\sqrt{34.5 MPa}} \approx 677\, mm \qquad (3\text{-}4)$$

Where d_b and f_{yc} are the column longitudinal reinforcement diameter and specified design yield strength, respectively, and f'_{cb} is the bent cap specified design concrete compressive strength. Since the as-built bent cap section provided only for a development length of 629 mm, there was the need to increase the height of the bent cap. The bent cap height was increased by a length of 152 mm for a total depth of 895 mm. This new height led to a total development length for the

column longitudinal reinforcement of 790 mm, which exceeds the required anchorage length of 677 mm.

3.3. JOINT DESIGN CONSIDERATIONS

3.3.1. Joint Principle Stress Evaluation

Recent earthquakes have demonstrated the high risks associated with joint shear failure that can lead to collapse of entire bridge systems. Joint shear failure has been attributed largely to poorly detailed joints, performing as weak links in RC frames (Mazzoni and Moehle, 2001). According to the National Cooperative Highway Research Program seismic design guidelines (NCHRP, 2003) and further corroborated by experimental investigation many existing bridges are vulnerable in the connection of the columns to the bent cap under seismic loads (Priestley et al., 1995; Yashinsky and Karshenas, 2003). Although flexibility in these connections is likely under seismic actions, these connections should retain reserved strength capacity under reversal cyclic loading in order to prevent large strength decreases in the system caused by shear failure of the joint core, or, as importantly, to prevent pull-out of the column longitudinal reinforcement.

Forces acting upon a typical bridge bent tee joint are depicted in Figure 3-6. Since large shear forces develop in bridge joints, as illustrated in Figure 3-6(c), conventional design methods that are based on joint shear forces typically demand considerable amounts of joint shear reinforcement. This design approach results in steel congestion within the joint regions creating difficulties in the construction of concrete bridge joints. A procedure that is nowadays used for the design of the joints is based on strut and tie models, which will be discussed in the next section.

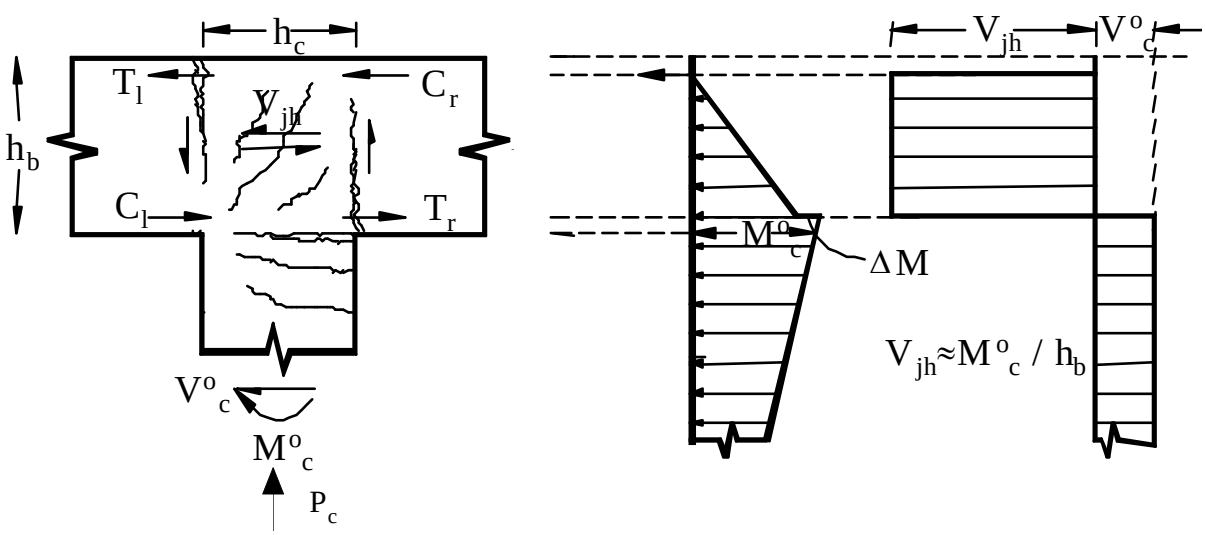

(a) Tee joint Forces (b) Joint Moments (c) Joint Shear Forces

Figure 3-6. Joint Shear Forces in Bridge Tee Joints

In this research program, design of the joint was preceded by an evaluation of the principle compressive and tensile stresses computed from a Mohr's circle of analysis in order to anticipate its seismic performance (Priestley, 1996; Silva, 1999; Sritharan, 2003). For the design of joints (Priestley, 1996; Sritharan and Ingham, 2003) the following values are limits that have been proposed to establish a criterion for the design of the joint shear reinforcement

$$p_c \leq 0.3 f_c^{'} \tag{3-5}$$

$$p_t \leq 0.25\sqrt{f_c^{'}}\,[MPa] \tag{3-6}$$

$$p_{t,m} \geq 0.42\sqrt{f_c^{'}}\,[MPa] \tag{3-7}$$

The principle compressive stress limit, p_c, stipulated by Eq. (3-5), corresponds to the value at which crushing of the diagonal compression strut through the joint region initiates. In this research program, the bent cap sizing was inspected to ensure that the computed principle compressive stresses were below this value. Based on the column moment demand and bent cap sizes the principle compressive stresses were evaluated at $0.13f^{'}_c$, which are significantly lower than the limit value of $0.30\,f^{'}_c$.

The principle tensile stress limit, p_t, stipulated by Eq. (3-6) indicates the limit at which diagonal cracking in the joint is initiated and nominal joint shear reinforcement is required. Eq. (3-7) stipulates the principle tensile stress limit, $p_{t,m}$, at which full joint shear reinforcement is required. Interpolation between nominal and full joint shear reinforcement is typically required between these two limits. Given the applied axial load in the column of 710 kN and using the retrofitted column's predicted ultimate moment capacity of 1,440 kN-m (see Figure 3-3), the joint shearing stress, v_j, and the axial stress, f_a, are

$$v_j = \frac{V_h}{b_{je}D_c} = \frac{21974kN}{0.826\,m \times 0.584\,m} = 4.09\,MPa \tag{3-8}$$

$$f_a = \frac{P}{\sqrt{2}D_c b_w} = \frac{710kN}{\sqrt{2} \times 0.584\,m \times 1.055\,m} = 0.82\,MPa \tag{3-9}$$

Where V_h is the shear force in the joint due to the applied moment, b_{je} is the width of the joint over which the shear force is applied, D_c is the inside diameter of the steel shell, and P is the axial force in the column, and V_h and b_{je} are given by

$$V_h = \frac{M_c^F}{d} \approx \frac{M_c^F}{0.8H_b} = \frac{1414\ kN-m}{0.8 \times 0.895\,m} = 1{,}974\,kN \tag{3-10}$$

$$\begin{aligned} b_{je} &= \sqrt{2}D_c \leq b_w \\ b_{je} &= \sqrt{2} \times 0.584\,m = 0.826\,m \leq 1.055\ m \end{aligned} \tag{3-11}$$

In Eq. (3-10), M_c^G is the ultimate moment capacity of the column derived from the moment curvature analysis. Using the Mohr's circle of analysis and the results from Eqs. (3-8) and (3-9), the principle stresses are then given by

$$p_c, p_t = \frac{f_a}{2} \pm \sqrt{\frac{f_a^2}{4} + v_j^2} = \frac{0.82}{2} \pm \sqrt{\frac{0.82^2}{4} + 4.09^2} = 4.5, -3.7\,(MPa) \qquad (3\text{-}12)$$

Normalizing the results derived from Eq. (3-12) in terms of the nominal design concrete compressive strength of 34.5 MPa for f'_c, yields the normalized principle compressive, p_c, and tensile stresses, p_t, of $0.13f'_c$ and $0.63\sqrt{f'_c}$ respectively. Joint principle tensile stresses, p_t, were then computed using the entire moment curvature envelope based on the retrofitted column section shown in Figure 3-3. As shown in Figure 3-7 results indicate that the principle tensile stresses, p_t, exceed the limits stipulated by Eq. (3-7) and, as such, full joint shear reinforcement was required in the joint. In the next section, the joint shear design is presented in further detail.

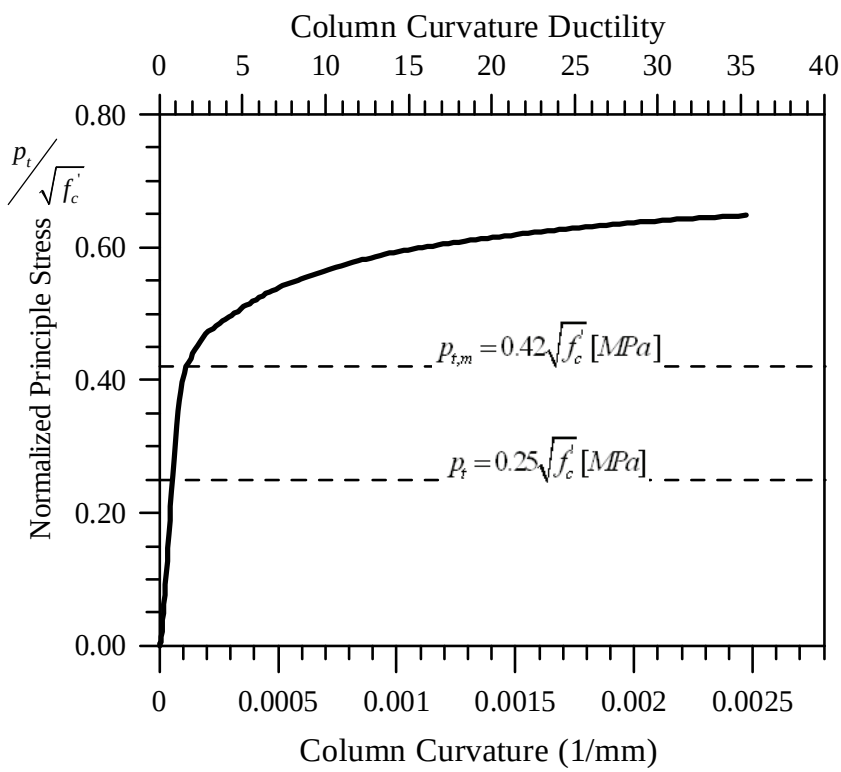

Figure 3-7. Joint Principle Tensile Stresses - Retrofitted Column

3.3.2. Joint Shear Reinforcement

Extensive information exists in the literature that clearly delineates the procedure of establishing strut and tie models for the design of joints and its benefits of transferring forces across the joint (Sritharan, 1999; Mazzoni, 2001). Sritharan (1999) has proposed a strut and tie model that has been successfully used to design the reinforcement in the joint region and was used in this

research program for the design of the joint shear reinforcement. Referring to Figure 3-8, design of the test unit upgrade scheme was based on the modified external strut force transfer model (Sritharan,1999).

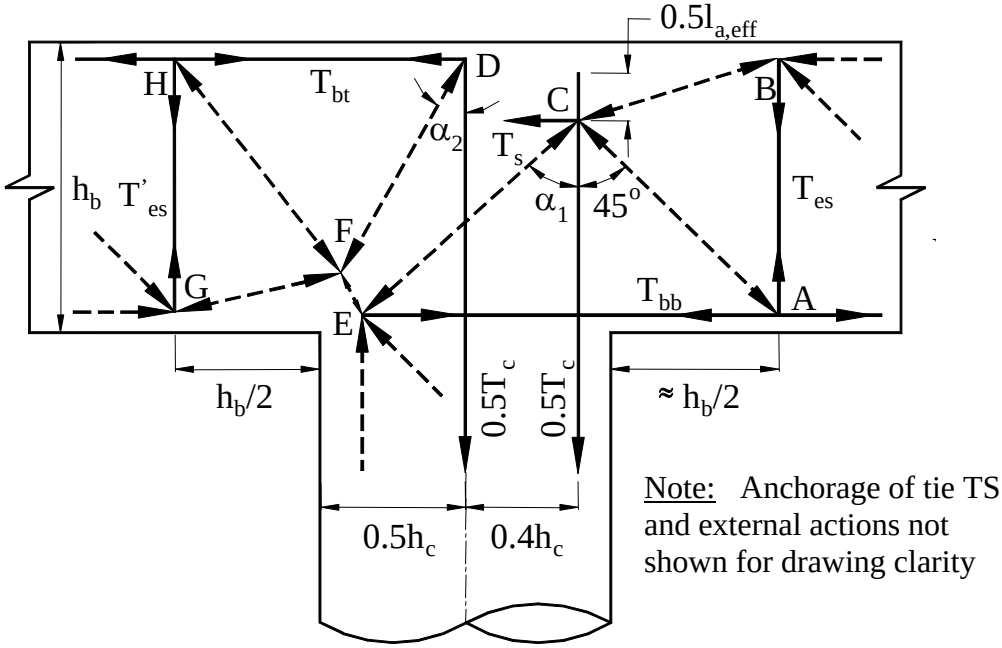

Figure 3-8. Joint Force Transfer Model (Sritharan, 1999)

This model typically requires the least amount of reinforcement when compared to other possible models. Design of joints using this approach has also been successfully used previously in the design of a three multiple column bridge bent (Silva *et al.*, 1999). Based on the strut and tie model of Figure 3-8, joint design includes (see Figure 3-9)

1. Top, $\Delta A_{tb,}$ and bottom, ΔA_{bb}, additional bent cap longitudinal reinforcement.
2. Vertical reinforcement outside and inside the joint region, A_{jv}, and
3. Horizontal joint reinforcement, A_{jh}.

Typically, the top, $\Delta A_{tb,}$ and bottom, ΔA_{bb}, longitudinal reinforcement is provided by additional reinforcement in the bent cap. Reference to top and bottom reinforcement are for a bent cap in its upright position; which in the test units these are inverted. The vertical reinforcement outside and inside the joint region, A_{jv}, is provided by closed stirrups or properly anchored headed reinforcement, and finally, the horizontal reinforcement, A_{jh}, is provided also by closed stirrups or headed reinforcement. Each of these along with the design requirements are described next.

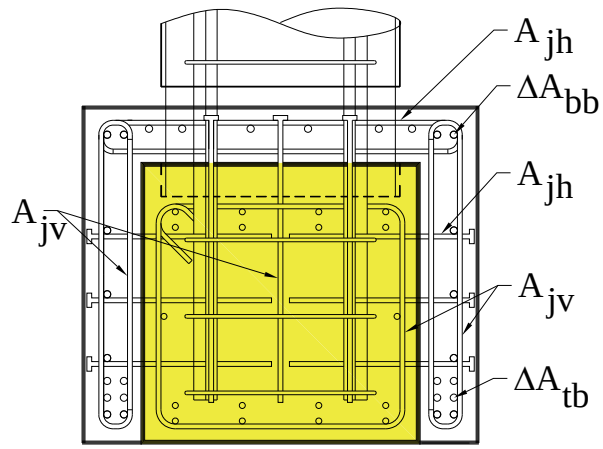

Figure 3-9. Joint Shear Reinforcements

3.3.3. Additional Longitudinal Reinforcement

Based on the strut and tie model presented in Figure 3-8 (Sritharan, 1999), additional longitudinal reinforcement is required to resist the joint shear forces and must be placed in the bent cap. As such, in addition to the required longitudinal reinforcement to satisfy flexural requirements, the area of additional top, ΔA_{tb}, and bottom, ΔA_{tb}, longitudinal reinforcement required was

$$\Delta A_{tb} = 0.17\lambda_0 A_{sc}\frac{f_{yc}}{f_{yb}} = 0.17\times 1.0\times 12\times 819.4\times\frac{519}{493} = 1{,}759\,mm^2 \qquad (3\text{-}13)$$

$$\Delta A_{bb} = 0.15\lambda_0 A_{sc}\frac{f_{yc}}{f_{yb}} = 0.15\times 1.0\times 9832.8\times\frac{519}{493} = 1{,}552\,mm^2 \qquad (3\text{-}14)$$

Where λ_0 is the material over-strength factor equal to 1.4 when the reinforcement design yield stress is used, otherwise $\lambda_0 = 1.0$, A_{sc} is the area of the column longitudinal reinforcement, f_{yc} is the column longitudinal reinforcement yield stress, and f_{yb} is the bent cap longitudinal reinforcement yield stress. It is required that this reinforcement be provided in addition to the reinforcement required to increase the yield moment capacity of the bent cap given by Eq. (3-2). Using a column longitudinal reinforcement of 12-D32 with a tested grade, f_{yc}, of 519 MPa, a tested grade for the additional bent cap longitudinal reinforcement (D19) of 493 MPa, along with using $\lambda_0 = 1.0$, the required limits for ΔA_{tb} and ΔA_{bb} were 1,759 mm^2 (7-D19) and 1,552 mm^2 (6-D19), respectively. From the bent cap longitudinal reinforcement provided, and subtracting the reinforcement required for the flexural capacity of the bent cap, 9-D19 and 10-D19 were available for ΔA_{tb} and ΔA_{bb}, respectively, which exceeds the required limits of 7 and 6, respectively.

3.3.4. Additional Internal and External Vertical Reinforcement

Based on the selected strut and tie model, the area of internal vertical joint shear reinforcement, A_{jv}^{int}, required within the joint region was (Silva 1999)

$$A_{jv}^{\text{int}} = 0.095\lambda_0 A_{sc}\frac{f_{yc}}{f_{yv}} = 0.095\times 1.0\times 9832.8\times\frac{519}{506} = 958\,mm^2 \text{ (Internal)} \qquad (3\text{-}15)$$

Where f_{yv} is the yield stress of the vertical stirrups. In addition, an area of external vertical joint shear reinforcement, A_{jv}^{ext}, was placed at a distance of h_b away from the column face (Silva 1999) given by

$$A_{jv}^{ext} = 0.125\lambda_0 A_{sc}\frac{f_{yc}}{f_{yv}} = 0.125\times 1.0\times 9832.8\times\frac{519}{506} = 1{,}261\,mm^2 \text{ (External)} \qquad (3\text{-}16)$$

In construction, D13 internal and external joint shear reinforcement was provided by closed stirrups. With a tested grade for the closed stirrups of 506 MPa the required A_{jv}^{int} was 958 mm^2 or 8 legs of D13, and A_{jv}^{ext} was 1261mm^2 or 10 legs of D13, respectively. Referring to Figure 3-1 and Figure 3-10, outside the joint region and within a distance of h_b, four D13 closed stirrups were provided on either side of the existing bent cap and within the joint three D13 stirrups were provided on either side of the existing bent cap, which exceeds the required reinforcement to satisfy A_{jv}^{int} and A_{jv}^{ext}, respectively.

3.3.5. Additional Horizontal Reinforcement

As in the previous two sections and based on the selected strut and tie model, an area of horizontal joint shear reinforcement, A_{jh}, was required within the joint region (Silva, 1999). In the design of new joints this reinforcement is typically provided in the form of spirals or hoops and installed along the anchorage length of the column longitudinal reinforcement.

In other retrofit projects this reinforcement is typically provided in the form of U-shaped hoops, but in this case the entire concrete within the joints must be removed in order to install the reinforcement (Ingham, 1995; Mazzoni and Moehle, 2001). In this research program a different detail was implemented in which the horizontal reinforcement was provided in the form of horizontal headed reinforcement. This reinforcement was embedded in pre-drilled holes; thus, avoiding the need to remove any concrete from the joints, which speeds up the construction process. Design of this headed reinforcement is discussed next.

Headed reinforcement was placed on all surfaces between the as-built and the retrofit sections. As such, the headed reinforcement extended halfway into the bent cap to form a mechanism to confine the concrete in the joint region due to insufficient detailing of the as-built section. This headed reinforcement was also effective in providing shear flow between the as-built section and the retrofit section ensuring composite action between these two sections. In addition, as shown

in Figure 3-1, horizontal D13 closed stirrups were also placed across the top of the bent cap and outside of the joint region to confine this portion of the new bent cap section.

Vertical headed reinforcement was also added on the top surface. According to this detailing the headed reinforcement extended to a depth equal to the depth of the column longitudinal reinforcement anchorage length. This vertical reinforcement was placed near the middle of the bent cap to ensure that the compression struts formed from the column longitudinal reinforcement, as shown in Figure 3-11, are balanced by the ties that develop from this vertical headed reinforcement. Priestley (1996) recommends a clamping confining pressure required to prevent excessive transverse strains in the concrete be no less than

$$f_l = 0.5\rho_s f_{sh} = \frac{0.23\lambda_0 A_{sc} f_{yc}}{D_c^{'} l_a} \qquad (3\text{-}17)$$

Where f_l is the confining pressure, ρ_s is the volumetric transverse reinforcement ratio, f_{sh} is the stress in the confining steel, l_a is the anchorage length of the column longitudinal reinforcement in the joint region ($l_a = 0.7\ h_b$), and $D_c^{'}$ is the diameter of the column concrete core. To prevent pullout of the column reinforcement, Priestley recommends limiting the strain in the concrete to 1.5 mm/m, which also leads to limiting the strain in the reinforcing hoops to 1.5 mm/m. For Grade 60 steel, this strain value is below the yield strain leading to the following force equilibrium

$$A_{st}\, 0.0015 E_s = 0.23\lambda_0 A_{sc} f_{yc} \Rightarrow A_{st} = \frac{0.23 \times 1.0 \times 9832.8 \times 519}{0.0015 \times 188{,}900} = 4{,}142\, mm^2 \qquad (3\text{-}18)$$

For this retrofit, using the tested ultimate strength of the column longitudinal reinforcement of 671 MPa and the tested modulus of elasticity of 189 GPa, leads to a required transverse reinforcement area, A_{st}, of 4,142 mm^2, which was provided by at least 20-D16. Figure 3-1 shows the final retrofit cross-section with the longitudinal reinforcement provided to increase the elastic moment capacity and additional vertical and horizontal joint shear reinforcement, where the spacing of the stirrups and headed reinforcement are shown in Figure 3-10.

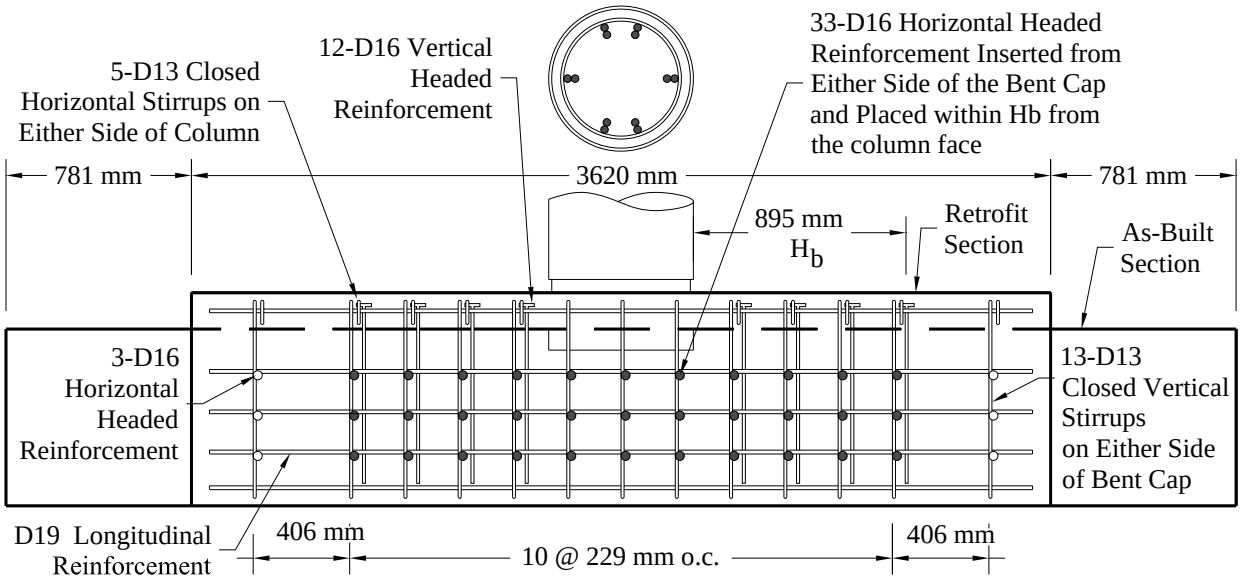

Note: As-built reinforcement not shown for drawing clarity

(a) Side View

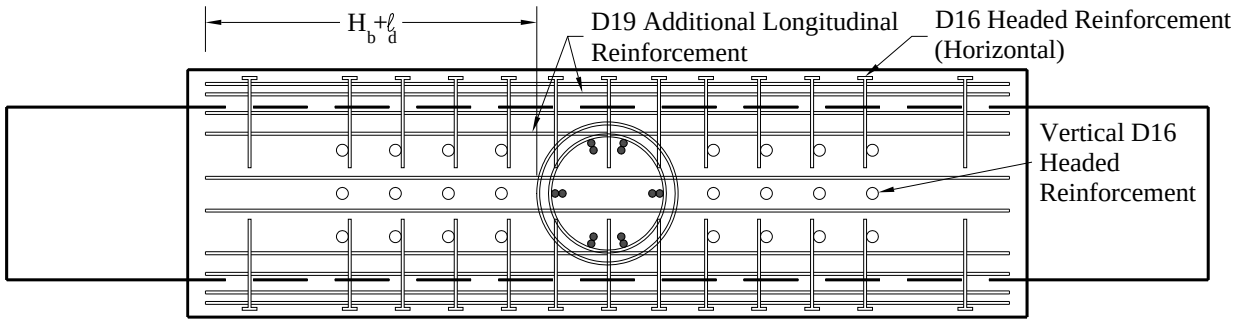

Note: Only headed and longitudinal reinforcement are shown for drawing clarity

(b) Top view

Figure 3-10. Unit 1 Bent Cap Reinforcement Layout

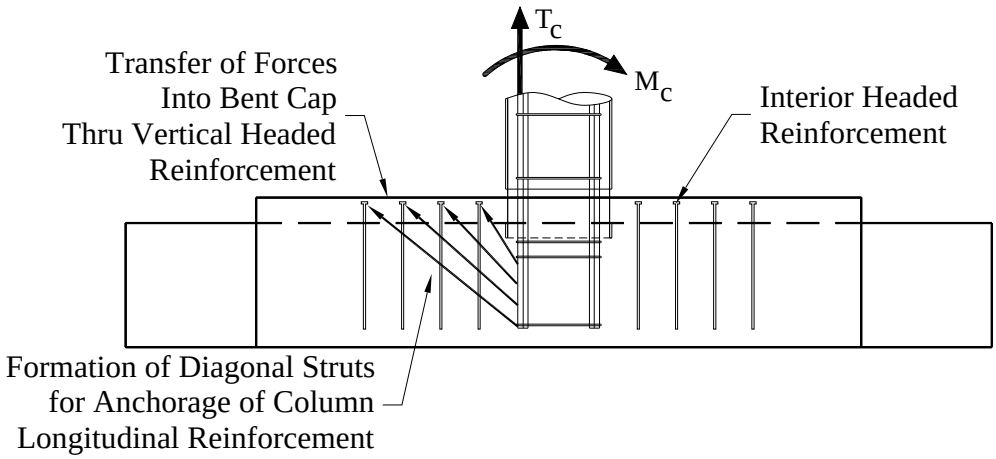

Figure 3-11. Column Strut Forces

3.4. CONSTRUCTION OF THE AS-BUILT SECTION

As previously discussed, the as-built section was identical in all the three test units. A brief description of the steps used in the construction of the as-built section is described next.

Initially, the bent cap and column reinforcement cages were assembled (see Figure 3-12 and Figure 3-13). This was followed by placing the bent cap reinforcing cage inside the form work and installation of the column reinforcement cage and steel shell casing, as shown in Figure 3-14 to Figure 3-16, respectively. With the column reinforcement cage and steel shell casing in place, the next step consisted of casting the bent cap, as shown in Figure 3-17. As a final step in the construction of the as-built sections, the load stub was assembled, followed by simultaneously casting the column and load stub (see Figure 3-18). The completed as-built section before any modifications were made is shown in Figure 3-19.

Figure 3-12. Column & Cap Reinforcing Cage

Figure 3-13. Bent Cap Reinforcing Cage

Figure 3-14. Bent Cap Inside Form Work

Figure 3-15. Colum Reinforcing Cage

Figure 3-16. Installation of Column Cage

Figure 3-17. Casting of the Bent Cap

Figure 3-18. Construction of the Load Stub

Figure 3-19. Completed As-Built Section

3.5. CONSTRUCTION OF UNIT 1 UPGRADE SECTION

As previously discussed, after the as-built section was constructed, modifications were implemented in order to install the reinforcement in the new bent cap section. As such, after the form work for the as-built section was removed (see Figure 3-19), the first step in the retrofit operation consisted of cutting the steel shell followed by cutting the column longitudinal reinforcement. This procedure is shown in Figure 3-2 and Figure 3-20. Next, the headed reinforcement was embedded in predrilled holes thru the as-built section (see Figure 3-21) by using U.S Anchor Corp.'s HS-200 epoxy. This is a rapid setting high strength structural epoxy. From an installation procedure, before embedding the headed reinforcement in the predrilled holes, these holes were first cleaned with compressed air in order to remove any loose particles

or dust. Then, the epoxy was injected into each hole until it was approximately half full. The rebar was inserted with a twisting motion to prevent any air voids for developing inside the holes. The installed headed reinforcement for the retrofit section is shown in Figure 3-21. As a procedural recommendation, the headed reinforcement should be installed before any other reinforcement is placed around the existing bent cap.

After the epoxy had cured, the retrofit longitudinal and vertical steel was tied in place, as shown in Figure 3-22 to Figure 3-24. The retrofit bent cap was then formed and the concrete was poured (see Figure 3-25). Finally, the retrofitted Unit 1 before testing is shown completed in Figure 3-26.

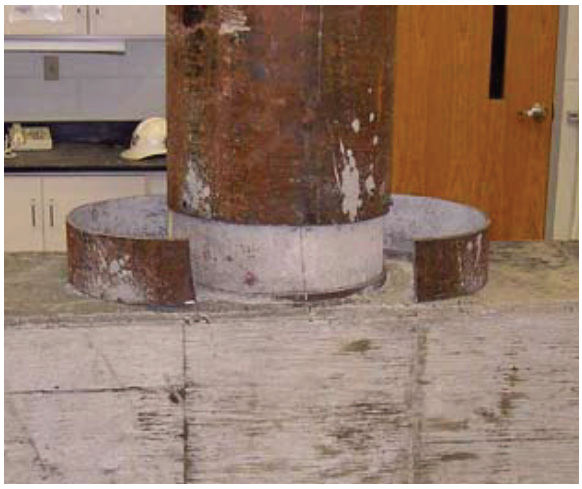

Figure 3-20. Cutting Steel Shell Casing

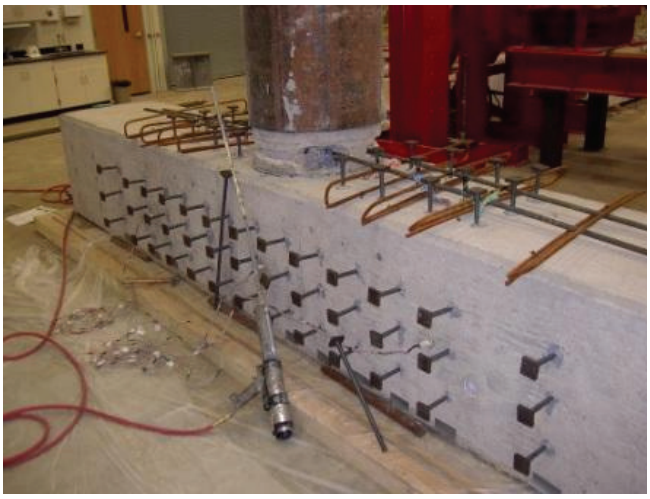

Figure 3-21. Installing Headed Reinforcing

Figure 3-22. Retrofit Section Reinforcing Cage

Figure 3-23. Joint Region Detail

Figure 3-24. Retrofit Section Reinforcing Cage

Figure 3-25. Forming Retrofit Section

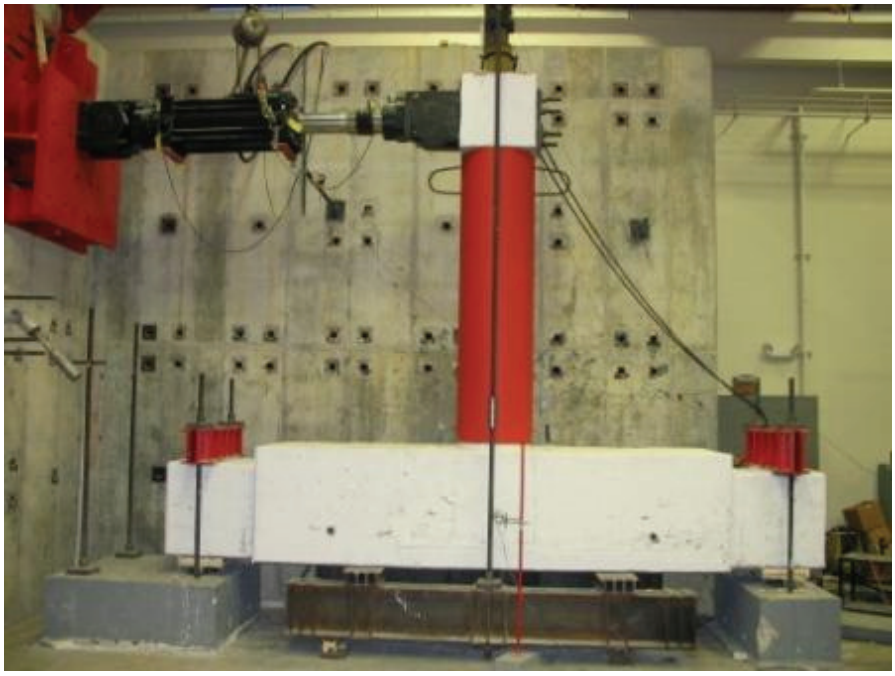

Figure 3-26. Completed Unit 1 Before Testing

4. RETROFIT AND UPGRADE DESIGN OF UNIT 2

Following testing of Unit 1 a few modifications were implemented for the construction of Unit 2. The main objective for these modifications was to increase the shear force transfer capacity through the joint and to improve the response of the test unit under cyclic loading. Description and reasoning behind these modifications are described next.

First, in Unit 1 the headed reinforcement was installed from either side of the bent cap leaving a gap between the reinforcement inside the joint region, as shown in Figure 3-1. Although this detail provided for an easier construction process, it was not sufficient in preventing excessive dilations in the transverse direction of the bent cap, as discussed in Section 8.1. As such, in Unit 2, the horizontal headed reinforcement was installed as a single continuous piece instead of two separate pieces. In order to accomplish this construction layout, a head was welded to the rebar and at the other end threads were used for the installation of the closing head. This type of headed reinforcement is commonly produced by companies specializing in the production of headed reinforcement. Figure 4-1 shows the continuous headed reinforcement running through the transverse direction of the bent cap.

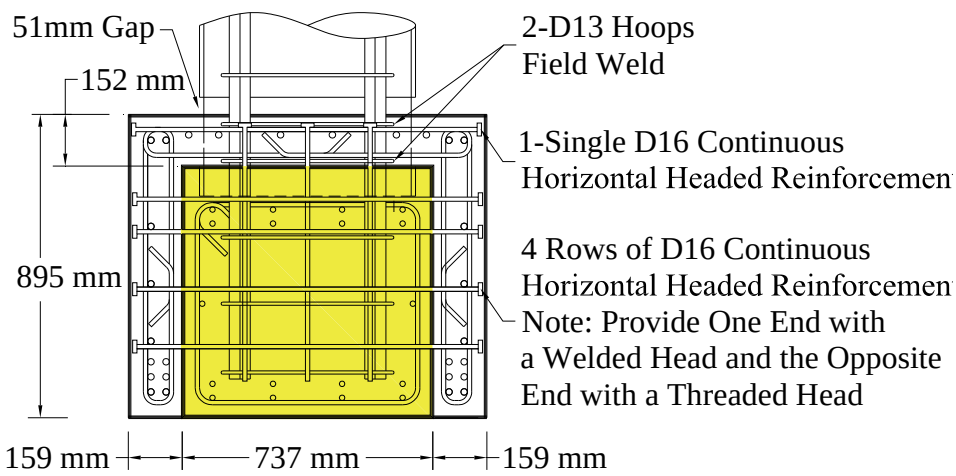

Figure 4-1. Unit 2 Retrofit Cross-Section

Second, during testing of Unit 1, it was observed that the column longitudinal reinforcement began to buckle immediately after crushing of the cover concrete. This was attributed to insufficient transverse reinforcement within the gap region. In order to improve the anti-buckling resistance for the longitudinal reinforcement, two additional D-13 field welded hoops were also provided within the steel shell gap region. This detail will be further discussed in the next section or Section 4.1.

Finally, during the final stages of testing of Unit 1 wide open cracks were observed in the bent cap near the column interface. As such, the following modifications were implemented as shown in Figure 4-2: (1) the D16 horizontal headed reinforcement within the joint region were placed at a much closer pattern near the joint, (2) an additional headed rebar was installed through the gap region and within the column longitudinal reinforcement, and (3) an additional D13 closed stirrup was provided on either side of the bent cap. The retrofit cross-section and reinforcing layout for the second unit are shown in Figure 4-1 and Figure 4-2.

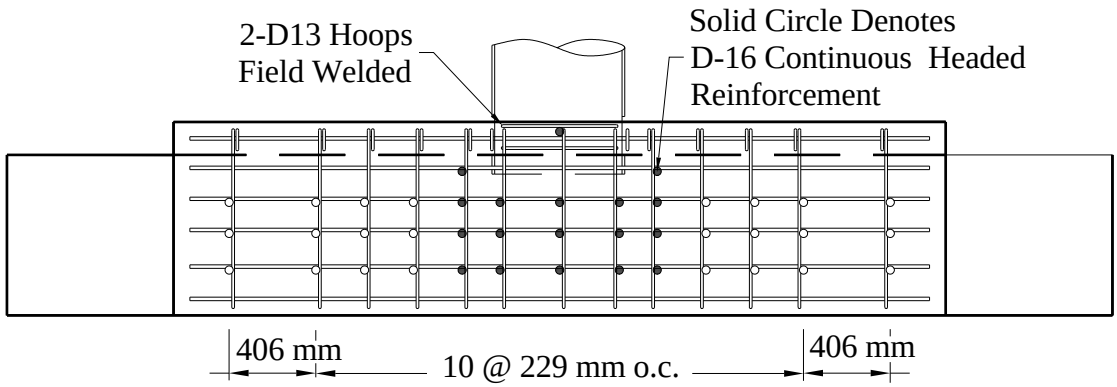

Figure 4-2. Unit 2 Retrofit Reinforcement Layout

4.1. CONSTRUCTION OF UNIT 2 UPGRADE SECTION

As in Unit 1, after the as-built section was constructed, modifications were implemented in order to install the new reinforcement. As before, the first step in the retrofit operation consisted of removing a protion of the steel shell followed by cutting the column longitudinal reinforcement (see Figure 4-3). Unlike Unit 1, in Unit 2, the next step consisted of removing first all of the concrete cover surrounding the column longitudinal reinforcement, as shown in Figure 4-3 and Figure 4-4.

Next, the continuous horizontal and vertical headed reinforcement was embedded in predrilled holes but in this unit the holes were predrilled through the entire width of the as-built section. After installation of the headed reinforcement, the closing head was threaded followed by installation of the remaining reinforcement, as shown in Figure 4-5 and Figure 4-6. Next, installation of the headed reinforcement and completion of the construction of the upgrade section followed the same procedures outlined in Section 3.5.

Figure 4-3. Detail at Bent Cap Interface

Figure 4-4. Detail at Bent Cap Interface

Figure 4-5. Bent Cap Retrofit Section

Figure 4-6. Bent Cap Retrofit Section

5. RETROFIT AND UPGRADE DESIGN OF UNIT 3

5.1. INTRODUCTION

The upgrade scheme was slightly modified for the third unit, and these modifications are described in this section. As discussed in Section 9.1, the continuous reinforcement though the joint region was adequate in preventing dilation of the bent cap in the transverse direction. In order to further enhance the strength capacity of the joint, a different detail was investigated, which consisted of replacing the horizontal headed reinforcement with post-tensioned rods. As previously stated, transverse prestressing is a good alternative for increasing the strength of the joint, because it actively confines the concrete and induces an increase in the bond strength provided to the column longitudinal reinforcement. In addition, the steel shell gap was reduced from 52mm to 13mm, to further reduce the propensity for buckling of the column longitudinal reinforcement. The retrofitted cross-section and the reinforcing layout for Unit 3 are shown in Figure 5-1 and Figure 5-2.

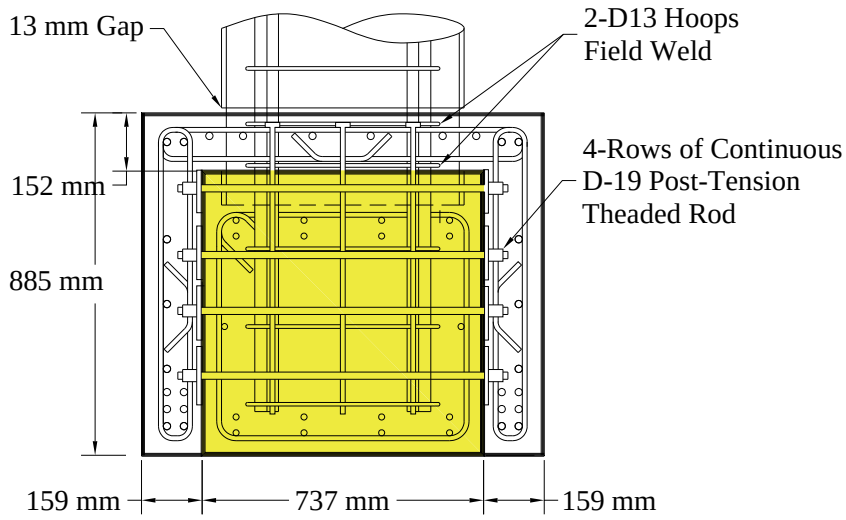

Figure 5-1. Unit 3 Retrofit Cross-Section

Since transverse stresses are only effective in improving the joint shear capacity and the bond strength of the column longitudinal reinforcement, the post-tensioned rods were only used within the joint region, as shown in Figure 5-3. Since placing the pre-stressing rods for the entire length of the bent cap would not lead to an increase in seismic performance, prestressing rods were only provided within the joint region further reducing construction time and costs. Each pre-stressing rod was 19 mm in diameter with a yield strength of 517 MPa according to the manufacturer. The pre-stressing rods were stressed to 60% of f_y by tightening a nut at each end of the rod, and the stress on the rods was measured by a calibrated torque wrench. It is important to note that the typical tensile strength of high-strength post-tensioning rods is 1,034MPA. Since in this research the rods provided by the manufacturer had a tensile strength of 517MPA, this only translated in a

higher pre-stress value applied to the rods but not a reduction in the performance of the joint. The stressed joint for Unit 3 is shown in Figure 5-3.

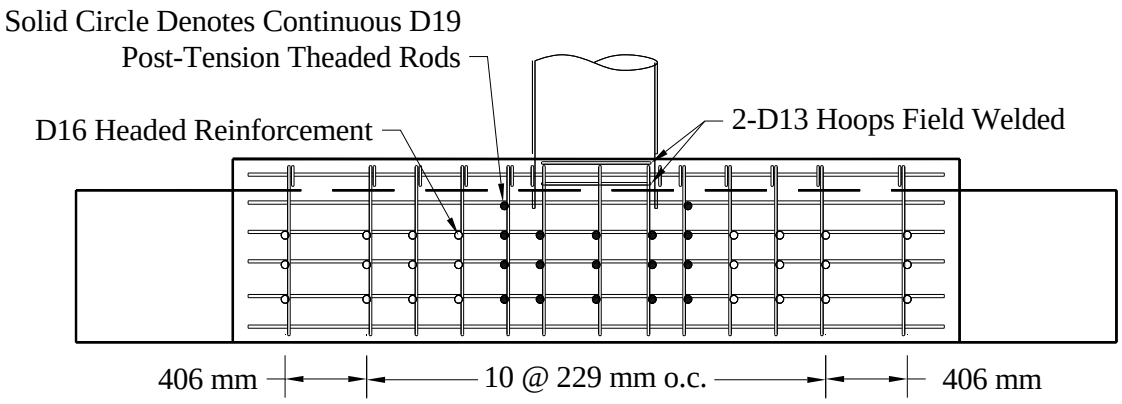

Figure 5-2. Unit 3 Retrofit Reinforcement Layout

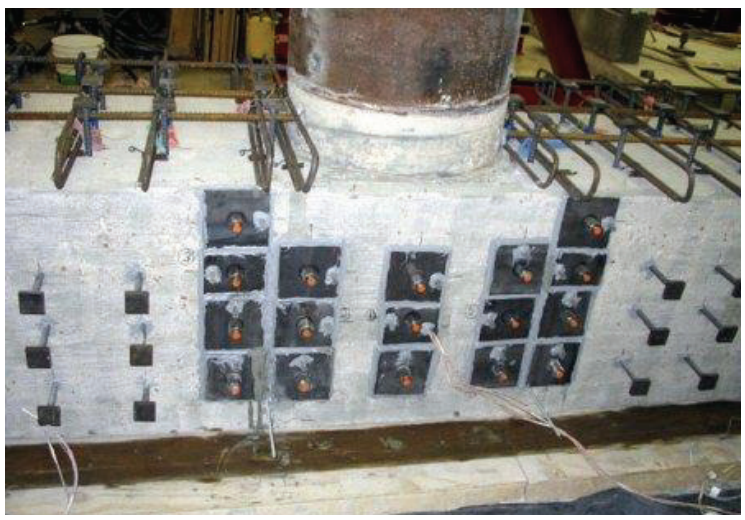

Figure 5-3. Unit 3 Pre-stressed Joint

5.2. MOMENT-CURVATURE ANALYSIS

Since the steel shell gap in the column of Unit 2 was identical to Unit 1 the moment curvature analysis for these two units' column was identical. In Unit 3 the steel shell gap was reduced from 51mm to 13mm and, as a result, a new moment-curvature analysis was performed for the column of the third unit. Results of this analysis are shown in Figure 5-4. In this unit, the column moment curvature analysis was nearly the same as in the previous two units to the exception that the concrete compression block was assumed confined by an equivalent spiral size and pitch of 13x13 mm and 13 mm, respectively. The moment curvature analysis for the test units are shown in Figure 5-4 and relevant data is outlined in Table 5-1. In Unit 3 the ultimate moment demand

for the modified column section was computed at 1,588 kN-m with an ultimate curvature ductility capacity of approximately 18, which was the same for the previous two units.

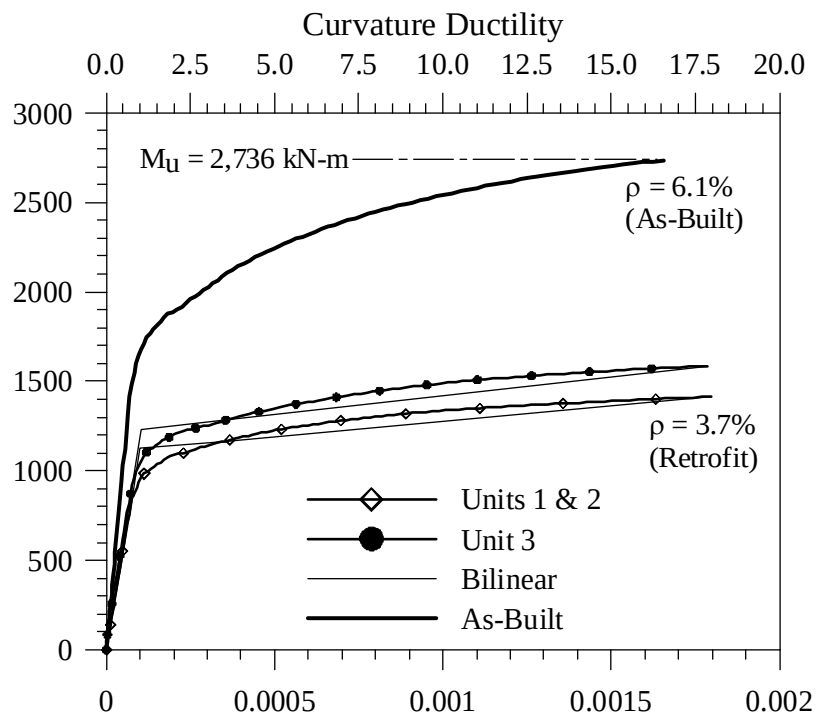

Figure 5-4. Unit 3 Moment-Curvature

Table 5-1. Bilinear Moment Curvature

Unit No.	First yield		Theoretical Yield		Ideal		Ultimate		
	ϕ'_Y (1/m)	M'_Y (kN-m)	ϕ_Y (mm)	M_Y (kN-m)	ϕ_I (1/m)	M_I (kN-m)	ϕ_U (1/m)	M_U (kN-m)	μ_ϕ
1 & 2	0.00007	790	0.00010	1125	0.00035	1168	0.00180	1,414	18
3	0.00008	903	0.00010	1232	0.00038	1290	0.00179	1,588	

5.3. JOINT PRINCIPLE STRESS DETERMINATION

Due to the additional pre-stress in the transverse direction, a principle stress analysis was implemented for a 3-dimensional stress cube, as shown in Figure 5-5. For a 3-D analysis the principle stresses are obtained by solving the determinant of the following stress matrix in terms of the scalar λ

$$\begin{vmatrix} \sigma_{xx} - \lambda & \tau_{xy} & \tau_{xz} \\ \tau_{yx} & \sigma_{yy} - \lambda & \tau_{yz} \\ \tau_{zx} & \tau_{zy} & \sigma_{zz} - \lambda \end{vmatrix} = 0 \qquad (5\text{-}1)$$

Where λ are the three principle stresses, σ_{xx} is zero because there is no pre-stressing in the longitudinal direction of the bent cap, σ_{yy} is f_a and is the stress due to the axial load, σ_{zz} is the stress due to the transverse stress force, τ_{xy} is equal to v_j and is the shear stress due to the applied column moment, and τ_{xz} and τ_{zy} are assumed zero or negligible due to the unidirectional applied column bending moment and that the applied pre-stress forces do not result in any significant shear stresses in these planes.

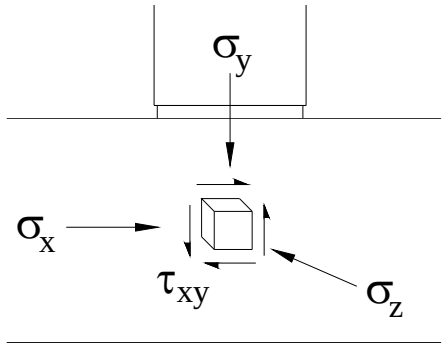

Figure 5-5. 3-D Stress Cube

As such, the determinant of Eq. (5-1) reverts to Eq. (3-12), which indicates that pre-stressing in the transverse direction has no effect on the joint principle compressive, p_c, and tensile, p_t, stresses in the longitudinal direction but only increases the joint principle compression stress in the transverse direction. As previously stated in Section 1.3 and unlike longitudinal prestressing, transverse prestressing does not lead to a reduction in the principle tensile stresses nor joint cracking, nor does it increases the bent cap shear and flexural strength. However, transverse prestressing merits by increasing the strength of the joint to resist the input tensile stresses. For example, test results clear suggest that the strength of the joint was increased from $0.42\sqrt{f_c^{'}}$ [MPa] to [$0.54\sqrt{f_c^{'}}$ [MPa], representing an increase over 25%. This has significant implications in retrofit applications; because, it significantly reduces construction costs and time.

As before, with an applied axial load on the column equal to 710 kN and referring to Eq. (3-9) the axial stress, f_a, is 0.82 MPa. Given the column's predicted ultimate moment capacity of 1,588 kN-m (see Table 5-1), the shear force in the joint, V_h, is

$$V_h = \frac{M_c^F}{d} \approx \frac{M_c^F}{0.8h_b} = \frac{1588\ kN-m}{0.8\times 0.895\,m} = 2{,}218\,kN \qquad (5\text{-}2)$$

Referring to Section 3.3, the joint shearing stress, v_j, is then

$$v_j = \frac{V_h}{b_{je}D_c} = \frac{2218\,kN}{0.826\,m\times 0.584\,m} = 4.60\,MPa \qquad (5\text{-}3)$$

As a last step, using the results from Eqs. (3-9) and (5-3), the principle stresses are then given by

$$p_c, p_t = \frac{f_a}{2} \pm \sqrt{\frac{f_a^2}{4} + v_j^2} = \frac{0.82}{2} \pm \sqrt{\frac{0.82^2}{4} + 4.60^2} = 5.02, -4.21(MPa) \qquad (5\text{-}4)$$

As before, normalizing the results of Eq. (5-4) in terms of the specified nominal concrete strength, f'_c, of 34.5 MPa yields the normalized principle compressive, p_c, and tensile stresses, p_t, of $0.15f'_c$ and $0.72\sqrt{f'_c}$. Joint principle tensile stresses, p_t, were computed for the entire moment curvature envelope shown in Figure 5-4 and using the retrofitted column sections. The principle tensile stresses were then normalized and plotted versus the curvature of the column as shown in Figure 5-6.

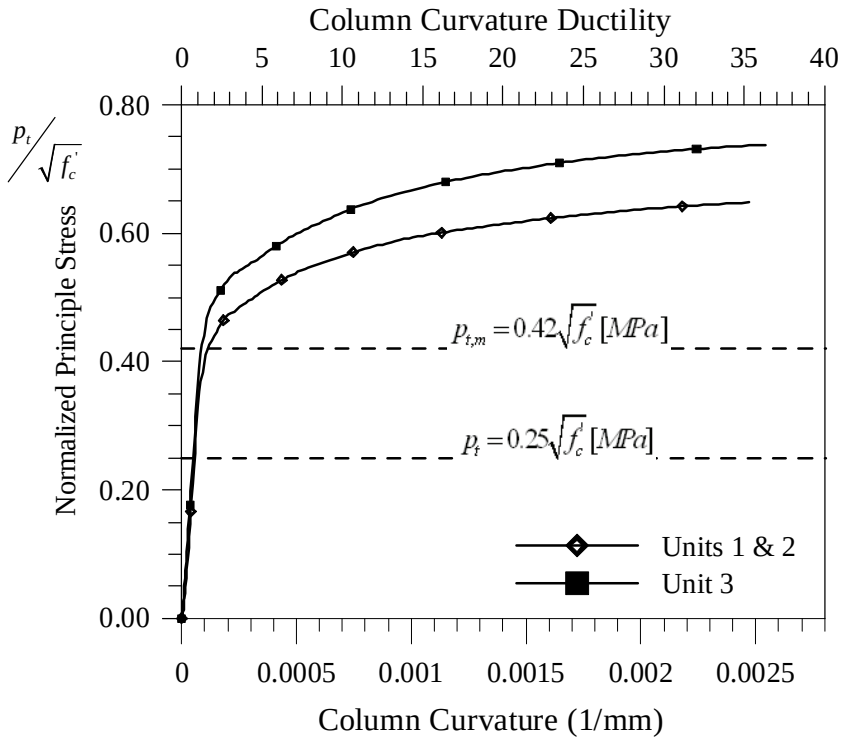

Figure 5-6. Unit 3 Principle Stresses

Again the principle tensile stresses, p_t, exceeded the limits stipulated by Eq. (3-7) and full joint shear reinforcement was required for design of the joint. It is important to note that although pre-stressing in the transverse direction does not lead to a reduction in the principle tensile stresses or demand in the joint, these stresses increase the bond strength of the column longitudinal reinforcement and subsequently the joint shear capacity. This suggests that a different moment rotation capacity should be proposed for units retrofitted according to the design details illustrated in this section.

5.4. CONSTRUCTION OF UNIT 3 UPGRADE SECTION

As before, the first step in the construction of the upgrade section consisted of cutting a portion of the steel shell and the designated column longitudinal bars, which was similar to the procedure shown in Figure 3-20. As specified, in this unit, the gap region was reduced to 13 mm.

As in Unit 2, the horizontal and vertical headed reinforcement were embedded in predrilled holes, as shown in Figure 5-7 and Figure 5-8. Installation of the headed reinforcement followed the same procedure outlined in Section 3.5. After installation of the headed reinforcement the pre-stress rods were installed and stressed by tightening a nut at each end of the rods. The stressed joint is shown in Figure 5-3, and the retrofit longitudinal and vertical steel was tied in place similar to Figure 3-22 and Figure 3-24, followed by forming and casting the upgrade section (see Figure 5-9). The completed Unit 3 during testing is shown in Figure 5-10.

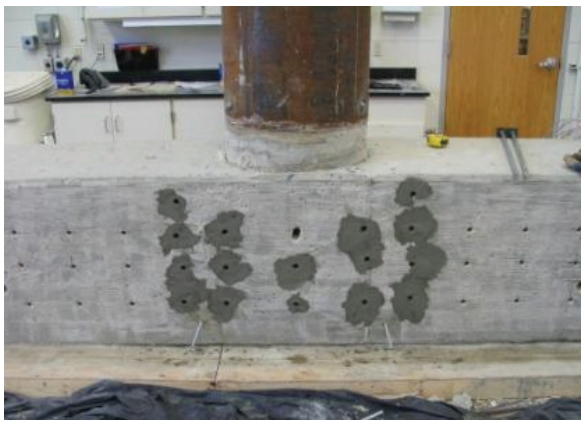

Figure 5-7. Pre-Drilled Holes

Figure 5-8. Installed Headed Reinforcement

Figure 5-9. Unit Before Casting of Upgrade Section

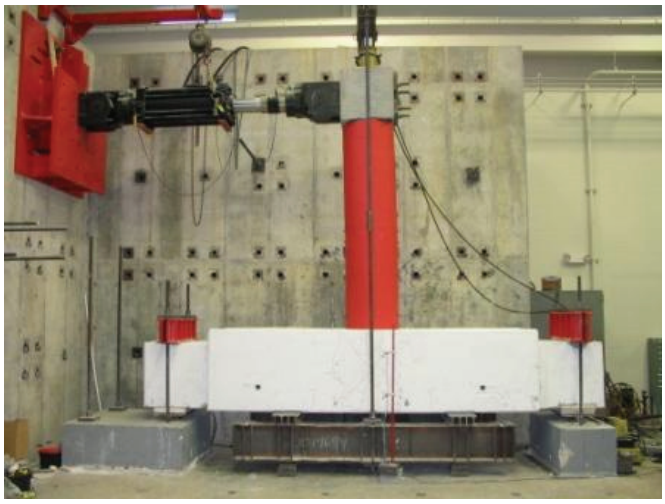

Figure 5-10. Completed Test Unit

6. INSTRUMENTATION LAYOUT

For each test unit, strain gauges were placed on the reinforcing steel, linear variable differential transducers (LVDT's) were affixed to the joint, and load cells were placed to measure the axial force in the column. The actuator used had an internal LVDT and load cell to measure the lateral displacement and force applied to the load stub atop the column. All instruments were connected to a data acquisition system that took data at preset time intervals. A detailed description of the instrumentation used is presented in the next three sections.

6.1. STRAIN GAUGES

Strain gauges were placed on the reinforcing steel on the as-built and the retrofit section, as shown in Figure 6-1 through Figure 6-7. Instrumentation of these reinforcement consisted of electric resistance strain gages produced by Tokyo Sokki Kenkyujo Co., Ltd. These strain gauges have a gage length of 5mm and a gage resistance of 120±0.3Ω.

6.1.1. Column Section

A description of the strain gauges mounted on the column reinforcement is discussed in this section. As shown in Figure 6-1, a total of 12 gauges were applied on the column longitudinal reinforcement, and 6 and 8 strain gauges were positioned vertically and horizontally in the steel shells, respectively.

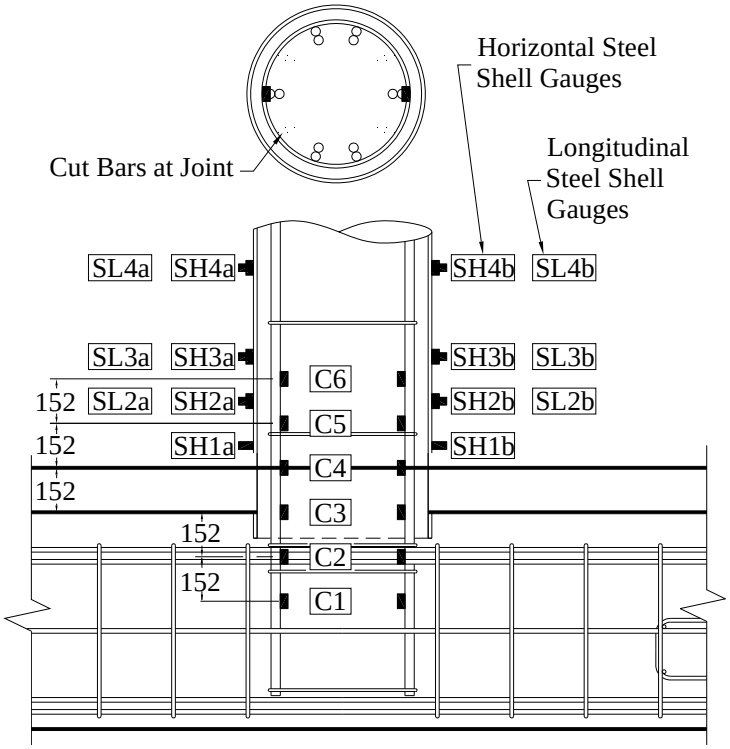

Figure 6-1. Column Reinforcement and Steel Shell Strain Gauges

6.1.2. Bent Cap As-Built Section

A description of the strain gages mounted on the bent cap as-built section reinforcement is discussed in this section. As shown in Figure 6-2, a total of 16 gauges were applied on the as-built section longitudinal reinforcement, and as shown in Figure 6-3, 6 strain gauges were positioned on the as-built section stirrups.

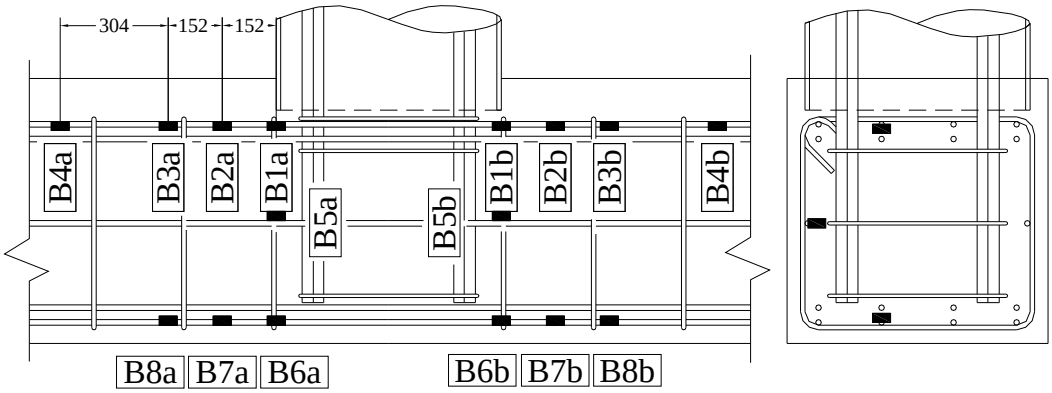

Figure 6-2. As-Built Bent Cap Strain Gauges

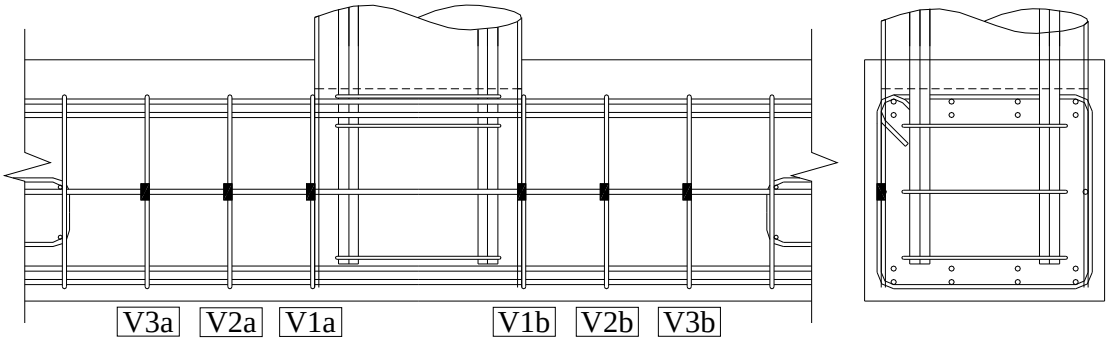

Figure 6-3. As-Built Bent Cap Shear Strain Gauges

6.1.3. Bent Cap Retrofit Section

A description of the strain gauges mounted on the bent cap upgrade section reinforcement is discussed in this section. As shown in Figure 6-4, a total of 16 gauges were also applied on the new section longitudinal reinforcement, and as shown in Figure 6-5, Figure 6-6, and Figure 6-7 15 strain gauges were positioned on the as-built section stirrups, 16 strain gauges were positioned on the horizontal headed reinforcement and 6 strain gauges were positioned on the vertical headed reinforcement.

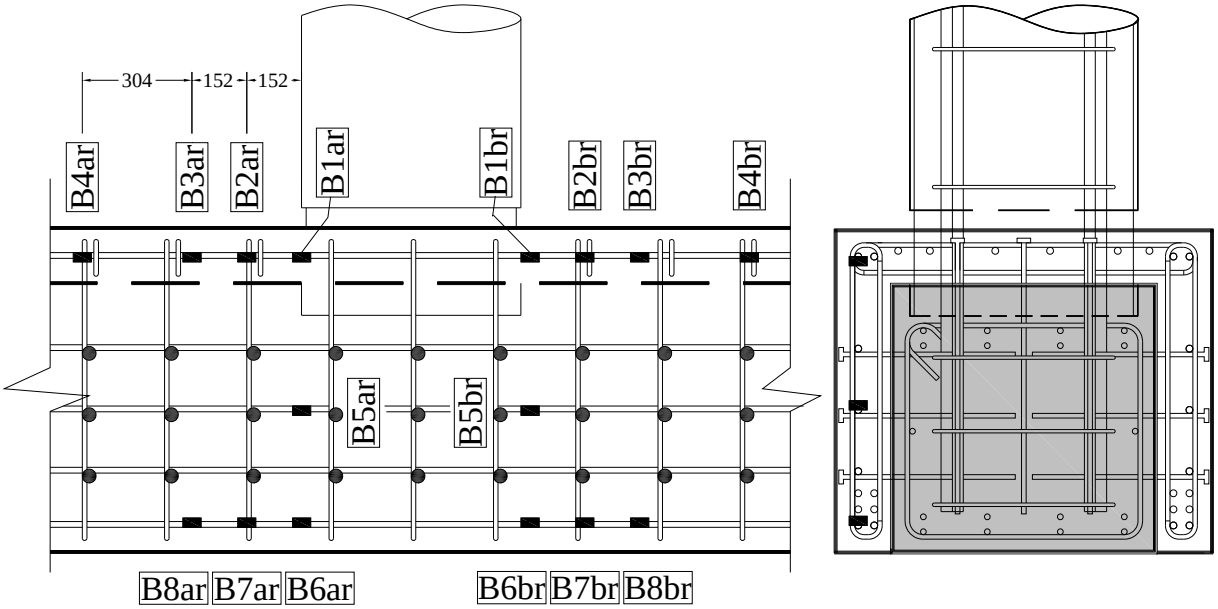

Figure 6-4. Retrofit Bent Cap Strain Gauges

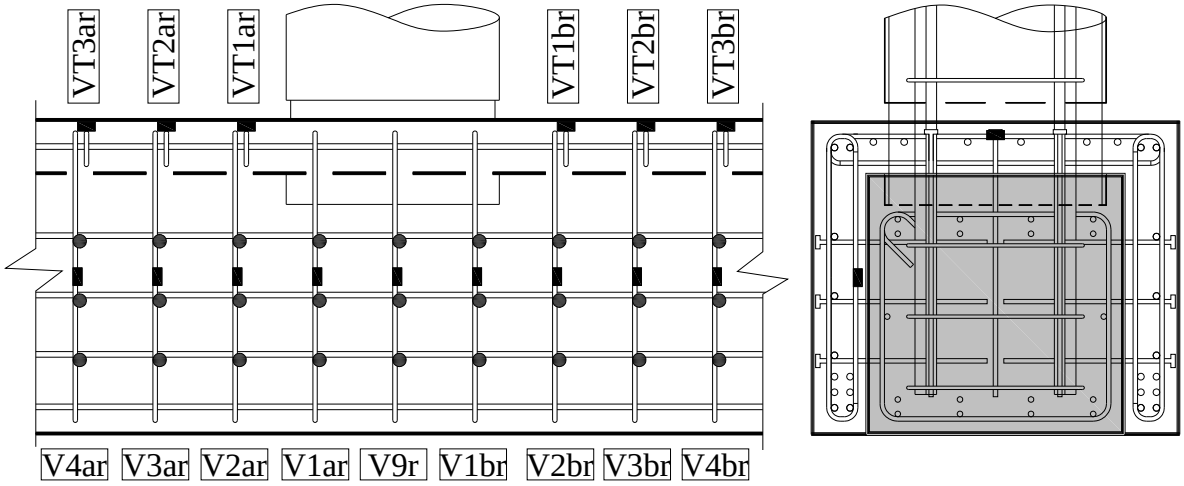

Figure 6-5. Retrofit Bent Cap Shear Strain Gauges

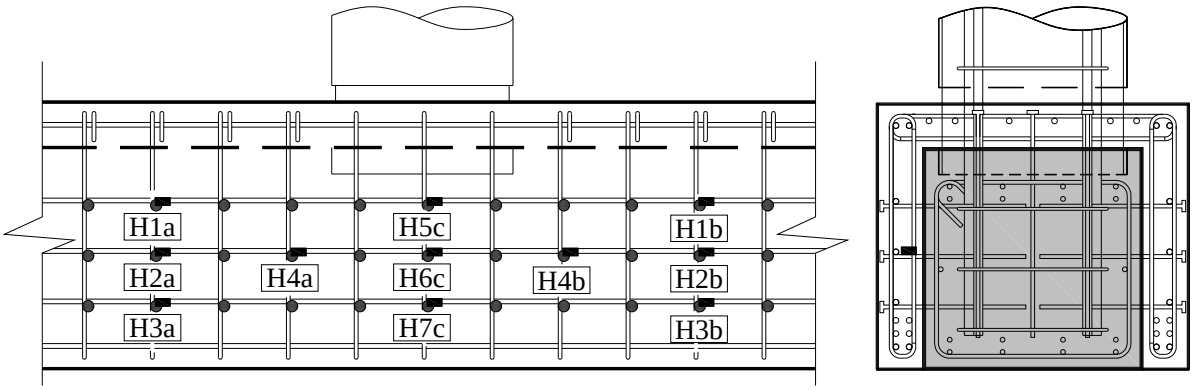

Figure 6-6. Retrofit Transverse Headed Reinforcement Strain Gauges

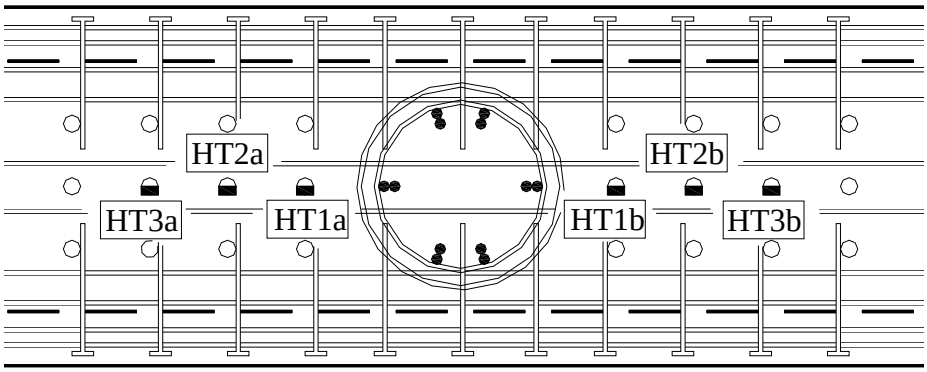

Figure 6-7. Retrofit Vertical Headed Reinforcement Strain Gauges

6.2. LOAD CELLS

Two load cells were placed on top of the reaction beam, which was used to transfer the applied axial load to the column, as shown in Figure 6-8. The axial load was held constant by a hydraulic pump with a control valve applying a constant pressure to the hydraulic jack placed on top of the column.

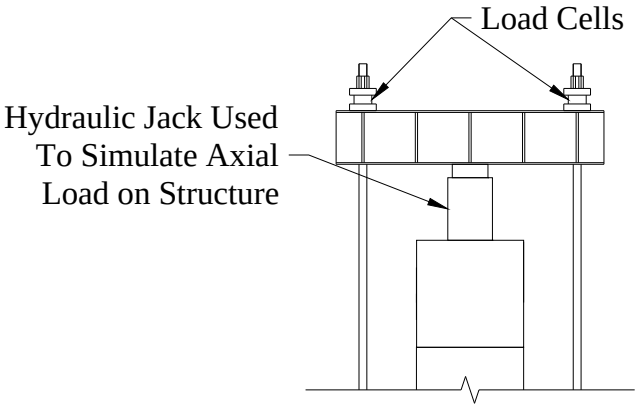

Figure 6-8. Load Cells for Axial Load

6.3. LVDT's

A total of 14 LVDT's were placed across the joint to measure the joint shear as shown in Figure 6-9. The deformations from LVDT's JHt, JHb, JVb, JVa, J1, and J2 were used to calculate the joint shear deformations and strains according to Figure 6-10.

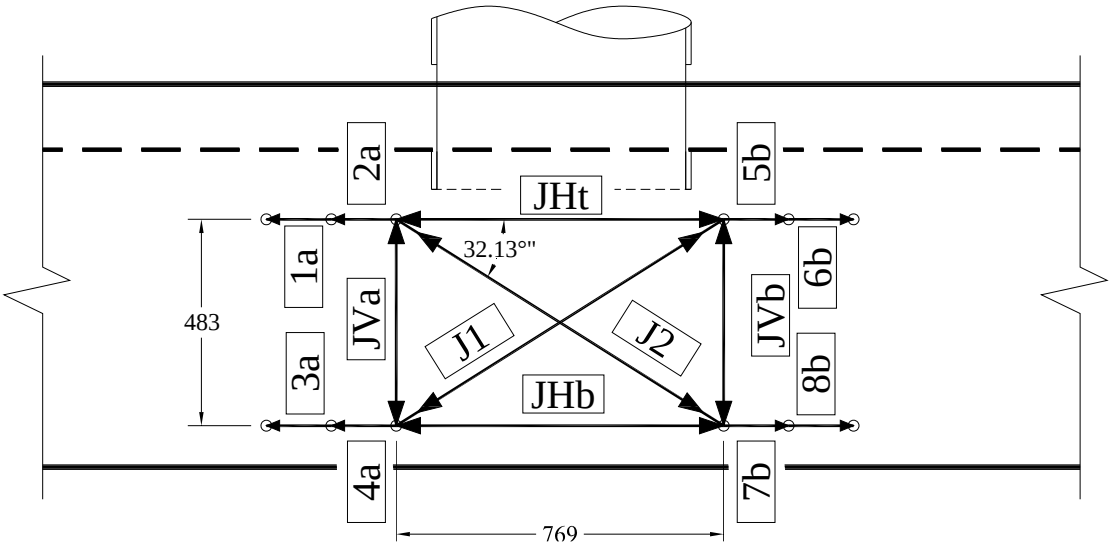

(a) Schematic

(b) Test Setup Installation

Figure 6-9. Joint LVDT's

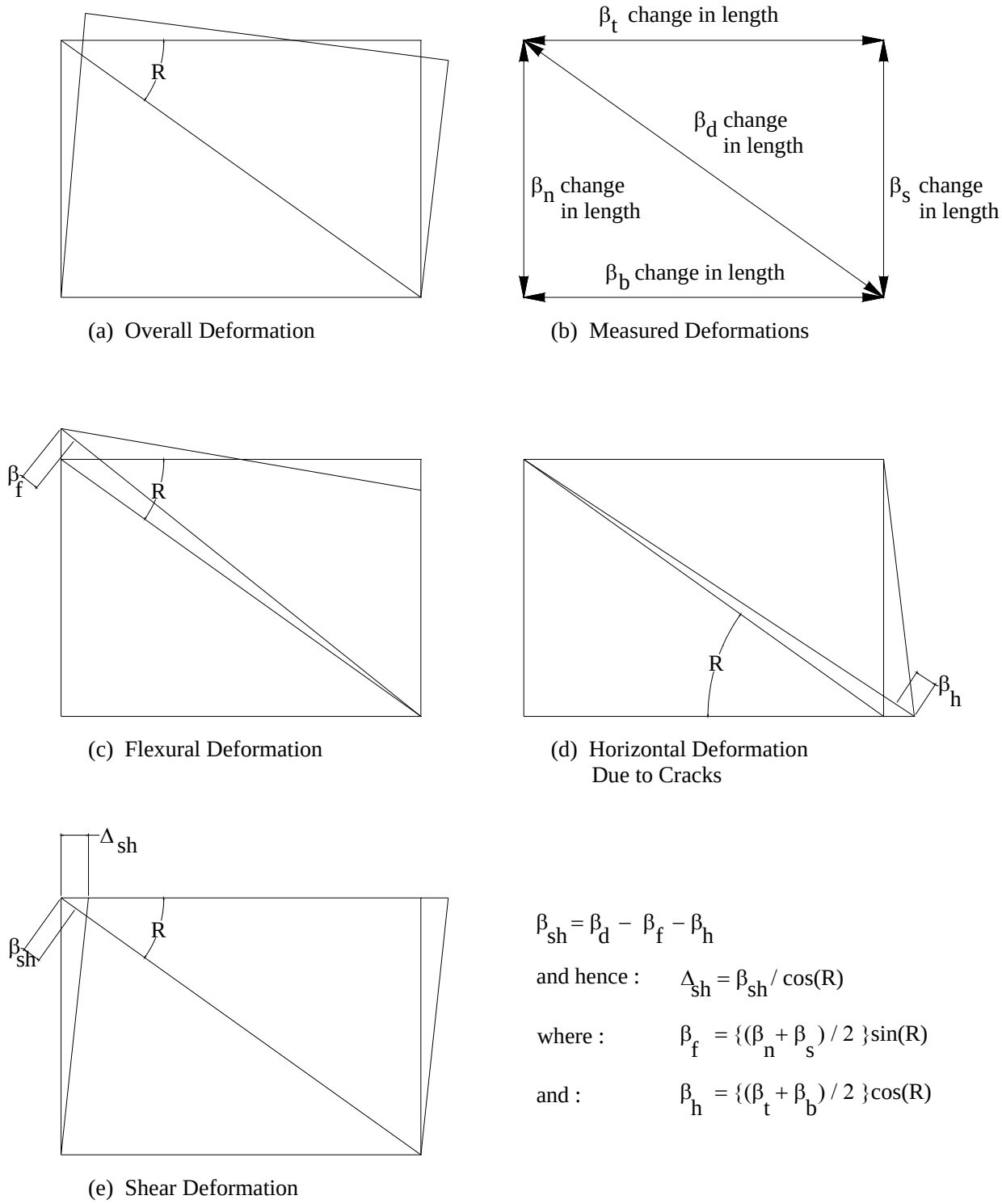

$$\beta_{sh} = \beta_d - \beta_f - \beta_h$$

and hence : $\Delta_{sh} = \beta_{sh} / \cos(R)$

where : $\beta_f = \{(\beta_n + \beta_s) / 2\}\sin(R)$

and : $\beta_h = \{(\beta_t + \beta_b) / 2\}\cos(R)$

Figure 6-10. Joint Strain Calculation

7. PREDICTED LOAD-DEFORMATION RESPONSE

7.1. ONE-COMPONENT NONLINEAR GIBERSON MODEL

The theoretical column top lateral deflection was established based on variables depicted in Figure 3-4, and according to the following expression:

$$\Delta V_i = \left(\frac{1}{K_{C,i}} + \frac{\left(L_c + h_b / 2\right)^2}{K_{B,i}} \right)^{-1} \times \Delta D_i \qquad (7\text{-}1)$$

Where ΔV_i and ΔD_i are the incremental column lateral load and top deflection, respectively, $K_{C,i}$ is the instantaneous tangential bending stiffness for the column bending response, and $K_{B,i}$ is the instantaneous tangential rotational stiffness of the bent cap contribution to the column top deflection expressed by Eq. (7-2). Furthermore in Eq. (7-1), the center of rotation of the bent cap was set at a distance of $L_c+h_b/2$, where h_b is the depth of the bent cap. The stiffness terms for the column and the bent cap were developed based on the one-component nonlinear Giberson model (Carr, 2000; Cheng, 2001). However, because of the test unit layout, this model was simplified for a base rotation due to the plastic hinge formation at one end only. As such, it was feasible to decouple the modes of deformation in the joint region in terms of plastic hinge plus bent cap rotation. In Eq. (7-1), the column and bent cap stiffness, $K_{C,i}$ and $K_{B,i}$, are, respectively:

$$K_{C,i} = \frac{3\, r_{i,C}\; EI_C^{'}}{L_C^2 \left[L_C\; r_{i,C} + 3\, L_{p,C} \left(1 - r_{i,C}\right) \right]}$$
$$K_{B,i} = \frac{12\, r_{i,B}\; EI_B^{'}}{\left[L_B\; r_{i,B} + 6\, L_{p,B} \left(1 - r_{i,B}\right) \right]} \qquad (7\text{-}2)$$

Referring to Figure 3-4, L_C is the column height measured from the centerline of the applied lateral load to the bent cap interface (i.e. L_C = 2.72 m), L_B is the length of the bent cap measured between supports blocks A and B (i.e. L_B = 4.57 m), and $r_{i,C}$ and $r_{i.B}$ are the column and bent cap instantaneous stiffness ratios, and $EI_C^{'}$ and $EI_B^{'}$ are the column and bent cap secant yield stiffness obtained from the column and bent cap moment curvature analyses. These quantities were further evaluated based on:

$$r_{i,C} = \frac{\Delta M_{i,c} / \Delta\phi_{i,C}}{EI_C^{'}} \quad \text{and} \quad r_{i,B} = \frac{\Delta M_{i,B} / \Delta\phi_{i,B}}{EI_B^{'}}$$
$$EI_C^{'} = \frac{M_{Y,C}}{\phi_{Y,C}} \qquad EI_B^{'} = \frac{M_{Y,B}}{\phi_{Y,B}} \qquad (7\text{-}3)$$

In addition, for the retrofitted units, $L_{p,C}$ and $L_{p,B}$ are, respectively, the column and bent cap plastic hinge lengths and were computed based on the following expressions (Priestley *et al.*, 1995; Caltrans, 2004):

$$L_{p,C} = g + 0.044 f_{yc} d_{bl}$$
$$L_{p,B} = D^{*} + 0.06H^{/} \qquad (7\text{-}4)$$

Where g is the steel shell gap length, f_{yc} is the column longitudinal reinforcement yield stress, d_{bl} is the bar diameter of the column longitudinal reinforcement, D^* is the least cross section dimension for rectangular sections, and H' is the length from the interface of the column to the point of contraflexure.

In Eq. (7-3) when the column is in the elastic range r_i is one, and the expression for $K_{C,i}$ reverts to the bending stiffness of a cantilever member given by $EI'_C/3L_C^3$. The procedure given by Eq. (7-1) can be used without the need to compute in advance the yield and ultimate conditions, which makes it suitable for the seismic assessment of system with multiple members with hinging at one end only. Hinging at both ends is a significantly more complex approach and was not covered in this research. Another attractive feature of the approach given by Eq. (7-1), is that the procedure is easily implemented for systems with multiple members responding within the inelastic range and for displacement control analysis, which were necessary conditions for this research program because the bent cap is likely to experience inelastic actions. Furthermore, in the Section 11 it will be shown that the influence of the inelastic deformations in the joint region will be easily handled with this approach.

7.2. FORCE-DISPLACEMENT RESPONSE NOT CONSIDERING JOINT DEGRADATION

Using the moment curvature analyses for the column and the bent cap previously outlined in Sections 3 and 5 and using the model developed based on Eq. (7-1), the corresponding predicted force-displacement responses for Units 1, 2 and 3 was performed and results of this analysis are shown in Figure 7-1.

Table 7-1 outlines values from this analysis at first yield, and other performance levels. From the moment curvature analyses described in Section 3.1.1, and Figure 3-3 first yield of the section was defined at yielding of the column longitudinal reinforcement. The ideal capacity was defined at the moment that develops a strain of ε_c=0.5 mm/m in the extreme compression fibers of the columns. Allowing for low cycle fatigue of the column longitudinal reinforcement due to cyclic loading and recognizing that the steel shell provides adequate resistance to prevent buckling of the column longitudinal reinforcement, rupture of these bars was predicted at a strain of 7%, which was based on previous laboratory tests. Numerical results at these performance levels are outlined in Table 7-1. Numerical analysis also indicates that the maximum expected displacement ductility capacity for the three tests units is within 9 and 10 with drift levels exceeding 10. These values indicate that the gap region was within values that can lead to displacement ductility levels that can ensure a safe seismic performance of RC bridge bents retrofitted according to the design details previously described.

It is important to emphasize that these predictions considered no strength degradation resulting from damage within the joint region. Based on test results, the test units experienced increasing levels of strength degradation at increasing levels of imposed displacement ductility, which was mainly attributed to joint damage. As such, in Section 11.5 three moment-rotation models were empirically developed from each of the test units test results. An empirical model was then developed to include the contribution of joint flexibility and damage into the lateral response of the test units. Furthermore, a detailed description of the implementation of these models in design is further outlined in Section 12.3.

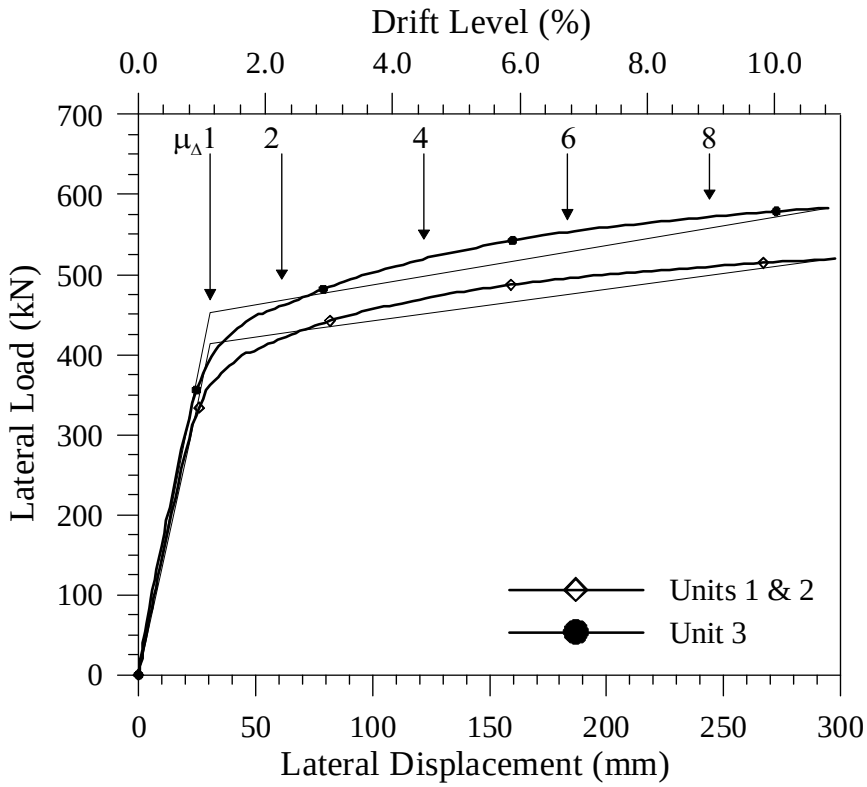

Figure 7-1. Predicted Force-Displacement Response of Units 1, 2 and 3

Table 7-1. Bilinear Force Deformation

Unit No.	First yield		Theoretical Yield		Ideal		Ultimate		
	Δ'_Y (mm)	V'_Y (kN)	Δ_Y (mm)	V_Y (kN)	Δ_I (mm)	V_I (kN)	Δ_U (mm)	V_U (kN)	μ_Δ
1 & 2	21.4	290	30.5	413	69.1	429	297.5	520	9.8
3	22.1	332	30.2	453	72.4	474	295.0	584	

7.3. LOADING PROTOCOL

Following the development of the load deformation response for the three test units the loading protocol was outlined for these units. For a direct comparison of test results the three units were loaded to the same load and displacement levels. Loading of the test units consisted of first applying the simulated gravity load followed by the cyclic lateral loads, which are described next.

The gravity load of the superstructure was simulated by a 710 kN axial load that was applied to the column by means of a hydraulic jack and the loading fixture shown in Figure 2-1. After applying the simulated gravity load, the units were tested according to the reversed cyclic loading protocol shown in Figure 7-2.

As discussed in Sections 8, 9, and 10, throughout testing, the three test units supported the applied gravity load. In the initial stages of testing, the three test units were loaded in force control with single cycles up to first yielding of the column longitudinal reinforcement. After first yielding, three cycles were applied in displacement control at intermediate displacement levels corresponding to the displacement ductility levels of 1, 1.5, 2, 4, and 6. At the displacement ductility level of 8, five cycles were applied to further investigate joint degradation under multiple reversed cyclic loading.

$$\Delta_{\mu 1} = \frac{\left(\left|\Delta^{T}_{y1}\right| + \left|\Delta^{T}_{y2}\right|\right)}{2}\frac{V_Y}{V_Y^{'}} \qquad (7\text{-}5)$$

Where $\Delta_{\mu 1}$ is the lateral displacement at $\mu_\Delta = 1$, V_Y is the lateral force at the theoretical yield, Δ^{T}_{y1} and Δ^{T}_{y2} are, respectively, the experimental lateral deflections recorded at first yield in the push and pull directions of loading. For Unit 1, in the push and pull directions these lateral deflections were recorded at 28.86 mm and 24.66 mm, respectively. Bilinear approximation of Unit 1 is presented in Figure 7-1. Thus, the lateral displacement of the test unit at the displacement ductility level of μ_Δ =1 was 38.10mm. It is important to emphasize that this number is different than the computed yield deflection presented in Table 7-1, which for Units 1 and 2 the yield deflection was 27.12 mm and for Unit 3 the yield deflection was 26.86 mm. However, the same force and ductility levels were used for testing of Units 2 and 3 to provide for a direct comparison of the test results.

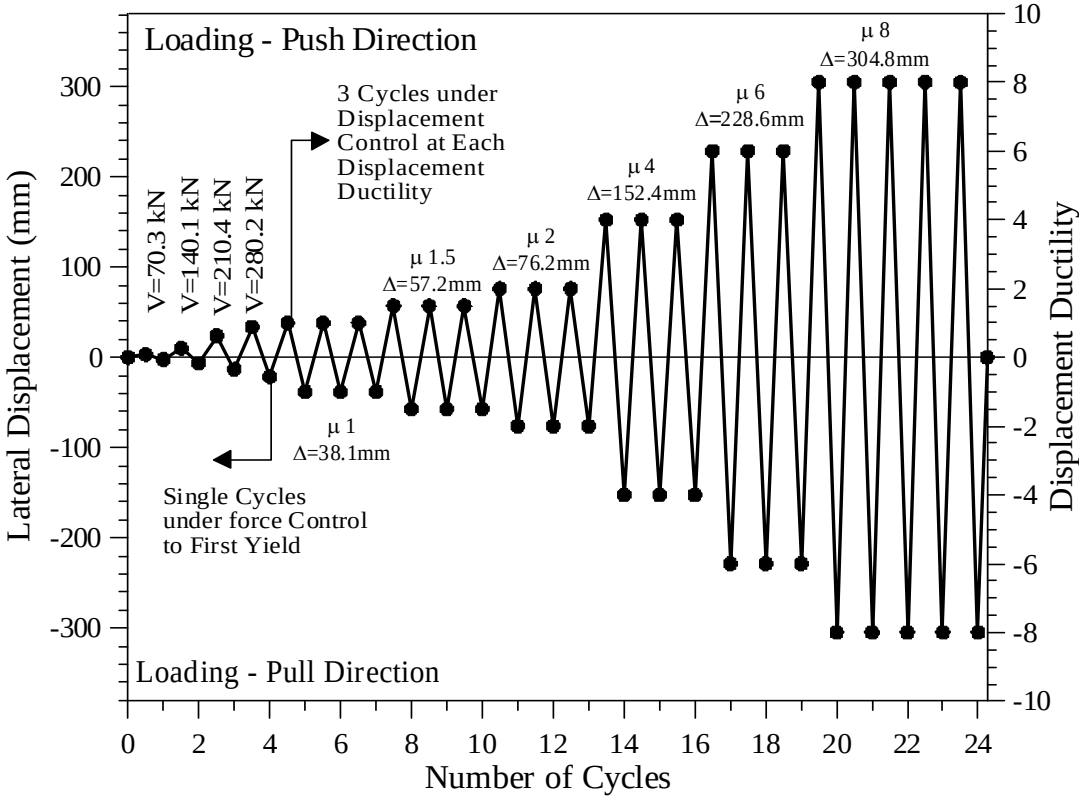

Figure 7-2. Loading Protocol Sequence

8. EXPERIMENTAL RESULTS – UNIT 1

This section presents observations recorded during testing, including load deformation and strain profiles for the column and bent cap reinforcement. The reversed cyclic loading protocol was previously described in detail in Section 7.3 and shown in Figure 7-2.

8.1. GENERAL TEST OBSERVATIONS

8.1.1. Force Control Load Cycles

Following application of the 710 kN axial load, the column was loaded during the first four reversed cycles in force control up to the theoretical first yield of the column longitudinal reinforcement. Theoretical yielding was previously defined in Section 3.1.1. Up to this load level, single fully reversed cycles were applied at $0.25V_y$, $0.50V_y$, $0.75V_y$, and $1.00V_y$ corresponding, respectively, to the lateral loads of 70.3, 140.1, 210.4, and 280.2 kN. At each peak cycle the load was held constant while damage was assessed and major observations were recorded for post-test evaluation.

During these four force-controlled cycles, inception of first cracking was detected during loading to $0.50V_y$. Micro-cracks were recorded at the interface between the column and the bent cap and within the steel shell gap region. Next at $0.75V_y$, these cracks propagated entirely around the column footprint and remained within widths smaller than 2mm. Then, as shown in Figure 8-1 and Figure 8-2, at $1.00V_y$ cracks propagated into the bent cap in a pattern emanating perpendicular to the column footprint. This crack pattern is indicative of onset of yielding of the column longitudinal reinforcement at the bent cap interface and development of yielding penetration into the joint region. This observation by itself indicates strong correlation to the predicted response, indicating yielding of the longitudinal reinforcement at this load level. As such, testing was continued and the theoretical displacement at ductility level 1 was calculated according to Eq. (7-5).

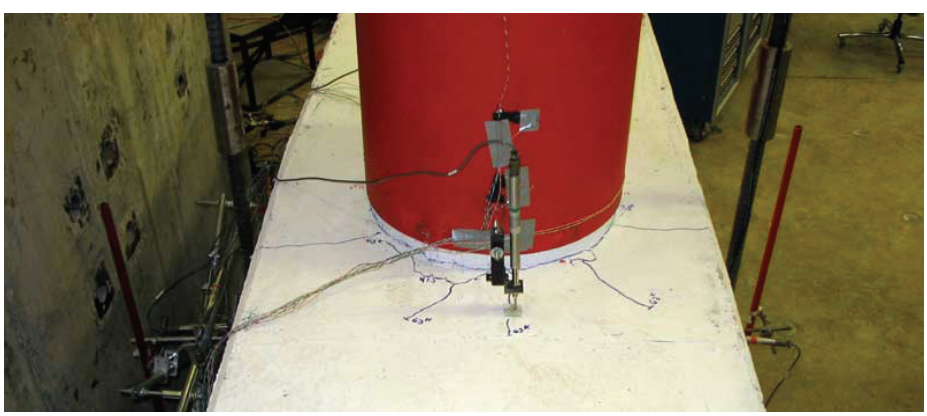

Figure 8-1. Bent Cap Cracking at $1.00V_y$

Figure 8-2. Bent Cap Cracking at 1.00 V_y

8.1.2. Displacement Control Load Cycles

After these four cycles the loading pattern was changed to displacement-control, as outlined in Section 7.3. At each peak displacement ductility level, testing was paused on the first and third cycles to visually inspect and record any damage to the test unit. It is important to emphasize that the ductility levels referenced in this section correlate to those described in Figure 7-2. However, during post-test evaluation different ductility levels were defined and these are referenced in Figure 8-22. The recorded damage at each ductility level is described next.

- *1.0 μ_Δ [38.1 mm]:* During the first cycle to this ductility level onset of joint shear cracking and flexural cracking of the bent cap was recorded, with the crack pattern recorded in Figure 8-3. It was also recorded that previously marked cracks increased in width along with onset of spalling of the cover concrete within the steel shell gap region, as shown in Figure 8-4.

- *1.5 μ_Δ [57.2 mm]:* Additional joint shear cracks were recorded including extension of previous cracks, as shown in Figure 8-5. An increase of strain penetration cracks occurred, as shown in Figure 8-6, along with further crushing of the column cover concrete.

- *2.0 μ_Δ [76.2 mm]:* Increase in the number of cracks and elongation of previous cracks was recorded in the joint, as seen in Figure 8-7. Separation of the cover concrete in the bent cap top surface further indicates continued strain penetrations into the bent cap (see Figure 8-8). At this damage level, further crushing and spalling of the column cover concrete were also recorded indicating onset of formation of a plastic hinge in the column. These two observations further confirm that up to this displacement level the joint was capable of sustaining the imposed joint shear stresses without significant strength degradation to the test unit.

- *4.0 μ_Δ [152.4 mm]:* At each successive cycle at ductility level 4, there was a loss of strength in the column combined with accumulated damage at the interface between the bent cap and column. There were no additional joint shear cracks and only minimal extensions of the existing cracks were recorded in Figure 8-9. In this figure and in Figure 8-10 are distinguishable concrete wedges lifting on the top surface of the bent cap and to either side of the column. Displacement of these wedges was more accentuated as the column was being displaced beyond ductility two, but then as the unit was progressively displaced lifting of these wedges stabilized. In addition, these wedges were limited to a distance corresponding to the first line of headed reinforcement, which prevented further extension of these cracks into the bent cap, as shown in Figure 8-10. The joint shear cracks remained within small widths as shown in Figure 8-11. At this level there was also further crushing of the column concrete cover as shown in Figure 8-12.

- *6.0 μ_Δ [228.6 mm]:* At this level the column strength continued to decrease; however, joint shear cracks neither extended further or increased in width as shown in Figure 8-13. Additional crushing of the column cover concrete was also recorded as shown in Figure 8-14. Onset of cracking on the underside of the bent cap was also observed indicating the typical pullout cone that is generally indicative of anchorage failure of the column longitudinal reinforcement. Further cycles accentuated the cracking and spalling of the cover concrete on the underside of the bent cap, as shown in Figure 8-15. Then as the longitudinal bars were pulled from within the joint core, under reversed cyclic loading, the steel shell was not as effective in preventing buckling of this reinforcement. As such during the last cycle at this level, buckling of the main column longitudinal bar was observed, as shown in Figure 8-16. Although some level of joint shear failure is clearly visible at this ductility level, complete failure of the test unit has not yet fully developed, as the unit is capable of sustaining significant amounts of lateral load.

- *8.0 μ_Δ [304.8 mm]:* There was a continual loss in capacity at this ductility level. The column bars that had previously buckled finally fractured under low cycle fatigue, as shown in Figure 8-18. Cracking continued on the underside of the bent cap and large wedge blocks separated from the bent cap as shown in Figure 8-19. However, cracks on the side of the bent cap remained within widths smaller than 3 mm with the corresponding cracking pattern shown in Figure 8-20. This observation suggests that joint damage was concentrated within the as-built section. Testing was stopped at this ductility level for safety reasons and more importantly because the sustained lateral load was rapidly decreasing to negligible levels.

After testing, all loose concrete was removed and the test unit was further inspected to evaluate the main failure mode. An important observation is that the extent of damage in the bent cap was confined to the first row of headed reinforcement, as shown in Figure 8-21. On the underside of the bent cap it was recorded that a wide open crack extended in the longitudinal direction of the bent cap. This indicates splitting of the bent cap and potential dilation of the bent cap in the

transverse direction. This indicates also that the transverse reinforcement through the bent cap was not effective in preventing this dilation and continuous reinforcement should be provided instead, as outlined in Section 4 while describing the design of Unit 2.

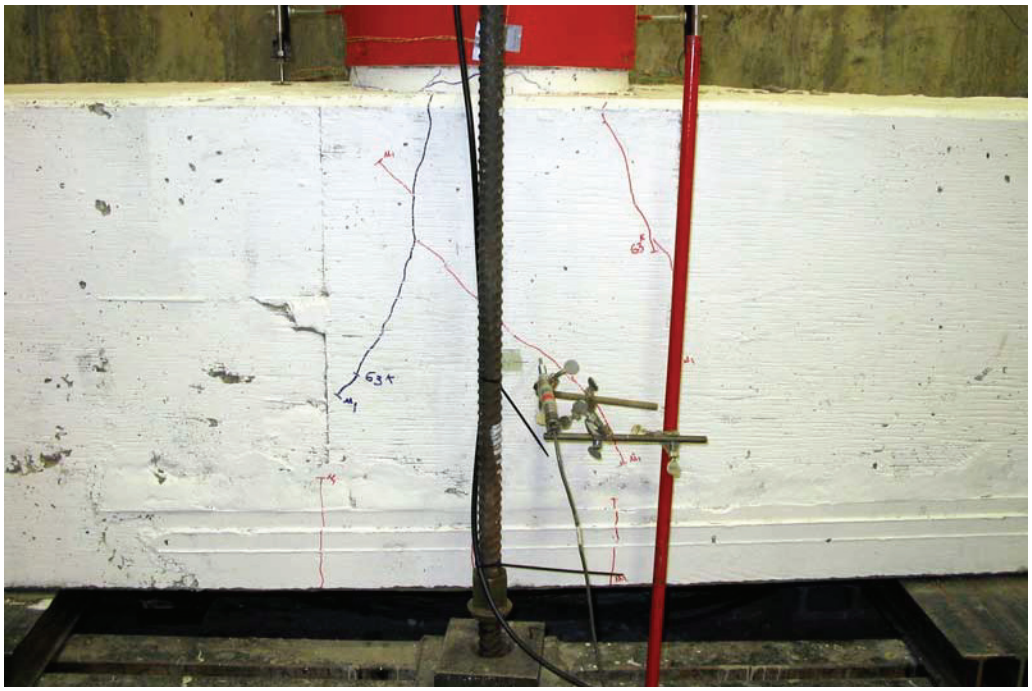

Figure 8-3. Joint Cracking at 1.0 μ_Δ

Figure 8-4. Bent Cap Cracking at 1.0 μ_Δ

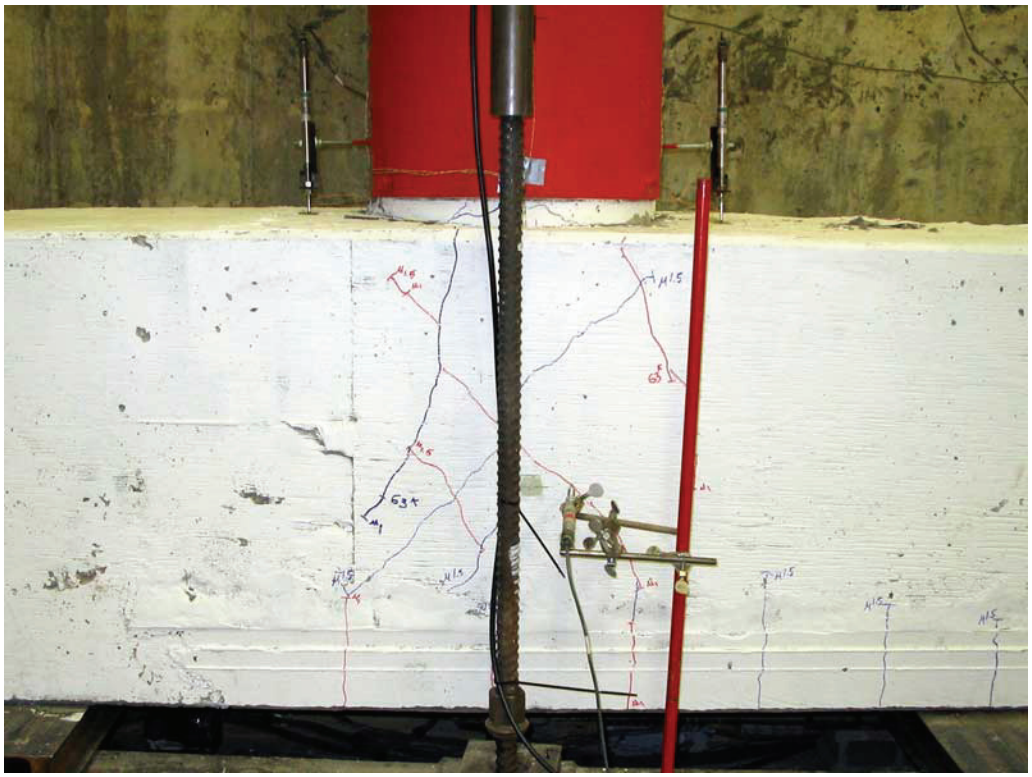

Figure 8-5. Joint Cracking at 1.5 μ_Δ

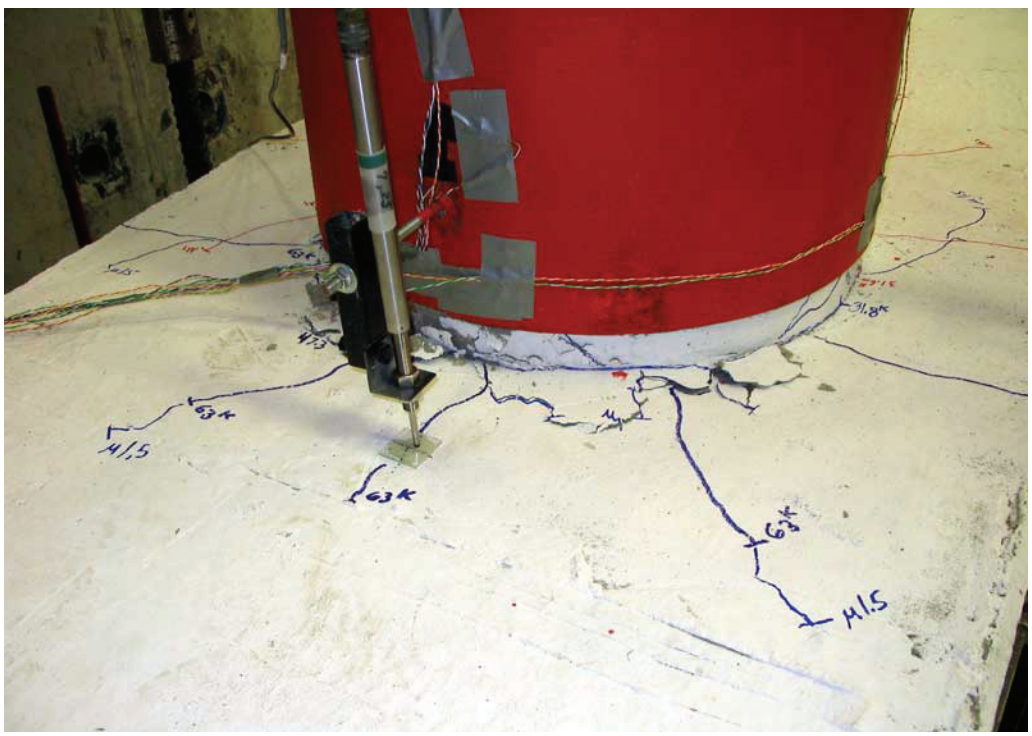

Figure 8-6. Bent Cap Cracking at 1.5 μ_Δ

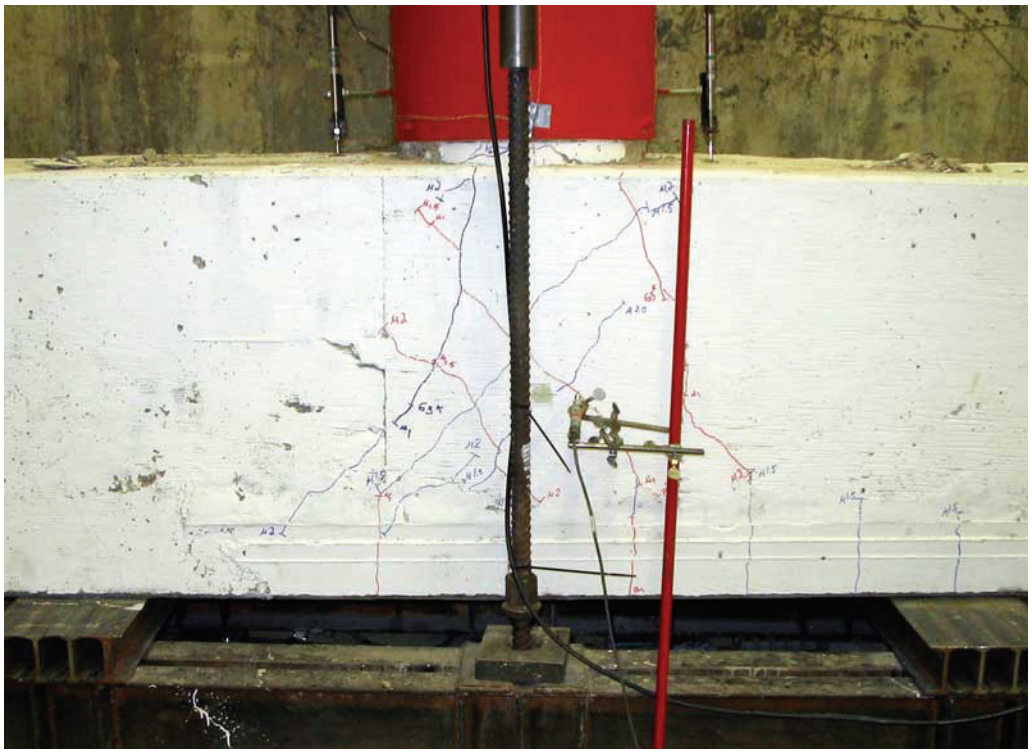

Figure 8-7. Joint Cracking at 2.0 μ_Δ

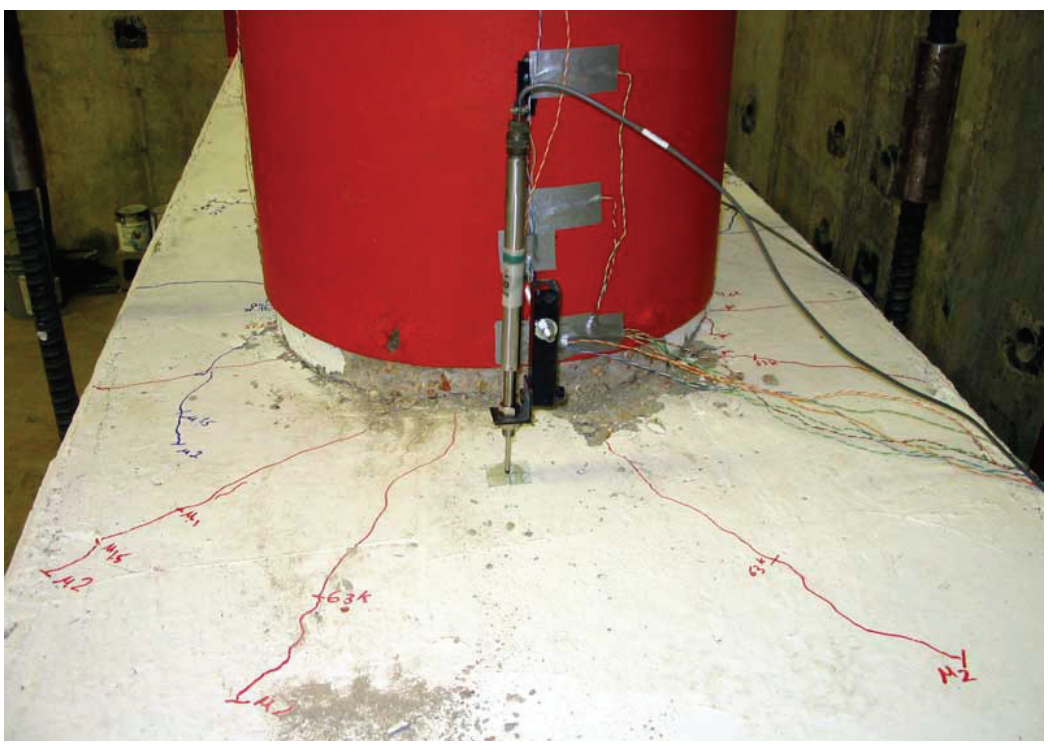

Figure 8-8. Bent Cap Cracking at 2.0 μ_Δ

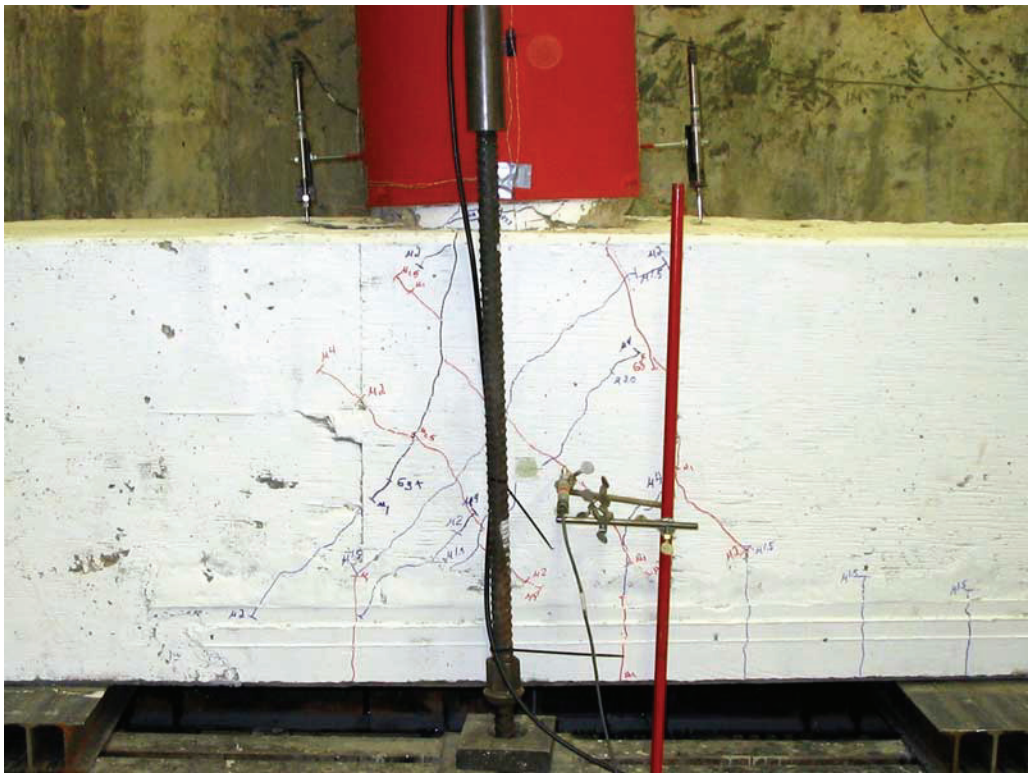

Figure 8-9. Joint Cracking at 4.0 μ_Δ

Figure 8-10. Bent Cap Cracking at 4.0 μ_Δ

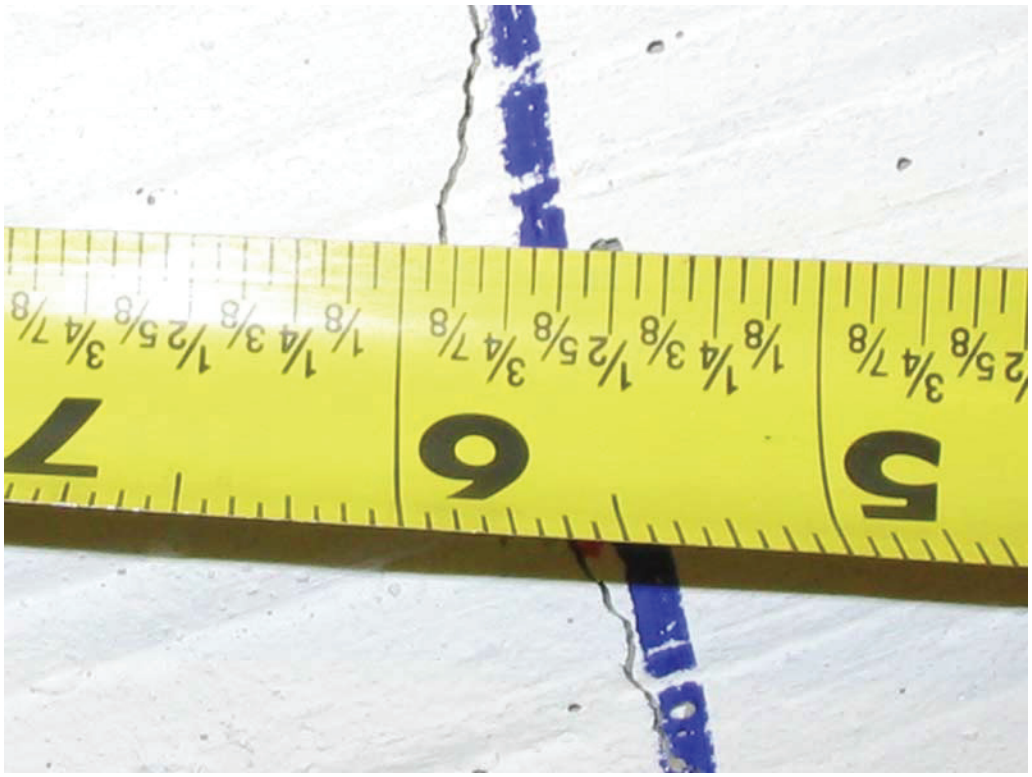

Figure 8-11. Joint Crack Width at 4.0 μ_Δ

Figure 8-12. Column Concrete Crushing at 4.0 μ_Δ

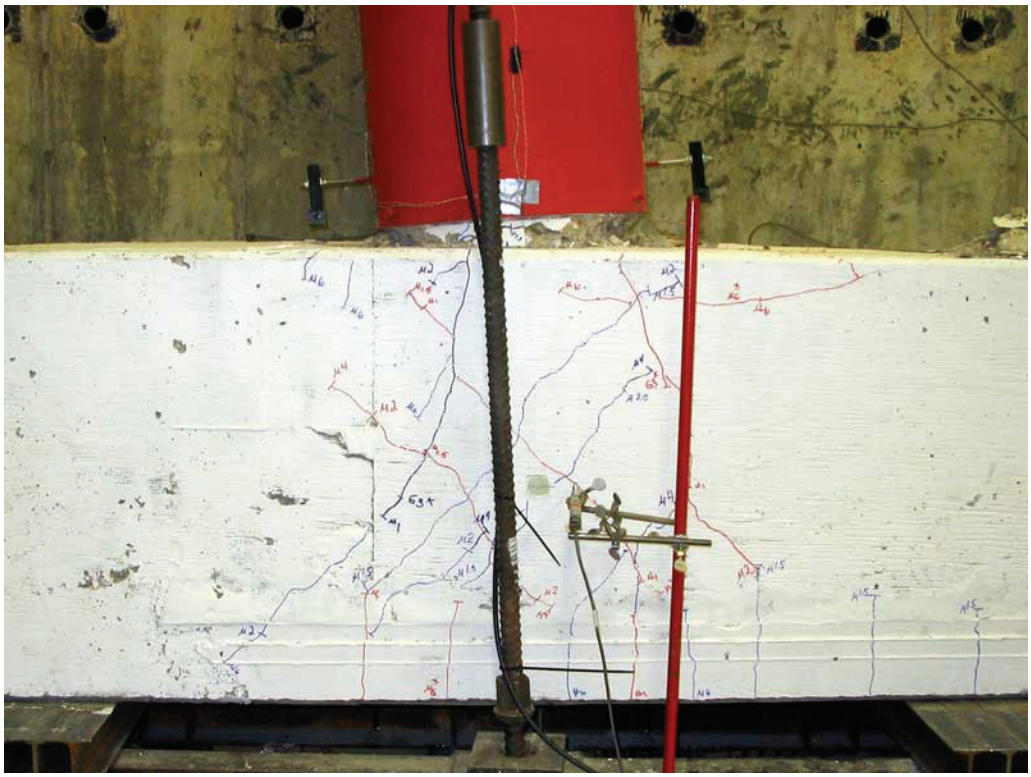

Figure 8-13. Joint Cracking at 6.0 μ_Δ

Figure 8-14. Column Concrete Crushing at 6.0 μ_Δ

Figure 8-15. Bent Cap Bottom Cracking at 6.0 μ_Δ

Figure 8-16. Column Longitudinal Bar Buckling at 6.0 μ_Δ

Figure 8-17. Bent Cap Cracking at 8.0 μ_Δ

Figure 8-18. Column Longitudinal Bar Fracture at 8.0 μ_Δ

Figure 8-19. Bent Cap Bottom Spalling at 8.0 μ_Δ

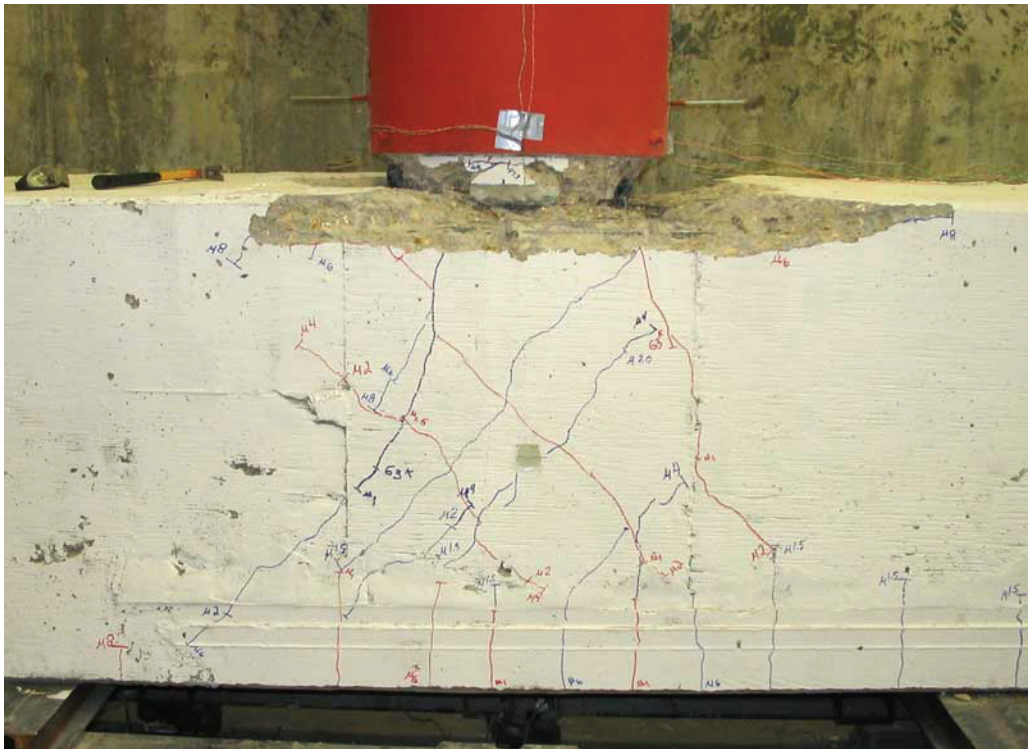

Figure 8-20. Joint Cracking at 8.0 μ_Δ

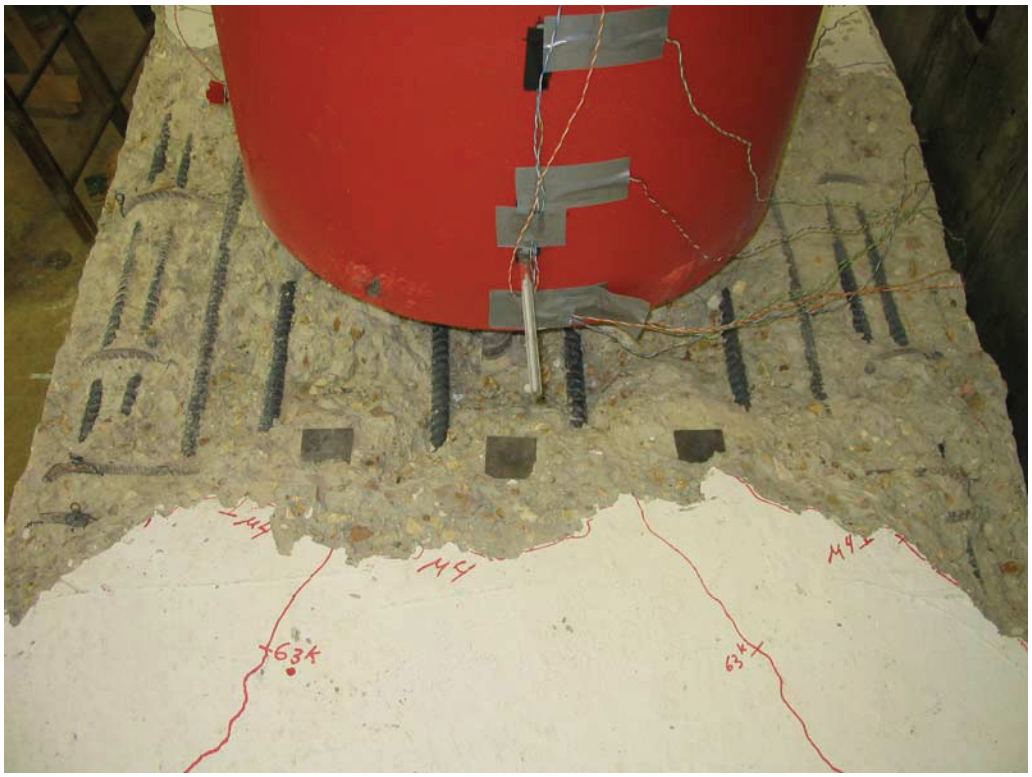

Figure 8-21. Bent Cap Ultimate Damage

8.2. LOAD DEFORMATION RESPONSE

The pre and post-test theoretical and experimental load vs. deformation curves for Unit 1 are shown in Figure 8-22. Development of the pre-test analysis curve was previously outlined in Section 7.1 and the post-test analysis is discussed in Section 11.5, which also describes the post-testing investigation for the three test units. After testing, the displacement at ductility level one was rectified to reflect directly the test results. Based on a direct investigation of the test results the new displacement at ductility level one was set at 31.5 mm, leading to the ductility levels shown in Figure 8-22.

The maximum lateral load was recorded during loading to the first cycle at the displacement of 152.4 mm or ductility level 5. At this cycle, in the push and pull directions the lateral loads were +421 and -442 kN, respectively. From the first to the second cycle the drop in the lateral load was approximately 17%, and from the second to the third cycle the drop in the lateral load was only 5%. In addition, during loading to the first cycle at the next displacement of 228.6 mm (or ductility 7) the degradation in the lateral load was less than 5% indicating stability in the response of the test unit. This suggests that at this level any damage that has developed within the joint region stabilized, and the reinforcement provided in the new bent cap section was effective in preventing further degradation to the test unit.

Then, during subsequent cycles a the continuous strength degradation was observed in combination with pinching in the hysteretic response of the test unit. The first significant drop in load below the theoretical yield load level was observed during the second cycle at this displacement level. Before this displacement ductility level, the hysteretic response of the test unit was reasonably stable with significant amounts of energy dissipation capacity. As previously stated, it is important to reemphasize that during loading to the first cycle at 228.6 mm the lateral load was nearly the same as the load registered to the third cycle at 152.4 mm. This indicates that load transfer within the joint region was still within limits capable of sustaining load levels within 80% of the maximum registered lateral load for displacement ductility levels less than 5. As such, a safe ductility level 4 was selected as the limiting ductility level for assessment and design using this retrofit procedure.

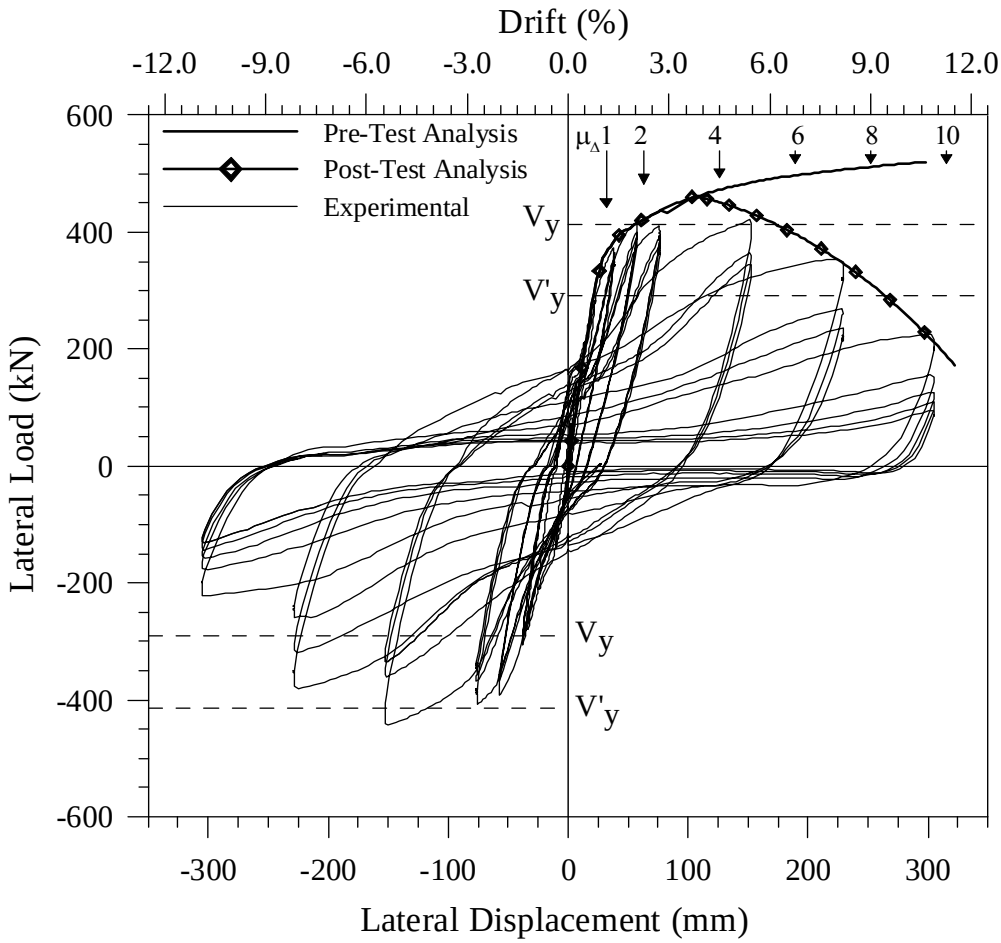

Figure 8-22. Unit 1 - Load Displacement Response

During the second cycle to 228.6 mm, cracks and then spalling of a concrete wedge were observed on the underside of the bent cap immediately below the column footprint. This indicates that severe joint degradation under reversed cyclic loading had initiated, which is also

evidenced by a drop in the lateral load during subsequent cycles. However, this damage level did not lead to complete loss in the lateral and axial load capacity of the test unit. In fact, during the first cycle to the displacement of 304.8 mm, low cycle fatigue of one of the column longitudinal rebar was detected, which shows that the joint had reserve capacity to prevent complete pull-out of the column longitudinal bars. Furthermore, the three cycles at the displacement ductility level of 228.6 mm exhibited considerable levels of energy dissipation capacity.

During the subsequent cycles at the displacement of 304.8 mm, large blocks of concrete separated from the bottom of the bent cap. Through visual inspection it was possible to distinguish a wide open crack running in the longitudinal direction and along the mid-width of the bent cap indicating a longitudinal splitting in the bent cap. This was accompanied by a significant drop in the lateral load capacity which indicates partial pullout failure of the column longitudinal reinforcement in addition to low cycle fatigue. These observations clearly suggest that the two-piece transverse reinforcement layout was not effective in preventing longitudinal splitting of the bent cap and this detail was revised for the construction of Unit 2, as described in Section 4.

8.3. LOAD VS. CURVATURE RESPONSE

Figure 8-23 shows the measured lateral load versus the computed curvatures at the interface of the column to the bent cap. The diagram depicted in this figure indicates a good correlation between the pre-test analysis and the experimental test results during the initial stages of testing. However, after peak load there is a considerable deviation between these two curves. These can be attributed to the fact that during the initial stages of testing most of the deformations are due to curvature along the length of the column, and at later stages of testing most of the column top deflection is a result of large rotations originating solely from within the joint region. Using these experimental results it was possible to back calculate any potential rotations within the joint region and propose models that can account for the contribution of the joint rotation on the column top deflection. This issue is further discussed in Section 11.

Curvatures presented in Figure 8-23 represent average values and were computed according to the expression:

$$\phi_{ave} = \frac{\Delta_1 - \Delta_2}{W_{cur} \times h_{cur}} \qquad (8\text{-}1)$$

Where Δ_1 and Δ_2 are the relative vertical displacements between the adjacent curvature rods in the extreme faces and on the opposite faces of the column, W_{cur} is the horizontal distance between the pair of linear potentiometers, and h_{cur} is the vertical distance between the adjacent linear potentiometers. During computations of curvatures at the pile cap interface the height of

the linear potentiometer cell h_{cur} include an additional term to account for tensile strain penetration into the bent cap by including the strain penetration length into the curvature cell height h_{cur} according to the expression:

$$h_{cur} = h + 0.0022\, d_{bl}\ f_s \qquad (8\text{-}2)$$

Where d_{bl} is the column main bar diameter and f_s is the column main bar stress obtained from the reinforcement strains obtained from the next section data. In the early stages of the testing procedure strain levels in the inner core reinforcement are minimum and f_s should be used instead of f_y and any tensile strain penetrations are negligible. Then at later stages of testing f_y was used.

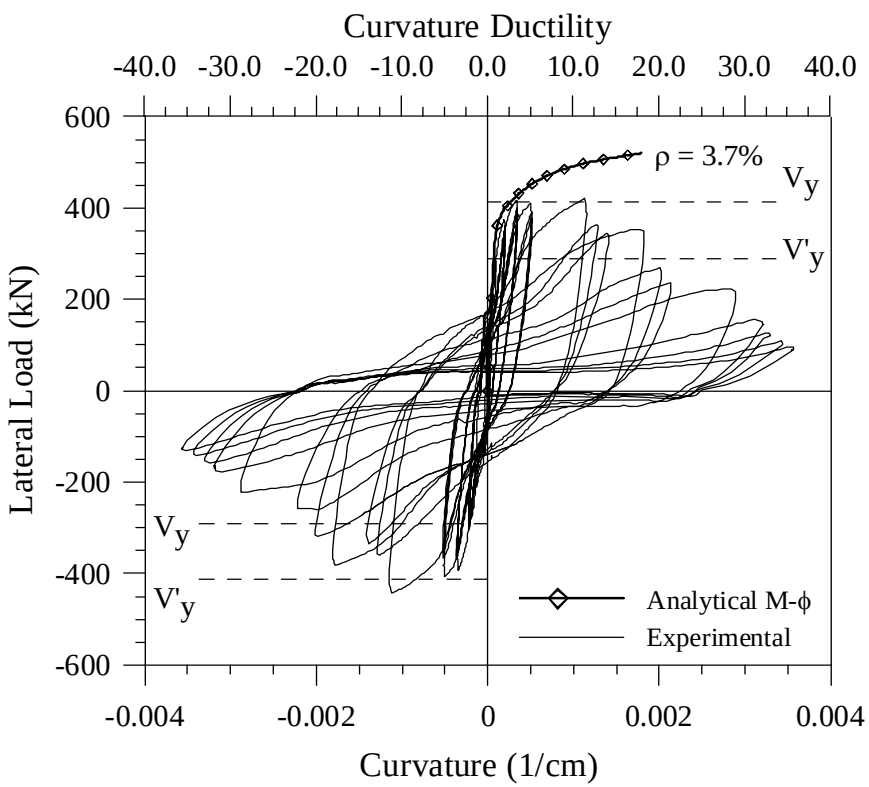

Figure 8-23. Unit 1 – Load versus Curvature Response

8.4. COLUMN LONGITUDINAL REINFORCEMENT STRAINS

Strains presented in this section and subsequent sections are indicated as positive when the bars are subjected to a tensile strain and negative when the bars are subjected to compressive strains. The strain histories of the column longitudinal reinforcement gauges at the interface of the column and bent cap for side "A" and side "B" are shown in Figure 8-24 and Figure 8-25, respectively. The yield strain of the column longitudinal reinforcement occurred at ±2,740με as determined from tensile testing and was previously indicated in the material properties section

and Table 2-2. The strain profiles for each side of the column are shown in Figure 8-26 and Figure 8-27. The onset of yielding of the main column longitudinal bars occurred at μ1.0 for each side of the column, which are within the predicted levels.

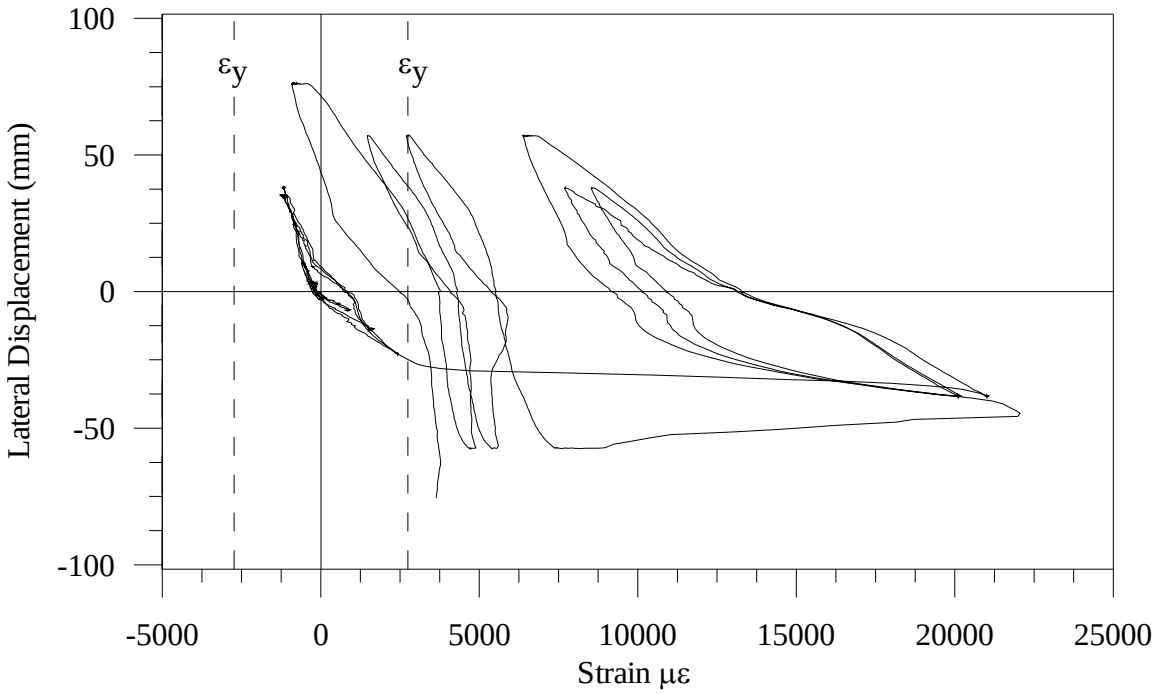

Figure 8-24. Strain Gauge History – C4a

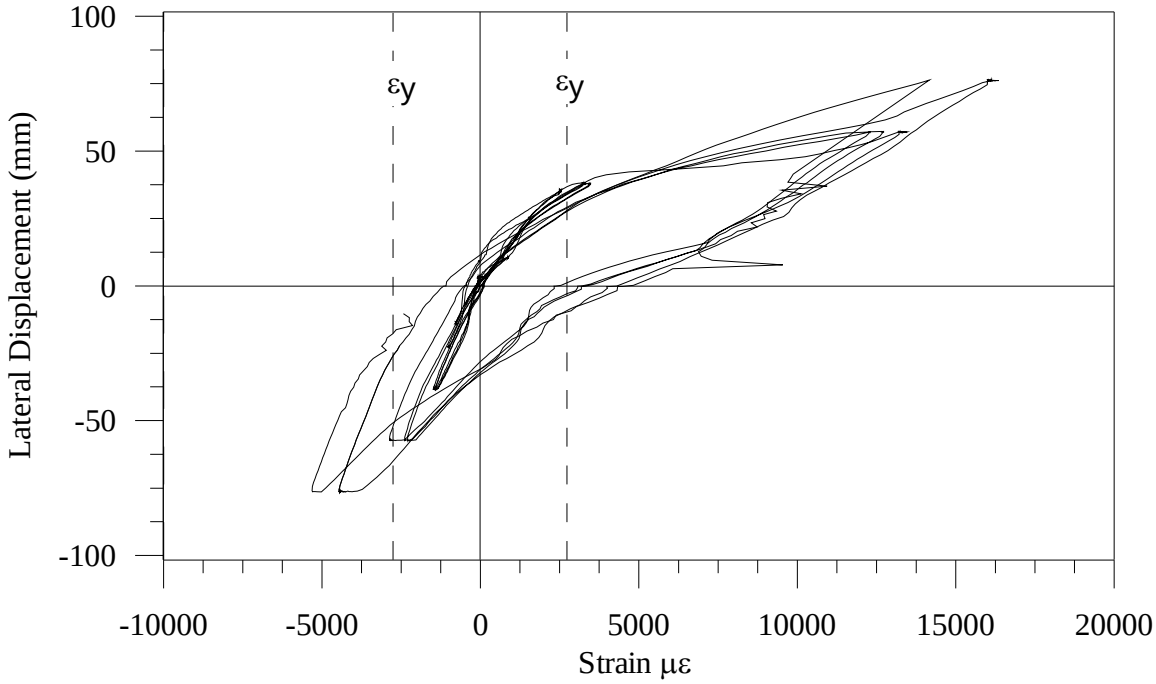

Figure 8-25. Strain Gauge History – C4b

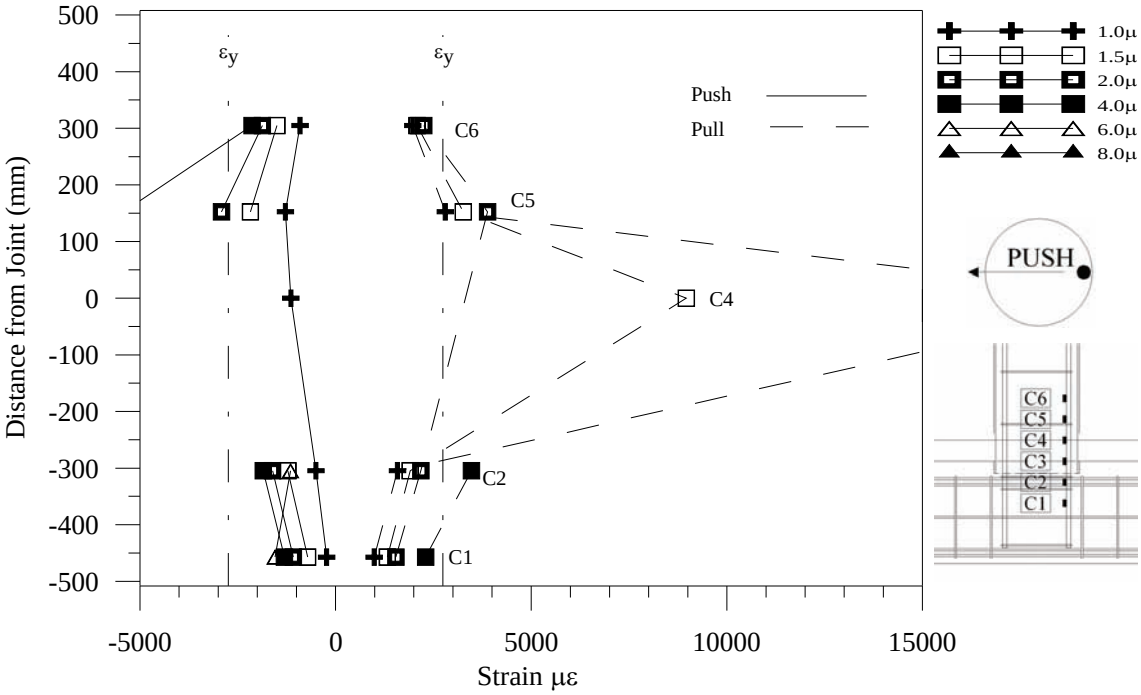

Figure 8-26. Strain Gauge Profile – Side "A"

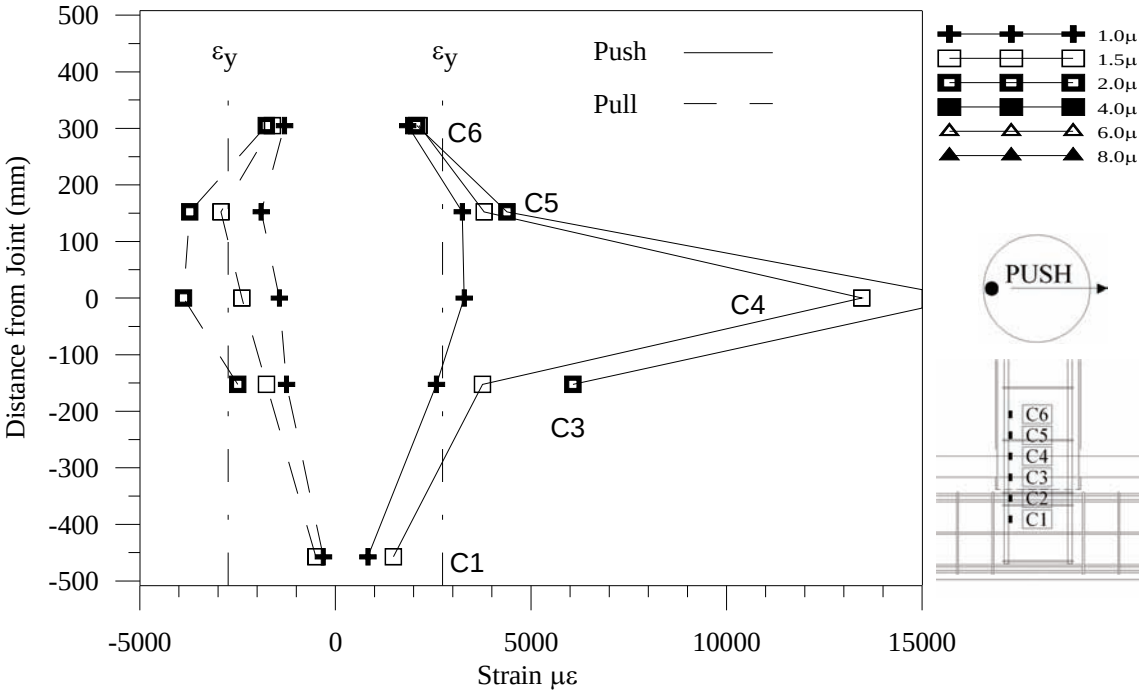

Figure 8-27. Strain Gauge Profile – Side "B"

8.5. JOINT SHEAR REINFORCEMENT STRAIN PROFILES

Strain profiles were developed from gauges mounted on the joint shear reinforcement and these profiles are presented in this section. As determined from the material characterization pull-out tests, the yield strain for the as-built shear reinforcement was measured at ±2,191με and the yield strain for the retrofit shear reinforcement was measured at ±2,340. Figure 8-28 and Figure 8-29 illustrate the strain profiles for the stirrups in the as-built and the retrofit sections, respectively. From these figures it is clear that the strain values registered in these stirrups stayed below yielding, which suggest that the cracks observed on the faces of the bent cap remained fairly small. This description matched closely the test observations described in Section 8.1, further indicating that joint shear failure in the longitudinal plane of the retrofit or the as-built bent cap sections was not the likely failure mode of the test unit.

Further comparisons between these strain profiles clearly indicate that during the initial stages of testing and up to ductility one the strains in either the as-built or the retrofit section were negligible. This statement corroborates the observation that diagonal joint shear cracking was not observed up to this ductility level, as shown in Figure 8-3. Another important observation that can help to explain the failure mode of this unit is that the strains in the as-built and the retrofit sections achieved similar profiles and nearly the same values. This is a strong indication that composite action was developed between these two sections and since it was not possible to investigate the damage within the as-built section, this eliminates the possibility for joint shear failure in the longitudinal plane of the as-built section.

In addition, at the centerline of the retrofit section the registered strains were nearly 50% higher than at the interface to the column, clearly showing that the reinforcement in this region was fully mobilized in preventing joint shear failure in the longitudinal plane of the bent cap section. Of equal importance to this study, the strains in the shear reinforcement rapidly dissipated away from the column faces. In fact beyond a distance of $h_b/2$ the strains were almost negligible, indicating that the vertical joint shears reinforcement is only active within this distance, and it should be placed within a distance of $h_b/2$ from the column faces, as stated per Section 3.3.4.

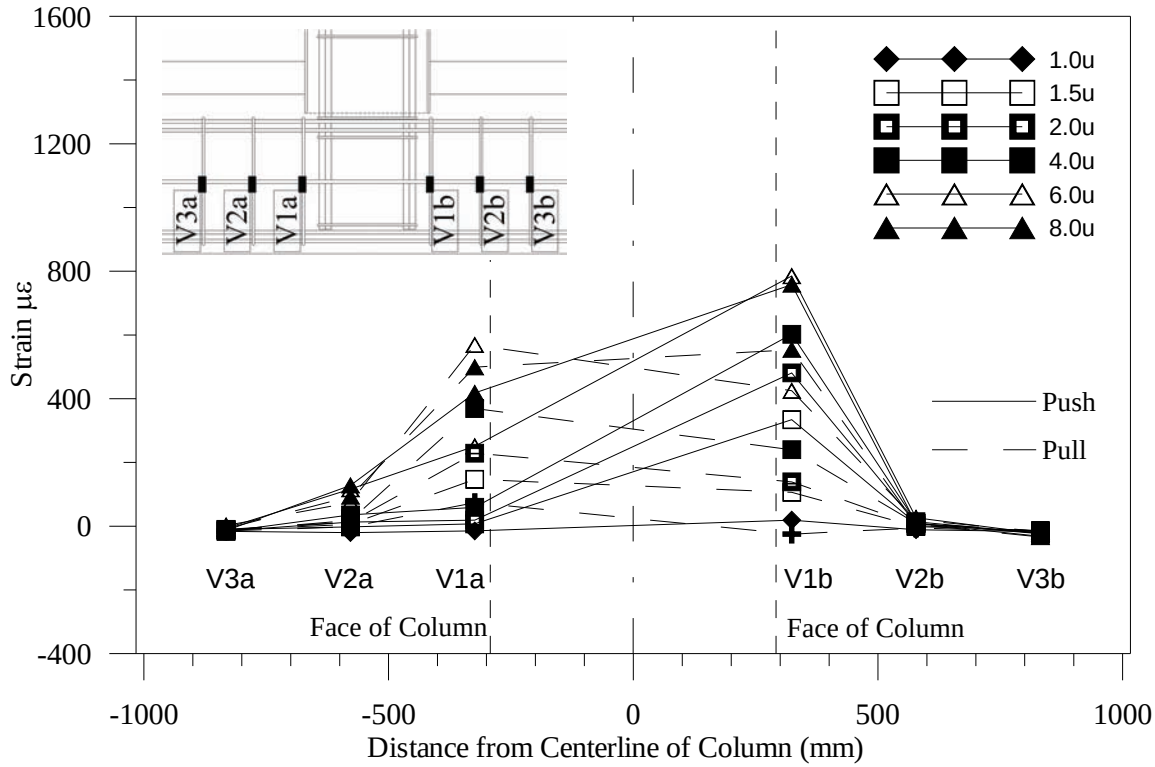

Figure 8-28. Strain Profiles – As-Built Section

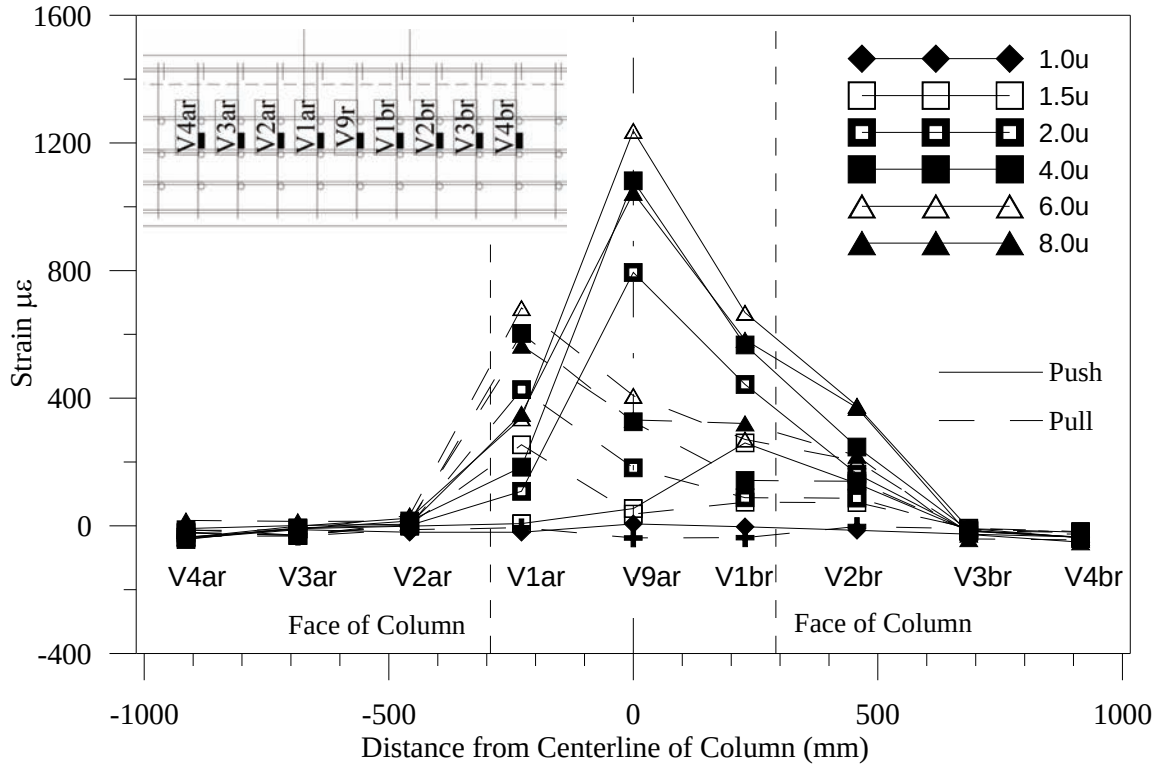

Figure 8-29. Strain Profiles – Retrofit Section

8.6. BENT CAP LONGITUDINAL REINFORCEMENT STRAINS

This section presents and discusses the strain profiles for the bent cap longitudinal reinforcement. The yield strains for the as-built and the retrofit longitudinal reinforcement were measured, respectively, at 2,807 με and 2,544 με.

8.6.1. Strain Profiles - Bottom Reinforcement

The strain profiles shown in Figure 8-30 and Figure 8-31 clearly indicate that the strains in either the as-built or the retrofit bottom reinforcements were above the measured yield strain values. These profiles also show that in similar locations, the strains in both these reinforcements achieved nearly the same strains levels, indicating that the bent cap was acting as one composite unit. Important to note that although after ductility level four the applied lateral load decreased and hence, the moment applied to the bent cap decreased, the strains in the longitudinal reinforcement at the bottom of the bent cap continued to increase as shown in these profiles.

This increase can be attributed to strains that develop as a result of joint stress demands as outlined by the strut and tie model shown in Figure 3-8 and the reinforcement demands per Eq. (3-13). Hence, based on the moment curvature analysis previously discussed in Section 3.2.1, the maximum achieved peak loads described in Section 8.2, and the stress demands per Eq. (3-13), it is feasible to estimate the strains that develop in this reinforcement by the expression

$$\mu\varepsilon_e = \frac{\mu\varepsilon_f \times n_f + \mu\varepsilon_j \times n_j}{n_t} = \frac{1{,}100 \times 11 + 2{,}544 \times 7}{20} = 1{,}495\mu\varepsilon \qquad (8\text{-}3)$$

Where $\mu_{\varepsilon f}$ was the estimated flexural strain which for a peak lateral load of 442 kN was estimated from the moment curvature analysis at 1,100με by considering 11-D16 bars, $\mu_{\varepsilon j}$ was the estimated strain at yielding by considering that only 7-D16 bars were effective in resisting the joint shear mechanism, n_{bf} and n_j are the number of bars from flexural and joint shear design considerations, and n_t is the total of bars provided at the bottom of the bent cap per Figure 3-1. As such, the estimated strains in these reinforcements per Eq. (8-3) were nearly 1,500με which are significantly lower than the maximum strain value of near 2,000με obtained from these strain profiles. These results suggest that other mechanism/s influenced the response of the joint.

Another mechanism that can be attributed to have caused this increase in strains beyond ductility level four is best depicted in Figure 8-32. According to this mechanism, after the wedges of concrete are formed at the bottom of the bent cap (see Figure 8-15) under reversed cyclic loading the column longitudinal reinforcement imposes downwards forces on these wedges. This increases the clamping mechanism that needs to be engaged by the bottom reinforcement in order to prevent complete punching shear failure of the column cage; Hence, imposing higher demands in these reinforcements.

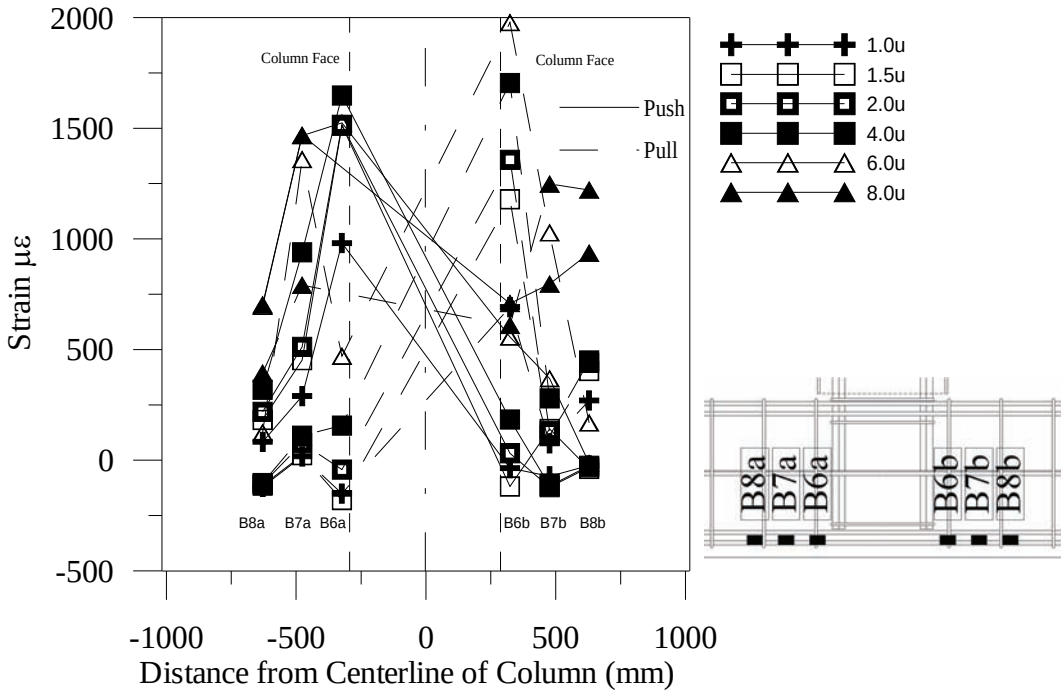

Figure 8-30. Strain Profiles – As-Built Section

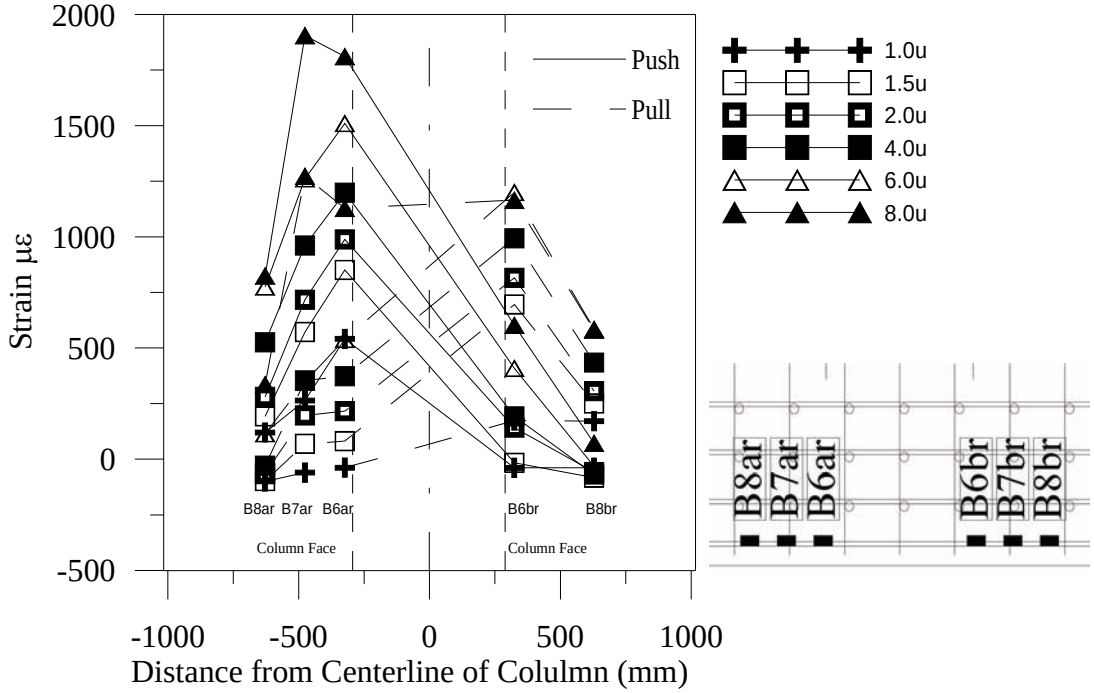

Figure 8-31. Strain Profiles – Retrofit Section

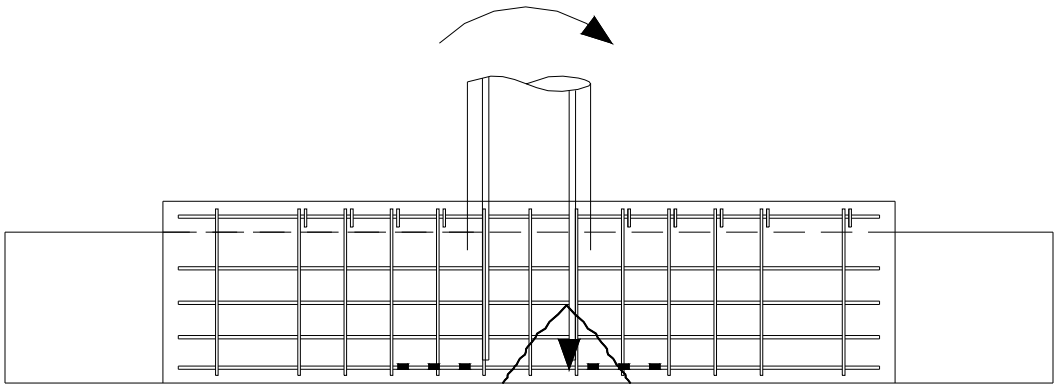

Figure 8-32. Confinement of Column Anchorage Failure

8.6.2. Strain Profiles - Top Reinforcement

As in the previous section, the strain profiles shown in Figure 8-33 clearly indicate that the strains in the retrofit top reinforcement were always below the measured yield strain values. These profiles also show that in the pull direction the maximum strains were registered at a distance of -550mm from the centerline of the bent, and from the strain profiles shown in Figure 8-31 the strains are highest at this location under the push direction which matches the expected moment demands per Figure 3-4(b).

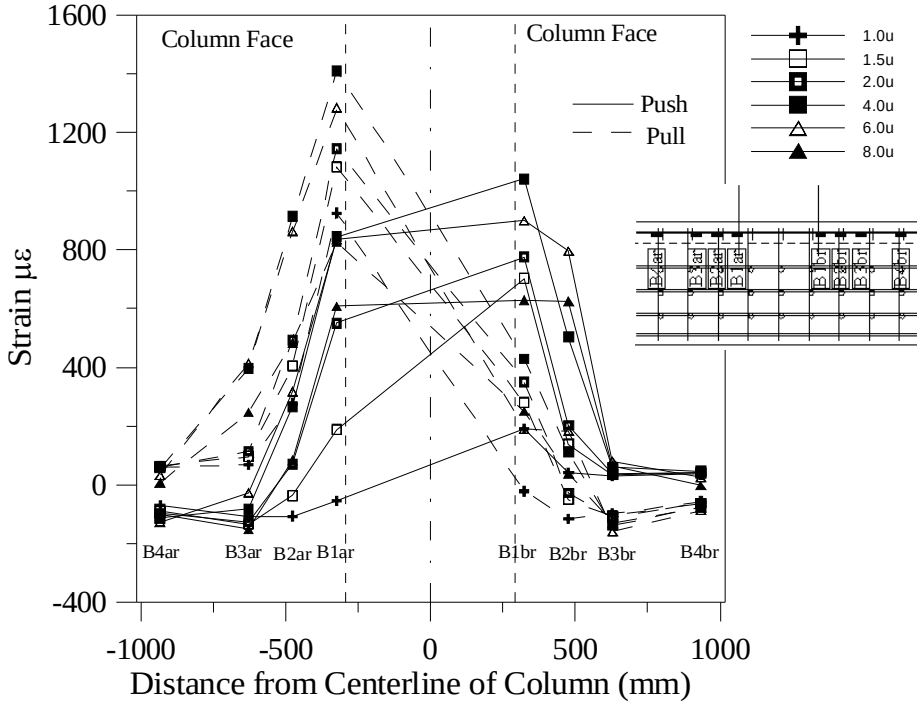

Figure 8-33. Strain Profiles – Retrofit Section

Performing similar calculations as in the previous section the estimated strain values in the top reinforcement were

$$\mu\varepsilon_e = \frac{\mu\varepsilon_f \times n_f + \mu\varepsilon_j \times n_j}{n_t} = \frac{500 \times 8 + 2{,}544 \times 6}{18} = 1{,}070\mu\varepsilon \qquad (8\text{-}4)$$

In this expression, the flexural strains are less than in Eq. (8-3) because of the reduction in moment demands in the top section per the bending moment diagram depicted in Figure 3-4(b). As before, the predicted strain values per Eq. (8-4) are also lower than the maximum strain values registered in the strain profiles, which indicate other mechanism/s were influencing the response of the test unit.

A reasonable mechanism, which can be used to justify this increase in top strains, was previously discussed while describing the importance of the mechanism shown in Figure 3-11, and matches well the observed damage substantiated per Figure 8-21. As such, under reversed cyclic loading the column longitudinal reinforcement is now clamped by wedges of concrete at the top of the bent cap which imposes upwards forces on these wedges; hence, imposing higher demands in these reinforcements.

8.7. JOINT SHEAR ANALYSIS

Referring to Figure 8-22 and based on a post-test investigation, it is reasonable to infer that the progressive loss in strength evidenced in this figure was mainly a result of flexibilities originating from within the joint region and, not necessarily a result of poor performance of the flexural or shear response of the column. It is also important to recognize that either of these column failure modes is associated with sudden losses in strength, which does not match the progressive loss of strength evidenced per Figure 8-22.

As important, load deformation responses of poorly detailed joints are associated with sudden losses in strength in excess of 30% per cycle, which also does not match the nature of the deformation response shown in Figure 8-22 figure. In addition, joint shear failures of poorly detailed joints are associated with large cracks and joint shear deformations on the face of the bent, which does not match the joint shear cracks marked on the sides of the bent cap. In fact, these marked cracks were rather small to justify any level of joint shear degradation. This is also evidenced by the computed shear deformations shown in Figure 8-34, which were rather small once again to justify joint shear failure. This also suggests that joint flexibility was not a result of lack of joint shear reinforcement but of the mechanisms previously associated with Figure 3-11 and Figure 8-32, which are typically associated with a more moderate loss of strength and do not necessarily lead to a sudden loss in strength.

Joint shear deformations shown in Figure 8-34 were computed based on the mathematical methodology presented in Figure 6-10 and using the experimental data obtained from the devices shown in Figure 6-9. Priestley (1993) developed a model for joint behavior using principle tensile stresses and joint shear strains that were obtained from tests conducted for unreinforced concrete joints. Based on his work Priestley developed a trilinear model which comprises of an initial joint stiffness based on the shear modulus of concrete, G_c, and is linear until cracking occurs at $0.29/\sqrt{f_c^{'}}$. The second slope of the joint stiffness model is based on the joint reinforcing steel stiffness of the cracked section where it peaks at $0.42/\sqrt{f_c^{'}}$ and at a corresponding strain of 0.007. Finaly, the third slope is based on a linear descent to an ultimate strain of 0.01 at zero principle tensile stress (Priestley 1993). In another model proposed by Mazzoni (2004) the second slope stays linear past $0.42/\sqrt{f_c^{'}}$ up to $0.62/\sqrt{f_c^{'}}$.

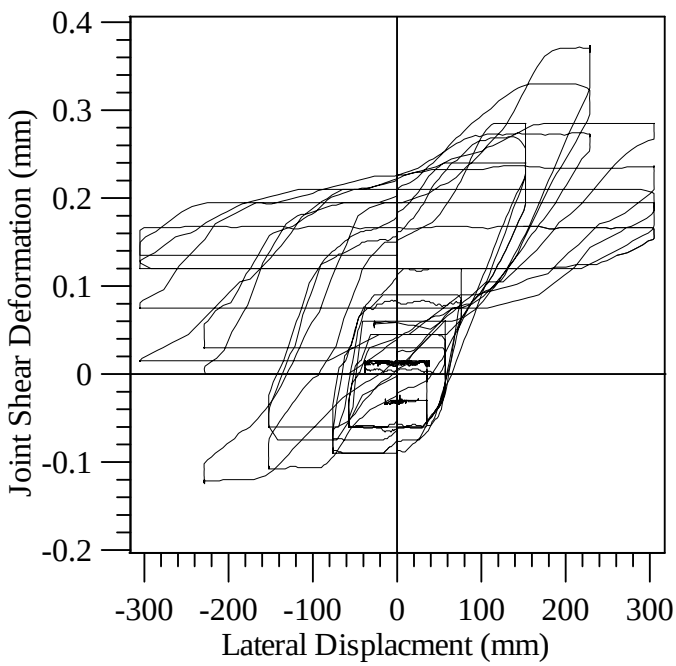

Figure 8-34. Joint Shear Deformation

In Figure 8-35 is shown the envelope of the joint shear strain versus the principle tensile stress for Unit 1, along with the models for the “weak” and the “intermediate” joints. Based on these results, it is clear that, for the most part during testing, the test data stays well above the “weak” joint limit curve. For poorly detailed joints and during subsequent reductions in the principle tensile stresses, which also reflect losses in the strength of the test unit, there is an associated significant increase in the joint shear deformations, which once again do not match the computed

data shown in this figure. In fact this moderate elastic behavior of the joint clearly indicates that joint shear failure was not the prevalent failure mode of the bent cap.

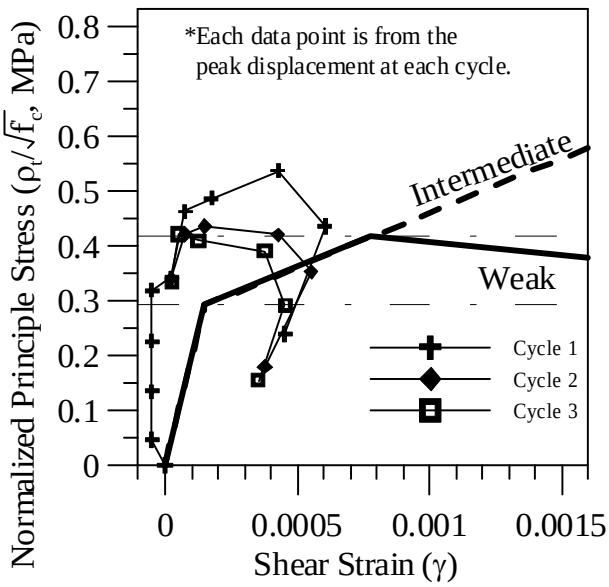

Figure 8-35. Unit 1 Principle Tensile Stress vs. Joint Shear Strain

Post-test investigations at the bottom of the cap clearly uncovered a longitudinal crack forming along the centerline of the bent cap, as shown in Figure 8-36. This indicates that the bent cap was splitting along this crack, leading to a partial anchorage failure of the column longitudinal bars and the mechanisms associated with Figure 3-11 and Figure 8-32.

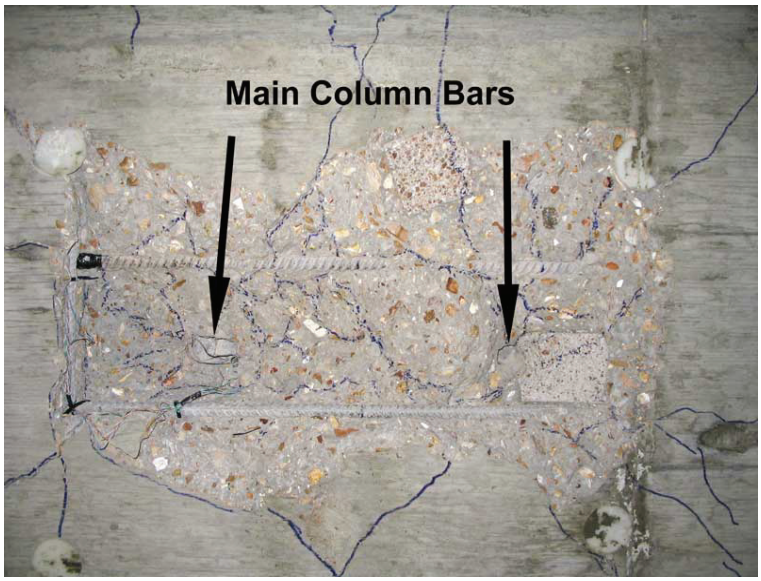

Figure 8-36. Underside of Bent Cap Cracking Pattern

8.8. RELEVANT EXPERIMENTAL RESULTS USED IN THE DESIGN OF UNIT 2

One of the main conclusions that can be drawn for these test results is that there was a progressive loss in strength due to joint shear failure, which resulted from the longitudinal splitting of the bent cap. This splitting was attributed to the fact that the transverse reinforcement going through the joint region was installed in two separate pieces leaving a gap between the two pieces. This detail solution resulted in a lack of a mechanism to proper clamp the bent cap in the transverse direction. As such, in the design of Unit 2 the transverse reinforcement going through the joint was installed continuous as described in Section 4. In Section 11.4 a different joint model is proposed and described in further detail using the data extracted from the curves shown in Figure 8-22 and Figure 8-23. This new model was then used in Section 11.5 to develop the post-test analysis for the test units, which is shown in Figure 8-22.

9. EXPERIMENTAL RESULTS – UNIT 2

This section presents observations recorded during experimental testing, including force-deformation and reinforcement strain profiles for the column and bent cap.

9.1. GENERAL TEST OBSERVATIONS

9.1.1. Force Control Load Cycles

Unit 2 was tested using the same loading protocol used for Unit 1 (see Figure 7-2). Similar observations were recorded for these two test units up to the first four cycles in force control. As in Unit 1, inception of cracking was detected at $0.50V_y$ with micro cracks developing at the bent cap interface. At this load level a single crack was observed on the bent cap, as shown in Figure 9-1. At $0.75V_y$ additional cracks developed due to strain penetrations along with cracking at the interface of the base of the column and the bent cap, as shown in Figure 9-2. At $1.00V_y$ extension of these strain penetration cracks were recorded (see Figure 9-3) along with onset of joint shear cracking as shown in Figure 9-4.

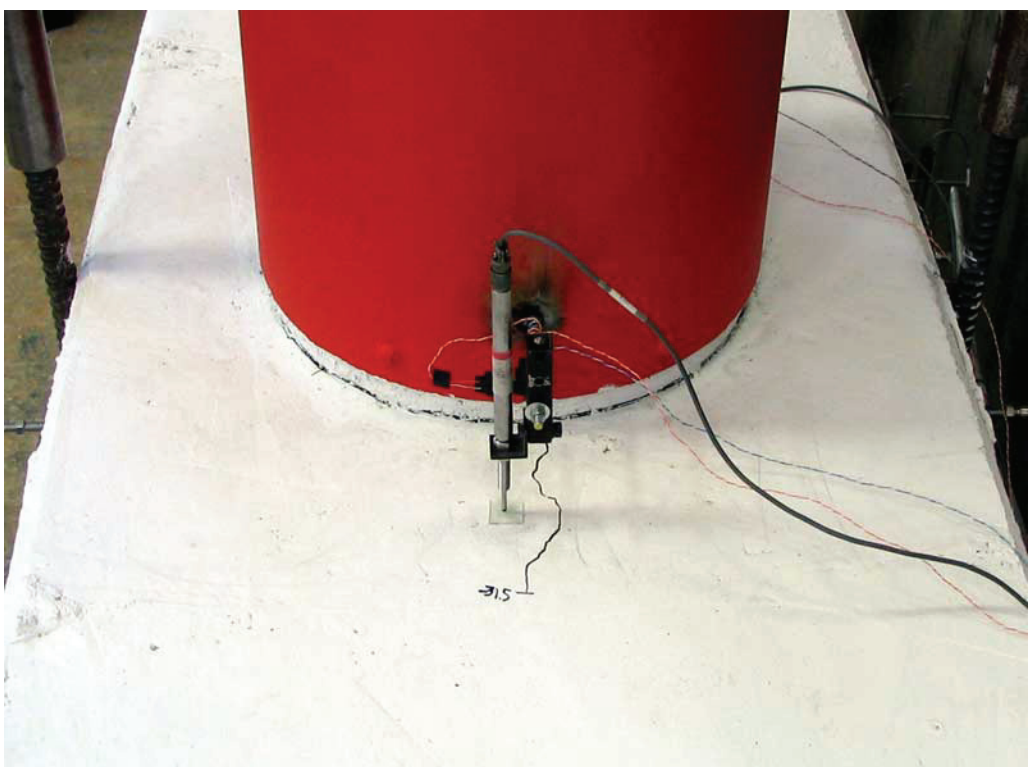

Figure 9-1. Bent Cap Cracking at $0.50V_y$

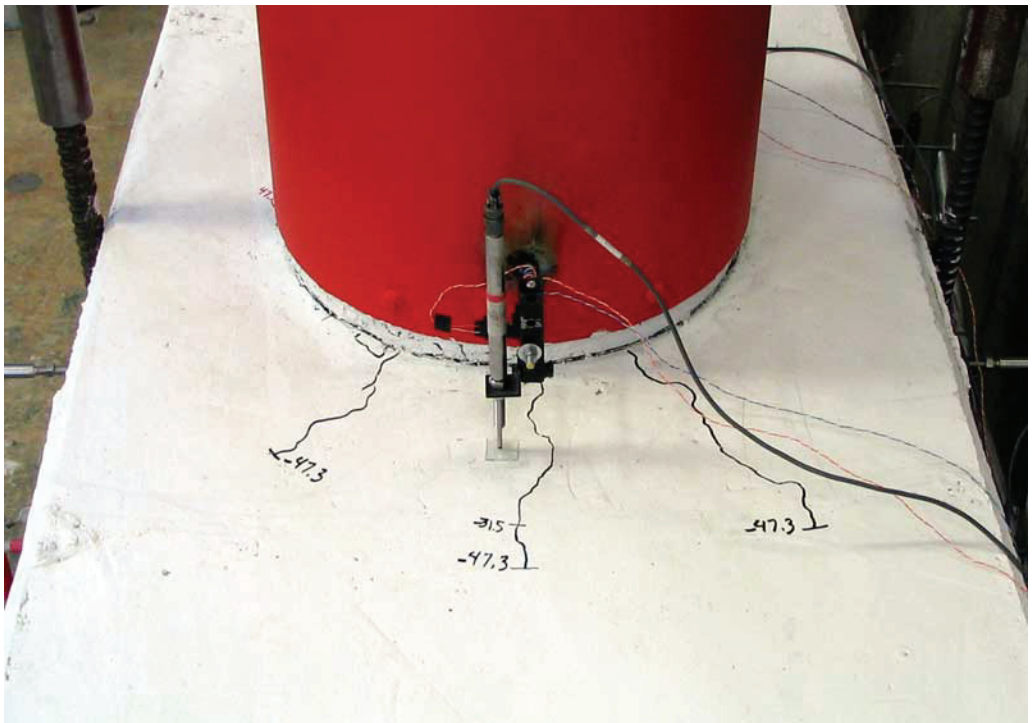

Figure 9-2. Bent Cap Cracking at 0.75V_y

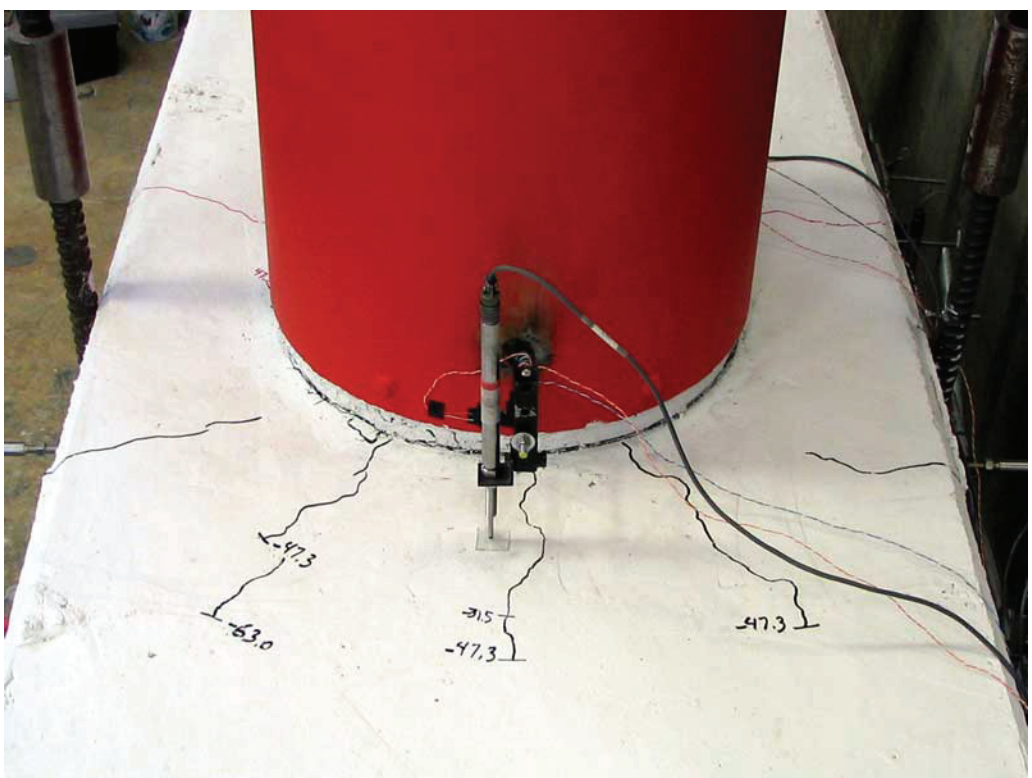

Figure 9-3. Bent Cap Cracking at 1.00V_y

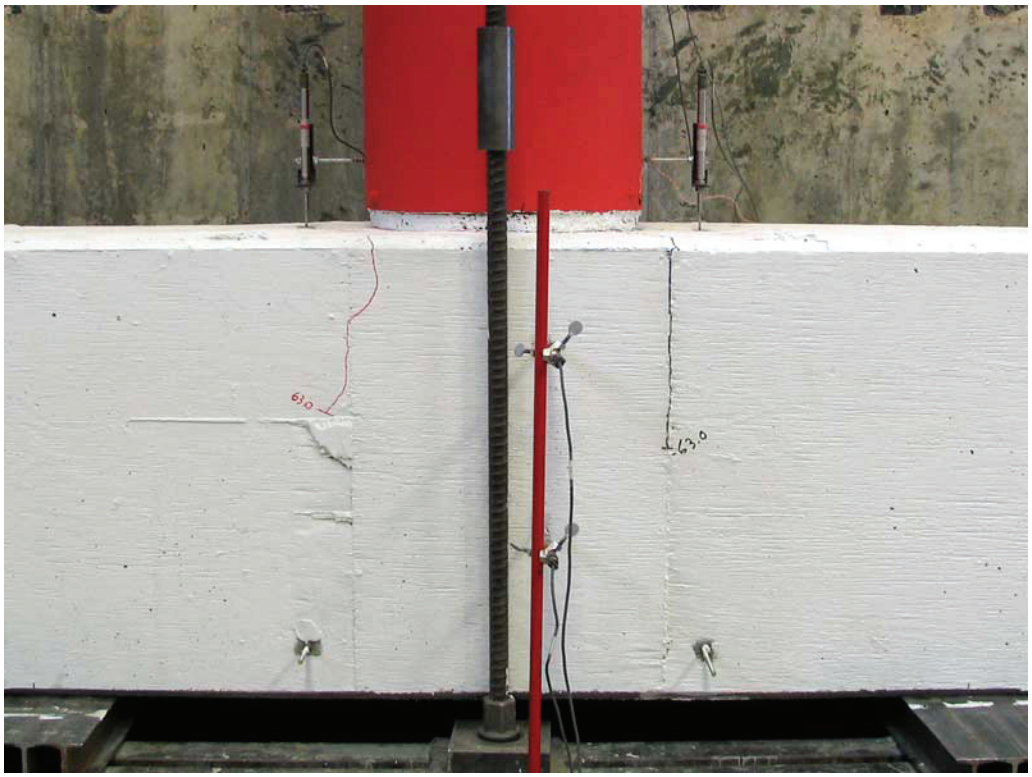

Figure 9-4. Joint Cracking at 1.00V_y

9.1.2. Displacement Control Load Cycles

After the force control load cycles the loading pattern was changed to displacement control as outlined in Section 7.3. As before, after reaching the peak displacement, at each ductility level, testing was paused on the first and last cycles to visually inspect and record damage to the unit.

- *1.0 μ_Δ [38.1 mm]:* Onset of joint shear cracking was observed in the joint region as shown in Figure 9-5. Strain penetration cracks around the column extended and onset of spalling of the cover concrete in the gap region was recorded, as shown in Figure 9-6.

- *1.5 μ_Δ [57.2 mm]:* At this level, additional joint shear cracks were recorded along with additional flexural cracking and extension to the previous marked cracks, as shown in Figure 9-7. An increase in the marked cracks resulting from strain penetration was observed by the increased cracking of the bent cap near the column, as shown Figure 9-8.

- *2.0 μ_Δ [76.2 mm]:* Additional joint shear cracking was observed along with the extension of existing joint shear cracks, as shown in Figure 9-9. Further cracking and lifting of wedges of concrete next to the column faces due to strain penetration was observed along with the onset of crushing of the column concrete, as shown in Figure 9-10.

- *4.0 μ_Δ [152.4 mm]* –After the fist cycle at ductility level 4.0, there was a moderate loss in the strength of the column. At this level, no additional joint shear cracks were recorded and only minimal extensions of the existing cracks were observed, as shown in Figure 9-11. Also it

may be concluded that at this level, the upward movement of the wedges of concrete, resulting strain penetrations, was prevented by the first line of vertical headed reinforcement, which is clear by inspection of Figure 9-12.

- *6.0 μ_Δ [228.6 mm]:* There was a continuous progression in the loss of strength of the test unit at this ductility level and at the subsequent cycles, but there were no additional joint shear cracks. Existing cracks did not extend further and remained within small widths, as shown in Figure 9-13. On the pull direction of the third cycle, additional crushing of the column concrete was observed along with buckling and fracture of one of the column longitudinal bars, as shown in Figure 9-14.

- *8.0 μ_Δ [304.8 mm]:* There was a continual decrease in the capacity of the test unit at this ductility level, but this decrease was mainly a result of the fracture of the longitudinal reinforcement. Additional fracture of the column longitudinal reinforcement was observed and detected during loading to this ductility level. Cracks propagated on the underside of the bent cap (see Figure 9-15); however, these cracks remained within small widths and no concrete wedges were separated from the bent cap, as observed during testing of Unit 1. In conclusion, joint shear cracks on the sides of the bent cap remained within small widths (see Figure 9-16), along with further crushing of the column cover concrete, as shown in Figure 9-17.

As before, after testing, all loose concrete was removed. In comparison to Unit 1 damage to the bent cap was significantly smaller, as shown in Figure 9-18. The extra two welded hoops that were placed below the interface of the bent cap and the column were effective in preventing an uncontrolled buckling of the column longitudinal reinforcement once the spalling of concrete occurred in the gap region; however, they could not prevent entirely the buckling to the column longitudinal reinforcement and the subsequent premature low cycle fatigue of this reinforcement, as shown in Figure 9-19 and Figure 9-20. As such, in the design of Unit 3 this issue was addressed by investigating the effects, either positive or negative, of reducing the steel gap region and install additional transverse reinforcement to further prevent buckling and premature low cycle fatigue of the longitudinal reinforcement. These issues were addressed during design of Unit 3 in Section 5, and will be further discussed in the body of this report.

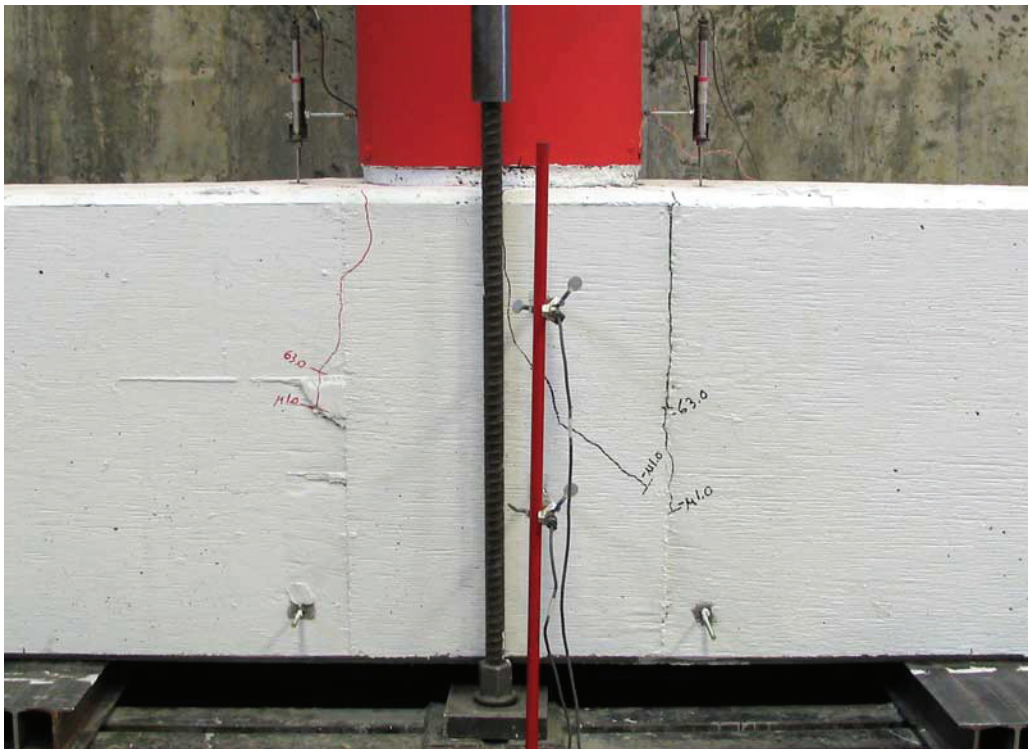

Figure 9-5. Joint Cracking at 1.0 μ_Δ

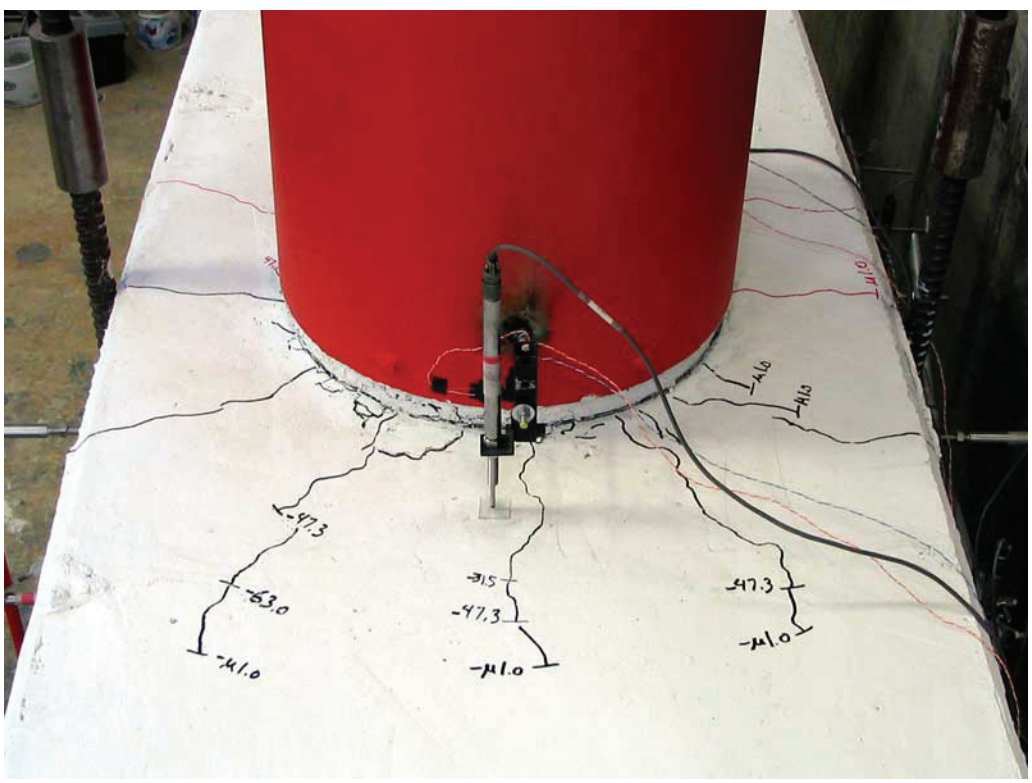

Figure 9-6. Bent Cap Cracking at 1.0 μ_Δ

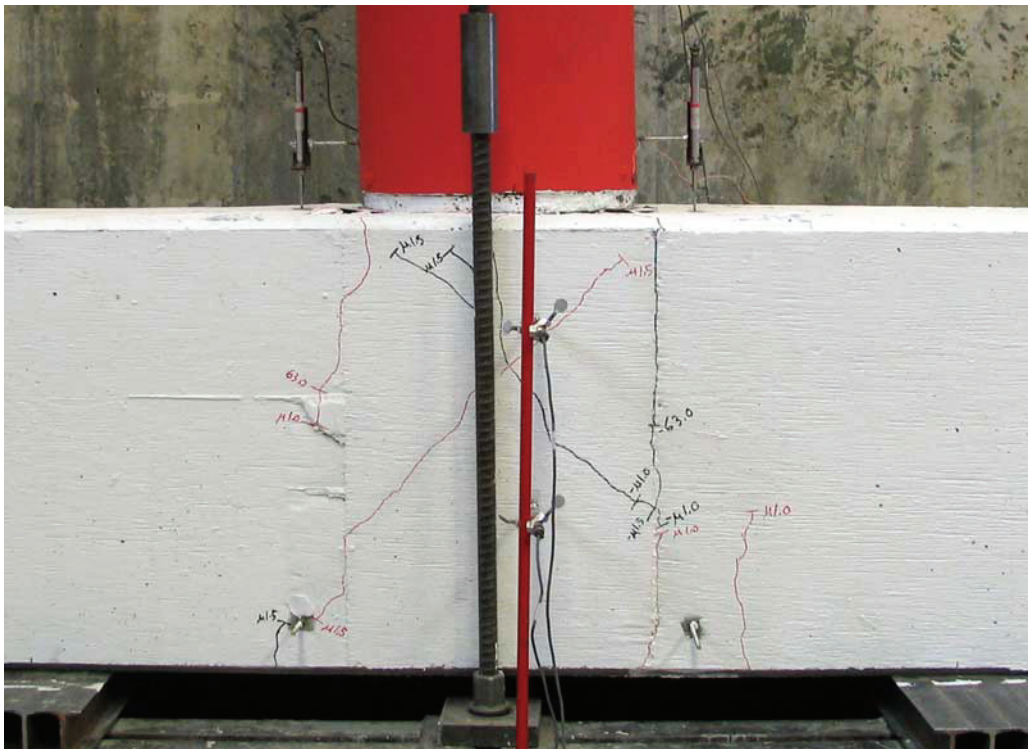

Figure 9-7. Joint Cracking at 1.5 μ_Δ

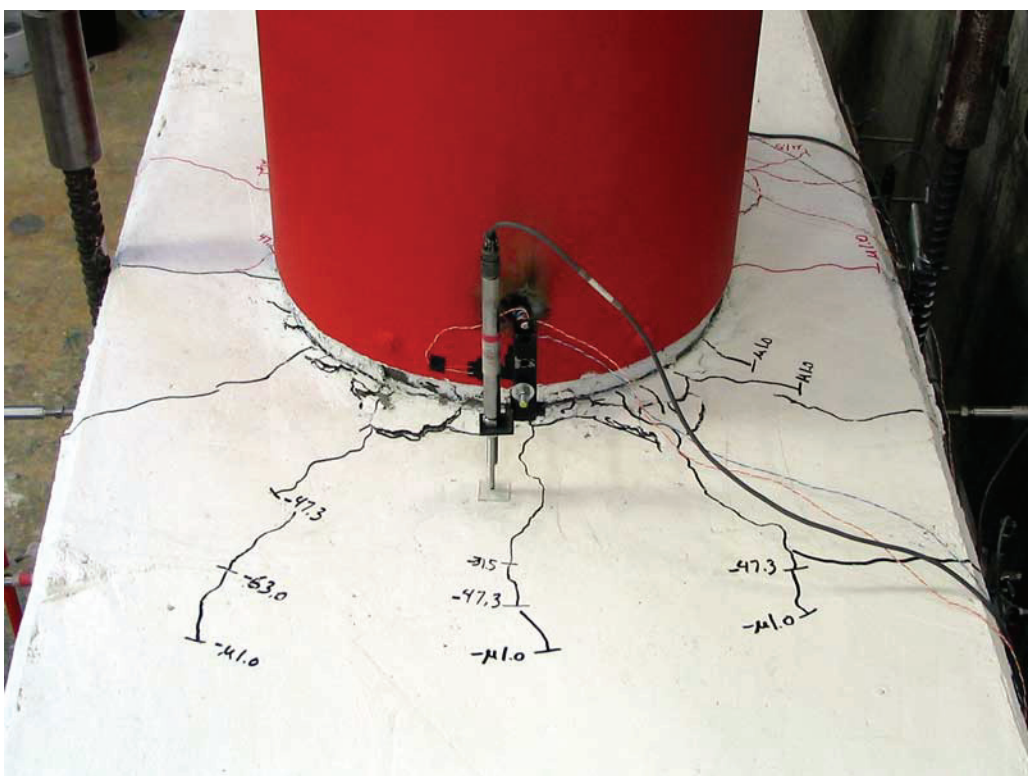

Figure 9-8. Bent Cap Cracking at 1.5 μ_Δ

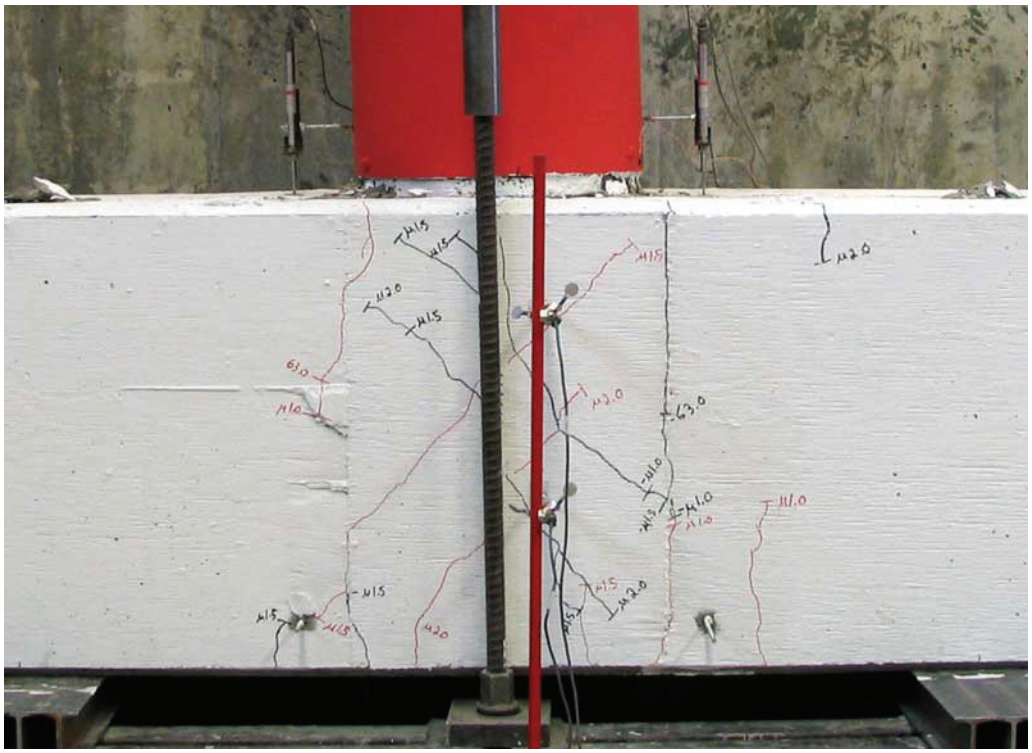

Figure 9-9. Joint Cracking at 2.0 μ_Δ

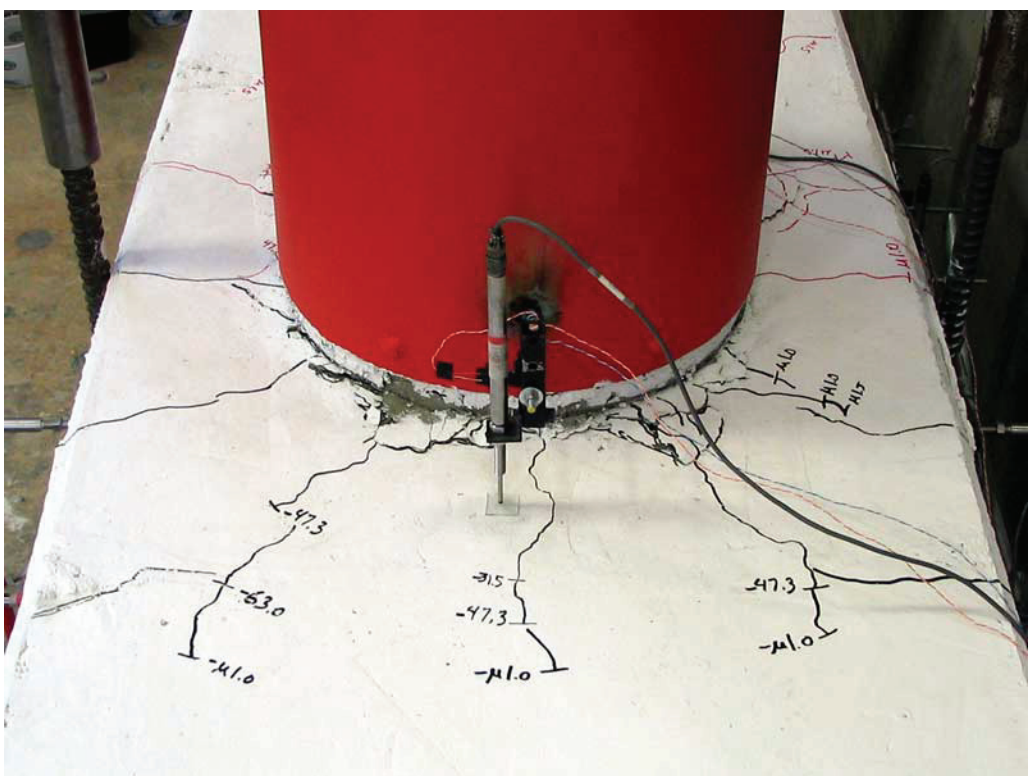

Figure 9-10. Bent Cap Cracking at 2.0 μ_Δ

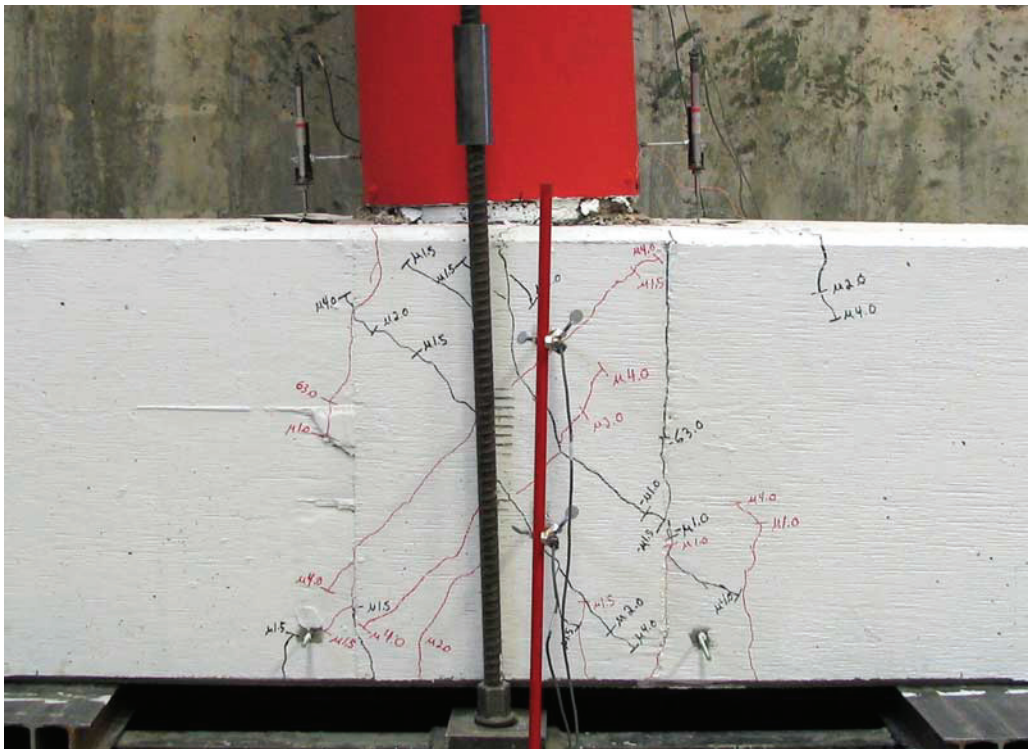

Figure 9-11. Joint Cracking at 4.0 μ_Δ

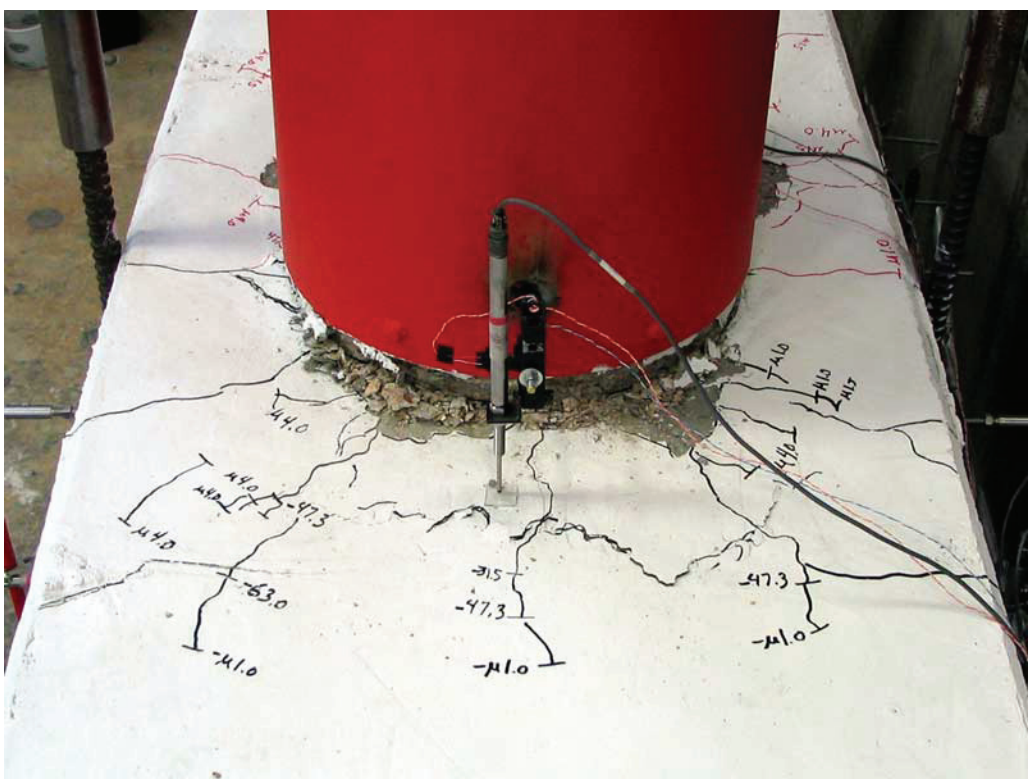

Figure 9-12. Bent Cap Cracking at 4.0 μ_Δ

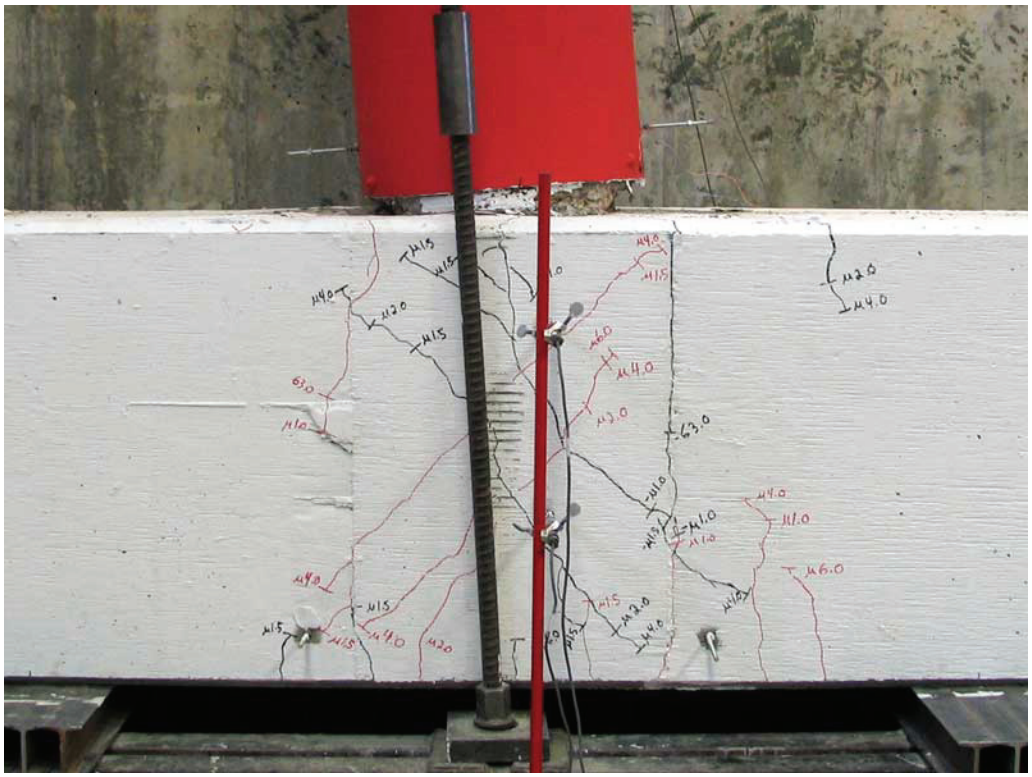

Figure 9-13. Joint Cracking at 6.0 μ_Δ

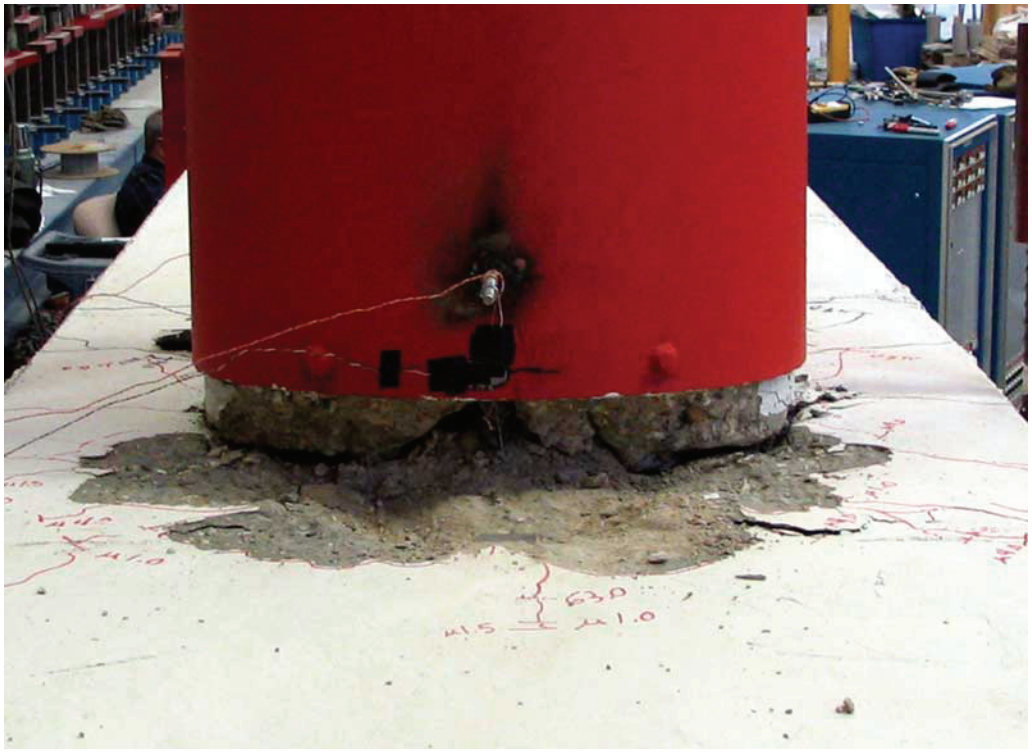

Figure 9-14. Bent Cap Cracking at 6.0 μ_Δ

Figure 9-15. Bottom Cracking at 8.0 μ_Δ

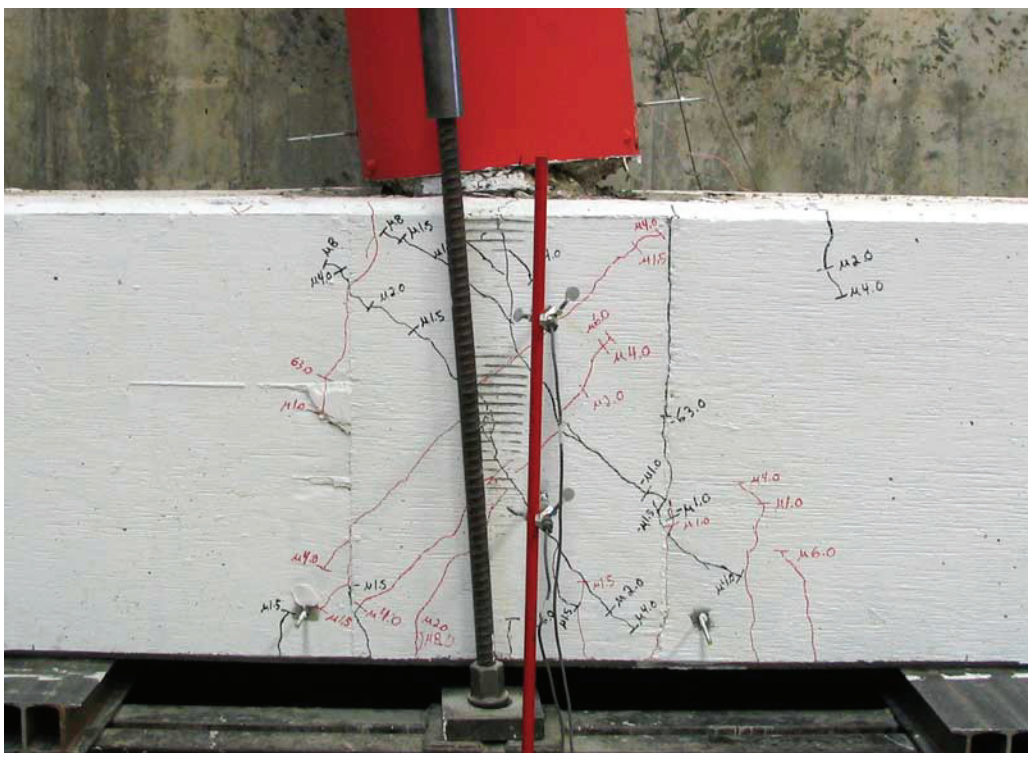

Figure 9-16. Joint Cracking at 8.0 μ_Δ

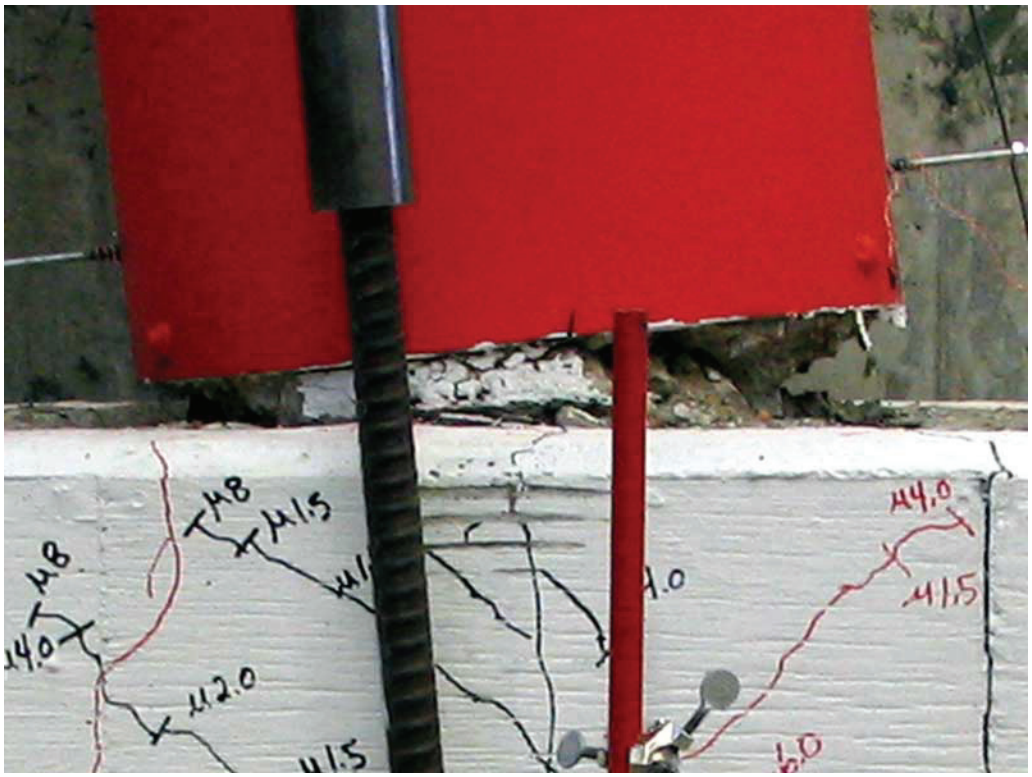

Figure 9-17. Column Crushing at 8.0 μ_Δ

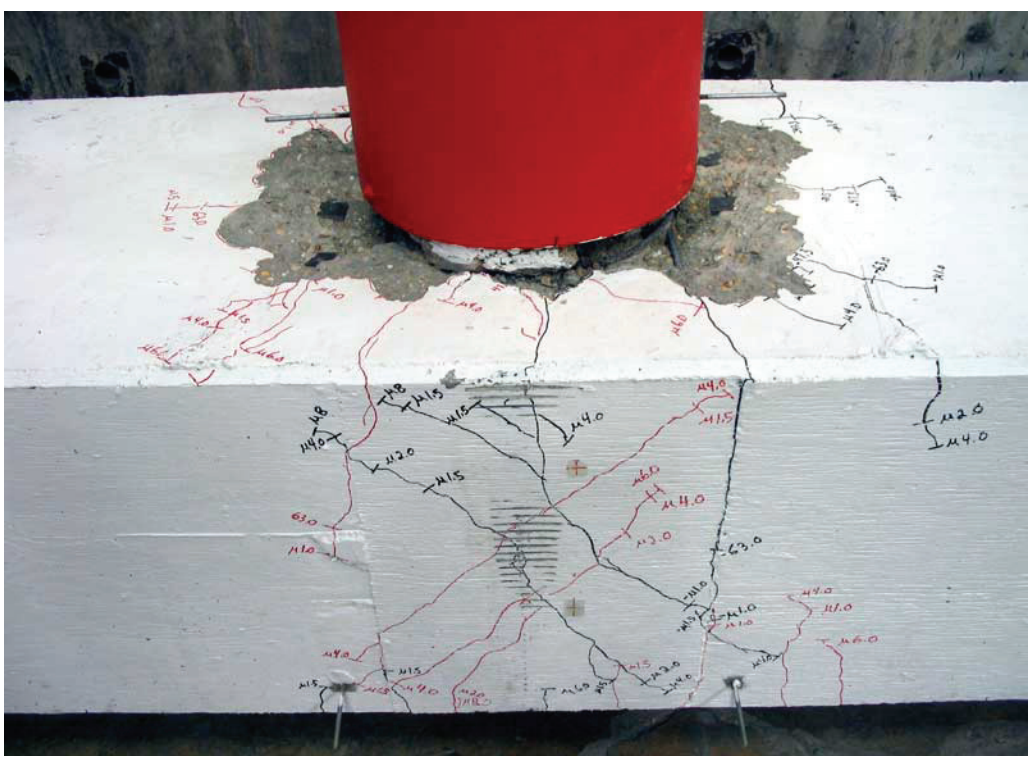

Figure 9-18. Final Damage

Figure 9-19. Hoop Buckling Side "A"

Figure 9-20. Hoop Buckling Side "B"

9.2. LOAD DEFORMATION RESPONSE

Unit 2 was tested following the loading protocol shown in Figure 7-2 and the load deformation response of Unit 2 is shown in Figure 9-21. This figure shows that Unit 2 response displayed similar features as those described for Unit 1. By comparing the load deformation response for these two test units, one may conclude that the response of Unit 2 displayed an improvement in the seismic response in terms of damage and load degradation at higher ductility levels. Further comparisons are described in greater detail in Section 11.1. As in Unit 1, based on a direct investigation of the test results the new displacement at ductility level one was also set at 31.5 mm.

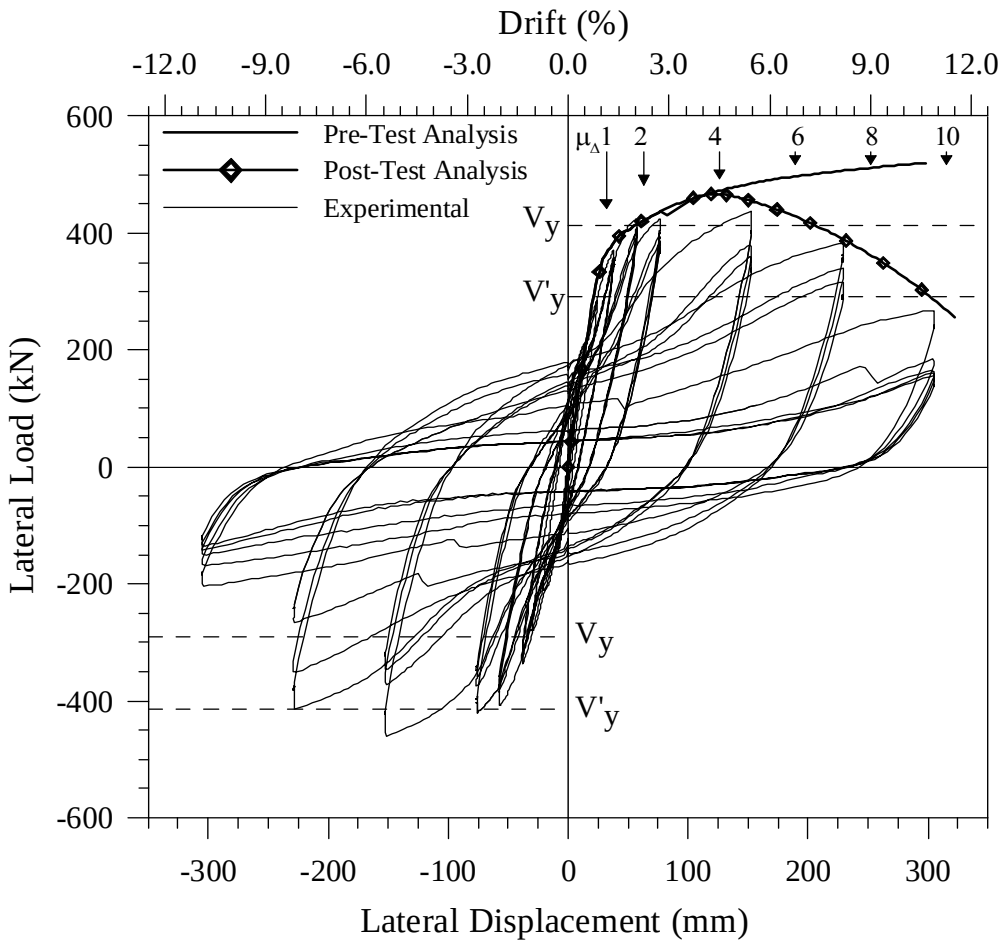

Figure 9-21. Unit 2 – Load Displacement Response

In Unit 2 the maximum registered lateral load was also recorded during the first cycle to the displacement of 152.4 mm. In the push and pull directions the registered lateral loads were +440 and -460 kN, respectively, which are slightly higher than those registered in Unit 1. Between the first and second cycles the drop in the lateral load was the same as in Unit 1 or approximately 17%, and between the second and third cycles the drop in the lateral load was 5%, indicating

stability in the response of this unit. Comparisons of load degradation at higher ductility levels are also described in further detail in Section 11.1.

In Unit 2 higher levels of load degradation were observed at the displacement level of 228.6 mm, which is one of the main differences in the response of these two units. As before, the unit exhibit significant levels of strain penetration around the column but this was limited to the first row of vertical headed reinforcement. Compared to Unit 1 these levels of strain penetration and corresponding damage extended much further in the bent cap (see Figure 9-22).

Unlike Unit 1, the first significant drop in the lateral load capacity of the test unit below the theoretical yield load level was not observed until the first cycle to the displacement of 304.8 mm. However, it is important to recognize that, when loading to the displacement of 228.6 mm and during the pull direction of the third cycle, low cycle fatigue fracture of the longitudinal reinforcement was observed, as previously discussed in Section 9.1.2. This is a clear indication that the loss in the strength of the test unit during the last cycles was predominantly due to fracture of the longitudinal reinforcement. In total, four column longitudinal bars buckled and fractured due to low cycle fatigue during displacement ductility levels 6 and 8 indicating reserve capacity in the joint against pullout of the column reinforcement.

In addition, cracking due to joint shear was minimal and all joint shear cracks were small as shown in Figure 9-22. Some level of cracking occurred on the underside of the bent cap but was significantly smaller than in Unit 1 as shown in Figure 9-23, which also indicates an improvement in the seismic response of the test unit.

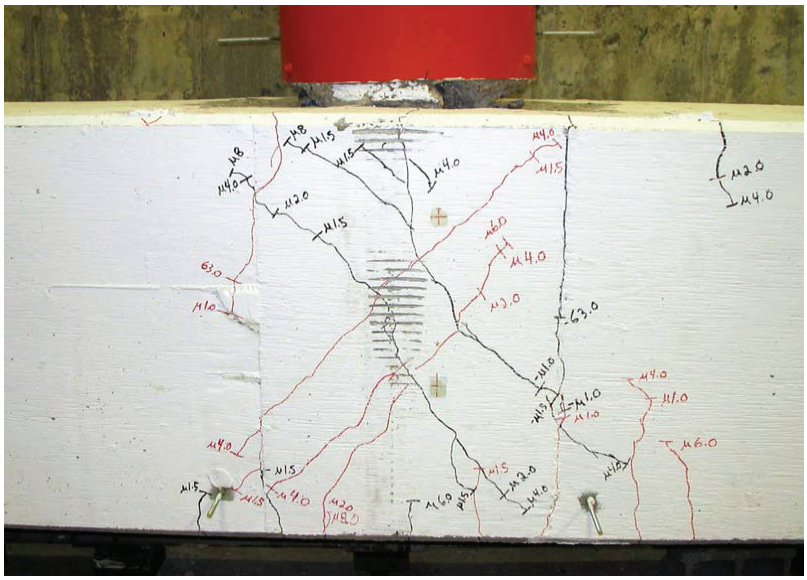

Figure 9-22. Unit 2 Joint Shear Cracks

Figure 9-23. Cracking on Underside of Bent Cap

9.3. LOAD VS. CURVATURE RESPONSE

Figure 9-24 shows the measured lateral load versus the computed curvatures at the column to the bent cap interface for Unit 2. As in Unit 1, the diagram depicted in this figure also indicates a good correlation between the pre-test analysis and the experimental test results during the initial stages of testing. However, after peak load there is a considerable deviation between these two curves. As in Unit 1, this can be attributed to joint flexibilities that where not considered during the pre-test analysis.

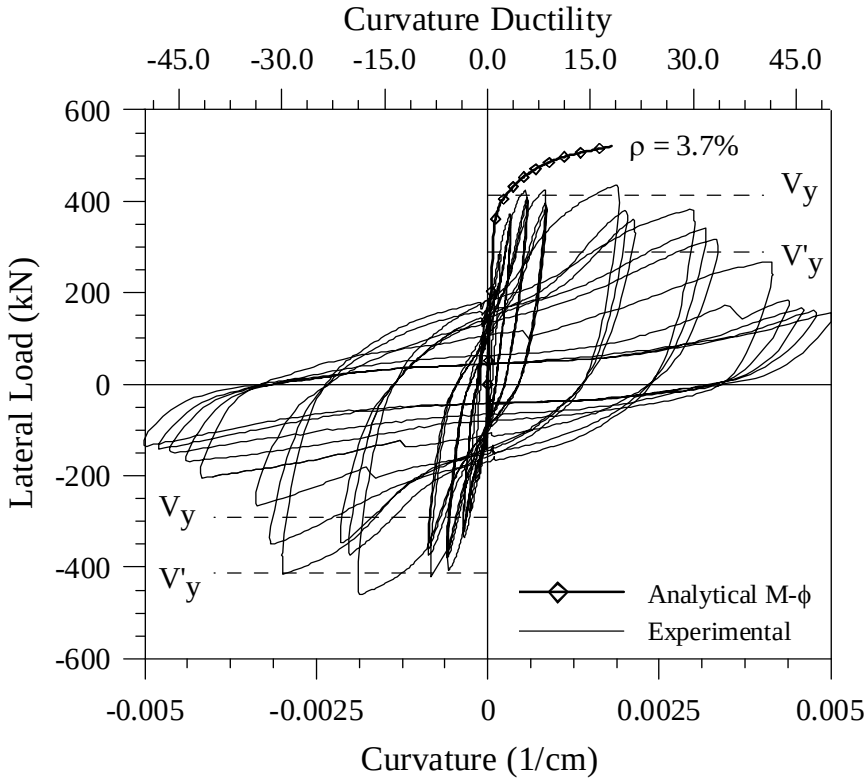

Figure 9-24. Unit 2 – Load versus Curvature Response

9.4. COLUMN LONGITUDINAL REINFORCEMENT STRAINS

The strain histories of the column longitudinal reinforcement gauges at the interface of the column and bent cap for side "A" and side "B" are shown in Figure 9-25 and Figure 9-26, respectively. The yield strain of the column longitudinal reinforcement occurred at ±2,740με as determined from tensile testing. The strain profiles for each side of the column are shown in Figure 9-27 and Figure 9-28. Onset of yielding of the main column longitudinal bars occurred at μ1.0 on either side of the column.

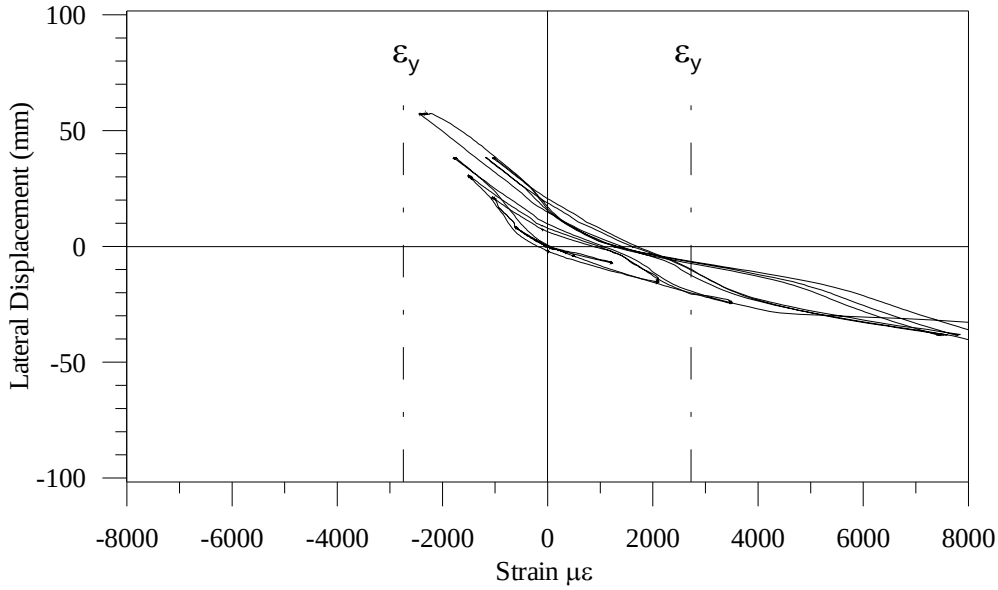

Figure 9-25. Strain Gauge History – C4a

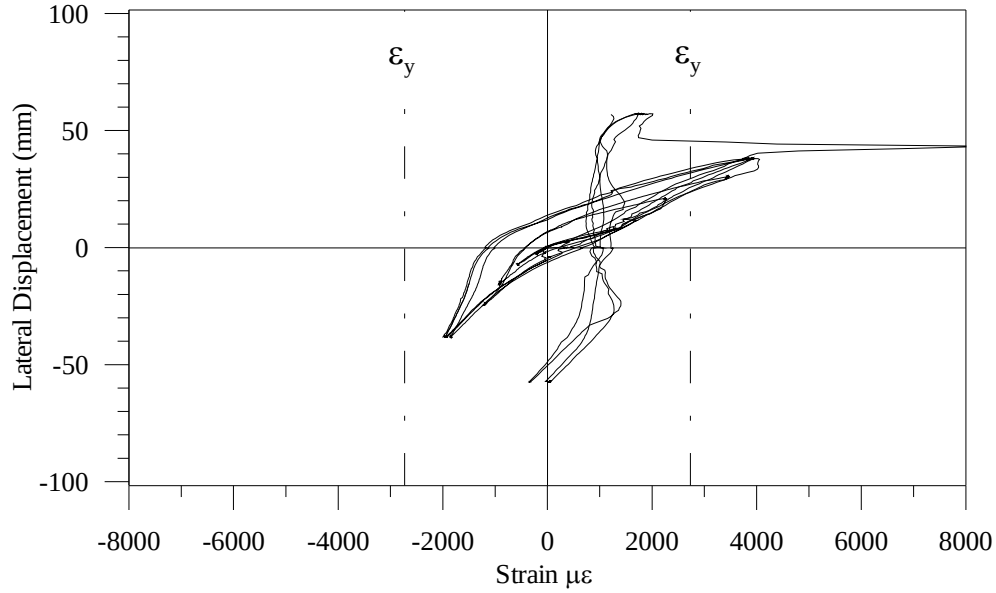

Figure 9-26. Strain Gauge History – C4b

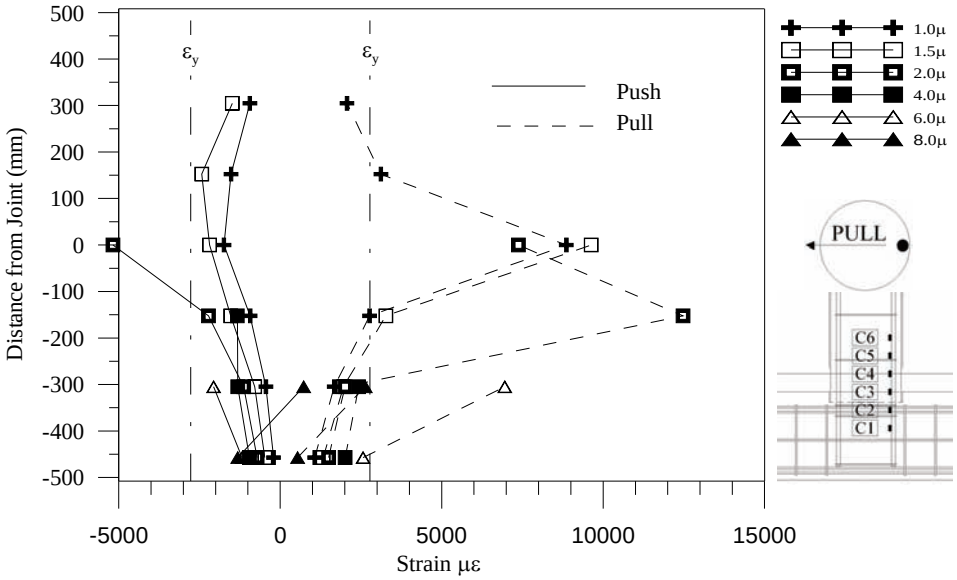

Figure 9-27. Strain Gauge Profile – Side "A"

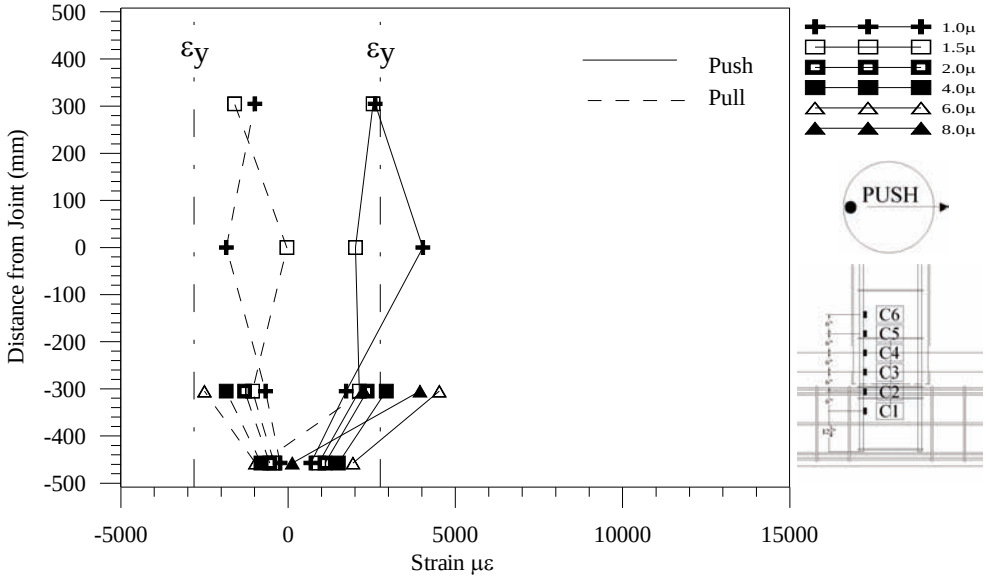

Figure 9-28. Strain Gauge Profile – Side "B"

9.5. JOINT SHEAR REINFORCEMENT STRAIN PROFILES

Strain profiles developed from gauges installed on the joint shear reinforcement are presented in this section. The yield strain of the as-built and retrofit shear reinforcement occurred, respectively, at ±2,191με and ±2,630 με, which were determined from tensile pull-out tests. Figure 9-29 and Figure 9-30 are the strain profiles for the stirrups in the as-built and retrofit sections, respectively. These strain profiles clearly show that these stirrups stayed below the yield level, which corroborate the observations recorded during testing that the diagonal cracks through the joint region remained small in width.

During the initial stages of testing and up to the ductility level of one, strain levels in these reinforcements were negligible, indicating no shear cracks had yet developed up to this level, which matched results observed during testing. At later stages of testing, strains in both the as-built and the retrofit reinforcement achieved approximately the same level of strain, which is a strong indication that once again composite action developed between these two sections. Beyond the column face, the strain in the stirrups quickly decreased, indicating that shear strains were primarily confined within a distance of $h_b/2$ away from the column faces, which matched the extent of diagonal cracking in the bent cap.

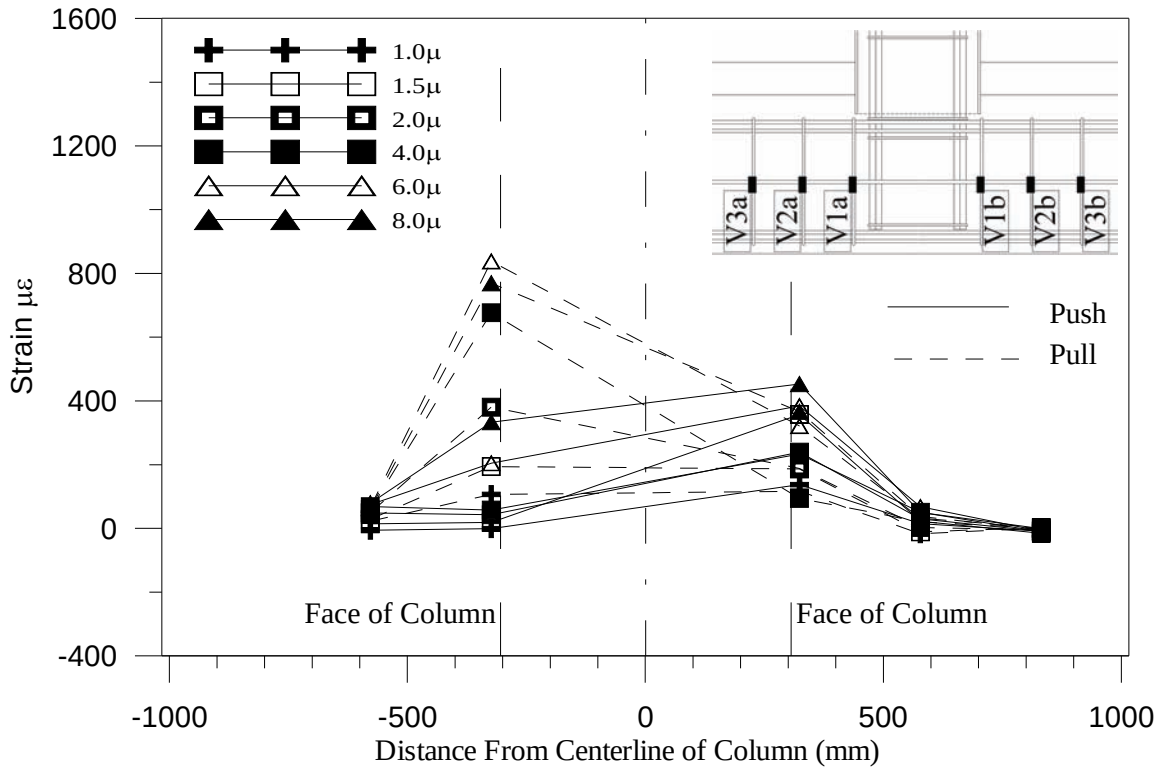

Figure 9-29. Strain Profiles – As-Built Section

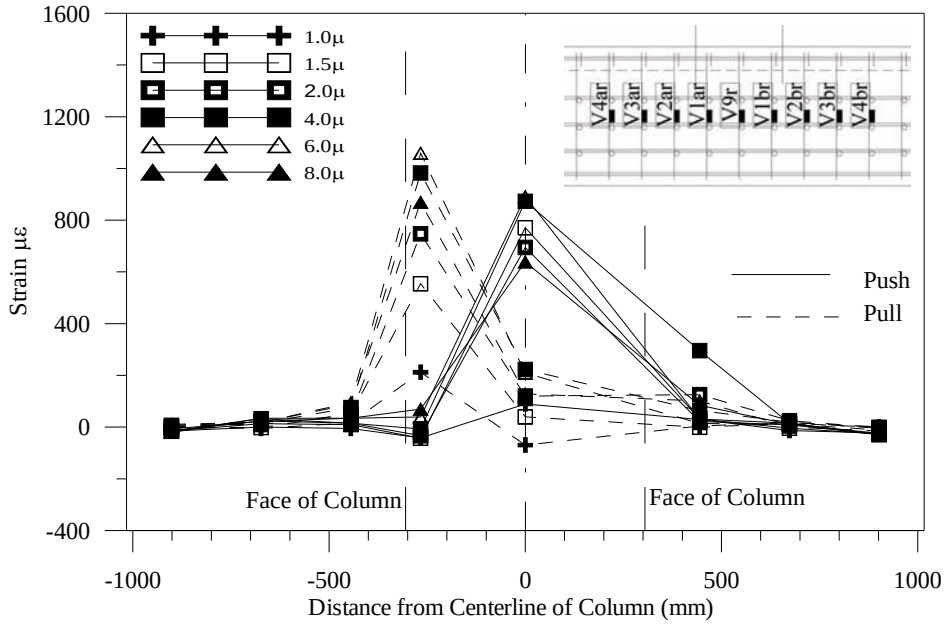

Figure 9-30. Strain Profiles – Retrofit Section

9.6. BENT CAP LONGITUDINAL REINFORCEMENT STRAINS

The following section presents the strain profiles developed for the bent cap longitudinal reinforcement. Based on tensile pull-out tests, the measured yield strain for the as-built longitudinal was 2,807 με. The yield strain for the retrofit longitudinal reinforcement was 2,604 με.

9.6.1. Strain Profiles - Bottom Reinforcement

Referring to the strain profiles depicted in Figure 9-31 and Figure 9-32, in both of the as-built and retrofit sections, the steel did not yield, indicating that the bent cap remained essentially elastic. For similar locations, the strains in both the retrofit steel and the as-built steel achieved similar strain profiles and values, indicating once again that the entire bent cap acted as one unit. As in Unit 1, although the applied lateral load decreased at higher ductility levels, the strains in the longitudinal reinforcement at the bottom of the bent cap continued to increase, as shown in these profiles. However, this increased was not as pronounced, and in fact the peak registered values in Unit 2 was nearly 1,000 με or half of those registered in Unit 1, which strongly suggested that any slipping of the column longitudinal reinforcement and its associated mechanisms as described by Figure 3-11 and Figure 8-32 were negligible.

Strain profiles for the top longitudinal reinforcement were not developed for this test unit because strain gages were malfunctioning at the onset of testing.

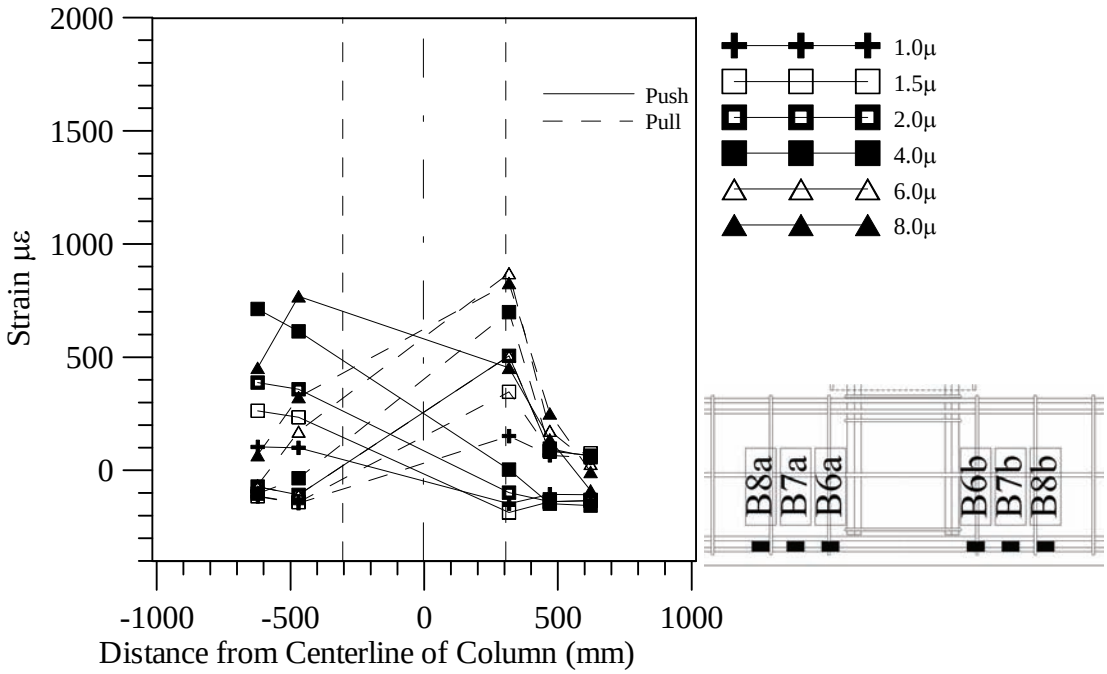

Figure 9-31. Strain Profiles – As-Built Section

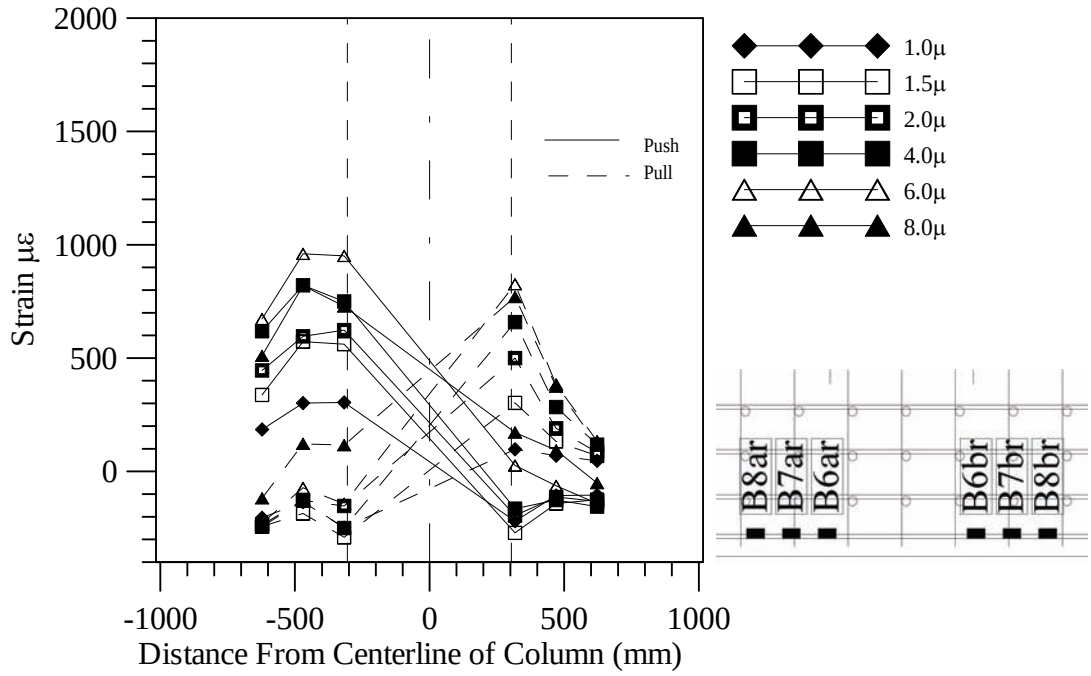

Figure 9-32. Strain Profiles – Retrofit Section

9.7. JOINT SHEAR ANALYSIS

As in Unit 1, the load deformation response for Unit 2 clearly shows a progressive loss in strength, and based on observations and experimental results, is mainly justified by flexibilities originating from within the joint region and, not necessarily a result of poor performance of the flexural or shear response of the column. Computed shear deformations are shown in Figure 9-33, which are nearly equal to those computed for Unit 1. These values once again do not justify typical values associated with joint shear failure.

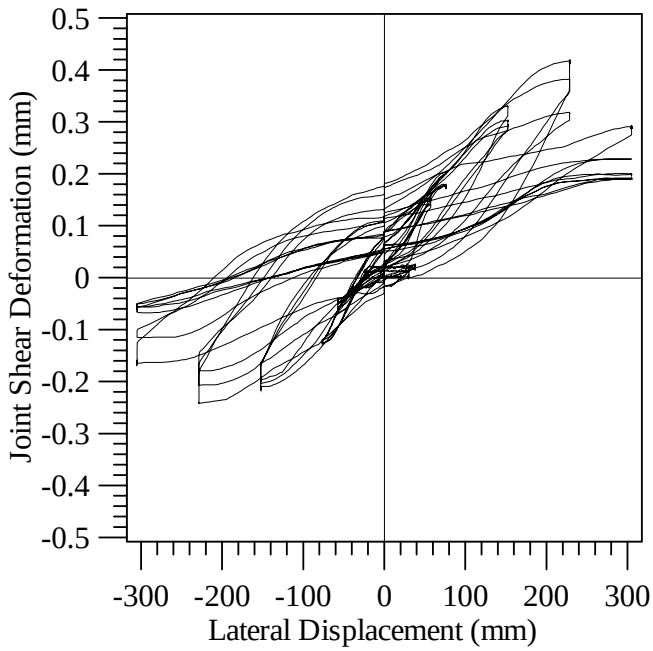

Figure 9-33. Specimen #2 Joint Shear Deformation

Furthermore, the maximum recorded strains in the bent cap top transverse reinforcement was 1,281με, while the maximum achieved strains in the transverse headed reinforcement was 506με, as shown in the strain histories presented in Figure 9-34 and Figure 9-35, respectively. These values are smaller than the 1,500με limit, which was stipulated in design given by Eq. (3-18) and recommended by Priestley (1996). This is an indication that the amount of reinforcement provided was adequate, and the continuous transverse headed reinforcement was effective in preventing splitting and excessive transverse dilations in the bent cap,

As in Figure 8-35, in Figure 9-36 is shown the envelope for Unit 2. Similar results may be inferred from this test data, which indicates that joint shear failure was not the prevalent failure mode which caused the unit's progressive loss in strength; but, instead low cycle fatigue fracture of the longitudinal reinforcement. Further comparisons between the response of these two test units is described in Section 11.

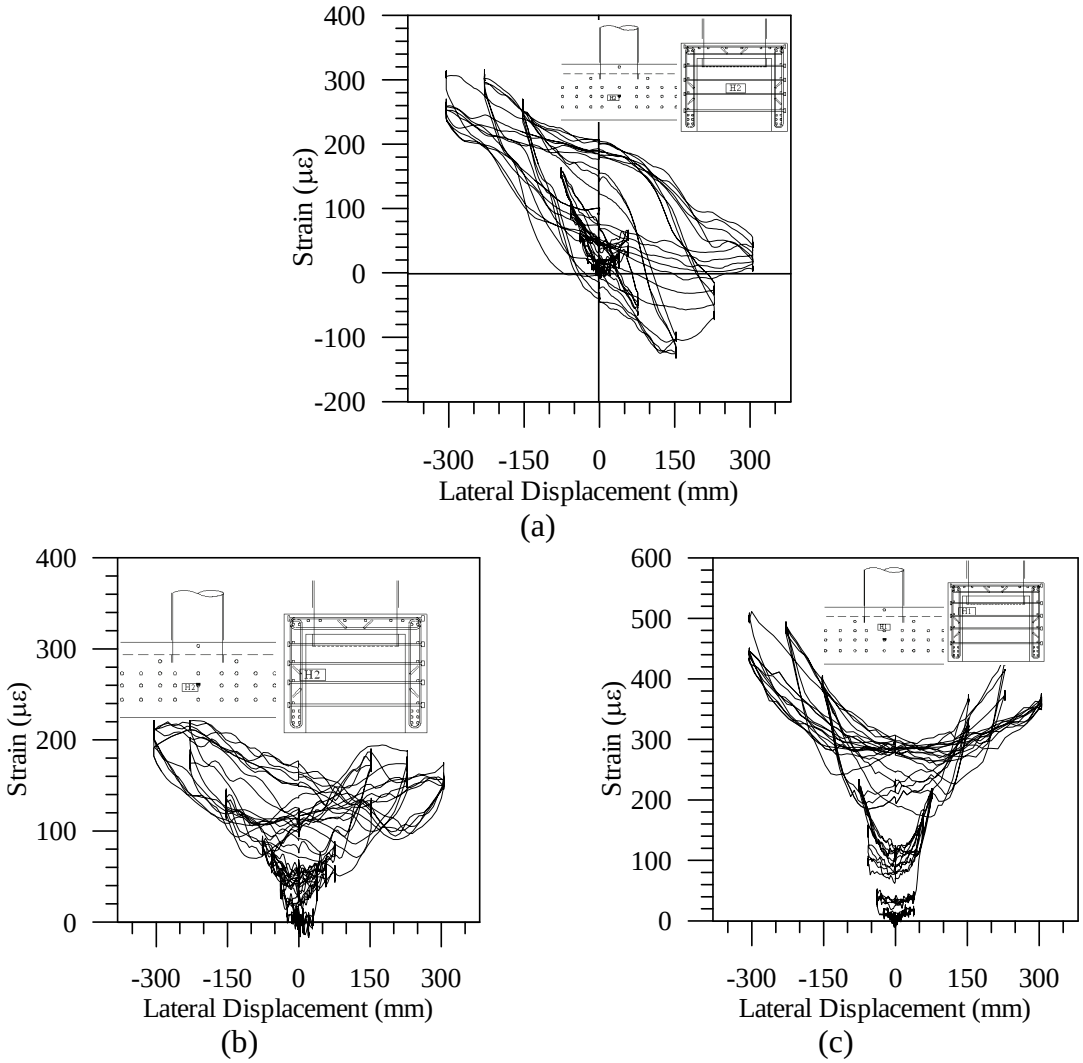

Figure 9-34. Unit 2 Headed Transverse Reinforcement Strain History

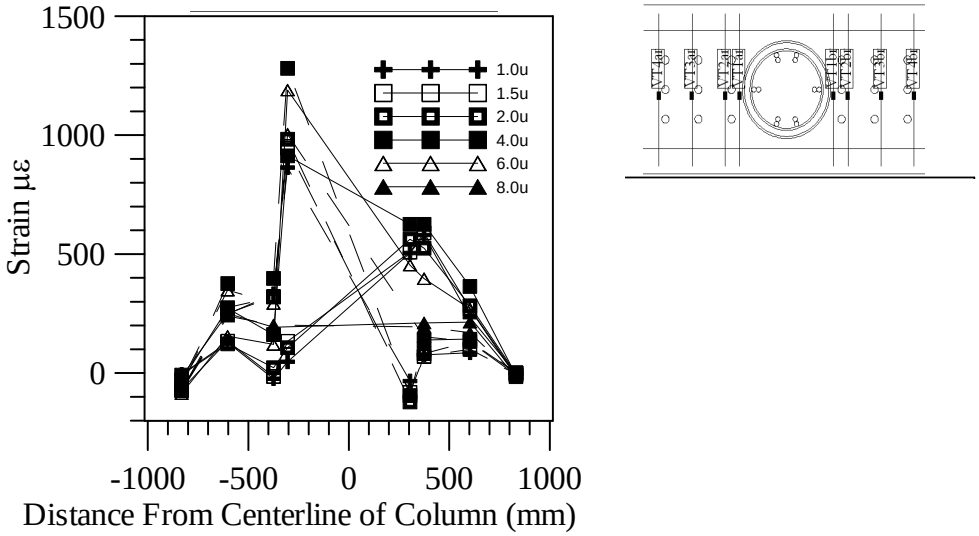

Figure 9-35. Unit 2 Top Transverse Reinforcement Strain Profile

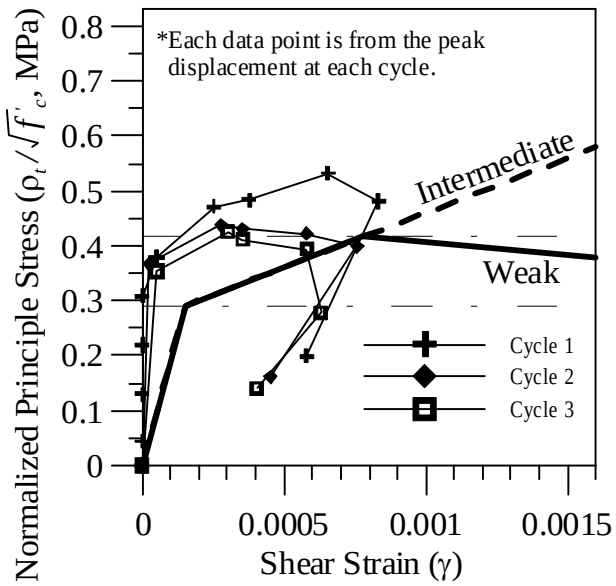

Figure 9-36. Unit 2 Principle Tensile Stress vs. Joint Shear Strain

10. EXPERIMENTAL RESULTS – UNIT 3

As in the previous two sections, this section presents observations recorded during testing, including force-deformation and reinforcement strain profiles for the column and the bent cap.

10.1. GENERAL TEST OBSERVATIONS

10.1.1. Force Control Load Cycles

Unit 3 was loaded following the loading protocol shown in Figure 7-2, which was identical to the loading protocol used for testing of Units 1 and 2. Onset of cracking was detected at $1.00V_y$ with cracks forming on the bent cap top surface, which once again indicates onset of strain penetration, as shown in Figure 10-1. During the force control cycles no other damage level was recorded for this test unit.

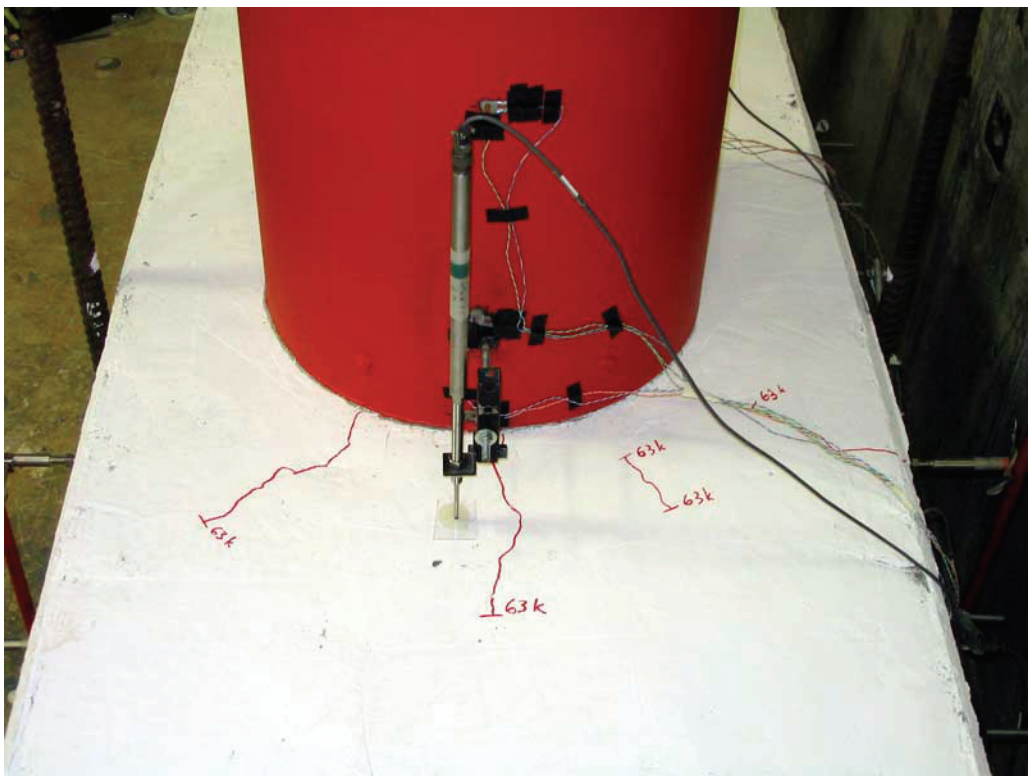

Figure 10-1. Bent Cap Cracking at $1.00V_y$

10.1.2. Displacement Control Load Cycles

After the four force control load cycles the loading pattern was changed to displacement control as outlined in Section 7.3. During the first and last cycle peak reversals and at each displacement ductility level testing was paused to visually inspect and record damage to the test unit. It is important to note that besides some minor differences nearly the same observations were recorded for the three units.

- *1.0 μ_Δ [38.1 mm]:* Onset of joint shear cracking was observed in the joint region as shown in Figure 10-2. As shown in Figure 10-3, previously recorded cracks depicting strain penetration grew in width, indicating the longitudinal bars were properly anchored to the joint.

- *1.5 μ_Δ [57.2 mm]:* There was additional joint shear cracking including extension of previous cracks along with the onset of flexural cracking in the bent cap as shown in Figure 10-4. Additional cracking on the bent cap due to strain penetration was minimal (see Figure 10-5).

- *2.0 μ_Δ [76.2 mm]:* Additional joint shear cracking and flexural cracking was observed along with the extension of existing joint shear and flexural cracks as shown in Figure 10-6. Additional cracking and extension of existing cracks was observed on the bent cap due to strain penetration along with onset of crushing of the column cover concrete as shown in Figure 10-7.

- *4.0 μ_Δ [152.4 mm]:* After the fist cycle at ductility level 4.0, there was a loss of capacity in the column, At this stage, no additional joint shear cracks were observed and minimal extension to the existing cracks was visible. Additional flexural cracks were observed on the side of the bent cap along with extension of existing flexural cracks, as shown in Figure 10-8. Similar to the previous two test units, concrete wedges originating from strain penetration on either side of the column lifted and the first line of headed reinforcement prevented further cracking into the bent cap, as shown in Figure 10-9.

- *6.0 μ_Δ [228.6 mm]:* At this ductility level, a progressive loss in the strength of the test unit was recorded; however, it is worth indicating that the first cycle at this ductility level matched the stiffness of the second and third cycles at 4.0μ. At the subsequent cycles a progressive loss in the capacity of the test unit was recorded but no additional joint shear cracks or extension of existing cracks were observed, as seen Figure 10-10. Additional crushing of the column cover concrete was observed along with the widening of one of the existing cracks on the surface of the bent, as shown in Figure 10-11. Onset of cracking on the underside side of the bent cap was observed at this level.

- *8.0 μ_Δ [304.8 mm]:* A continual loss in capacity was recorded at this ductility level. No further extension of joint shear cracks was observed and previously recorded cracks stayed within constant widths for the remaining of the test. As before, concrete wedges developing as a result of strain penetrations from the column longitudinal reinforcement extended on the sides of the bent cap as indicated by the horizontal crack shown in Figure 10-12. On the top surface of the bent cap, it is visible the lifting of these concrete wedges, as shown in Figure 10-13 and Figure 10-14. On the bottom surface of the bent cap and as shown in Figure 10-15, concrete wedges separated from the bent cap , which is indicative of onset of anchorage failure of the column longitudinal reinforcement.

As in the previous two test units, after testing all loose cracked concrete was removed. The extent of damage to the bent cap was limited to the first row of headed reinforcement, as shown

in Figure 10-16. Reducing the gap region to 13 mm prevented excessive crushing of the column concrete as shown in Figure 10-17. This also prevented buckling of the column longitudinal reinforcement after spalling of the cover concrete and subsequently premature low cyclic fatigue fracture of this reinforcement. The extent of the cracking on the underside of the bent cap is shown in Figure 10-18. Further comparisons and discussions with Units 1 and 2 are discussed in Section 11.

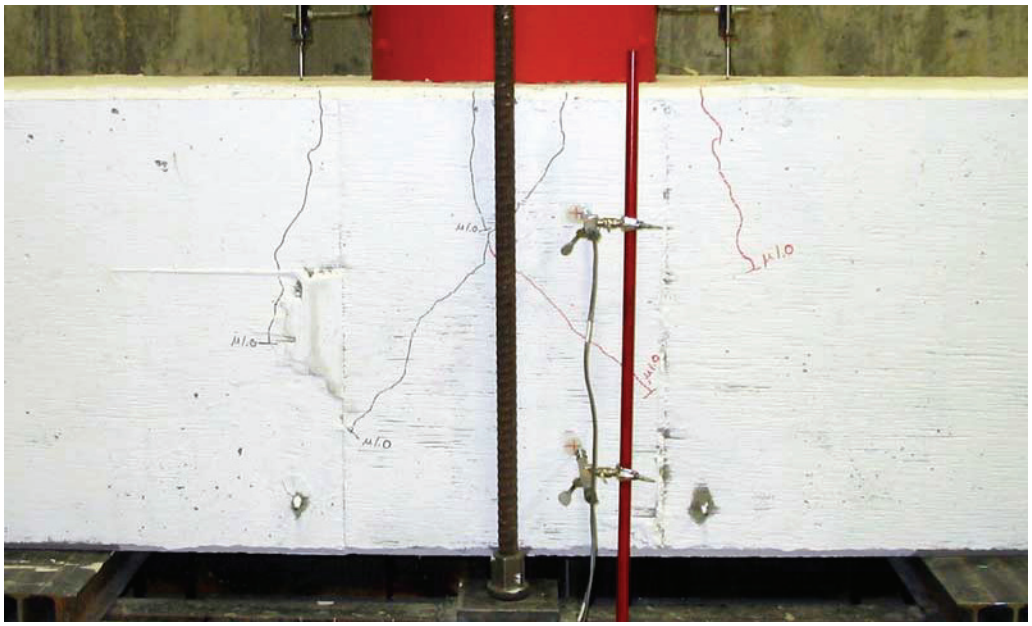

Figure 10-2. Joint Cracking at 1.0 μ_Δ

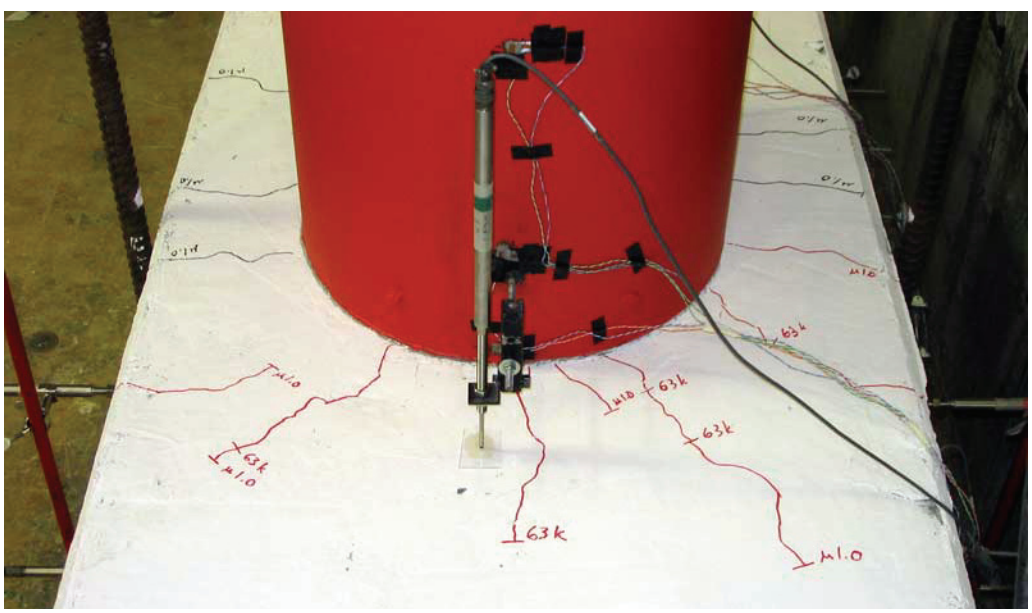

Figure 10-3. Bent Cap Cracking at 1.0 μ_Δ

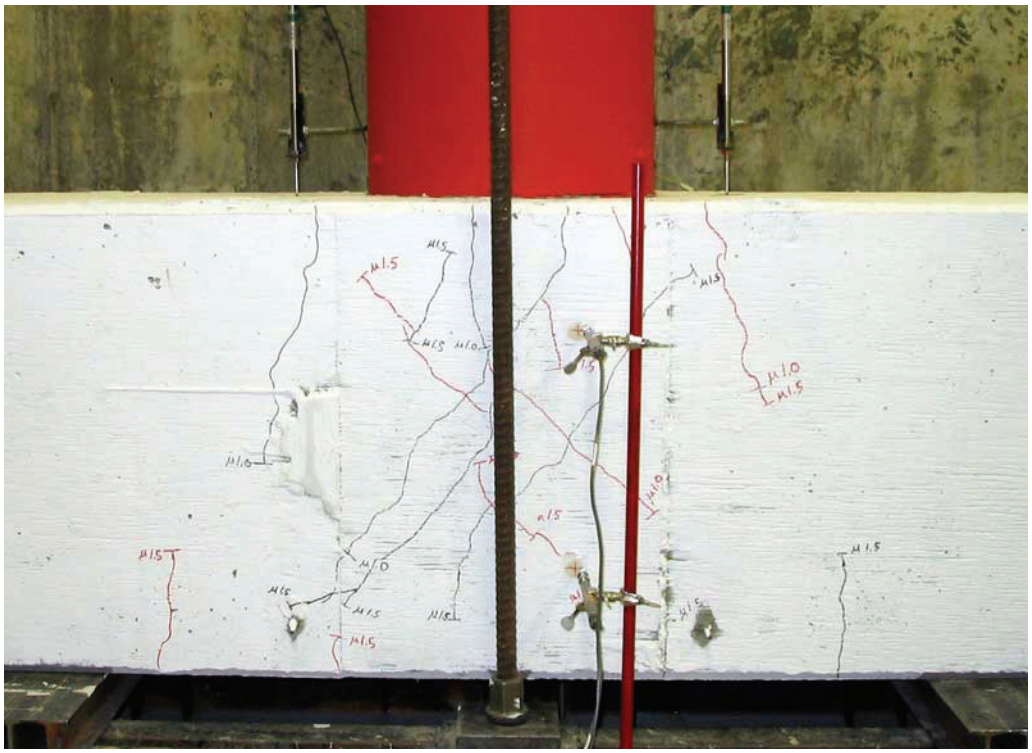

Figure 10-4. Joint Cracking at 1.5 μ_Δ

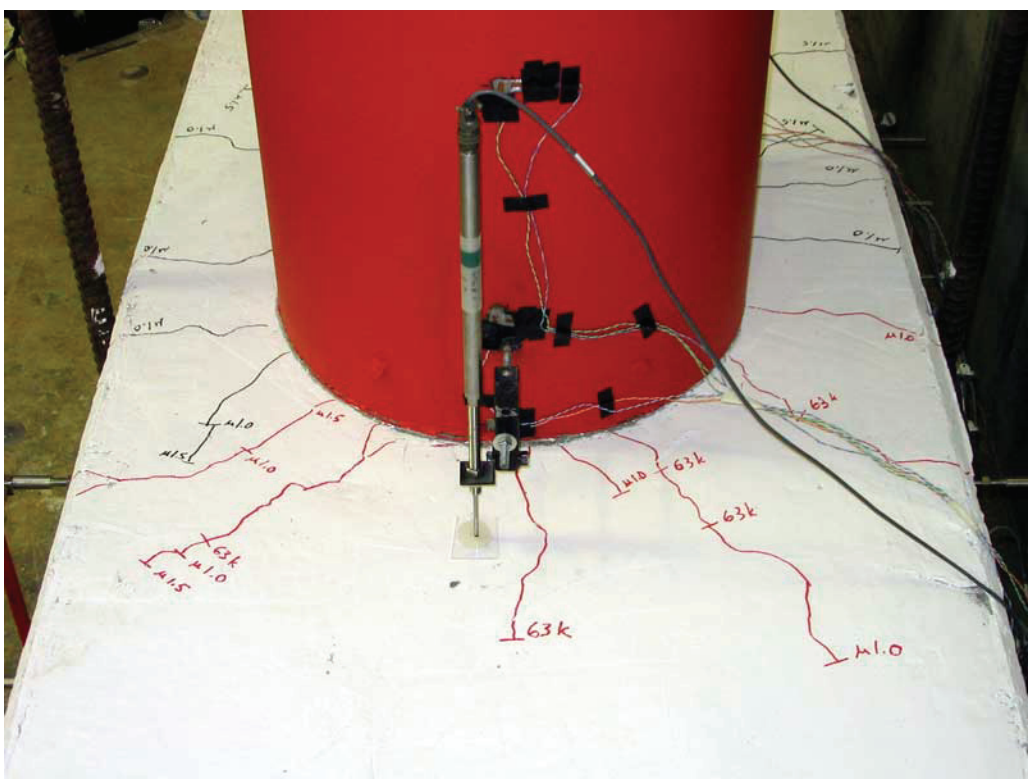

Figure 10-5. Bent Cap Cracking at 1.5 μ_Δ

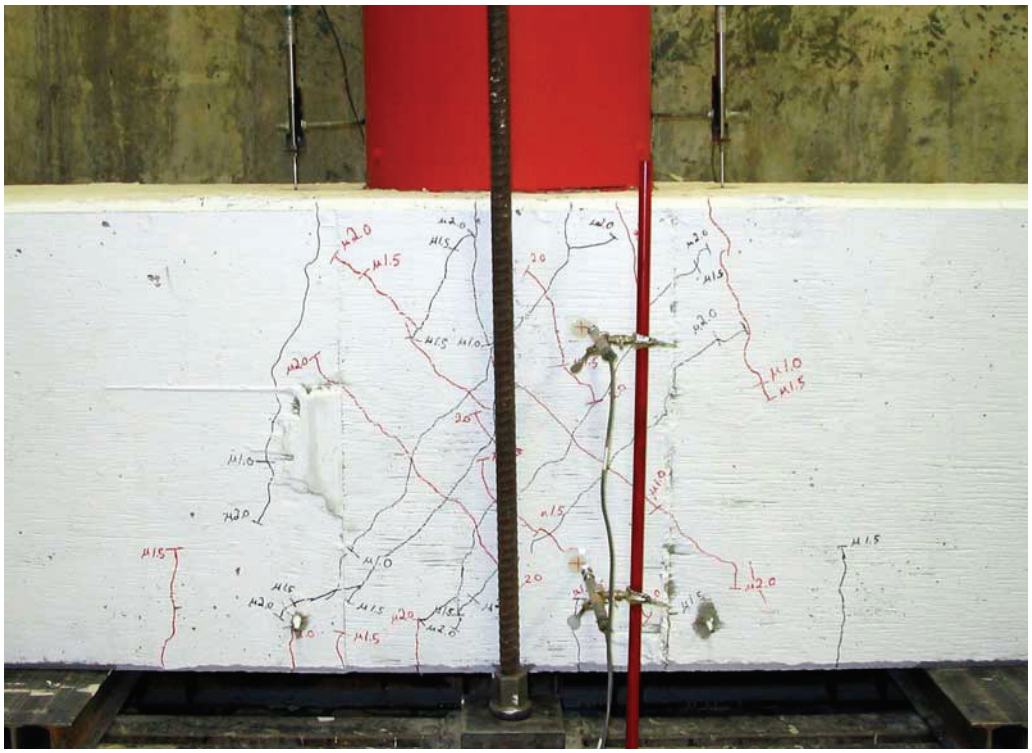

Figure 10-6. Joint Cracking at 2.0 μ_Δ

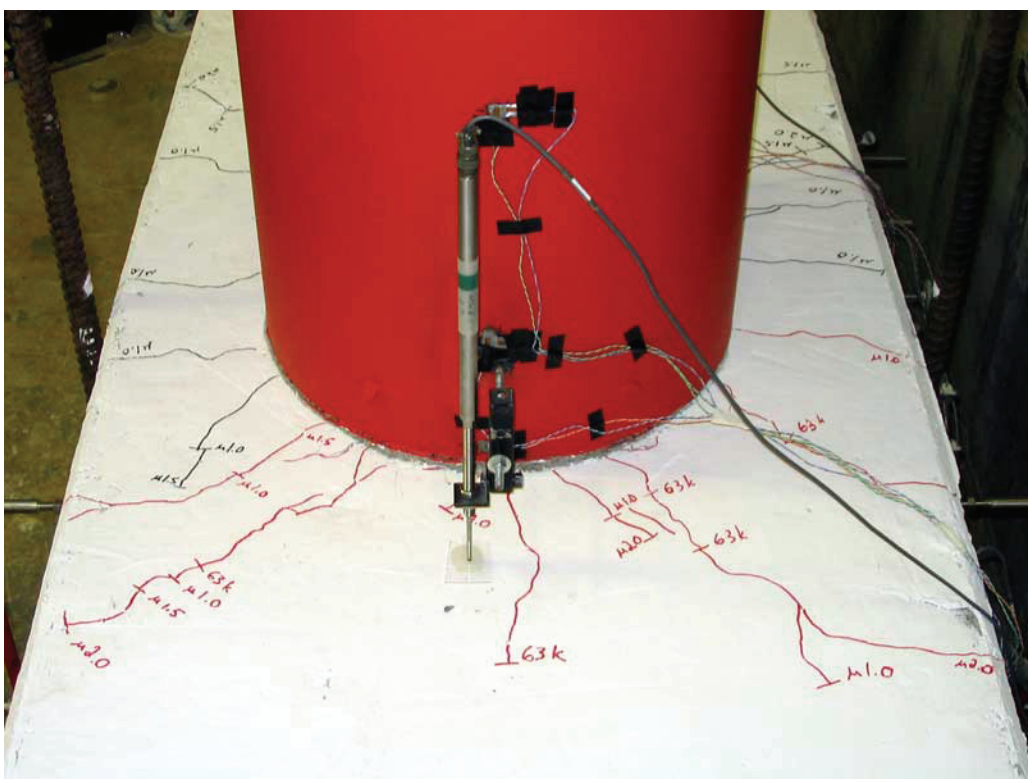

Figure 10-7. Bent Cap Cracking at 2.0 μ_Δ

Figure 10-8. Joint Cracking 4.0 μ_Δ

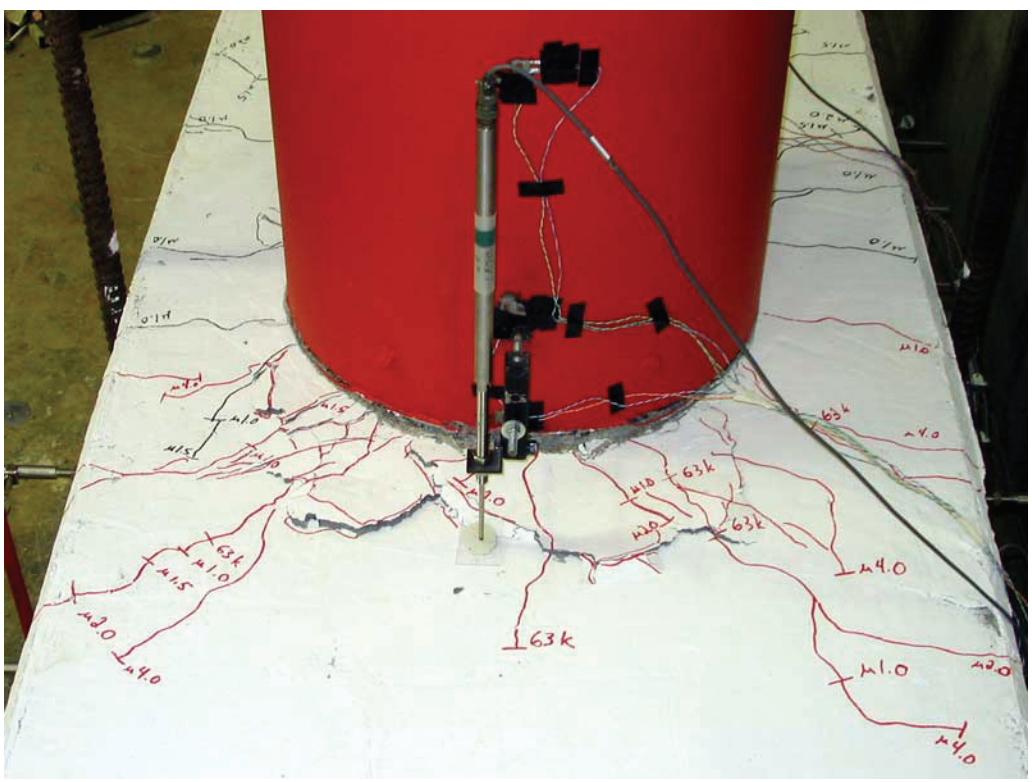

Figure 10-9. Bent Cap Cracking at 4.0 μ_Δ

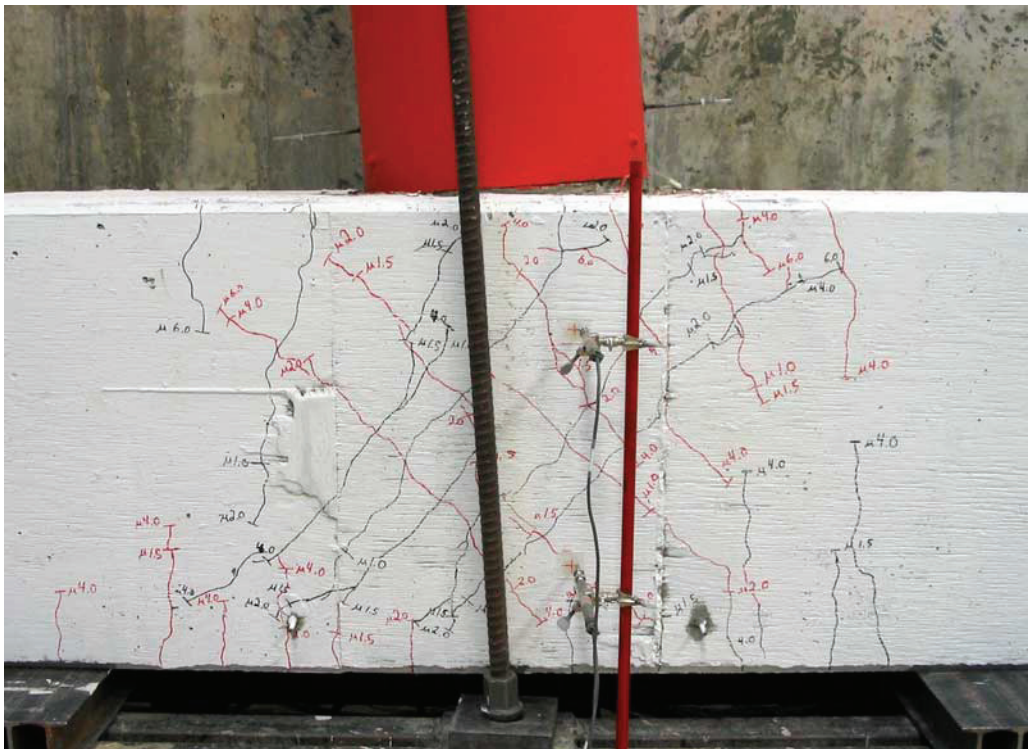

Figure 10-10. Joint Cracking at 6.0 μ_Δ

Figure 10-11. Bent Cap Cracking at 6.0 μ_Δ

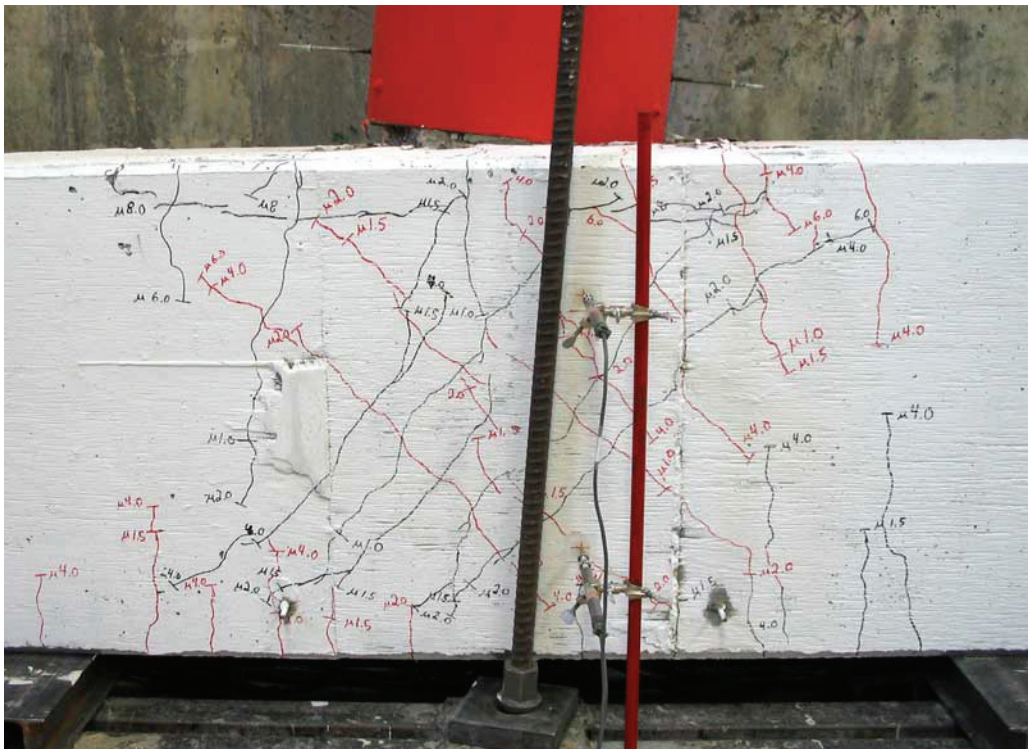

Figure 10-12. Joint Cracking at 8.0 μ_Δ

Figure 10-13. Bent Cap Cracking – Side "A" at 8.0 μ_Δ

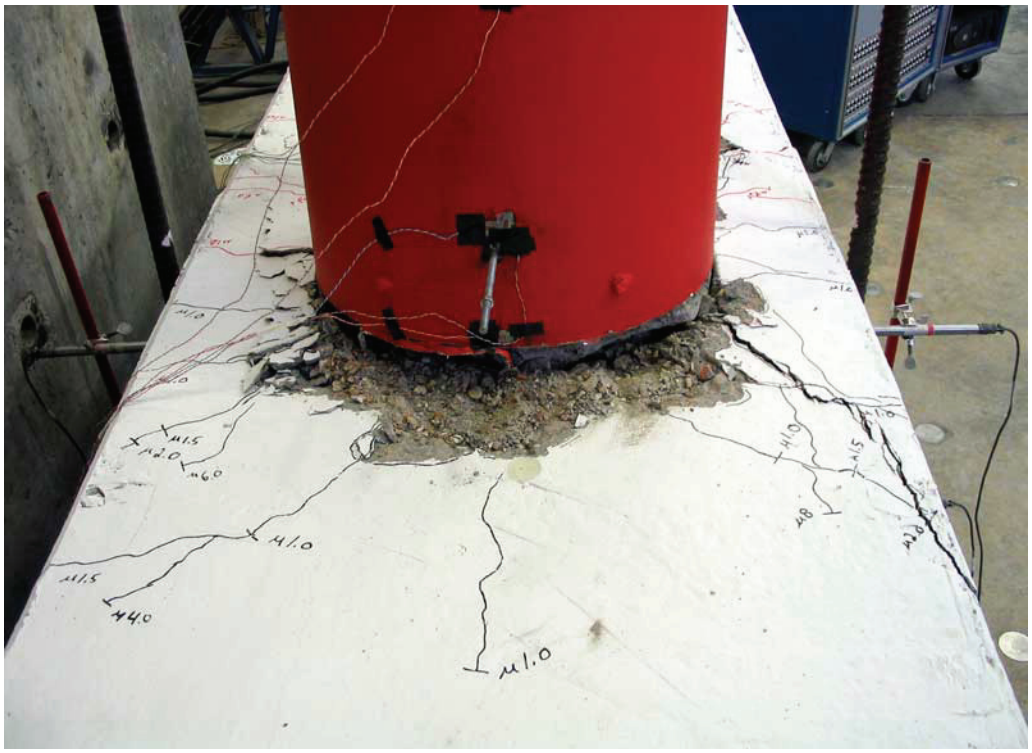

Figure 10-14. Bent Cap Cracking – Side "B" at 8.0 μ_Δ

Figure 10-15. Bent Cap Underside Cracking at 8.0 μ_Δ

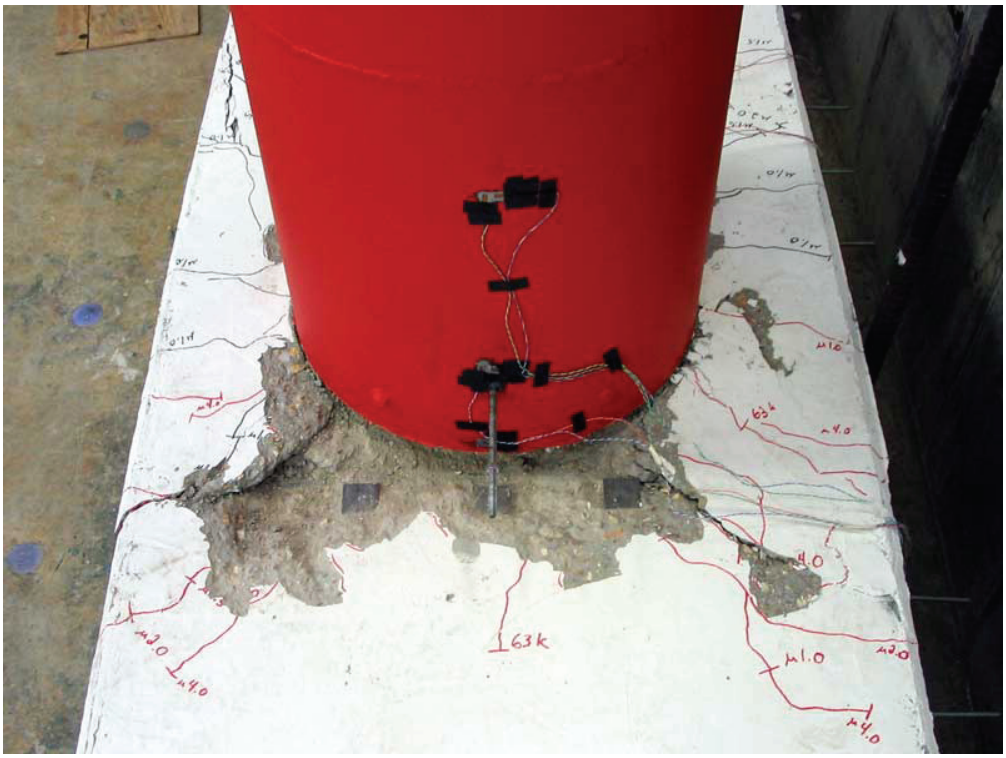

Figure 10-16. Bent Cap Cracking Ultimate Damage

Figure 10-17. Column Crushing Ultimate Damage

Figure 10-18. Underside of Bent Cap Ultimate Damage

10.2. LOAD DEFORMATION RESPONSE

The load deformation response of Unit 3 is shown in Figure 10-19. After the displacement of 228.6 mm the unit experienced the first significant loss in capacity, which is thought to result from significant strain penetration cracks around the column, especially after the displacement of 228.6 mm.

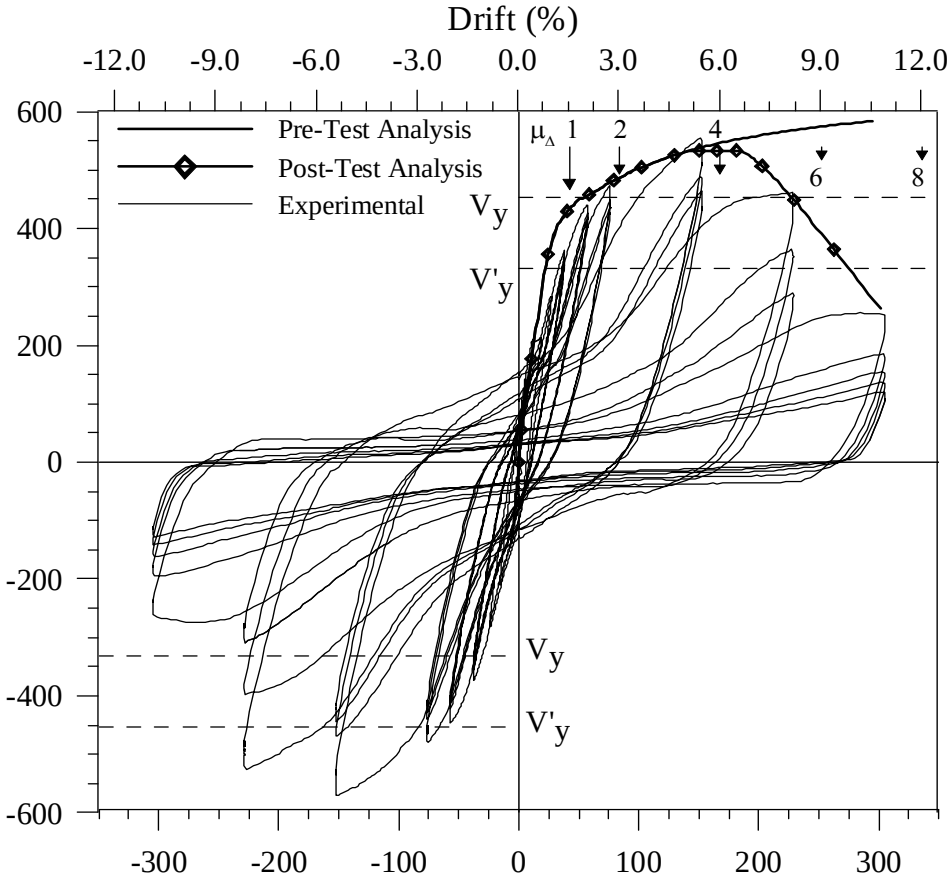

Figure 10-19. Unit 3 - Load Displacement Response

An immediate conclusion from these test results clearly indicate that reducing the steel shell gap to 13mm prevented excessive crushing of the concrete cover, and buckling of the column longitudinal bars, as previously described in Unit 1 and 2. This further accentuates the conclusion that the reduction in the lateral load observed in the previous two units was likely from flexibilities originating from within the joint and not due to buckling of the column longitudinal reinforcement, as one may have originally anticipated. This also accentuates the need to develop refined joint models that can account for these joint flexibilities, which is the central topic discussed in Section 11.5. Cracking on the sides of the bent cap resulting from joint shear was minimal and all cracks stayed small as shown in Figure 10-20. The crack pattern was more distributed than in Units 1 and 2. Cracking and spalling of large wedges of concrete occurred on the underside of the bent cap indicating once again onset of anchorage failure of the column longitudinal reinforcement, as shown in Figure 10-18.

Figure 10-20. Unit 3 Joint Shear Cracks

In Unit 3 the maximum registered lateral load was also recorded during the first cycle to the displacement of 152.4 mm. In the push and pull directions the registered lateral loads were +555 and -570 kN, respectively, which are nearly 20% higher than those registered for the previous two units. Between the first and second cycles the drop in the lateral load was the same as in Unit 1 or approximately 14%, and between the second and third cycles the drop in the lateral load was 5%, indicating once again stability in the response of Unit 3. Comparisons of load degradation at higher ductility levels are also described in further detail in Section 11.1. The first significant drop in the lateral load capacity of Unit 3 below the theoretical first yield load level was observed during the third cycle at the displacement of 228.6 mm. This indicates similar load degradation, which indicates that reducing the steel shell gap did not translate directly into an improvement of the seismic response of the test unit, but it certainly prevented premature low

cycle fatigue of the reinforcement. This suggests, that the steel shell gap should not be reduced below levels that can lead to significant increase in the load capacity of the unit, leading to higher principle tensile stress demands in the joint. For Unit 3 and based on a direct investigation of the test results the new displacement at ductility level one was set at 42.1 mm, translating in the displacement ductility levels shown in the Figure 10-19..

10.3. LOAD VS. CURVATURE RESPONSE

As before, Figure 10-21 depicts the measured lateral load versus the computed curvatures at the column to the bent cap interface for Unit 3. As in the previous Units 1 and 2, the diagram depicted in this figure also indicates a good correlation between the pre-test analysis and the experimental test results during the initial stages of testing. However, after peak load there is a considerable deviation between these two curves. As in Units 1 and 2, this can be attributed to large rotations originating solely from within the joint region, which indicates that the response of the three units was very similar.

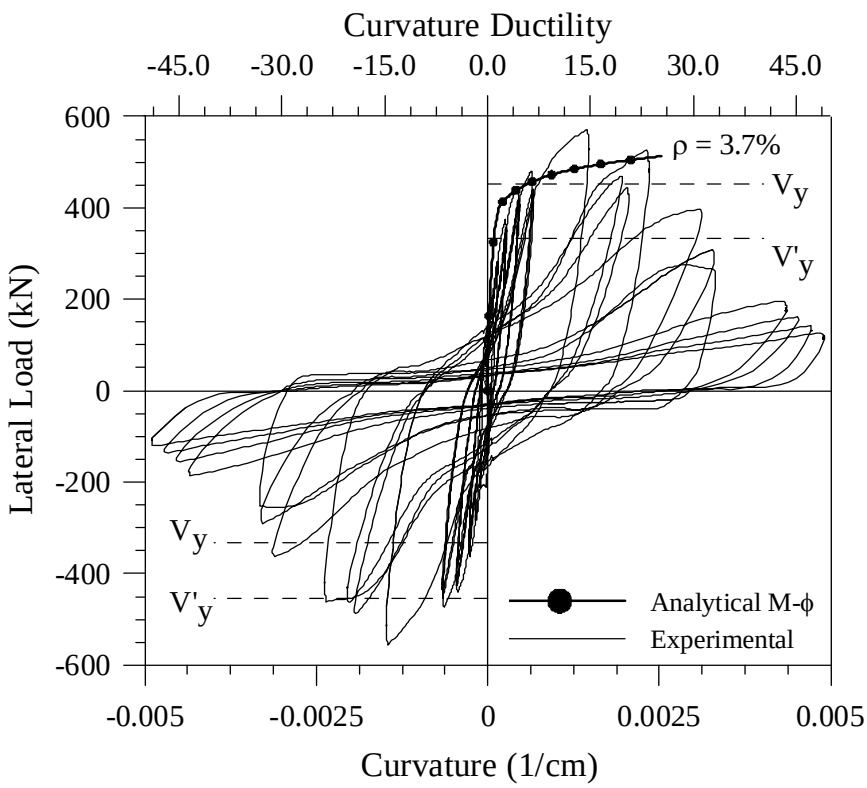

Figure 10-21. Unit 3 – Load versus Curvature Response

10.4. COLUMN LONGITUDINAL REINFORCEMENT STRAINS

The strain histories of the column longitudinal reinforcement gauges at the interface of the column and bent cap for side “A” and side “B” are shown in Figure 10-22 and Figure 10-31,

respectively. The yield strain of the column longitudinal reinforcement occurred at ±2,376με as determined from tensile testing. The strain profiles for each side of the column are shown in Figure 10-24 and Figure 10-25. The onset of yielding of the main column longitudinal bars occurred at μ1.0 for each side of the column.

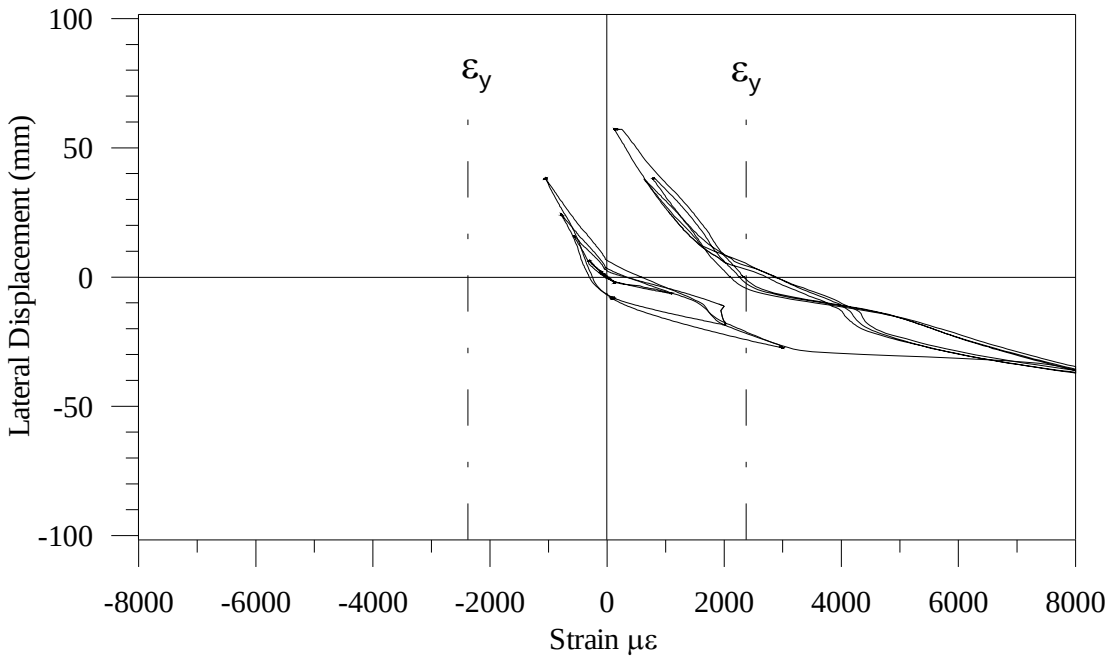

Figure 10-22. Strain Gauge History – C4a

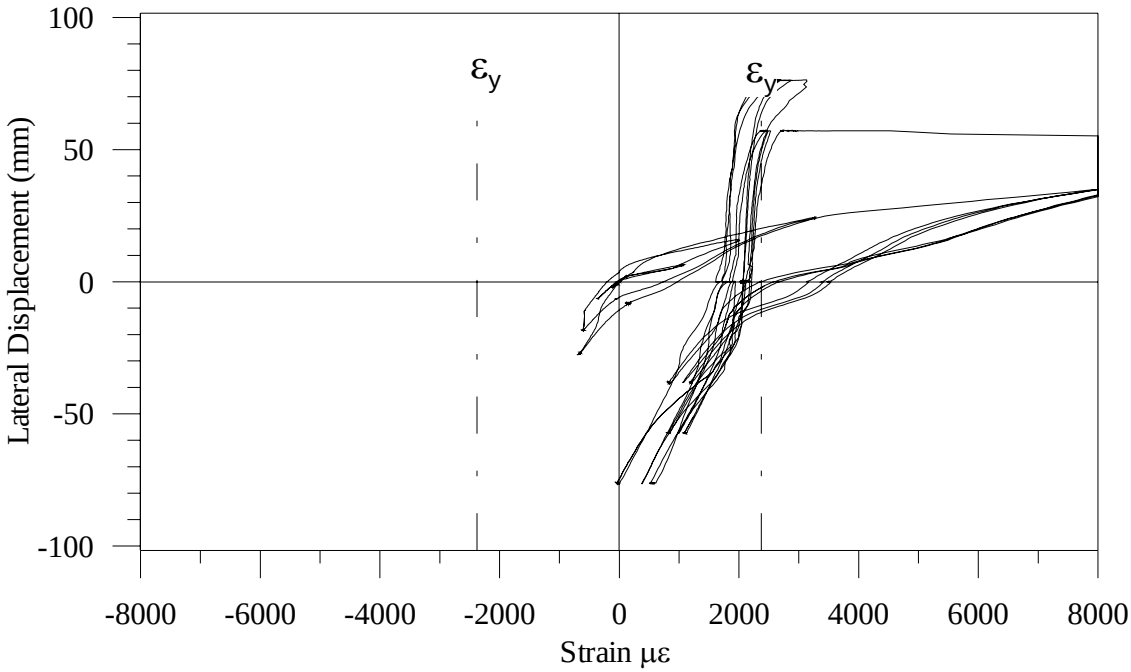

Figure 10-23. Strain Gauge History – C4b

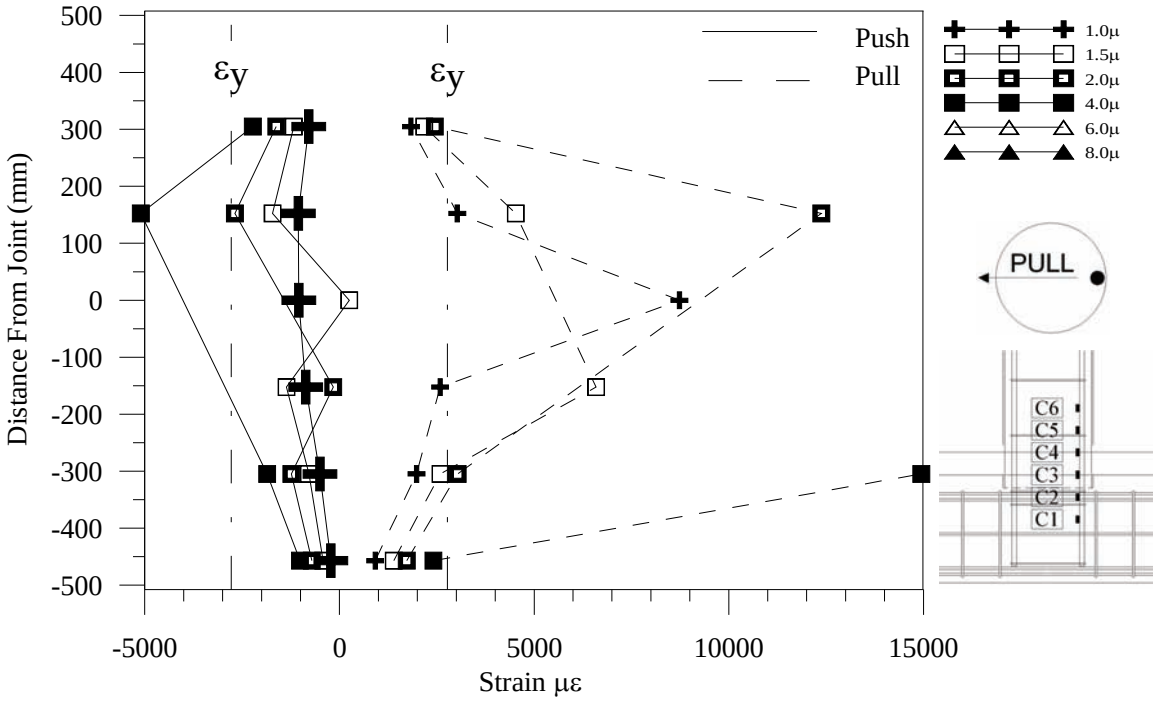

Figure 10-24. Strain Gauge Profile – Side "A"

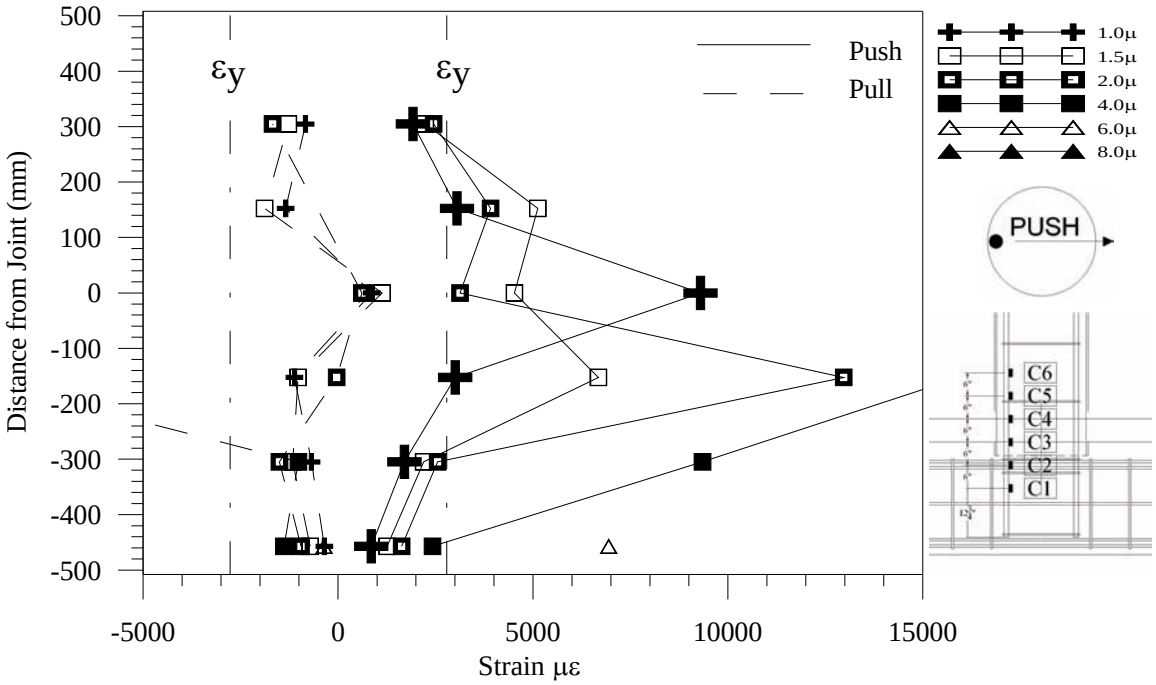

Figure 10-25. Strain Gauge Profile – Side "B"

10.5. JOINT SHEAR REINFORCEMENT STRAIN PROFILES

The strain gauges from the shear reinforcement are presented in this section. The yield strain of the as-built and retrofit shear reinforcement occurred at ±2,626 as determined from tensile testing. Figure 10-26 and Figure 10-27 show the strain profiles for the stirrups in the as-built concrete and the stirrups in the retrofit concrete, respectively. The stirrups stayed below the yield point indicating that joint shear did not occur in the longitudinal plane of the bent cap.

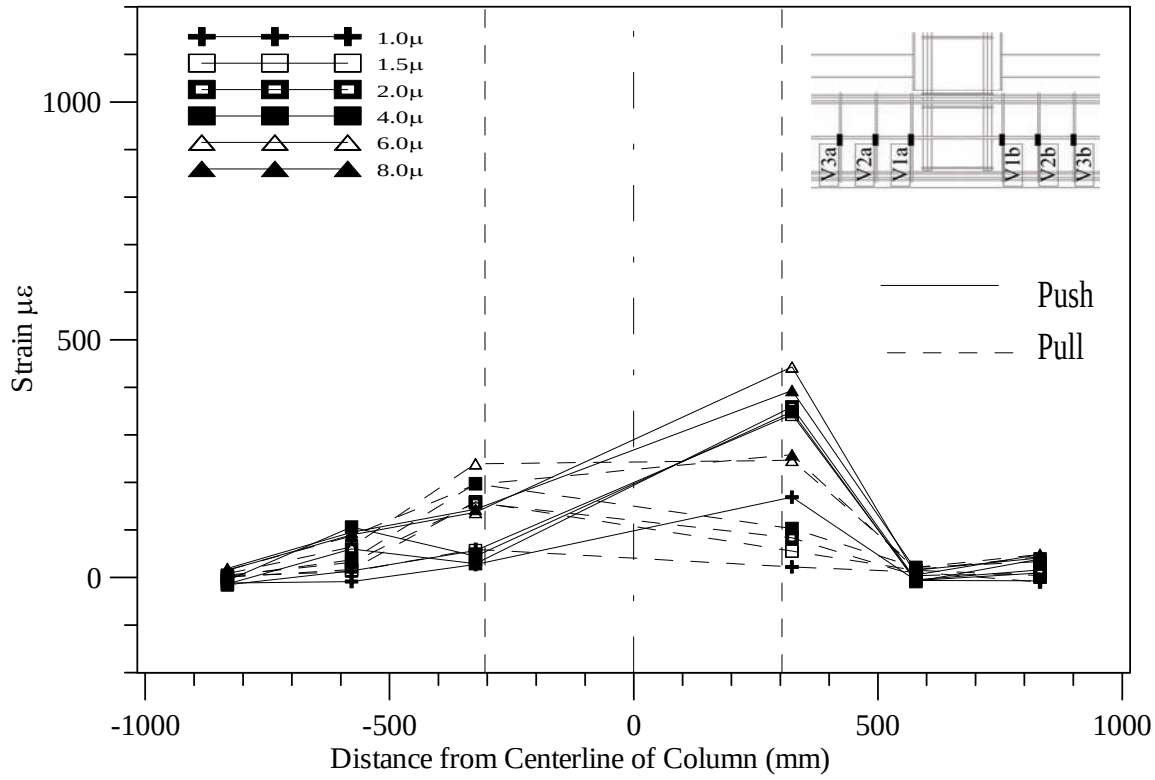

Figure 10-26. Strain Profiles – As-Built Section

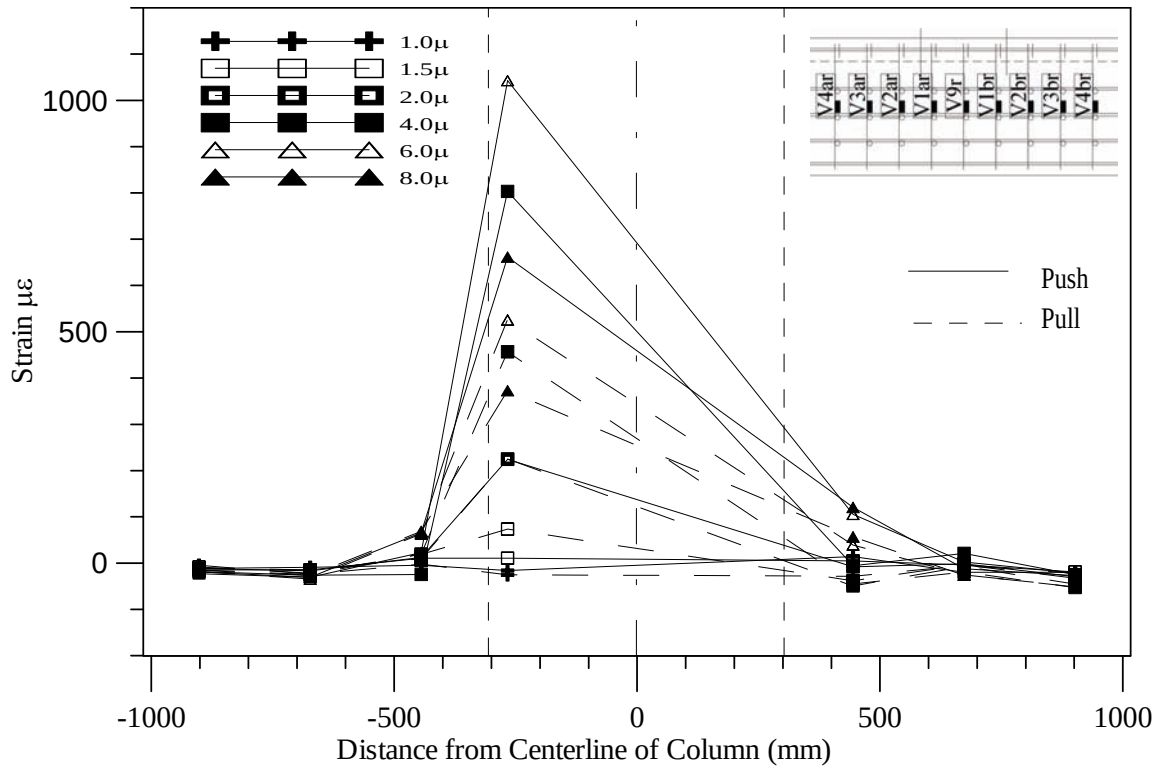

Figure 10-27. Strain Profiles – Retrofit Section

10.6. BENT CAP LONGITUDINAL REINFORCEMENT STRAINS

The following section presents the strain in the bent cap longitudinal steel. The yield strain for the as-built longitudinal steel was measured at 2,438 με, and tThe yield strain for the retrofit longitudinal steel was measured at 2,604 με. For both the as-built and the retrofit steel, the steel did not yield, indicating that the bent cap stayed within the elastic range. Also for similar locations, the strain in both the retrofit steel and the as-built steel had strain levels that were very close indicating that the entire bent cap acted as one unit. The strain profiles for the bent cap bottom longitudinal reinforcement for the as-built and retrofit sections are shown in Figure 10-28 and Figure 10-29, respectively.

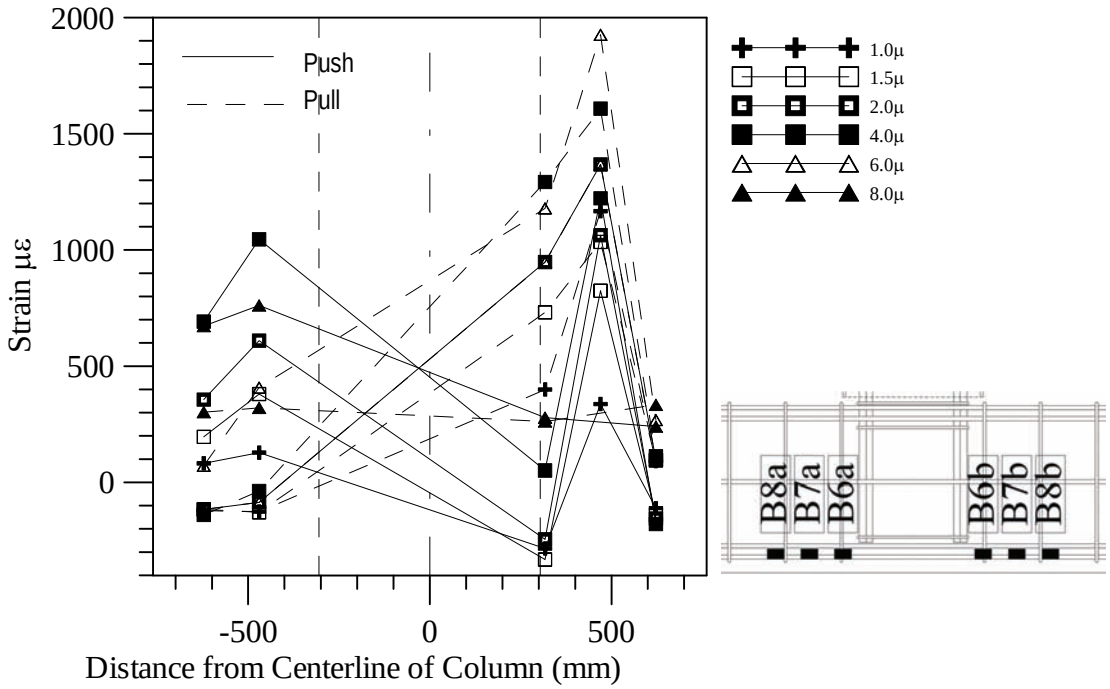

Figure 10-28. Strain Profiles – As-Built Section

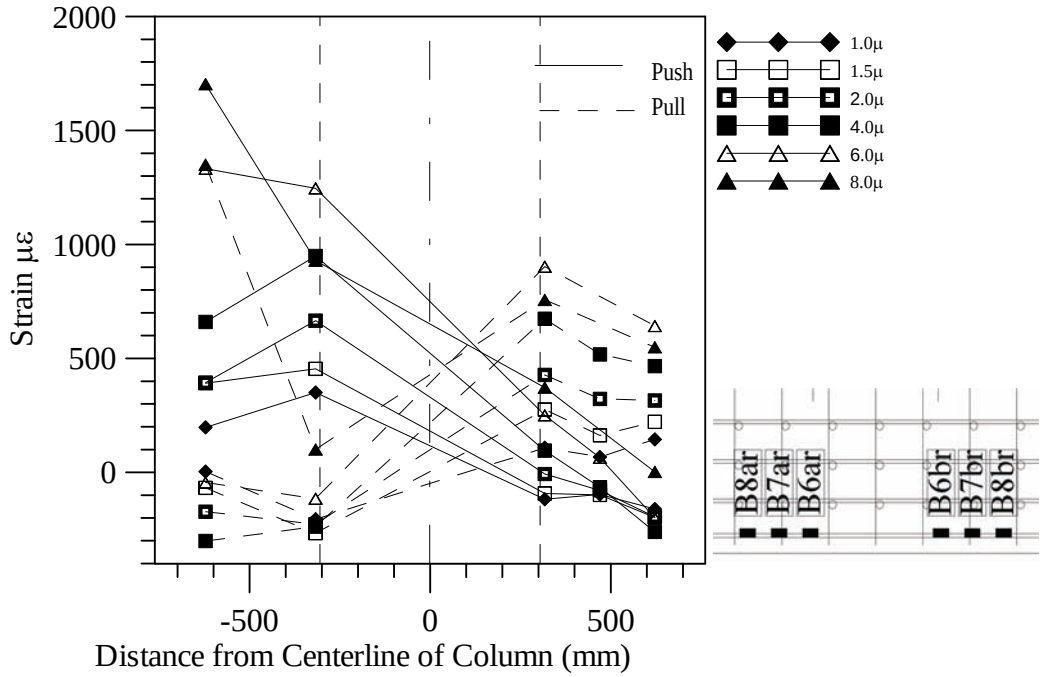

Figure 10-29. Strain Profiles – Retrofit Section

10.7. JOINT SHEAR ANALYSIS

Damage within the joint was attributed to cause the progressive degradation of the lateral load as observed by the load deformation response curve shown in Figure 10-19. Computed joint shear deformation were slightly larger than the previous two units, as shown in Figure 10-30. also, the post tensioning mechanism prevented excessive dilation of the bent cap preventing large strains in the top transverse reinforcement as shown in Figure 10-32.

The bent cap flexural and shear reinforcement stayed below yield and had similar levels of strain for the as-built and retrofit reinforcement as shown in Figure 10-28 and Figure 10-29, respectively. As with the previous two units, this indicates composite action between the as-built and retrofit cross-sections and that the bent cap stayed elastic forcing the plastic hinge to form in the column.

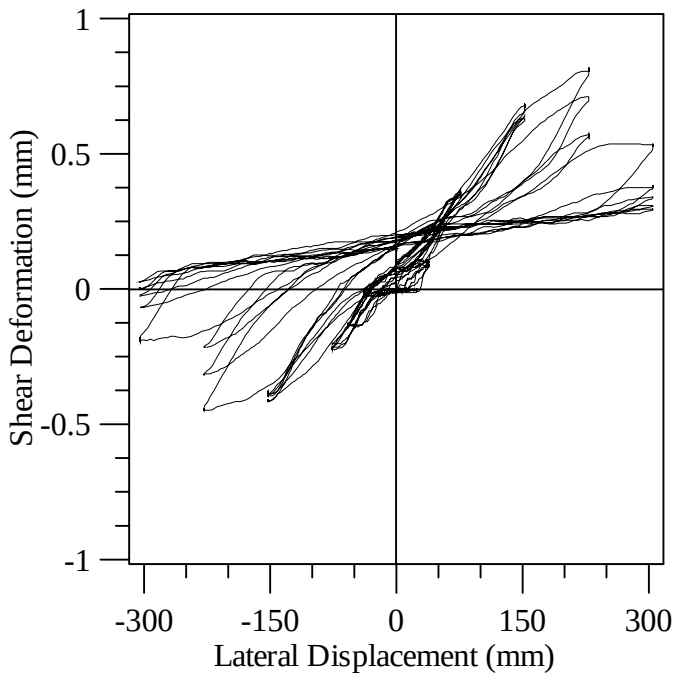

Figure 10-30. Unit 3 Joint Shear Deformation

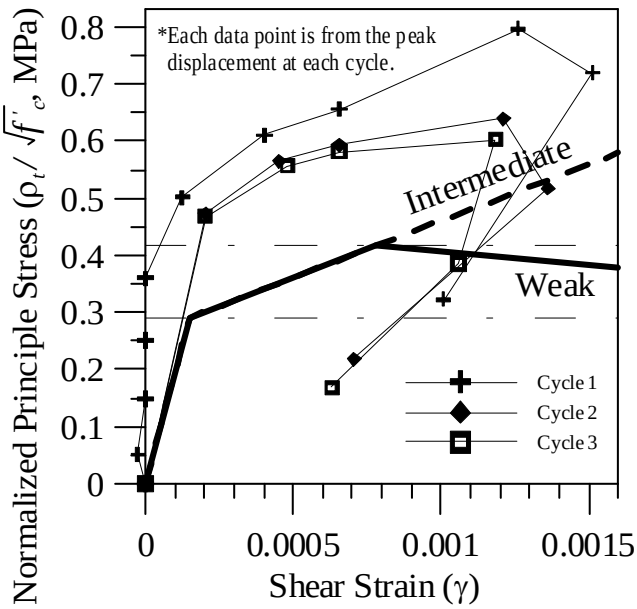

Figure 10-31. Unit 3 Principle Tensile Stress vs. Joint Shear Strain

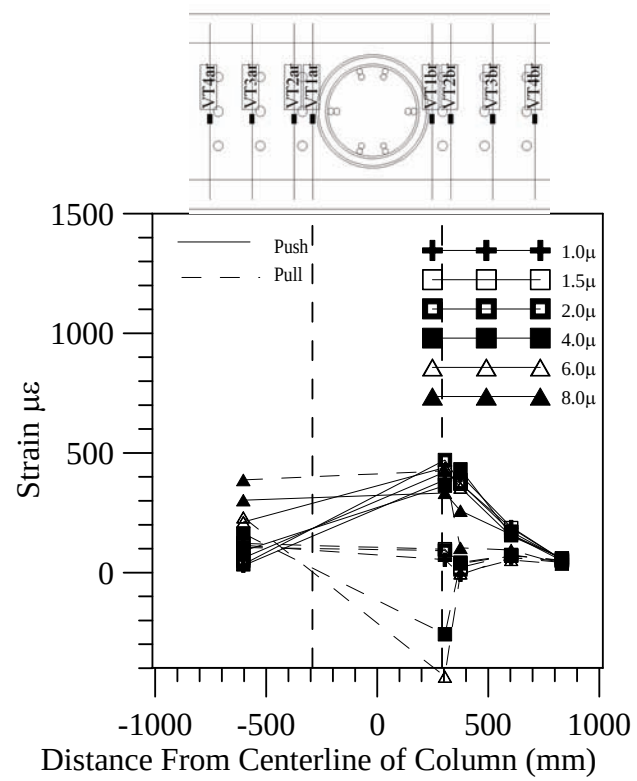

Figure 10-32. Unit 3 Top Transverse Reinforcement Strain Profile

11. DISCUSSION OF EXPERIMENTAL RESULTS

11.1. GENERAL

As previously shown in Sections 8.2, 9.2, 10.2, the load deformation response for the three units are very similar; however, slight deviations in the response of each of these three test units can be outlined either in terms of energy absorption capabilities, maximum achieved lateral load, strength degradation under increased reversed cyclic loads, and damage levels. A brief summary of some of the results derived from the experimental program are shown in Table 11-1. Peak lateral loads and peak principle tensile stresses for the three test units are shown in this table for a direct comparison of the test results. A reasonable comparison among the three test units was performed in terms of the energy dissipated through the system, and strength degradation under reversed cyclic loading. These parameters are discussed in the next two sections.

Table 11-1. Peak Values

Unit	Peak Values (kN)			Energy (kN-m)	
	Load	Stress	Rate*	Dissipated	Rate*
1	+421 -442	0.39 -0.41	-	986	-
2	+440 -460	0.41 -0.43	1.05 1.04	1,154	1.17
3	+555 -570	0.53 -0.55	1.32 1.29	1,007	1.02

* Normalized values in terms of Unit 1 results

11.2. COMPARISON OF DISSIPATED ENERGY FOR THE THREE TEST UNITS

In this section a comparison of energy dissipated through the three test units is used in the context of assessing joint performance. The energy dissipated through the structural system was calculated from the area of the hysteretic loops at each displacement level and results of these analyses are shown in Figure 11-1. The total cumulative energy dissipated for Units 1, 2, and 3 was 986 kN-m, 1,154 kN-m, and 1,007 kN-m, respectively, which shows that Unit 2 had a slightly higher capacity to dissipate the hysteretic energy by nearly 15%. Also as shown in this figure, Unit 2 was capable of dissipating higher levels of energy beyond 228.6 mm, which can also be set as the limit for onset of joint shear degradation for Units 1 and 3. Also the higher energy dissipation capacity associated with Unit 2 is evident by the reduced pinching of the hysteresis loops for this unit in comparison to those of Units 1 and 3. This suggests an improved performance for the joint of Unit 2 and hence a greater capacity to dissipate energy.

Referring to Table 11-1 it is important to note that although Unit 3 was not able to dissipate the same level of energy as Unit 2, the principle tensile stresses for this unit exceeded those of Unit

2. As such, reducing the steel shell gap from 51 mm to 13 mm for Unit 3 provided better confinement of the concrete cover; thus, preventing buckling and low cyclic fatigue fracture of the column longitudinal bars. However, the significant increase in the load capacity of Unit 3 led to an increased demand in the joint region. This observation suggests that in design practice combining details of Units 2 and 3 are likely to lead to an improved joint performance. Based on these results, it is desirable to limit the steel shell gap to within 38 to 51 mm, and in design situations where higher joint shear capacity may be needed one may opt for post-tensioning of the joint.

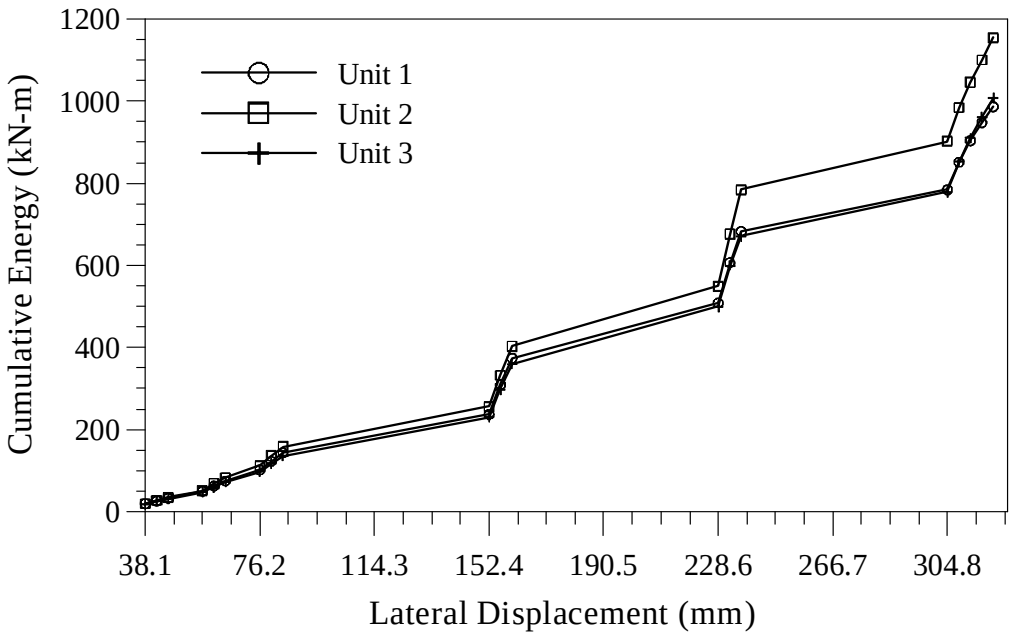

Figure 11-1. Cumulative Dissipated Energy

11.3. STRENGTH DEGRADATION UNDER REVERSED CYCLIC LOADING

Referring to Figure 11-2(a) it is clear that the three test units reached their peak capacity at the displacement level of 152.4 mm. Also, the peak load achieved in Units 1 and 2 was nearly 1.5 times the section yield capacity. In Unit 3 the maximum achieved lateral load was nearly twice as the yield capacity. This increase in the ultimate capacity of Unit 3 was a direct result of reducing the steel shell gap from 51 mm to 13 mm, which increased the confinement action on the concrete core. As such, one of the immediate conclusions derived from this research project is to stipulate a limit for the steel shell gap length as a means to control the capacity of the column, which is discussed in further detail in Section 12.3.1.

As in the previous section, in this section a comparison of strength degradation under reversed cyclic loading is used in the context of assessing joint performance. In comparison to the analytical models it is expected that under reversed cyclic loading reinforced concrete sections

will experience degradation in the lateral strength due to buckling of the longitudinal reinforcement and joint degradation. However for the three test units, buckling of the longitudinal reinforcement was more prevalent in Units 1 and 3. In addition, Unit 1 experienced the first drop in the lateral load capacity below the theoretical yield load level during the second cycle to the displacement level of 228.60 mm. Similarly, Units 2 and 3 experienced the first drop in the lateral load capacity below the theoretical yield load level during the first cycle to the displacement level 304.8 mm. These results were used in Section 12.3.3 to establish displacement ductility levels for the design and upgrade of existing bridge bents.

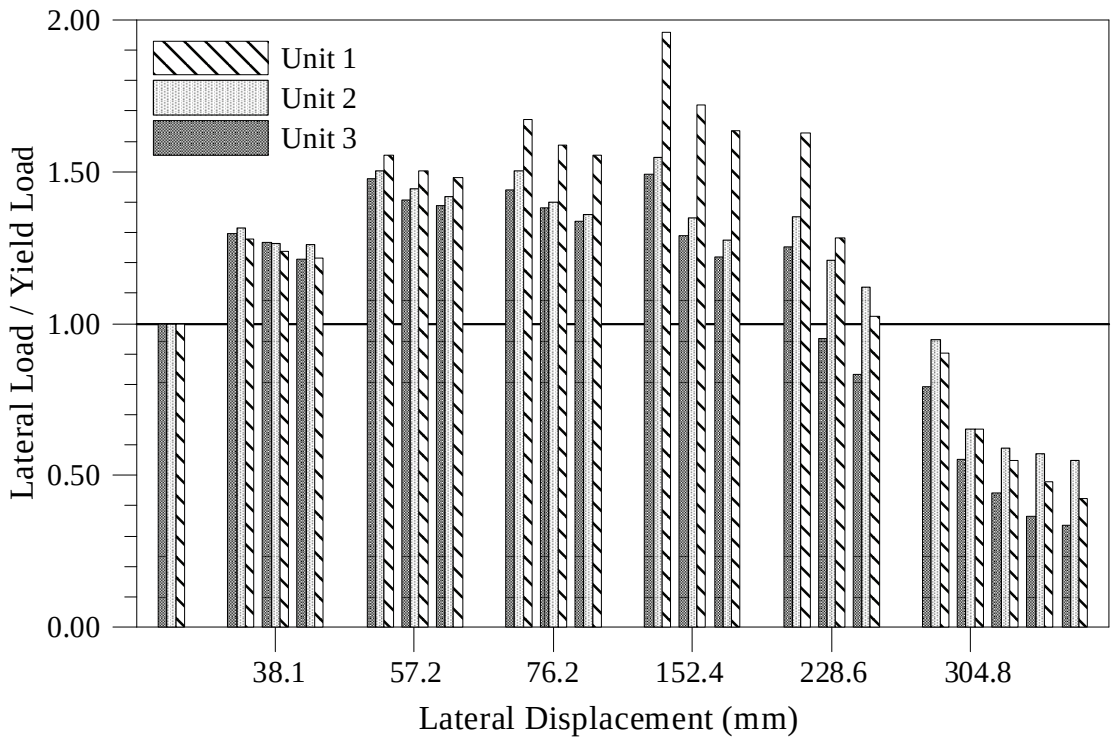

Figure 11-2. Strength Degradation under Reversed cyclic loading

11.4. JOINT PERFORMANCE

Priestley (1993) developed a three point joint stress-strain response model for poorly confined joints using the two principle tensile stress limits stipulated in Eqs. (3-6) and (3-7) as starting points for joint design and assessment. These two points were empirically derived from testing of 26 outrigger-bent knee joints. However, it is important to note that there is no single joint stress-strain model that can represent the complex behavior of all possible joints (Mazzoni and Moehle, 2001), and the model developed by Priestley has been used by Caltrans (SDC, 2004) as a starting point for seismic design and assessment of bridge joints.

In the post-test evaluation of the three test units, three different joint models were developed to evaluate the lateral response of the test units. These proposed models are shown in Figure 11-3 along with the experimentally derived normalized principle tensile stresses versus joint rotation. The proposed models for each of the joints of Units 1, 2, and 3 are shown in Figure 11-4(a). A direct comparison of these figures shows that the joint in Unit 3 achieved higher principle tensile stresses, and the joint in Unit 2 shows lower levels of strength degradation under increased joint rotations. In Figure 11-3 are also shown the models originally developed by Priestley (1993) and Mazzoni and Moehle (2001). These two models have been proposed in the literature, and as previously stated these have been used to evaluate joint performance under reversed cyclic loads. Joint model *I* is used in the evaluation of unconfined joints and was proposed by Priestley (1993), and Joint model *II* is used in the evaluation of confined joints and was proposed by Mazzoni and Moehle (2001). Both of these joint models are tri-linear models, in which the first two branches are the same for both models with expressions given by

$$\rho_t = \begin{cases} 1944.444 \times \theta_j \; ; & \theta_j \le 0.00015\,(rad) \Rightarrow \textit{Joint Model I \& II} \\ 0.2576 + 227.273 \times \theta_j \; ; & \theta_j \le 0.0007\,(rad) \Rightarrow \textit{Joint Model I \& II} \\ 0.4480 - 44.804 \times \theta_j \; ; & 0.0007 < \theta_j \le 0.01\,(rad) \Rightarrow \textit{Joint Model I} \\ 0.625 \; ; & \theta_j > 0.00162\,(rad) \Rightarrow \textit{Joint Model II} \end{cases} \tag{11-1}$$

Where θ_j is the joint shear/rotation measured in radians and ρ_t is the normalized principle tensile stresses. The principle tensile stresses were then converted to a moment relation based on the Mohr circle of analysis and on the relation

$$M_t = w_b \left(0.8 \times h_b\right)^2 \sqrt{\left(\rho_t \chi_i^N \times \sqrt{f_c^{'}} + \frac{f_a}{2}\right)^2 - \frac{f_a^{\,2}}{4}} \tag{11-2}$$

Where w_b and h_b are the bent cap width and depth, respectively, $f^{'}_c$ is the concrete compression strength, and f_a is the axial stress on the joint derived from the axial load, P, and is given by $P/w_b h_b$, χ is a damage parameter and is a piecewise linear function that was empirically derived from the test results for each test unit that was developed to simulate the damage that develops within the joint region, and the power N in χ is the cycle number under consideration. The damage parameter χ was then given for each test unit by

$$\chi = \begin{cases} 1.00 \; ; & \theta_j \le 0.00015\,(rad) \Rightarrow \textit{Joint Model Units 1 and 2} \\ 1.00 - 15.0 \times \theta_j ; & \theta_j \le 0.0007\,(rad) \Rightarrow \textit{Joint Model Unit 1} \\ 1.00 - 5.0 \times \theta_j ; & \theta_j \le 0.0007\,(rad) \Rightarrow \textit{Joint Model Unit 2} \end{cases} \tag{11-3}$$

Next, substituting the piecewise Eqs. (11-3) and (11-1) into Eq. (11-2) the moment-rotation envelope for each of the test units is obtained and the relations for the three test units are shown in Figure 11-4(b). Results from this section were then used to develop the post-test analysis outlined in the next section.

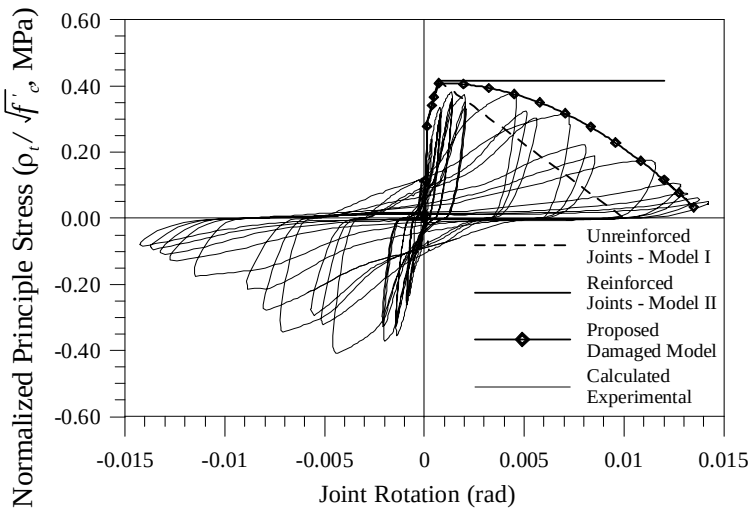

(a) Unit 1

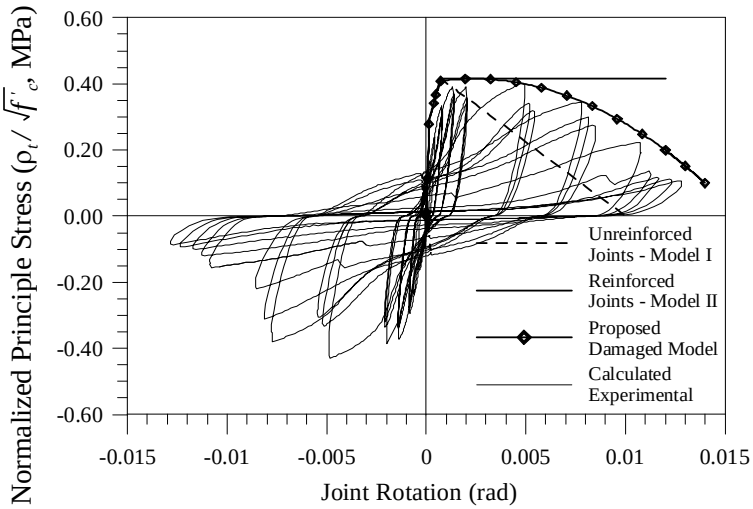

(b) Unit 2

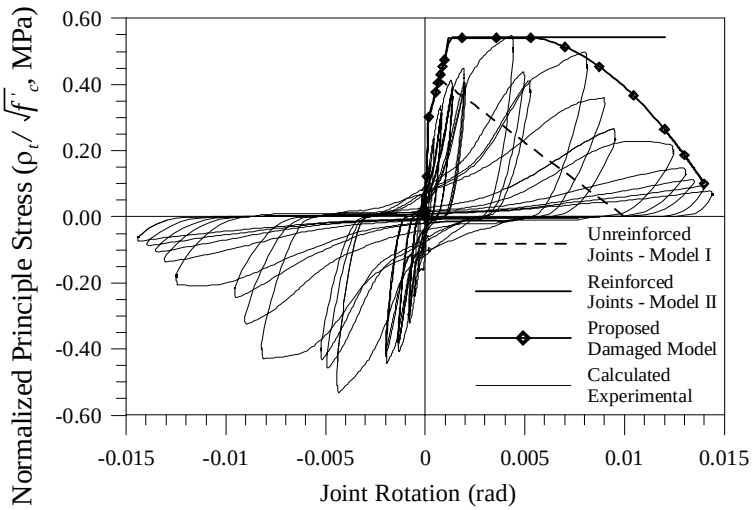

(c) Unit 3

Figure 11-3. Normalized Principle Stresses vs. Computed Joint Rotation

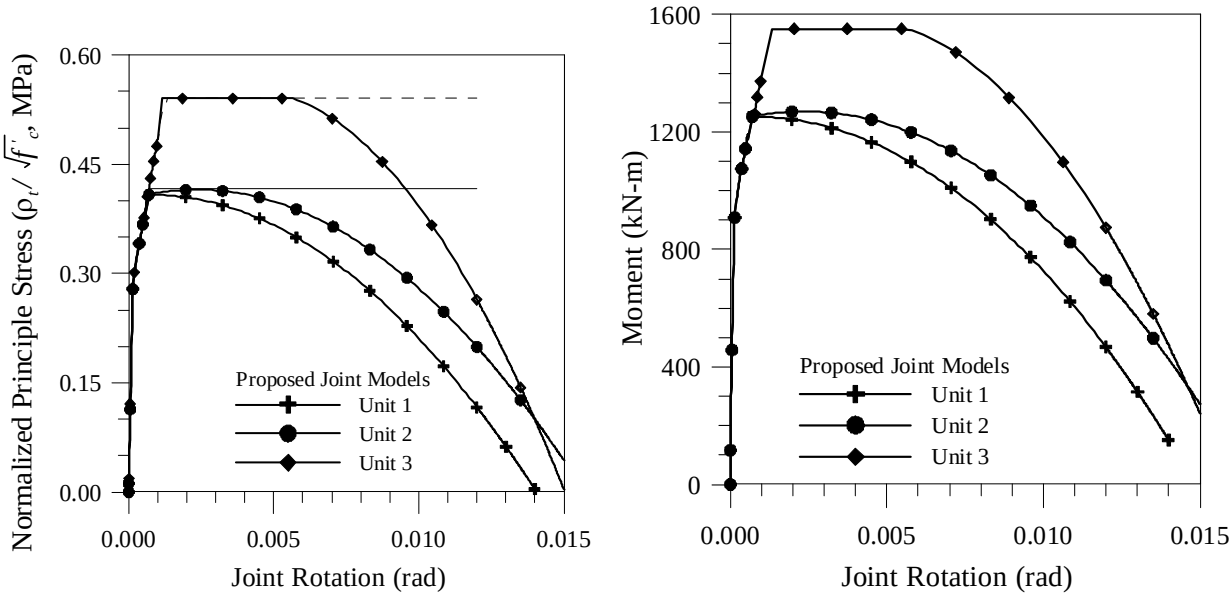

(a) Normalized Stresses (b) Moment Rotation Envelope

Figure 11-4. Joint models

11.5. POST-TEST ANALYSIS

The pre-test analyses for Units 1, 2 and 3, as described in Section 7.2, were developed without considering any increases in deflections or loss in load capacity deriving from flexibility or damage in the joint. This approach leads to satisfactory results in developing the envelope response of members built with joint shear reinforcement designed according to current seismic design provisions, in which joint flexibility is negligible. However, prior to the 1970's joints were built with insufficient joint shear reinforcement and for these structures other mechanisms of deformation must also be considered in the analysis.

These mechanisms should consider rigid body rotations at the ends of members due to joint flexibility and elongation combined with slip of the longitudinal reinforcement from the joint core. Mazzoni and Moehle (2001) have successfully used these mechanisms combined in a rigid body moment rotation relation. As such, in this research program these additional modes of joint deformation were considered in the analysis in terms of the relation

$$\Delta V_i = \left(\frac{1}{K_{C,i}} + \frac{\left(L_C + h_b/2\right)^2}{K_{B,i}} + \frac{\left(L_C + h_b/2\right)^2}{K_{J,i}} \right)^{-1} \times \Delta D_i \qquad (11\text{-}4)$$

Where as before, ΔV_i and ΔD_i are the incremental column lateral load and top deflection, respectively, and $K_{C,i}$ and $K_{B,i}$ are the instantaneous tangential bending stiffness for the column and bent cap, respectively, and were obtained in terms of Eq. (7-2). In this form the first two terms consider only the column and bent cap flexibility, and the last term considers the rigid

body rotation at the base of the column due to joint flexibility combined with bar elongation and slip. As such, $K_{J,i}$ is the rotational stiffness of the joint considering joint flexibility plus bar elongation and slip. The joint rotational stiffness was empirically derived for each of the test units by employing a rotational spring element with zero length and moment rotation relation developed based on the joint stress-strain/rotation diagrams presented earlier for joint models *I* and *II*.

Based on the three moment-rotation models shown in Figure 11-4(b) and the analytical model expressed by Eq. (11-4) the curve envelopes for each of the test units was developed and results from this analysis are shown in Figure 11-5. These three curves were then superimposed with the load deformation response curves for each of the three test units shown in Sections 8.2, 9.2, and 10.2. Referring to these experimental results sections there is a good correlation between the proposed joint model results and the experimental curves.

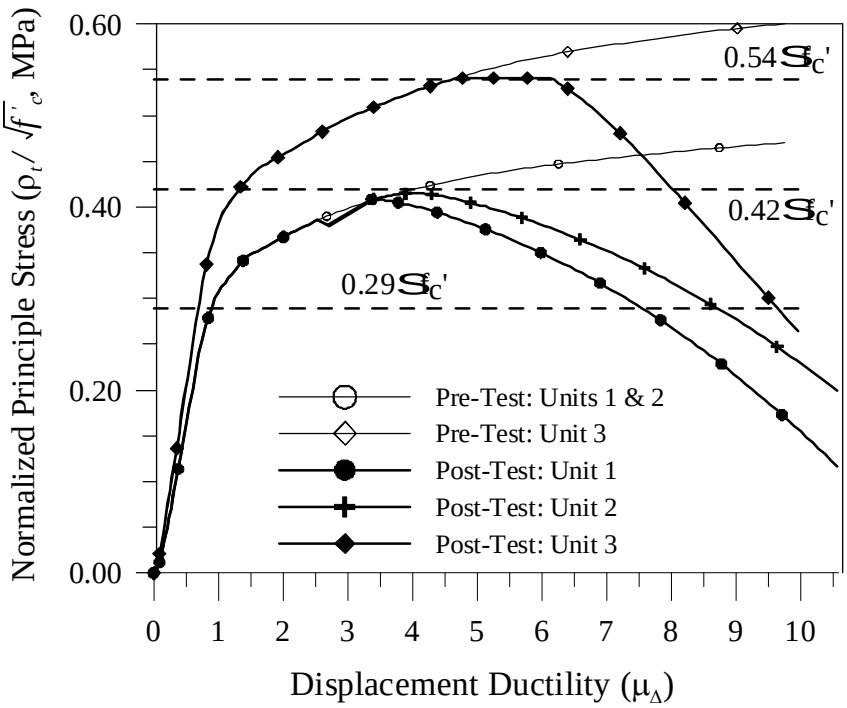

Figure 11-5. Post-Test Analysis

12. CONCLUSIONS

12.1. GENERAL OVERVIEW

This report discusses in detail experimental and analytical findings from a research program conducted for the State of Alaska Department of Transportation and Public Facilities. Part of this research program a total of three 4/5 scale units were cast, retrofitted, and tested under simulated fully-reversed cyclic lateral loading. These three units consisted of a cast in place steel shell (CISS) column foundation shaft and a bent cap configured to form a tee connection. In addition, these units were built to model a bridge bent and tested under simulated seismic loads at the University of Missouri Rolla experimental facilities. Based on these research program, an upgrade method was investigated that can be implemented in field conditions for improving the seismic performance of bridges built in the state of Alaska. Based on the research findings overall design recommendations are discussed in this Section 12.3.

A prototype as-built unit consisting of an interior column and corresponding bent cap was designed and constructed in a T-configuration by including the following design deficiencies: (1) the CISS column foundation shafts have excessive longitudinal reinforcement ratios, (2) the yield moment capacity of the bent cap is below the maximum feasible moment that develops at the column faces, (3) the steel shells are partially embedded in the joint region, which under low levels of rotation impose extensive damage on the bent cap, and (4) the joints have inadequate amounts of joint shear reinforcement to sustain the levels of principal tensile stresses that develop within the joint region, which leads to anchorage failure of the column longitudinal reinforcement and significant strength degradation at low ductility levels.

After construction of the as-built units, the units were modified in order to investigate seismic improvements and propose procedures for field implementation, according to the following seismic improvements: (1) the moment capacity of the column was reduced by cutting a portion of the column longitudinal reinforcement at the connection to the bent cap to levels that can ensure a proper ductile seismic response, (2) a section of the steel shell was cut and removed leaving a gap between the steel shell and the bent cap, and (3) the bent cap dimensions were increased to i) install the additional flexure and joint shear reinforcement thereby increasing the moment capacity of the bent cap, ii) provide adequate reinforcement spacing, iii) reduce the principle tensile stresses, iv) provide for a better transfer of stresses within the joint region, v) increase the development length of the column longitudinal reinforcement, and v) reduce reinforcement congestion in the joint region.

12.2. GENERAL CONCLUSIONS

Overall, experimental results from the three test units cyclic tests showed that the three test units displayed a ductile response up to the displacement ductility of 5 without significant decreases in the strength of the test units, inelastic actions due to flexural yielding of the bent cap, shear failure of the bent cap or joint shear failure. Realizing that for a column with an aspect ratio of 4.5, Priestley *et. al* (1995) recommends that the displacement ductility capacity of multiple column bridge bents should not be any less than 4, experimental results indicate that the displacement ductility levels achieved are within the recommended values.

Beyond the ductility level of 5, the main failure mode of Unit 1 was attributed to joint shear failure due to excessive transverse dilations within the joint region. This was attributed to the transverse horizontal headed reinforcement not been made continuous though the joint region. As such it is recommended that this detail practice not be used in regions prone to seismic events with a combined ductility demand near 4 and under multiple reversed cycles.

An improved joint detail was implemented for Units 2 and 3, in which this transverse reinforcement was made continuous through the joint region. In Unit 2, the main failure mode was attributed to low cyclic fatigue of the column longitudinal reinforcement. Extensive joint degradation was recorded beyond the displacement ductility of 7. In Unit 3 the joint was post-tensioned in the transverse direction while also decreasing the gap length between the steel shell and the bent cap. Beyond ductility level 7 degradation of the lateral load capacity of the column occurred due to joint shear failure. Detailed description for the design of these units and experimental results are discussed within this report.

Based on the experimental results the research team proposes that a displacement ductility of 4 be implemented in the retrofit design using the details proposed for Units 2 and 3. At this level it is expected that some level of strength degradation will be observed in the column, but this will not either cause significant decrease in the column axial capacity nor significant wide open cracks in the joint region. Furthermore, any cracks at this level will close under the gravity loads. In addition, for columns with lower reinforcement ratios or deeper bent cap the full dependable moment capacity and displacement ductility of the column can be expected to develop. As such, for these columns higher displacement ductility levels may be accepted for assessment investigation. This is further addressed in the next section.

12.3. SEISMIC DESIGN RECOMMENDATIONS

Following on the discussion of the experimental results presented in Section 11, this section outlines design recommendations to establish an improved seismic performance of bridge bents

built in the state of Alaska using CISS columns. Based on the design and performance of the three test units, the following design recommendations are made for seismic retrofit/upgrade design of multi-column bridge bents with circular CISS-columns. It is assumed that multi-column bents are designed using the capacity design philosophy with hinges forming at the column end.

12.3.1. Column Design

The following seismic upgrade design procedures are proposed for the seismic rehabilitation of circular CISS-columns built with reinforcement ratios greater 4% and/or the steel shell embedded into the bent cap:

i) A section of the steel shell must be cut and removed in order to leave a gap between the steel shell and the new bent cap section, as previously discussed in Sections 3, 4, and 5 during construction of the test units, see Figure 3-2. All the concrete surrounding the column longitudinal reinforcement and located below the line of the new bent cap section should be removed as shown in Figure 4-3.

ii) Following up on the previous recommendation, confining reinforcement shall be required in terms of field welded hoops installed below the steel shell gap region and placed immediately in contact with the column longitudinal reinforcement, as shown in Figure 4-4. Higher number of welded hoops may be required to satisfy the following anti-buckling spacing, *s*, requirements (Caltrans, 2004):

$$s \leq 6d_{bl} \tag{12-1}$$

Where d_{bl} is the bar diameter of the column longitudinal reinforcement. This detail is necessary to prevent buckling of the column longitudinal reinforcement within the gap region beyond the damage level corresponding to crushing of the cover concrete.

iii) The steel shell gap should be limited between 38 and 51 mm. The lower gap value will limit increases in the flexural capacity of the column due to excessive confinement of the inner core. The upper bound will be within values that can ensure sufficient displacement ductility capacity, minimum confinement of the plastic hinge region and prevent shear failure of the column.

iv) The column longitudinal reinforcement ratio should be reduced to limits below 4% but not lower than 1% using the procedures outlined in Section 3.5 and 4.1. The upper limit avoids significant amounts of joint shear reinforcement and practical difficulties involving construction of the upgrade bent cap section in columns with large reinforcement ratios.

v) In the evaluation of the flexural capacity of circular CISS columns with a gap region the concrete core should be assumed confined by an equivalent spiral confined section with a spiral

area corresponding to the square of the steel shell thickness and a pitch equivalent to the gap length.

12.3.2. Bent Cap Design

The following seismic upgrade design procedures are proposed for the seismic rehabilitation of reinforced concrete bridge bent caps built with insufficient longitudinal, shear and joint shear reinforcement capable of ensuring plastic hinges to form at the column ends:

i) The minimum width of the upgrade bent cap section must be within 1.5 times the outside diameter of the steel shell. This limit will ensure a uniform flow of forces through the joint region. However, as previously discussed in Section 3.2.2, the minimum width of the bent cap, W_b, must satisfy current ACI (ACI 2002) bar spacing and cover concrete specifications for the installation of the new bent cap flexural and joint shear reinforcement.

ii) Redesign of the bent cap height shall be dimensioned according to limits stipulated by Eq. (3-4) (Priestley, 1996), which was established based on the required development length for the column longitudinal reinforcement. A higher bent cap height may be necessary in order to reduce the principle tensile stresses within the joint region as stipulated in Section 12.3.3.

iii) As previously discussed in Section 3.2.1 and Eq. (3-1), the maximum moment demand placed on the bent cap can be established at the column face and may included the effects of the axial load on the columns.

iv) Based on the maximum moment demand computed from Eq. (3-1) increase in the yield moment capacity of the bent cap must be achieved in terms of Eq. (3-2).

v) Referring to a section in its upright position, when an increase in the bent cap bottom longitudinal reinforcement is required (that is top in the test units) at least a minimum of 4 bars shall be placed within the width of the exiting bent cap section, as shown in Figure 3-22. If at least 4 bars are already present in the as-built section this limit shall be considered null. Furthermore, at least two of these bars must be placed through the existing concrete core as shown in Figure 3-23.

12.3.3. Reinforced Concrete Joint Design

Design of the reinforcement within the joint region should follow the procedure outlined in Section 3.3.1, which establish design of the joints in terms of the principle compressive and tensile stress limits. Furthermore, design of the joint shear reinforcement shall be performed in terms of the strut and tie model presented in Section 3.3.2.

i) In addition to the longitudinal reinforcement required to increase the yield moment capacity of the bent cap given by Eq. (3-2), additional longitudinal reinforcement shall be

required to resist the joint shear forces and shall be placed in the bent cap according to the design strategy discussed in Section 3.3.3.

ii) Additional internal and external vertical joint shear reinforcement required within the joint region shall be provided according to the limits defined in Section 3.3.4.

iii) An area of horizontal joint shear reinforcement is required within the joint region according to the design philosophy presented in Section 3.3.5.

Based on the experimental results and observed damage levels the following methodology is recommended in addition to the design parameters set by Section 3.3.5.

iii.a) For an upgrade bent cap section when the principle tensile stress are less than $\phi_f \times 0.42\sqrt{f_c^{'}}\,(Mpa)$, installation of the transverse reinforcement may be provided in terms of any of the details used in the construction of Unit 1 (two pieces, see detail in Figure 3-1), Unit 2 (single piece, see detail in Figure 4-1), and/or Unit 3 (single piece post-tensioned, see detail in Figure 5-1). At this principle tensile stress limit no reduction in the available displacement ductility capacity of the system is imposed.

iii.a.1) In retrofit situations that meet Unit 3 design and when the principle tensile stress limits are less than $\phi_f \times 0.55\sqrt{f_c^{'}}\,(Mpa)$; once again, no reduction in the available displacement ductility capacity of the system shall be imposed.

iii.b) For bent cap sections with the height, h_b, initially computed based on Eq. (3-4) and that do not meet the limits set above, the bent cap height may be computed based on the following expression:

$$h_b = \frac{1}{\phi_f\, 0.8}\sqrt{\frac{M_U}{w_b\sqrt{\left(\rho_{all} \times \sqrt{f_c^{'}} + \frac{f_a}{2}\right)^2 - \frac{f_a^{\,2}}{4}}}} \qquad (12\text{-}2)$$

Where M_U is the ultimate moment capacity of the column, ϕ_f is the flexural strength reduction factor equal to 0.9, f_a is the axial stress in the joint and is computed based on Eq. (3-9), $f^{'}_c$ is the nominal design concrete compressive strength, and ρ_{all} is the allowable principle tensile stress limit in the joint in terms of the values shown in Table 12-1. Bent caps meeting the requirements set by this expression shall have no required reduction in the available displacement ductility capacity of the system.

iii.c) For bent cap designed according to Eq. (12-2) the maximum available displacement ductility capacity must be set in terms of the values shown in Table 12-1.

Table 12-1. Allowable

Transverse Reinforcement Details	Allowable ρ_{all}	Allowable μ_{Δ}
Two Pieces per Figure 3-1	ϕ_f 0.42	4
Single Piece per Figure 4-1	ϕ_f 0.42	8
Post-Tensioned per Figure 5-1	ϕ_f 0.55	8

iii.d) Reductions in the displacement ductility capacity of the system as shown in Table 12-2 are required when the principle tensile stress limits exceed $\phi_f \times 0.42\sqrt{f_c^{'}}(Mpa)$ for Units 1 and 2 details, and $\phi_f \times 0.55\sqrt{f_c^{'}}(Mpa)$ for uUnit 3 details.

Table 12-2. Modified Displacement Ductility Capacity

Transverse Reinforcement Details	Number of Peak Cycles, N_f		
	$N_f \leq 2$	$2 \leq N_f \leq 4$	$N_f > 4$
Two Pieces per Figure 3-1	6	4	2
Single Piece per Figure 4-1	6	6	2
Post-Tensioned per Figure 5-1	6	4	2

*Maximum number of peak cycles, N_f, is computed based on Eq.(12-3).

In Table 12-2 the number of cycles of loading, N_f, expected at the maximum displacement amplitude may be estimated from (NCHRP, 2003):

$$N_f = 2 \leq 3.5 \times T_N^{-\frac{1}{3}} \leq 10 \qquad (12\text{-}3)$$

Where T_N is the natural period of vibration of the structure.

When a multiple column bridge bent is designed based on the above recommendations, a ductile seismic response can be expected up to the design drift limit state.

REFERENCES

AASHTO, "Standard Specification for Highway Bridges, Sixteenth Edition," American Association of State Highway and Transportation Officials, 1996.

ATC-32, (1996), "Improved Seismic Design Criteria for California Bridges: Provisional Recommendations," Applied Technology Council, Redwood City, California.

Buckle, I. (2000), "Passive Control of Structures for Seismic Loads." *Proceedings of the 12th World Conference on Earthquake Engineering*, Auckland, New Zealand, 2000, Paper No. 2825

California Department of Transportation (Caltrans), (2001), "Bridge Design Specifications," Sacramento, CA, 2001.

California Department of Transportation (Caltrans), (2004), "Seismic Design Criteria," Version 1.3, Sacramento, CA, USA, February 2004.

Chai, H. Y., Priestley, M. J. N., Seible, F., (1991), "Seismic Retrofit of Circular Bridge Columns for Enhanced Flexural Performance," *ACI Structural Journal*, Vol. 88, No. 5, September – October 1991, pp. 572-584.

Chen, G., Anderson, N., Luna, R., Stephenson, R.W., El-Engebawy, M., Silva, P.F., and Zoughi, R., Earthquake Hazards Assessment and Mitigation: A Pilot Study in the New Madrid Seismic Zone Report FHWA, Turner-Fairbanks Highway Research Center, Federal Highway Administration, McLean, Virginia, August 2005.

DesRoches, R., and Fenves, G.L., (2001), Simplified Restrainer Design Procedure for Multiple-Frame Bridges, *EERI Earthquake Spectra*, Vol. 17, No. 4, Nov. 2001, pp. 551-567.

Ereckson, N.J., Silva, P.F., Chen, G., (2002), "Seismic Evaluation of Bent Cap/Column Joints in Missouri," Preliminary Report for Task 6, Earthquake Hazards Mitigation Research Program for Highway Systems.

Gergely, I., Pantelides, C.P., and Reaveley, L.D., (2000). "Shear strengthening of R/C T-Joints using CFRP Composites." ASCE Journal of Composite for Construction, Vol. 4, No. 2, May 2000, pp. 56-64.

Ingham, J. M., (1995), "Seismic Performance of bridge Knee Joints." Doctoral Dissertation, University of California, San Diego, 1995.

Krawinkler, H. (1995), "New Trends in Seismic Design Methodology," *Proceeding of the l0th European Earthquake Engineering*, Rotterdam, Netherlands, Aug. 28 – Sep. 2, 1995, Vol. 2, pp. 821-830.

Krawinkler, H. (1999), "Challenges and Progress in Performance-Based Earthquake Engineering." *Proceedings of International Seminar on Seismic Engineering for Tomorrow – in Honor of Professor Hiroshi Akiyama*, Tokyo, Japan, 1999, pp. 1-10.

Lowes, Laura N., Moehle, Jack P., (1999), "Evaluation and Retrofit of Beam-Column T-Joints in Older Reinforced Concrete Bridge Structures," ACI Structural Journal, V. 96, No. 4, July-August 1999.

Mazzoni, S., Moehle, J.P., (2001). "Seismic Response of Beam-Column Joints in Double-Deck Reinforced Concrete Bridge Frames," *ACI Structural Journal*, Vol. 98, No. 3, May-June 2001, pp. 259–269.

Mazzoni, S., Fenves, G. L., Smith, J. B. (2004) Effects of Local Deformations On Lateral Response of Bridge Frames," Report to California Department of Transportation, Contract No. 59A201, EEC-9701568.

Priestley, M.J.N., (1993), "Assessment and Design of Joints for Single-Level Bridges with Circular Columns," University of California, San Diego, Structural Systems Research Project, Report No. SSRP-93/02.

Priestley, M.J.N., Seible, F., Calvi, G.M. (1995) "Seismic Design and Retrofit of Bridges," John Wiley & Sons, Inc.

Sanders, D., Laplace, P., Saiidi, M. & El-Azazy, S. (2002) "Seismic performance of reinforced concrete bridge columns," Third National Seismic Conference and Workshop on Bridges and Highways: Advances in Engineering and Technology for the Seismic Safety of Bridges in the New Millennium, Portland, Oregon, April 2002: pp. 345–356.

Silva, P.F., Seible, F., Priestley, M.J.N., (1997), "Response of Standard Caltrans Pile-to-Pile Cap Connections Under Simulated Seismic Loads," Department of AMES, University of California San Diego, La Jolla, California, November 1997, Report SSRP-97/09.

Silva, P.F., Sritharan, S., Seible, F., Priestley, M.J.N. (1999), "Full-Scale Test of the Alaska Cast-in-Place Steel Shell three Column Bridge Bent," University of California, San Diego, Report to Alaska Department of Transportation and Public Facilities, Juneau, Alaska, Report No. SSRP 98/13.

Sritharan, S. (1998), "*Analysis of Concrete Bridge Joints Subjected to Seismic Action*", Doctoral Dissertation, Department of AMES - Division of Structural Engineering, University of California San Diego, La Jolla, California.

Sritharan, S. Sri, Priestley, M.J.N., Seible, F., (1999), "Enhancing Seismic Performance of Bridge Bent cap-to-Column Joints Using Prestressing," *PCI Journal*, V. 44, No. 4, July-August 1999.

Sritharan, S., Ingham, Jason M., (2003), "Application of Strut-and-Tie Concepts to Concrete Bridge Joints in Seismic Regions," *PCI Journal*, Vol. 48, No. 4, July-August 2003, pp.66-90.